Report on the PHT Scientific Validation for OLP Version 7.0

Ulrich Klaas and Mario Radovich

with contributions by the PHT OLP Validation Team:
Ingolf Heinrichsen, Linda Cornwall, Phil Richards,
Huw Morris, Martin Haas, Viktor Toth,
Helen Walker and Carlos Gabriel

and

with contributions by the PIDT/MPIA Calibration Team:
Bernhard Schulz, José Acosta, Hector Castañeda, Uwe Herbstmeier,
Peter Ábrahám, Steffen Huth, Michael Braun, Thomas Müller,
Michael Kunkel and Rene Laureijs

SAI/98–049/Rp

Version 2.0

July 20, 1998

Contents

1 Results and Achievements by PHT OLP V7.0 Scientific Validation 7
1.1 Calibration Upgrades from OLP6 to OLP7 . . . 7
1.2 Photometric Accuracies of Staring Modes . . . 7
1.2.1 Photometric Accuracy Limitations . . . 9
1.3 Re-validation of Staring Mode Photometry and PHT-S . . . 9
1.3.1 Reset Interval Correction . . . 9
1.3.2 Orbit Dependent Dark Current Subtraction . . . 10
1.3.3 Multi-filter Staring Modes . . . 10
1.3.4 Absolute Photometric Modes . . . 10
1.3.5 Spectroscopic Mode . . . 10
1.3.6 Mapping Modes . . . 11
1.4 Validation . . . 11
1.4.1 Color Correction . . . 11
1.4.2 Extended Source Photometry . . . 11
1.4.3 Chopped Photometry . . . 11
1.5 Error Calculation and Propagation . . . 12
1.6 Status of Scientific Validation of PHT AOTs . . . 12
1.7 General Points . . . 13
1.8 Limitations and Caveats . . . 13

2 Known Limitations and Caveats 14
2.1 Validity Ranges of FCS Calibration Files . . . 14
2.2 PHT-C External Flat-fields . . . 15
2.3 Inhomogeneous FCS Illumination of PHT-P Apertures . . . 15
2.4 Non-geometric Aperture Beam Size Scaling . . . 16
2.5 Signal Dependence on Reset Interval . . . 17
2.6 Non-linearity of Detector Responsivity with Flux . . . 17
2.7 Detector Signal Transients . . . 17
2.8 Long Term Detector Drifts . . . 18
2.9 Dark Current Variations along the Revolution . . . 18
2.10 Error Calculation and Propagation . . . 19
2.11 Actual versus Intended Pointing . . . 19
2.12 Missing Measurements and Chopper Correction . . . 19
2.13 Limitations in Use of PHT Color Correction Factors . . . 19
2.14 Empirical PPSF Correction Factors for Array Centered C200 Photometry . . . 20

3 Prerequisites for OLP Scientific Validation 22

4 Results from OLP 7 Scientific Validation Period 1 23
4.1 Empirical Chopper Frequency Correction (Black Box Test) . . . 24
4.1.1 Data Analysis . . . 24
4.1.2 Narrative . . . 24
4.1.3 Problems Identified . . . 24
4.1.4 Concerns . . . 24
4.1.5 Evaluation Log . . . 25
4.2 REPORT on Scientific Validation of PIA/OLP 7.0, AOT P22, P32, P37 . . . 28
4.2.1 Summary . . . 28
4.2.2 Data Sets . . . 28
4.2.3 Data Reduction . . . 28
4.2.4 Notes on the Bugs Found and Additional Improvements Recommended 29
4.2.5 Results . . . 31

5 Revalidation Tests (Results from OLP 7 Scientific Validation Period 2) 34
5.1 PHT-C Multi-filter Relative Calibration . . . 35
5.1.1 Motivation . . . 35
5.1.2 References to Calibration Analysis and Software Change Documentation 35
5.1.3 Method . . . 35
5.1.4 Results . . . 35
5.1.5 Conclusions . . . 37
5.1.6 Evaluation Log . . . 37
5.2 Signal Dependence on Reset Interval Correction . . . 40
5.2.1 Motivation . . . 40
5.2.2 References to Calibration Analysis and Software Change Documentation 40
5.2.3 Method . . . 40
5.2.4 Results . . . 41
5.2.5 Conclusions . . . 42
5.2.6 Evaluation Log . . . 50
5.2.7 CAL-G Files Affected by Reset Interval Correction . . . 52
5.2.8 Independent Check of the Quality of the Reset Interval Correction . . 53
5.3 Extension of PHT SPD Data Records for Improved Error Handling . . . 56
5.3.1 Motivation . . . 56
5.3.2 Reference to Software Change Documentation . . . 56
5.3.3 Method . . . 56
5.3.4 Results . . . 56
5.4 Use of Improved Pointing Information for PHT Maps . . . 58
5.4.1 Motivation . . . 58
5.4.2 References to Calibration Analysis and Software Change Documentation 58
5.4.3 Method . . . 58
5.4.4 Results . . . 58
5.4.5 Conclusions . . . 58
5.5 Power Ranges of FCS Cal-G Files . . . 63
5.5.1 Motivation . . . 63
5.5.2 References to Calibration Analysis and Software Change Documentation 63
5.5.3 Method . . . 63
5.5.4 Results . . . 63
5.5.5 Conclusions . . . 64
5.6 Orbit Dependent Dark Current Subtraction for the PHT-S Spectrum of the Faint Star HR 6514 . . . 65
5.6.1 Motivation . . . 65
5.6.2 References to Calibration Analysis and Software Change Documentation 65
5.6.3 Method . . . 65
5.6.4 Results . . . 65
5.6.5 Conclusions . . . 65
5.7 Orbit Dependent Dark Current Subtraction for the Absolute Surface Brightness Photometry of the Earth Straylight Measurements . . . 68
5.7.1 Motivation . . . 68
5.7.2 References to Calibration Analysis and Software Change Documentation 68
5.7.3 Method . . . 68
5.7.4 Results . . . 68
5.7.5 Conclusions . . . 69
5.7.6 Evaluation Log . . . 70
5.8 PHT Photometry Color Correction Factors . . . 72
5.8.1 Motivation . . . 72
5.8.2 References to Calibration Analysis and Software Change Documentation 72
5.8.3 Method . . . 72
5.8.4 Results . . . 72
5.8.5 Final Color Correction Values for CAL-G V4.0 . . . 73
5.9 Converting PHT OLP to Run on the DEC Alpha Platform . . . 78
5.9.1 Motivation . . . 78
5.9.2 Summary of Software Changes for Port to Alpha Platform . . . 78
5.9.3 Results . . . 78

5.10 Error Message Log and Ramp Statistics in PHT SPD and Cal-A Headers . . 79
5.10.1 Motivation . . . 79
5.10.2 References to Calibration Analysis and Software Change Documentation 79
5.10.3 Method . . . 79
5.10.4 Results . . . 79
5.10.5 Conclusions . . . 80
5.11 Wavelength Dependent Solid Angles of PHT-C Arrays . . . 81
5.11.1 Motivation . . . 81
5.11.2 References to Calibration Analysis and Software Change Documentation 81
5.11.3 Method . . . 81
5.11.4 Results . . . 81
5.11.5 Conclusions . . . 83
5.11.6 Evaluation Log . . . 84
5.12 Subtracted Source Flux for Chopped PHT AA Products . . . 86
5.12.1 Motivation . . . 86
5.12.2 References to Calibration Analysis and Software Change Documentation 86
5.12.3 Method . . . 86
5.12.4 Results . . . 86
5.12.5 Conclusions . . . 88
5.13 Change in Error Handling for PHT OLP . . . 89
5.13.1 Motivation . . . 89
5.13.2 References to Calibration Analysis and Software Change Documentation 89
5.13.3 Method . . . 89
5.13.4 Results . . . 89
5.13.5 Conclusions . . . 89
5.14 General Re-validation of PHT03 and PHT22 Staring Mode: The SED of α Bootes (HR 5340) . . . 91
5.14.1 Motivation . . . 91
5.14.2 Method . . . 91
5.14.3 Results . . . 91
5.14.4 Conclusions . . . 93
5.14.5 Evaluation Log . . . 95
5.15 General Re-validation of PHT03 and PHT22 Staring Mode: The SED of Arp 220 . . . 96
5.15.1 Motivation . . . 96
5.15.2 Method . . . 96
5.15.3 Results . . . 96
5.15.4 Conclusions . . . 99
5.15.5 Evaluation Log . . . 100
5.16 General Re-validation of PHT Multi-filter (PHT03/PHT22) and PHT Absolute (PHT05/PHT25) Staring Mode Photometry: The SED of γ Draconis (HR 6705) . . . 101
5.16.1 Motivation . . . 101
5.16.2 Method . . . 101
5.16.3 Results . . . 101
5.16.4 Conclusions . . . 105
5.16.5 Evaluation Log . . . 105
5.17 General Re-validation of PHT Staring, Nodding and Mini-map Modes: The SED of Sirius (HR 2491) . . . 107
5.17.1 Motivation . . . 107
5.17.2 Method . . . 107
5.17.3 Results . . . 107
5.17.4 Conclusions . . . 107
5.17.5 Evaluation Log . . . 109
5.18 General Re-validation of PHT03 Staring Mode: Photometric Reproducibility Aspects in the Case of the SED of Vega (HR 7001) . . . 110
5.18.1 Motivation . . . 110
5.18.2 Method . . . 110
5.18.3 Results . . . 111

5.18.4 Conclusions . . . 111
5.18.5 Evaluation Log . . . 113
5.19 General Re-validation of C200 Absolute and Mapping Photometry of Ceres . 115
5.19.1 Motivation . . . 115
5.19.2 Method . . . 115
5.19.3 Results . . . 115
5.19.4 Conclusions . . . 115
5.19.5 Evaluation Log . . . 118
5.20 General Re-validation of C200 Absolute and Mapping Photometry of Uranus 119
5.20.1 Motivation . . . 119
5.20.2 Method . . . 119
5.20.3 Results . . . 119
5.20.4 Conclusions . . . 119
5.20.5 Evaluation Log . . . 121
5.21 C200 Mini-map Photometry of the Faint Star ε Lep (HR 1654) . . . 122
5.21.1 Motivation . . . 122
5.21.2 Method . . . 122
5.21.3 Results . . . 122
5.21.4 Conclusions . . . 122
5.21.5 Evaluation Log . . . 123
5.22 Reproducibility of Photometry Processed by OLP for the C200 MFAINT Program on γ Dra (HR 6705) . . . 124
5.22.1 Motivation . . . 124
5.22.2 Method . . . 124
5.22.3 Results . . . 124
5.22.4 Conclusion . . . 125
5.22.5 Evaluation Log . . . 125
5.23 General Re-validation of PHT-40: Spectra of Line and Continuum Sources (HR 6705, HR 6817, NGC 7023, NGC 6543) . . . 128
5.23.1 Motivation . . . 128
5.23.2 References to Calibration Analysis and Software Change Documentation 128
5.23.3 Method . . . 128
5.23.4 Results . . . 128
5.23.5 Conclusions . . . 132
5.23.6 Evaluation Log . . . 132

6 Validation of the Chopped Point Source Photometry 143
6.1 Motivation . . . 143
6.2 References to Calibration Analysis and Software Change Documentation . . . 143
6.3 Method . . . 143
6.4 Validation of PHT03 and PHT22 Chopped Mode: The SED of IRAS 03068-5346 144
6.4.1 Motivation . . . 144
6.4.2 Method . . . 144
6.4.3 Results . . . 144
6.4.4 Conclusions . . . 145
6.4.5 Evaluation Log . . . 148
6.5 Validation of PHT03 and PHT22 Chopped Mode: The FIR Excess SED of Vega . . . 150
6.5.1 Motivation . . . 150
6.5.2 Method . . . 150
6.5.3 Results . . . 150
6.5.4 Conclusions . . . 150
6.5.5 Evaluation Log . . . 154
6.6 Comparison of Chopped and Staring Mode Photometry of Standard Stars from the Empirical Signal Correction Calibration Program . . . 155
6.6.1 Motivation . . . 155
6.6.2 Method . . . 155
6.6.3 Results . . . 155
6.6.4 Conclusions . . . 155

6.6.5 Evaluation Log . . . 158
6.7 OLP Chopped and Staring Mode Photometric Results for the Faint Point Source Detection Limit Program . . . 160
6.7.1 Motivation . . . 160
6.7.2 Method . . . 160
6.7.3 Results . . . 160
6.7.4 Conclusions . . . 161
6.7.5 Evaluation Log . . . 162
6.8 Comparison of Chopped and Staring Mode Photometry of Stars Observed by the MFAINT and CFAINT Programs . . . 164
6.8.1 Motivation . . . 164
6.8.2 Method . . . 164
6.8.3 Results . . . 164
6.8.4 Conclusions . . . 164
6.8.5 Evaluation Log . . . 169
6.9 General Conclusions from Chopped Photometry Analysis . . . 171

7 Conclusions and Outlook **172**

1 Results and Achievements by PHT OLP V7.0 Scientific Validation

1.1 Calibration Upgrades from OLP6 to OLP7

In Table 1 we list the major calibration upgrades which were implemented for OLP7 and describe which AOTs or AOT submodes were affected by the individual upgrades.

Table 1: Calibration upgrades from OLP 6 to OLP 7 and impact on the different AOT modes

	calibration upgrade	**affects AOT**
1)	reset interval dependence	all AOTs, except PHT40
2)	FCS calibration	all AOTs, except PHT40
3)	PHT-C filter-to-filter	PHT22, PHT37/38/39, PHT32
4)	orbit dependent dark current	all AOTs in staring mode
5)	chopper offset	PHT22, PHT32
6)	chopped signal correction	PHT03, PHT04, PHT22 in chopped mode
7)	orbit dependent responsivity	PHT03, PHT04, PHT22 in chopped mode
8)	solid angles per filter	PHT22, PHT25, PHT32, PHT37/38/39 extended sources

1.2 Photometric Accuracies of Staring Modes

Global calibration accuracies have been estimated from the investigation of the test cases and the comparison with published reference photometry. (for a dependence on flux, see Table 2 below). They can be applied, if not one of the caveats on photometry applies, cf. Sect. 2.
The terms **absolute accuracy**, **relative accuracy** and **reproducibility** have been defined in the following context:

- **absolute accuracy** is the accuracy achieved w.r.t. the reference photometry, if the filter measurement had a corresponding FCS transfer measurement in the same filter. Hence, the quality of the FCS calibration against celestial standards is directly verified. Note that no calibration accuracy of the reference photometry (models, IRAS) has been taken into account, as this is beyond the scope of this report. A typical order of the absolute accuracy of the reference photometry is 2 – 10%. Table 2 lists the achieved values per detector and flux range.

- **relative (filter-to-filter) accuracy** is the accuracy achieved w.r.t. the reference photometry, if the filter measurement was not performed in the filter in which the FCS calibration was done. Currently, assumptions about the constancy of the responsivity over the full flux range and for all filters, and, related to that relative filter-to-filter correction factors, apply. It has been proven that this is in general not correct, and it is considered that in future OLP versions corrections for non-linearities of the responsivity with the in-band power will be applied. Hence, the relative uncertainty can be much larger than the absolute one in multi-filter measurements with certain source SEDs. Table 2 lists the achieved values per detector and flux range. The number of

suitable test cases performed in multi-filter mode is much smaller than the number of test cases in any of the absolute measurement modes (i.e. with an FCS measurement in the respective filter). The relative filter-to-filter accuracy could only be established for a minor subset with no test case for C200.

- absolute and relative accuracy are assumed to add to the total photometric uncertainty. In multi-filter measurements with one FCS measurement the absolute measurement uncertainty is subtracted from all measurements in non-FCS filters in order to derive the relative measurement accuracy.
- **reproducibility** is the relative consistency of measurements repeated several times with the same measurement set-up. It is a measure of the internal stability of the instrument and describes also the current limitations in signal processing. Table 3 lists the achieved values per detector both for a bright secondary standard and a faint source. These values were obtained from special calibration monitoring programs performed during ISO's Routine Phase [21].

In summary, the following calibration accuracies have been achieved per detector:

P1: 10% absolute accuracy and 20% relative accuracy for bright sources (> 50 Jy). For fainter sources the absolute accuracy is within 30%.
The relative reproducibility accuracy is 5% for bright sources and 10% for faint sources.

P2: Better than 15% absolute accuracy and 10% relative accuracy.
The relative reproducibility accuracy is 2% for bright sources and 12% for faint sources.

P3: 15% absolute accuracy and 20% relative accuarcy down to $\sim$ 0.5 Jy. For fainter sources the absolute accuracy is around 30 %.
The relative reproducibility accuracy is 7% for bright sources and 7% for faint sources. Under extreme Space Weather conditions and for the very end of the science window the achieved accuracy for faint sources is poorer.

C100: 15% absolute accuracy and 10% relative accuracy down to $\sim$ 0.5 Jy. For fainter fluxes the absolute accuracy in mini-map mode is $\sim$ 30%.
The relative reproducibility accuracy is 3% for bright sources and 20% for faint sources.

C200: $\sim$ 20% absolute accuracy for brighter sources. Note that in array centered mode accuracies are poorer for the 180 and 200 μm filters due to an inadequate PSF correction factor. Photometry in these filters has to be corrected in general by 20–30% towards higher flux values. For fainter sources (< 1 Jy) the accuracy achieved in mini-map mode is $\sim$ 30%. There was no suitable test case allowing to judge the relative filter-to-filter accuracy. The investigated test cases of standard stars (α Boo, γ Dra and Sirius did not give conclusive results due to their faintness in the C200 range and application of less optimal observing modes.
The relative reproducibility accuarcy is around 10% both for bright and faint sources.

Table 2: Absolute and relative (filter-to-filter) calibration accuracies per detector achieved for various flux ranges in multi-filter mode with OLP V7.0b2. For quoted PHT-S accuracies refer to Ref. [13].

detector	AOT mode	flux range [Jy]	abs. accuracy [%]	rel. accuracy [%]	standard
P1	P03 off & on	300 - 6000	**10**	15	α Boo
P1	P03, P05 off & on	70 - 1250	**10**	20	γ Dra
P1	P03, P05 off & on	50 - 1000	**10**	**10**	Sirius
P1	P03 nodding	2 - 10	30	–	HR 6817
P1	P03 nodding	2	35	–	HR 5986
P1	P03 nodding	< 0.1	20	–	HD 172323
P2	P03 off & on	100 - 200	≤ 5	5	α Boo
P2	P03, P05 off & on	25 - 40	10	10	γ Dra
P2	P05 off & on	~ 20	**15**	–	Sirius
P2	P03 nodding	3 - 6	≤ 25	–	HR 6132
P2	P03 nodding	3.5	≤ 5	–	HR 7310
P2	P03 nodding	0.5	≤ 10	–	HR 5986
P3	P03 off & on	10 - 25	**10**	20	α Boo
P3	P03 nodding	6 - 20	15	–	α Tau
P3	P03, P05 off & on	~ 5	**10**	30	γ Dra
P3	P03 nodding	~ 3.5	**15**	–	Sirius
P3	P03 nodding	0.6	≤ 15	–	HR 7310
P3	P17/18/19	< 0.2	30	–	HR 5981
C100	P22 off & on	6 - 25	5	10	α Boo
C100	P22, P25 off & on	~ 5	**10**	–	γ Dra
C100	P22 nod & minimap	~ 3.5	**15**	–	Sirius
C100	P22 minimap	0.2 - 0.6	5	–	HR 7310
C100	P37/38/39 4 times	< 0.2	30	–	HR 5981
C100	P37/38/39 2 times	< 0.1	30	–	SAO248381
C100	P37/38/39 2 times	< 0.1	30	–	IRC+60228
C200	P22 minimap	600 - 900	$<$ **10**	–	Uranus
C200	P22 minimap	50 - 120	25 (> 170 μm)	–	Ceres
	P22 minimap, P25		15 (< 170 μm)	–	
C200	P22 minimap	~ 0.5	15	–	γ Dra
C200	P25 off & on	~ 0.5	30	–	γ Dra
C200	P22 minimap	0.2 - 0.4	30	–	HR 1654
SS	P40 off & on	2 - 5000	< 30	< 30	
SL	P40 off & on	1 - 5000	< 30	< 30	

1.2.1 Photometric Accuracy Limitations

The multi-filter staring off/on photometry shows drastically reduced photometric accuracy as soon as the source-to-background contrast goes below 0.75 (1:1.3). For this reason the C200 photometry of the standard stars α Boo and γ Dra cannot be used for the establishment of absolute and relative calibration accuracies. This issue needs follow-up, in particular in the context of the responsivity non-linearity with flux investigations.

1.3 Re-validation of Staring Mode Photometry and PHT-S

1.3.1 Reset Interval Correction

The correction for signal dependence on reset interval was implemented successfully and homogenizes the signals for most read-out combinations. A prerequisite for this was a consistent treatment of a significant fraction of the PHT calibration files which were provided for this OLP version.

Table 3: Relative Calibration Reproducibility Accuracy per Detector for Bright and Faint Fluxes from Monitoring Programs.

detector	target	**flux** [Jy]	**relative accuracy** $1\ \sigma$ [%]
P1	NGC 6543	8	5
P1	HD 172323	0.085	10
P2	NGC 6543	100	2
P2	HR 5986	0.67	12
P3	NGC 6543	100	7
P3	HR 7310	0.67	7
C100	NGC 6543	50	3
C100	HR 7310	0.23	20
C200	NGC 6543	11	10
C200	HR 6705	0.67	7

1.3.2 Orbit Dependent Dark Current Subtraction

The orbit dependent dark current subtraction was implemented successfully for all detector systems. For PHT-S faint source measurements clear improvements of the final flux calibrated spectra showing less scatter and more accurate absolute levels could be demonstrated. The statistical approach of deriving an average orbit dependent dark current has its limitations, if detectors show peculiar behaviour on specific revolutions.

1.3.3 Multi-filter Staring Modes

The PHT staring photometric modes PHT03 and PHT22 OLP processing was sucessfully re-validated. In general both the absolute and relative calibration are improved by this OLP version, see Sect. 1.2 above.

1.3.4 Absolute Photometric Modes

The PHT absolute photometric modes PHT05 and PHT25 OLP processing was successfully re-validated. The absolute calibration of PHT-P is improved for this version, see Sect. 1.2 above.

The following points were noted which need to be addressed in further detail:

- For the investigated test case C100 absolute photometry gives less accurate results than the multi-filter mode.
- For C200 similar restrictions apply as for the multi-filter mode due to the faintness of the standard stars in this wavelength range.

1.3.5 Spectroscopic Mode

The PHT spectroscopic mode PHT40 OLP processing was successfully re-validated. Spectral shapes and features are maintained.

Under the following conditions significant deviations in flux from the OLP 6 occur:

- The newly introduced orbit dependent dark signal subtraction shows noticeable differences in the resulting fluxes for continuum levels below 6 10^{-14} W m^2 μm^{-1} for SS and 4 10^{-14} W m^2 μm^{-1} for SL, respectively (for staring mode observations).

- For faint continuum sources changes in the continuum level of about 50% can occur w.r.t. OLP V6 results. For the investigated test case (NGC 6543) no final conclusion could be drawn by comparison with reference spectroscopy (IRAS LRS and CAM-CVF) and further refined cross calibration is necessary. The line fluxes are in general not affected, if the peak intensity is above the levels where dark current subtraction becomes crucial (see above).

1.3.6 Mapping Modes

The mapping modes of PHT03 and PHT22 were successfully technically re-validated, using now the best pointing information. A slight qualitiative improvement (sharpness, flat-field, border smothness, etc.) was observed, too.

1.4 Validation

1.4.1 Color Correction

Color correction tables have been successfully tested in the context of absolute and relative filter-to-filter calibration. Color correction figures have to be consequently applied in order to achieve the best photometric accuracy.

1.4.2 Extended Source Photometry

Wavelength dependent solid angles for the PHT-C arrays derived from refined beam calculations have been successfully tested and make the surface brightness values for all investigated test cases comparable to COBE annual map results.
The PHT22 AOT extended source photometry can therefore be declared scientifically validated with an absolute accuracy of 30% and a relative filter-to-filter accuracy of 20%.
The PHT03 AOT extended source photometry needs still further refinement of the solid angles and a detailed check-out of the dependence on the aperture size.

An overview per detector and flux range is presented in Table 4 Note that the accuracy of COBE annual maps for 140 and 240 μm is typically 20%. For weekly maps it can be even worse. For wavelengths less equal than 100 μm the quoted accuracy is in general $\leq$ 1%.

Table 4: Calibration Accuracy per Detector for Extended Sources for Various Flux Ranges with OLP V7

detector	**flux range** [MJy sr^{-1}]	**absolute accuracy** [%]	**relative accuracy** [%]	**standard**
C100	5 - 15	20	< 30	COBE/DIRBE
C200	4 - 10	20	< 30	COBE/DIRBE

1.4.3 Chopped Photometry

On the basis of the investigated test cases the chopped photometry of AOTs PHT03 and PHT22 can not yet be declared scientifically valid.

The most reliable results have been found for chopped P2 photometry for which in many cases an absolute calibration accuracy of around 20% could be achieved.

This non-declaration of scientific validation is based on the following findings:

- In particular for P3 and C100 a general over-correction of the chopped photometric fluxes w.r.t. reference photometry from the literature or ISOPHOT staring mode photometry is observed.
- In multi-filter modes the scatter of the photometric data points, including non-detection of the source, or discontinuitites in the resulting SEDs larger than 30% are found which do not allow a sound scientific analysis.

Reasons for this behaviour of the chopped modes which need follow-up investigations are supposed to be:

- Limitations in the usage of an average default responsivity (the orbit dependence alone appears to be too weak to account for the variation of the responsivity values).
- A not yet sufficient signal evaluation for chopped measurements. In particular for C100 the restriction to use the central pixel only in the case of chopped point source photometry seems to be mandatory taking the test results into account.
- Not yet final signal correction factors. Here, more calibration data have been acquired.

1.5 Error Calculation and Propagation

Whenever possible uncertainties had been included in the Cal-G files. It turned out, however, that the simple propagation of relative uncertainties as originally specified did not yield reasonable results, as the uncertainties are of different types: statistical and systematic uncertainties and photometric bias. The relative contribution of these different types of uncertainty depends on the details of the measurement mode.

OLP V7.0 is now restricted to the pure statistical uncertainty from signal evaluation. This can be seen as a minimal error. For an estimate of the total uncertainty associated with a specific measurement the dedicated documentation must be refered to (cf. Sect. 2.10).

1.6 Status of Scientific Validation of PHT AOTs

With the finalisation of the OLP7 validation the status per AOT submode is the following as given in Table 5. The table also provides an overview of the next steps to further upgrade both validated and non-validated modes and for which OLP version improvements can be expected.
It should be noted that in the case of AOT PHT22 raster maps are partly validated: It has been demonstrated in this report that mini-maps give reliable results for faint source photometry. Most of the photometric accuracy numbers presented for faint source measurements of C100 and C200 are based on mini-map photometry. However, in order to validate PHT22 raster maps in general, the following items must be verified before:

- valid results for all different combinations of raster parameters
- conservation of flux independent of the raster parameters and the re-gridding algorithm.

These checks are less related to calibration upgrades but more to the establishment of a sufficiently large test data set and inspection of the observations case by case.
In Table 6 we list the validated modes per detector sub-system. For completeness we have added the polarisation modes which can only be evaluated interactively using PIA and special FORTRAN routines.

Table 5: Scientific Validation of OLP AOT Processing, July 98

AOT	**submode**	**scientifically valid since**	**next upgrades**	**foreseen in OLP Vx.y**
PHT03	staring point source	V6	non-lin R & FCS aper	8.2
	staring extended source	no	beam	8.2
	nodding	V6	non-lin R & FCS aper	8.2
	chopped point source	no	chop	8.2
	raster map	no	map cal & drift	8.2/9.2
PHT04	staring point source	no	beam & FCS aper	8.2
	staring extended source	no	beam	8.2
	chopped point source	no	chop & beam	8.2
PHT05	staring point source	V6	FCS aper	8.2
	staring extended source	no	beam	8.2
PHT17/9	staring point source	V6	non-lin R & FCS aper	8.2
	staring extended source	no	beam	8.2
PHT22	staring point source	V7	non-lin R	8.2
	staring extended source	V7	non-lin R	8.2
	nodding	V7	non-lin R	8.2
	chopped point source	no	chop	8.2
	raster map	no	map cal & flat-field	9.2
PHT25	staring point source	V7		
	staring extended source	V7		
PHT32	chopped mapping	no	chop & map cal	9.2
PHT37/9	staring point source	V7	non-lin R	8.2
	staring extended source	V7	non-lin R	8.2
PHT40	staring point source	V5		
	staring extended source	V6	beam	8.2
	chopped point source	V6		

1.7 General Points

- The PHT OLP was successfully ported to the DEC Alpha platform. One item which turned out to be crucial for maintenance was the Archive Configuration Table.
- This report provides useful input for the general instrument cross-calibration (PHT photometric results of calibration standards).
- This report demonstrates what can be done scientifically with PHT OLP Auto Analysis Results (AAR). Most of the comparisons with models and reference photometry performed in the Scientific Validation Period 2 are based on AAR results, without any fine tuning of data with PIA, but background subtraction and color correction were done as extra steps.

1.8 Limitations and Caveats

Limitations and Caveats are summarized in the subsequent section.

Table 6: Scientifically Validated Observing Modes per Detector, July 98

detector	**scientifically validated mode**	**AOT**
P1	absolute photometry point sources	PHT05
	staring multi-filter photometry point sources	PHT03
	faint source multi-filter nodding	PHT03
	multi-filter sparse map	PHT17/18/19
P2	absolute photometry point sources	PHT05
	staring multi-filter photometry point sources	PHT03
	faint source multi-filter nodding	PHT03
	multi-filter sparse map	PHT17/18/19
	polarimetry (PIA)	PHT50
P3	absolute photometry point sources	PHT05
	staring multi-filter photometry point sources	PHT03
	faint source multi-filter nodding	PHT03
	multi-filter sparse map	PHT17/18/19
C100	absolute photometry point sources	PHT25
	absolute photometry extended sources	PHT25
	staring multi-filter photometry point sources	PHT22
	staring multi-filter extended sources	PHT22
	faint source multi-filter nodding	PHT22
	multi-filter sparse map	PHT37/38/39
C200	absolute photometry point sources	PHT25
	absolute photometry extended sources	PHT25
	staring multi-filter photometry point sources	PHT22
	staring multi-filter extended sources	PHT22
	faint source multi-filter nodding	PHT22
	multi-filter sparse map	PHT37/38/39
	polarimetry (PIA)	PHT51
SS/SL	staring point source spectroscopy	PHT40
	extended source spectroscopy	PHT40
	chopped point source spectroscopy	PHT40

2 Known Limitations and Caveats

This section addresses the limitations and caveats of the PHT calibration file Version 4.0 and the OLP implementation 7.0 which have been identified during the scientific pipeline validation process. It addresses also which caveats from calibration file Version 3.0 and OLP version 6.0 have been closed out by this latest version.

2.1 Validity Ranges of FCS Calibration Files

OLP 6.0 contained the following caveats concerning the validity ranges of the FCS calibration files (cf. Report on the Scientific Validation of PHT OLP 6.0 [1]:

1 *OLP 6.0 Caveat:* For observations with FCS power settings outside the validity range strong deviations from the expected results can occur.

2 *OLP 6.0 Caveat:* The FCS calibration for P3, C100 and C200 before revolution 94 suffers from a lack of calibration observations, which can not be recovered. Therefore, the quality of the FCS calibration of observations before revolution 94 can be poorer as compared to observations taken later in the mission.

SCREW 338 was introduced in order to handle this problem. Limits for the validity of the FCS ranges were included into the headers of the relevant FCS calibration files and outside this validity range the s/w used default responses. In the framework of the scientific validation it was found, that this behaviour of the OLP led to unsatisfactory results

for multi-detector AOTs, as it tended to introduce "discontinuities" in the spectral energy distributions. Consequently SCREW 338 was amended by SCREW 351 which imposes that always the responsivity as derived from the FCS calibration is used. Only a warning is written to the file headers indicating the limit violation and possible degradation in calibration. To derive responsivities for the full range of electrical FCS powers used in the AOTs the lower and upper ends of the calibrated ranges were extrapolated using a model of the FCS (grey body). It should be noted that for CAL-G Version 4.0 associated with OLP V7.0 the calibrated ranges of several filters could be extended due to a large amount of additional data from the routine calibration. Sometimes, the limits are more restricted w.r.t. OLP V6.x. This comes from a more rigid quality control discarding doubtful data.
Therefore, the following (but considerably restricted) caveat remains for OLP Version 7.0:

Caveat 1: A poorer calibration accuracy can be expected for observations for which the headers of the PHT data products indicate that the FCS power settings were outside the validity range given in the header of the P*FCSPOW*.FITS CAL-G files. The deviation is larger for extrapolations further away from the validity range.

Concerning OLP 6.0 caveat 2) above, the calibration accuracy could be improved in the OLP 6.0 version also for the time before revolution 94 by using better reduction algorithms, however, the coverage of the calibration curves by standard sources is less good than for the rest of the mission. This affects only a small number of routine observations (from rev. 79 to rev. 93):

Caveat 2: The FCS calibration for P3, C100 and C200 before revolution 94 is less well sampled with standard calibration observations, than after revolution 94. Therefore, the quality of the FCS calibration of observations before revolution 94 can be poorer as compared to observations taken later in the mission. This also applies for the FCS flat-field calibration for the C100 and C200 detectors.

Table 7 compares the valid ranges of the main FCS, FCS1, for OLP V6.x and OLP V7.0 (in mW of electrical FCS power). In general the ranges of OLP V7.0 are wider. However, a more rigid data quality assurance removed some doubtful data points which occurred in most cases at the lower end of the calibration range, so that for some filters the ranges are actually narrower. Note that strictly speaking for PHT-P the power range is associated with the corresponding standard aperture (cf. Sect. 2.3 for a table of the standard apertures per PHT-P filter and additional caveat).

2.2 PHT-C External Flat-fields

For OLP 6.0 it was not possible to integrate the FCS flat-field corrections in time for the release of the s/w. For Version 7.0 the related calibration files PC1ILLUM* and PC2ILLUM* have been updated in the framework of the general calibration file delivery. Therefore, the

1 *OLP 6.0 Caveat:* In multi-filter AOTs measurements in filters other than the one of the corresponding FCS calibration measurement can show a poorer flat-field correction of the PHT-C arrays.

does no longer apply for OLP 7.0 products.

2.3 Inhomogeneous FCS Illumination of PHT-P Apertures

The illumination of the both the PHT-P apertures and the PHT-C arrays by the internal Fine Calibration Source (FCS) is not flat. As a result the illumination of the detector does not scale with the area of the aperture. This effect is corrected for in the case of PHT-C by the so-called illumination matrix (PC1ILLUM and PC2ILLUM cal-G files). Currently, for PHT-P linearity with the aperture area is assumed and the corresponding PHT-P CAL-G files (PP1FCSAP, PP2FCSAP and PP3FCSAP) only contain correction factors of 1 (i.e. they do not imply any correction).

Table 7: Validity Ranges of FCS Tables (for FCS1 only)

	up to revolution 93				after revolution 93			
	OLP V6.x		OLP V7.0		OLP V6.x		OLP V7.0	
Filter	**min**	**max**	**min**	**max**	**min**	**max**	**min**	**max**
P_3.29	17.48	49.99	17.48	50.00	17.48	49.99	17.48	50.00
P_3.6	9.49	50.02	11.29	50.01	9.49	50.02	11.29	50.01
P_4.85	10.00	39.30	13.30	35.34	10.00	39.30	13.30	35.34
P_7.3	7.59	20.00	7.48	22.13	7.59	20.00	7.48	22.13
P_7.7	8.60	24.41	8.59	24.41	8.60	24.41	8.59	24.41
P_10	4.77	11.49	4.47	11.49	4.77	11.49	4.47	11.49
P_11.3	4.99	9.07	4.81	8.92	4.99	9.07	4.81	8.92
P_11.5	3.31	8.25	3.50	9.49	3.31	8.25	3.50	9.49
P_12.8	3.24	7.69	4.00	7.63	3.24	7.69	4.00	7.63
P_16	2.66	6.58	2.66	6.58	2.66	6.58	2.66	6.58
P_20	1.72	4.00	1.72	4.00	1.72	4.00	1.72	4.00
P_25	1.50	3.25	1.40	3.61	1.50	3.25	1.40	3.61
P_60	0.93	2.98	1.34	2.98	0.54	2.17	0.42	2.13
P_100	0.42	1.47	0.42	1.84	0.20	1.08	0.27	1.84
C_50	1.03	4.23	1.93	4.23	1.03	2.78	0.59	4.36
C_60	1.09	3.88	1.23	3.88	1.23	3.17	0.77	3.05
C_70	0.74	4.03	0.75	4.03	0.74	2.49	0.43	3.15
C_90	0.54	1.93	0.54	1.93	0.29	1.94	0.29	1.94
C_100	0.46	2.03	0.46	2.03	0.23	1.59	0.20	1.75
C_105	0.40	2.22	0.40	2.22	0.20	1.34	0.20	3.09
C_120	0.31	1.86	0.31	1.86	0.29	3.47	0.24	3.47
C_135	0.27	1.34	0.27	1.34	0.20	2.66	0.17	2.66
C_160	0.22	1.16	0.22	1.16	0.20	1.16	0.13	1.62
C_180	0.27	1.90	0.27	1.90	0.17	2.91	0.18	2.91
C_200	0.22	0.59	0.22	0.81	0.16	4.46	0.13	5.78

Therefore the following caveat remains in place:

Caveat 3: In case the FCS calibration of an observation is performed in a non-standard aperture of this filter (cf. Table 1) strong deviations (factor $\simeq 2$) of the correct responsivity and thus the derived fluxes can occur. The deviations are strongest for the usage of the largest apertures in combination with P1 filters.

2.4 Non-geometric Aperture Beam Size Scaling

By evaluation of multi-aperture measurements on flat backgrounds it has been found that in some filters strong non-linear behaviour w.r.t. the geometrical aperture area occurs (in particular for the largest apertures, $\geq$ 120", of the 11.5 micron filter). This means, that, if observations are performed in apertures deviating strongly from the ones used in calibration (cf. Table 8), deviations from the correct flux can occur. This is especially of importance for multi-aperture measurements, because often background measurements are performed in different (larger) apertures than the related source observations and are scaled to the corresponding on-source aperture size.
Evaluation of the relevant calibration measurements to correct for this effect is underway. The extended source calibration and the correction for non-geometric beam size effects will be one key issue of OLP 8.0. Currently, the s/w uses the geometrical beam sizes only. Therefore the following caveat applies:

Table 8: ISOPHOT Standard Calibration Apertures

Filter	**Standard Aperture**
P_3.29	23"
P_3.6	23"
P_4.85	23"
P_7.3	23"
P_7.7	23"
P_10	52"
P_11.3	52"
P_11.5	52"
P_12.8	52"
P_16	52"
P_20	79"
P_25	79"
P_60	180"
P_100	180"

Caveat 4: If observations are performed in apertures, which are different in diameter from the ones used in standard calibration, deviations from the correct flux calibration can occur. This implies especially for extended source or background observations using the largest apertures with P1 and P2.

2.5 Signal Dependence on Reset Interval

For OLP 7.0 a correction for the dependence of the signal on the reset interval has been introduced (SCREW-322). For OLP 6.0 the following caveat was formulated:

1 *OLP 6.0 Caveat:* If the reset interval for either the source or the FCS measurement deviates strongly from the optimum (0.2-1.0 V dynamic range) an impact on the calibrated result can be expected.

which is no longer applicable for OLP version 7.0.

2.6 Non-linearity of Detector Responsivity with Flux

There are meanwhile strong indications from the huge data base of standard star measurements that ISOPHOT detectors do not behave linear in their response with incident flux. By design of the AOTs the PHT uplink logic matches the FCS flux to the expected source flux and consequently the non-linearity should be minimal in many cases. However, in multi-filter AOTs it is possible, that the flux in one filter deviates quite strongly from the flux in the filter in which the FCS calibration is performed (especially for P1). In these cases the filter that deviates most from the inband power used for the FCS calibration (usually the first measurements of an AOT sequence) can show calibration problems due to this effect. Similar problems can occur for maps and for multi-aperture observations, which show a wide dynamic range in flux.
This effect is not corrected for in OLP verson 7.0, therefore, the following caveat remains:

Caveat 5: Measurements with inband powers far away ($\geq$ factor 10) from the ones used for the related FCS measurement(s) have poorer calibration accuracy.

2.7 Detector Signal Transients

PHT OLP does not use physical (Fouks) or empirical (exponential, signal jump) signal transient correction functions, as they are available in the PIA, because those require still

a highly interactive mode. Currently OLP detects detector transients by statistical trend analysis methods and discards parts of a measurement found to be affected by drifts. This method works reasonably well, if a given measurement reaches stability, i.e. for bright sources and for very long observations. The condition that stability is achieved is that the variation of the signals during the considered time interval is less than 5%. Then the signals within the stability period are used to derive the final signal per chopper plateau. In case this criterium is not met, OLP uses the weighted mean of the last 8 signals.

Caveat 6: The transient correction only works satisfactory for measurements longer than the detector transient time constant at a given illumination. The transients are very often the limiting factor for the achieved accuracy. Measurements flagged by the OLP software as *"plateau data affected by residual drift"* can show strong deviations (residual drift is greater than 5%) from the correct result.

Note: The quality of an observation, w.r.t. drift and other criteria is coded into the SPD field **PxxSFLAG** where xx identifies the detectors as follows: C1, C2, P1, P2, P3, SS and SL. The flags are given for each chopper plateau individually and are defined in the OLP include file SPP_PIX_FLAGS_PAR.INC. The following table gives an overview:

Table 9: Quality flags for PHT SPD Data

Flag	**Description**
0	normal
1	calibration measurement saturated
2	part of plateau data affected by drifts
3	all ramps on plateau rejected
4	plateau data affected by residual drift
5	zero standard deviation
7	zero signal for plateau

2.8 Long Term Detector Drifts

For single pointing measurements with one FCS measurement per detector no attempt is made by PHT OLP 7.0 software to correct for long term detector responsivity drifts, i.e. stability of the detector responsivity during the execution time of an AOT is assumed. For raster pointing observations and sparse maps OLP does a linear interpolation with time of the responsivity values derived from the two bracketing FCS measurements. Detailed investigation of PHT-C maps has shown that the detector long term drift is not linear, but very often shows an exponential behaviour due to switch-on effects. Therefore, models of the detector behaviour or baseline fits would be required for optimum results.

Caveat 7: PHT OLP does not correct (in case of single pointings) or correct only with a linear interpolation (in case of maps) for long term detector drifts within an AOT.

2.9 Dark Current Variations along the Revolution

For OLP Version 6.0 a caveat was formulated concerning the variability of the detector dark current along the revolution:

1 *OLP 6.0 Caveat:* The AAR data obtained for observations with signals close to the dark signals can show high deviations from the expected results due to variations of the dark current along the revolution and scatter from revolution to revolution.

Evaluation of the routine calibration dark current measurement data base has established a CAL-G file providing the dark current dependence on the orbital phase (cf. SCREW-336). The caveat does no longer apply.

2.10 Error Calculation and Propagation

The automatic derivation of measurement uncertainties is extremely difficult for a complex instrument like ISOPHOT due to the mixture of systematic and statistical errors. The PHT OLP performs only a statistical error propagation, based on the assumption of Gaussian noise. It makes no attempt to estimate the systematic uncertainties of the various calibration steps in separate terms.
In fact, for a clean separation of different types of uncertainties, all systematic error terms introduced in previous pipeline versions have been taken out and uncertainties provided by OLP 7.0 are pure statistical errors from signal evaluation (SCREW 336). In order to assess all other uncertainties it is necessary to refer to the related documentation on PHT calibration in combination with the OLP products. (cf. ISO Data User Manual (IDUM) [2] and document "flow of corrections made during processing" [3]).

Caveat 8: The PHT OLP software does only provide an uncertainty from the statistical signal evaluation. It does not give any estimates of the systematic uncertainties of all performed calibration steps. Therefore, OLP 7.0 uncertainties are **minimal** errors. It is essential to refer to special documentation which provide an overview of the uncertainties introduced step by step. These depend on the exact observing conditions and evaluation steps which may even not be completed inside OLP (e.g. background subtraction in maps or from independent staring measurements).

2.11 Actual versus Intended Pointing

With the introduction of SCREW 324 "Use of improved pointing information for PHT maps" PHT OLP uses the best available actual pointing information (accuracy $\simeq$ 1-2") as provided in the IRPH file, when constructing maps. For measurements on revolutions before rev. 452 the actual pointing is more accurate than the intended pointing, as there were systematic pointing inaccuracies which could be assessed a posteriori. After rev. 452 intended and actual pointing should be virtually indistinguishable. Therefore, the following cavet does no longer apply for PHT OLP version 7.0:

1 *OLP 6.0 Caveat:* The PHT OLP uses intended rather than actual spacecraft pointing information.

2.12 Missing Measurements and Chopper Correction

The current version of OLP does not perform a consistency check whether the number of measurements which were actually performed does match the number of measurements expected from the EOHA beyond an initial check during DERIVE_SPD. In case there are measurements missing in an AOT it is possible that there is a mismacth between the keywords written into the SPD header concerning the chopper correction parameters, w.r.t. the measurement number and the filter number that was actually used in a measurement.

Caveat 9: In case there are measurements missing from an AOT there may be a mismatch between the chopper correction keywords and the related filter number.

2.13 Limitations in Use of PHT Color Correction Factors

With the OLP V7.0 and CAL-G V4.0 for the first time CAL-G files with color correction factors for several different SEDs are provided. These color correction factors are not applied by PHT OLP, but can be applied inside PIA. They have been calculated from the bandpass transmission files currently available, which have typically about 300 data points equally spaced in wavelength. Two different interpolation and integration methods have been

used to derive the color correction factors and they give equal results except for the cases where steep Wien branches are convolved with the bandpass transmission numbers. Furthermore, the bandpass transmission files used are centred on the main throughput range. All wavelengths for which the transmission was below 10^{-4} have been excluded. Taking into account the latest available data sets of all transmission components (filter transmission, field less transmission, blocking material transmission, spectral detector responses) the bandpass transmission of some filters (in particular P1 filters) need some update and refinement, because they show minor credible transmission peaks outside the main range. In case of extreme source SEDs these "leaks" can make a significant contribution to the resulting inband power and hence alter the corresponding color correction factor considerably.
Therefore, the following caveats have to be put onto the CAL-G V4.0 color correction factors:

Caveat 10: For the establishment of the color correction factors provided by CAL-G Version 4.0 not yet final PHT filter bandpass data including a wide wavelength range outside the nominal bandpass have been used. For some filters and in the case of extremely rising or falling SEDs this can mean an underestimate by out-of-band contributions. Color correction factors above 2 should be considered as less accurate and factors above 4 only as an indication of the order of the correction, as they clearly depend on the integration and interpolation method used. This applies in particular for SEDs of cold sources in combination with the P1 filters which fall onto the steep Wien branch of these SEDs. In these cases it is recommended to contact the ISO Data Centres for the most recent bandpass transmission and establish the color correction factor yourself.

2.14 Empirical PPSF Correction Factors for Array Centered C200 Photometry

During OLP V6 Scientific Validation it had been realised that the theoretically calculated point spread function correction factors (PPSF) for photometry with the source centered on the C200 array were not the correct ones. Hence, empirical correction factors were established by comparing the relative intensities in the pixels for targets which had been measured both in array centered and pixel raster mode. These empirical correction factors compare with the theoretical ones as shown in Table 10:

Table 10: PPSF Factors for Array Centered C200 Photometry

C200 Filter	theoretical PPSF	empirical PPSF
C_120	0.900	0.574
C_135	0.864	0.668
C_160	0.810	0.708
C_180	0.782	0.972
C_200	0.736	1.054

A plausible explanation for the reverse behaviour (increasing PPSF with wavelength instead of decreasing PPSF) is diffraction at the edges of the field lenses which are mounted with an inter-pixel gap of about 100 μm, so that the effect is expected to be strongest for the short wavelength C200 filters.
Detailed investigation of several test cases during OLP V7 Scientific Validation clearly points out that the photometry in the C_180 and C_200 filters always gives too low fluxes. Comparison with reference photometry suggests that the PPSF factors for the two filters must be some 20 to 30% smaller, hence close to the theoretical value. This issue will be followed up in a detailed calibration program to establish refined PPSF correction factors for array centered C200 photometry.
Therefore, the following caveat has to be put onto the CAL-G V4.0 empirical PPSF correction factors for array centered C200 photometry:

Caveat 11: The correction factors for the filters C_180 and C_200 appear to be too large by 20 to 30%. Photometric fluxes derived for both filters in array centered mode should be corrected towards larger values by this percentage (as the uncorrected flux value is divided by the PPSF factor).

3 Prerequisites for OLP Scientific Validation

The scientific validation of the PHT pipeline follows the guidelines as out-lined in the e-mail by Martin Kessler, "Scope of OLP Scientific Validation - IDT AI #8/16" from 18-JUL-1995. The major goals of the scientific validation process according to this note are to:

- confirm that the applied processing has had the expected effect(s) on the data;
- establish that sufficient processing has been applied to the data so that the products are usable by the observer;
- demonstrate that the processing is reliable, stable and repeatable;
- establish the level of accuracy of the calibration;
- document any known caveats or concerns with the processing and/or calibration;
- demonstrate that, with the aid of the relevant ISO Data Users Manual (IDUM), Observers can further process products to a publish-able form.

The scientific validation process is restricted to PHT Standard Processed Data (SPD) and Auto-Analysis Products. Edited Raw Data (ERD) were declared scientifically valid for data products generated with OLP version 4.0 or higher, during the "OLP V4.0 AND BEYOND REVIEW MEETING" on the 24th of April 1996. Therefore, all tests outlined here assume the correctness of all ERD data.
All test data sets were reprocessed with the PIDT stand-alone pipeline version 7.0beta. Reprocessing with a delta version of 7.0beta was performed as necessary in order to validate OLP modules which have been improved during the validation process. This approach requires to check that the validity of the results is preserved in the integration process of the PHT part of the pipeline into the OLP system.

4 Results from OLP 7 Scientific Validation Period 1

During the Scientific Validation Period 1 it was not yet possible to perform a comprehensive scientific check-out, as the software was not stable. Nevertheless several software bugs could be pointed out and suggestions for further improvement of the software be made, as outlined in the reports below. The following table gives an overview of the changes, both in software in calibration files, after validation period 1, documented in the following SCREWs and SPRs (excluded are SPRs related to the port to Alpha, see Section 5.9 for an overview):

Table 11: Change Record for OLP 7 and CAL-G 4 at the end of scientific validation period 1

Title	**SPR**	**SCREW**
PHT DERIVE SPD problems with the use of default responsivity in staring mode AOTs		351
Subtracted source flux for chopped PHT AA products		353
Change in error handling for PHT OLP		356
FITS header keywords for electrical power range in CAL-G files P%%FCSPOW	2510	
PHT AA: Change length of IRPH record	2527	
OLP 7.0 beta: Warning message MCRVER called too often	2543	
OLP 7.0 beta test processing for PHT stuck in endless loop	2545	
Correct dark current subtraction for absolute photometry	2553	
OLP 7.0 beta PHT Derive SPD: Wrong interpolation for dark current	2555	
OLP 7.0 beta PHT Derive SPD: Wrong interpolation for default response	2557	
Modify calculation of no. of image pixels in PHT map	2558	
Old version of PC1D.DES accidently finds its way into OLP v7.0b1	2560	
OLP 7.0 PXXOMEGA contain wrong solid angles	2589	
No chopped mode correction for PHT-S	2597	
Low background values in PHT AAR	2598	
OLP 7.0 Update of P##RESP_##.FITS CAL-G files	2600	
Update of solid angles in PHT OLP	2608	
Use corrected position to define centre of PHT images	2610	
Zeros in PHT-S OLP products	2627	
PHT AA: return of PBOR messages	2628	

4.1 Empirical Chopper Frequency Correction (Black Box Test)

- author: Helen Walker, RAL
- date: 8 March 1998

4.1.1 Data Analysis

- P detector subsystem data checked
- Means used throughout
- Data have been processed in PIA interactively, not in batch mode

4.1.2 Narrative

The data have been reduced from ERD using PIA7.0.p. From ERD to SPD, the data have the following corrections applied:

- non-linearity,
- deglitching,
- 1st order polynomial fits to ramps (no subdivision used),
- reset interval correction
- deglitching,
- dark current removal

The actual mean responsivity from FCS1 is used, and the orbit dependent default responsivity. A trial where dark current was not removed (for a chopped observation) made no (or very little) difference to the values determined. OLP did not remove the dark current when the observation was chopped, and did use the default responsivity (as required). Staring mode observations did have the dark current subtracted and used actual responsivities (unless out of limits). During my visit (23/2/98 - 8/3/98) the OLP data were reprocessed twice. (I think I have used the latest products here, available from 5/3/98). Consequently two datasets have been thoroughly investigated, those for HD166620 and those for HR7001.

4.1.3 Problems Identified

- Orbit dependent correction of FCS default in OLP incorrect ⇒ SPR 2557
- Orbit dependent correction of Dark Current in OLP incorrect ⇒ SPR 2555
- Reading of multi P detector data AAR in PIA (PP not recognised)
- Limits on FCS range set so that only default used in OLP ⇒ SCREW 351
- FITS header for SPD and AAP overwritten in PIA
- Flag showing default responsivity used not reset when a second detector used in P03

4.1.4 Concerns

- Concern as to whether reset interval correction errors are correct, or correctly displayed in PIA (the graph shows them as very large). ⇒ SCREW 356
- 20 μm fluxes seem low (AAP output in log-log domain shows 20 μm point below straight line of other points for HD166620).
- Warning about FCS out of limits in PIA fades before it can be read and the decision about selecting responsivity made.
- Errors grow very quickly. Default responsivities meant that 30% errors were being combined (with square and add technique) to give very large numbers for chopped observations. ⇒ SCREW 356

4.1.5 Evaluation Log

```
1. HD166620

1.1 08500342 HD166620 P03 rectangular chopping using P1,P2,P3

I think the processing is satisfactory for P1, but I am not convinced that
all is well for the P2 and P3 detectors. The observer does not appear to
have entered good estimates of the fluxes expected.

Responsivities used
    Actual  Default
P1   0.887   1.17
P2   0.555   0.67
P3  15.279  21.594

SPD data
P1.2 background data contains a large glitch.
              OLP                PIA (Default resp)      PIA (Actual resp)
       -75"         +75"          -75"       +75"         -75"      +75"
P1.1 2.39734e-15 6.77410e-15   1.5837e-15 5.9600e-15   2.0893e-15 7.8628e-15
P1.2 1.56489e-15 1.74385e-14   0.8259e-15 1.6656e-14   1.0895e-15 2.1974e-14
P1.3 1.31163e-15 2.68061e-14   0.5204e-15 2.6043e-14   0.6866e-15 3.4358e-14
P2   2.16691e-15 2.81591e-15   2.6968e-15 3.3218e-15   3.2550e-15 4.0094e-15
P3   1.50317e-15 1.58852e-15   1.5874e-15 1.6628e-15   2.2435e-15 2.3502e-15

Subtracted SPD data
Chopper correction applied to default responsivity processed data
       OLP         PIA(chopper) PIA(default) PIA(actual)
P1.1 4.3768e-15    4.3763e-15   4.3763e-15   5.7735e-15
P1.2 1.5873e-14    1.5830e-14   1.5830e-14   2.0885e-14
P1.3 2.5495e-14    2.5523e-14   2.5991e-14   3.4289e-14
P2   6.4900e-16    6.2495e-16   6.2496e-16   7.5432e-16
P3   8.5348e-17    9.8857e-17   7.547e-17   10.6668e-17

AAR/AAP data
Last Off plateau has high value compared to the others for P3.
   Plateau Off +/-  OLP  On   +/-      PIA(def) On    PIA(act) On
P1.1  4 0.6549 0.0305  1.8503 0.0788   0.4328 1.6289  0.5710 2.1489
P1.2 16 0.1561 0.0063  1.8690 0.0462   0.0889 1.7932  0.1173 2.3657
P1.3 16 0.1632 0.0075  3.8002 0.0942   0.0737 3.6895  0.0973 4.8674
P2    4 0.5958 0.0170  0.7964 0.0225   0.7479 0.9212  0.9027 1.1119
P3    8 2.8638 0.5788  3.0205 0.5836   2.8914 3.0289  4.0865 4.2808

Subtracted AAR/AAP data
   Filter     OLP  +/-     PIA(chopper)   PIA(default)   PIA(actual)
P1.1 11.5  1.1955 0.0845  1.1961 0.0888   1.1961 0.0525  1.5779 0.0693
P1.2  7.3  1.7020 0.0477  1.7043 0.1025   1.7043 0.0103  2.2484 0.0136
P1.3  3.6  3.6322 0.0948  3.6158 0.2169   3.6158 0.0159  4.7702 0.0209
P2     20  0.2008 0.0282  0.1733 0.0132   0.1733 0.0122  0.2092 0.0147
P3     60  0.1801 0.8237  0.1801 0.2290   0.1375 0.1687  0.1943 0.2384

Expected source flux (from AAR header)

11.5um 3.5Jy
7.3um  1.14Jy
3.6um  0.43Jy
20um   0.4Jy
60um   5.5Jy

1.2a 09101385 HD166620 P03 triangular chopping using P2
1.2b 36901485 HD166620 P03 triangular chopping using P2 (repeat)

I am not convinced that all is well with this data processing.
Data and FCS were drifting badly.
```

```
Responsivities used
                Actual    Default (from OLP)
09101385 P2     1.182     1.798879
36901485 P2     1.245     1.780565

SPD data
1st point (-90") always low, positions 2 - 3 used for chopped calculations.
          Off    OLP   On        Off  PIA (default) On   Off PIA (actual) On
091-90 10.5334e-15 12.2850e-15  9.50093e-15 11.3241e-15  5.38401e-15 6.37718e-15
   +90 11.6748e-15              10.6473e-15              6.03364e-15
369-90 7.29941e-15 8.66660e-15  6.44221e-15 7.97006e-15  3.46674e-15 4.28892e-15
   +90 8.12416e-15              7.18151e-15              3.86458e-15

Subtracted SPD data
      OLP         PIA(chopper) PIA(default)  PIA(actual)
091 5.00276e-16   4.9663e-16   12.500e-16    6.6836e-16
369 4.65277e-16   5.5340e-16   11.582e-16    6.2326e-16

AAR/AAP data
       Off    +/-   OLP  On    +/-      Off PIA(def) On  Off PIA(act) On
091 8 2.53703 0.12357  2.84625 0.10845  2.33871 2.61268  1.32539 1.48056
369 8 1.78163 0.06760  2.05978 0.07501  1.58147 1.86348  0.85104 0.99574

Subtracted AAR/AAP data
          OLP  +/-    PIA(chopper)   PIA(default)    PIA(actual)
091 25 0.3064 0.1644  0.1153 0.0220  0.1153 0.0217   0.0653 0.0123
369 25 0.2480 0.1019  0.1285 0.0407  0.1285 0.0405   0.0691 0.0218

Expected source flux (from AAR header) 0.2Jy

2. HR7001

2.1 10601103 HR7001 P04 staring using P2 detector
I am satisfied with the comparison of OLP and PIA.
Using default responsivities in PIA gave results which agreed well with
early OLP runs when default used there.

Responsivities used
Actual 0.628  Default 0.67

SPD data
          OLP          +/-         PIA(default)   PIA(actual)   +/-
1103.1   3.96888e-14 1.56238e-15   3.72679e-14    3.97789e-14 3.97668e-16
1103.2   5.19052e-14 7.44651e-16   4.85965e-14    5.18708e-14 1.55041e-16
1103.3   6.12298e-14 7.56196e-16   5.74931e-14    6.13667e-14 1.62327e-16
1103.4   7.23344e-14 9.47823e-16   6.78650e-14    7.24375e-14 2.34502e-16
1103.5   8.55099e-14 1.03501e-15   8.03153e-14    8.67647e-14 2.20982e-16
1103.6  13.9485e-14  1.66880e-15  13.1022e-14    13.9850e-14  3.63826e-16

AAR/AAP data
        OLP     +/-    PIA(default)  PIA(actual) +/-
1103.1 12.0143 0.4730   11.2814       12.0415 0.1204
1103.2 12.0505 0.1729   11.2824       12.0426 0.0360
1103.3 13.7884 0.1703   12.9469       13.8192 0.0366
1103.4 15.9838 0.2094   14.9962       16.0066 0.0518
1103.5 18.7081 0.2264   17.5716       18.9826 0.0483
1103.6 30.0965 0.3601   28.2706       30.1753 0.0785

2.2 10601104 HR7001 P04 staring using P3 detector
I am satisfied with the comparison of OLP and PIA using default responsivities.
Default responsivity used in OLP, because FCS power (FCS1 had 1.17919) out of
calibrated range.
```

```
Responsivities used
Actual 23.6515 Default 1104.1 23.7222  (from PIA)
                       1104.2 23.7344
                       1104.3 23.7470
                       1104.4 23.7596
                       1104.5 23.7732

SPD data
            OLP       +/-       PIA(default)  +/-        PIA(actual)  +/-
1104.1 5.41538e-15 1.62549e-15  5.30450e-15 1.58685e-15  4.61005e-15 4.72478e-17
1104.2 7.54901e-15 2.28148e-15  7.54148e-15 2.25470e-15  6.55756e-15 6.25721e-17
1104.3 8.62859e-15 2.59783e-15  8.56519e-15 2.55919e-15  7.45166e-15 6.47366e-17
1104.4 9.15432e-15 2.75476e-15  9.12827e-15 2.72587e-15  7.94573e-15 6.55673e-15
1104.5 11.4398e-15 3.43357e-15  11.2541e-15 3.35882e-15  9.80177e-15 8.26566e-17

AAR/AAP data
         OLP     +/-    PIA(default) +/-  PIA(actual) +/-
1104.1  12.9101 3.8751   12.6457 3.7830   10.9902 0.1126
1104.2  14.4782 4.3756   14.4637 4.3243   12.5767 0.1200
1104.3  15.7011 4.7320   15.6015 4.6616   13.5732 0.1179
1104.4  16.5990 4.9950   16.5517 4.9427   14.4075 0.1189
1104.5  20.1608 6.0511   19.8335 5.9194   17.2740 0.1457

2.3 10601105 HR7001 P03 staring using P2, P3

Responsivities used
1105.1 P2 actual 0.682 default 0.67
1105.2 P3 actual 23.86 default 23.78 (from OLP)

SPD data
           OLP       +/-          PIA(default)  PIA(actual)
1105.1  8.73649e-14 4.67079e-16   8.88520e-14   8.74182e-14
1105.2  3.28319e-15 9.81165e-16   3.27238e-15   3.09744e-15

AAR/AAP
          OLP     +/-   PIA(default) +/-  PIA(actual) +/-
1105.1   18.8506 0.1008  19.1715 0.5729    18.8621 0.0363
1105.2    5.7861 1.7291   5.7670 1.7149     5.4587 0.0485

2.4 HR7001 - Background subtracted multi-aperture photometry
Not really part of test since OLP does not combine AOTs.

HR7001 fluxes  25um 11.8Jy  60um 10.1Jy
AAP subtracted fluxes from PIA
        Default    Actual            Default  Actual
1103.1  -15.62Jy   -14.42
1103.2   -9.35      -8.25   1104.1    4.84Jy   3.61
1103.3   -7.06      -5.87   1104.2    8.19     6.64
1103.4   -4.64      -3.31   1104.3    9.64     7.93
1103.5   -1.87      -0.14   1104.4   10.62     8.79
1103.6    9.10      11.31   1104.5   14.07    11.82
```

4.2 REPORT on Scientific Validation of PIA/OLP 7.0, AOT P22, P32, P37

- authors: Martin Haas and Viktor Toth, MPIA Heidelberg
- date: 12-Mar-1998

4.2.1 Summary

C100 and C200 measurements in all filters were examined using OLP V7.0b1 and the automatic processing sequence in PIA V7.0, with the CALG V4.0 set. The AOTs investigated were P22 (staring, raster scans and chopped), P37/39 (sparse maps) and - only qualitatively - P32 (chopped maps).
The staring modes were revalidated with the newly implemented reset interval correction and the chopped modes are validated with the additional vignetting and chopper frequency signal correction and the orbit position dependent responsivity.
A couple of errors and inconsistencies were found and their origins have been located. In case these errors are fixed, the OLP and PIA results agree well and for the flux range above 0.5 Jy and larger than 10% of the background the automatic data reductions can obtain the source fluxes at an accuracy of better than 50% within the predictions. For fainter sources additional interactive analysis has to be applied for scientific applications.

4.2.2 Data Sets

TABLE 1. Observations

No.	Object	TDT Number	AOT	Observing mode	Detector
1	HR7001	10601101	P22	chopped multifilter	C1+C2
2	IRAS0306-5346	81101906	P22	chopped multifilter	C1
3	IRAS0306-5346	81102008	P22	chopped multifilter	C2
4	IRAS0306-5346	81101907	P22	multifilter raster=3x2	C1
5	IRAS0306-5346	81102009	P22	multifilter raster=3x2	C2
6	Alpha Bootes	45200203	P22	multifilter pointing off	C1+C2
7	Alpha Bootes	45200204	P22	multifilter pointing on	C1+C2
8	Arp244	06903805	P37	multifilter pointing off	C1
9	Arp244	06903806	P39	multifilter pointing on	C1
10	Arp244	06903807	P37	multifilter pointing off	C2
11	Arp244	06903808	P39	multifilter pointing on	C2
12	M51	17200618	P32	multifilter raster=11x15 with chopper	C1

4.2.3 Data Reduction

The data were reduced from the ERD level to AAP/AAR level using OLP V7.0b1 and the automatic processing sequence in PIA V7.0, and the CAL-G set V4.0.
As far as available, both the default and the actual responsivities were used and the resulting SPD levels were analysed.
The resulting fluxes (AAP/AAR level) were PSF and color corrected. The fluxes obtained with OLP and PIA were compared against each other and with predicted values from models/IRAS or V6.0/V3.0 results.

4.2.4 Notes on the Bugs Found and Additional Improvements Recommended

1) OLP: the brightness on the background is by a factor "npix" too high, npix = 9 for C100 and npix = 4 for C200. This leads to a wrong background subtraction, hence wrong source flux determination. This bug can be easily fixed.

2) OLP and PIA: the error bars are generally very high, so that even a bright source does not appear as 3 sigma detection. E.g the systematic errors from the reset time correction should not be included into the formal errors. In addition, for OLP there might be a multiplication instead of division in the error propagation. This is more serious for the 9 pixel C100 than for the 4 pixel C200 array. This bug can be easily fixed. ⇒ SCREW 356

3) OLP and PIA: though P22 staring and P37/39 measurements should use the actual responsivities, they switch to the default responsivity, if the FCS data are outside the well calibrated range. This may lead in a multi-filter series with several FCS measurements for different detectors and/or on-off source pointings to the mixed usage of responsivities, hence to spurious jumps in the resulting SEDs of 100%. ⇒ SCREW 351

4) OLP: for P22 chopped measurements the AAR header should provide the flux for pure source and not for the sum source+backgound. This is important, because the user can only perform the average background subtraction, but not the differential background subtraction (= background subtraction for each individual chopper plateau) which is the main advantage of the chopped mode, in particular in the case of long term drifts. ⇒ SCREW 353

5) OLP: for P22 raster maps (scans) the AAR file may contain more records than raster points. (If the the space craft axis is not parallel to north-south or east-west, the raster map is embedded in a larger north-south oriented map.) However with respect to the space craft axis, this makes the identification of the raster points and their fluxes extremely difficult, particularly for the common case of mini maps. A more canonical relation between the records and the measured raster points would be desired. ⇒ SPR 2633 (no real s/w problem, consequence of not matching file size information in the early test versions)

6) OLP: the P32 map was inspected only qualitatively/morphologically without check of photometry, and it appeared similar to the former published maps obtained with PIA.

7) CAL-G: the reset interval correction appears ok.

8) CAL-G: the vignetting correction appears ok, compare intensity distributions of the faint source HR166620 with and without vignetting correction in Figs. 1 and 2.

9) CAL-G: the chopper frequency signal correction appears ok (cf. Fig. 3).

10) CAL-G: the orbit position dependent responsivity appears quite ok. Nevertheless, the responsivity seems to be a non-linear function of the signal (illumination strength): FCS measurements within a few minutes at faint background and bright source levels yield a responsivity increase for faint and a decrease for high illuminaton. This would also naturally explain why in maps in which the whole dynamic range is calibrated using one single intermediate responsivity value the background appears too high compared with the bright sources (and this is not due to beam profile effects as thought before). Therefore a signal dependent responsivity calibration is recommended for OLP/PIA V8.0 and CALG V5.0.

11) CAL-G: the 90 μm fluxes are systematically too low.

12) OLP and PIA and CAL-G: the omega factors applied are different from the new theoretical numbers. This possibly explains some of the discrepancies between OLP and PIA results, in particular for C2. ⇒ SPR 2589

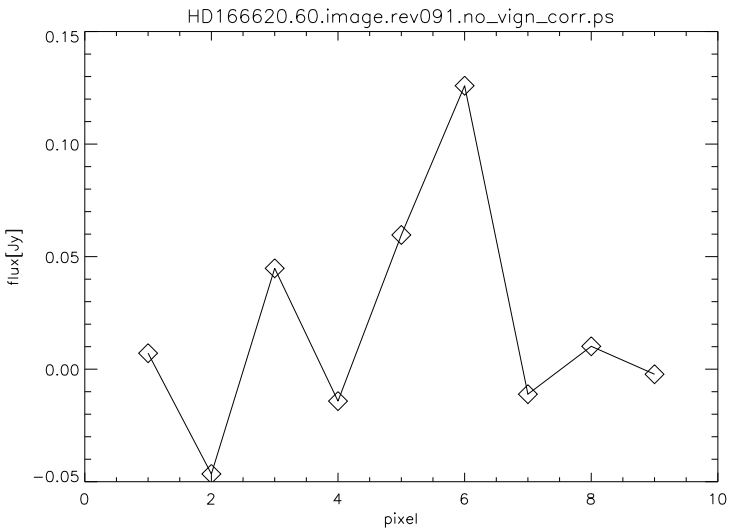

Figure 1: Intensity distribution over the 9 C100 pixels in a chopped image without any vignetting correction for the star HD 166620 at 60 μm.

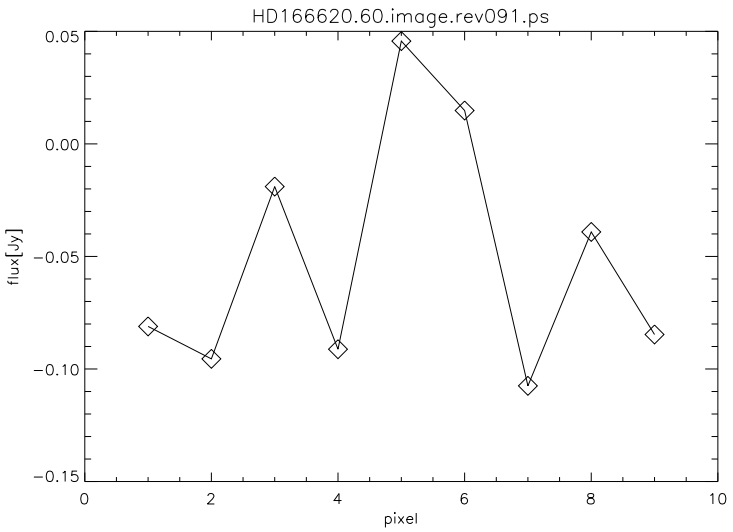

Figure 2: Resulting intensity distribution over the 9 C100 pixels in the chopped image of the star HD 166620 at 60 μm after vignetting correction.

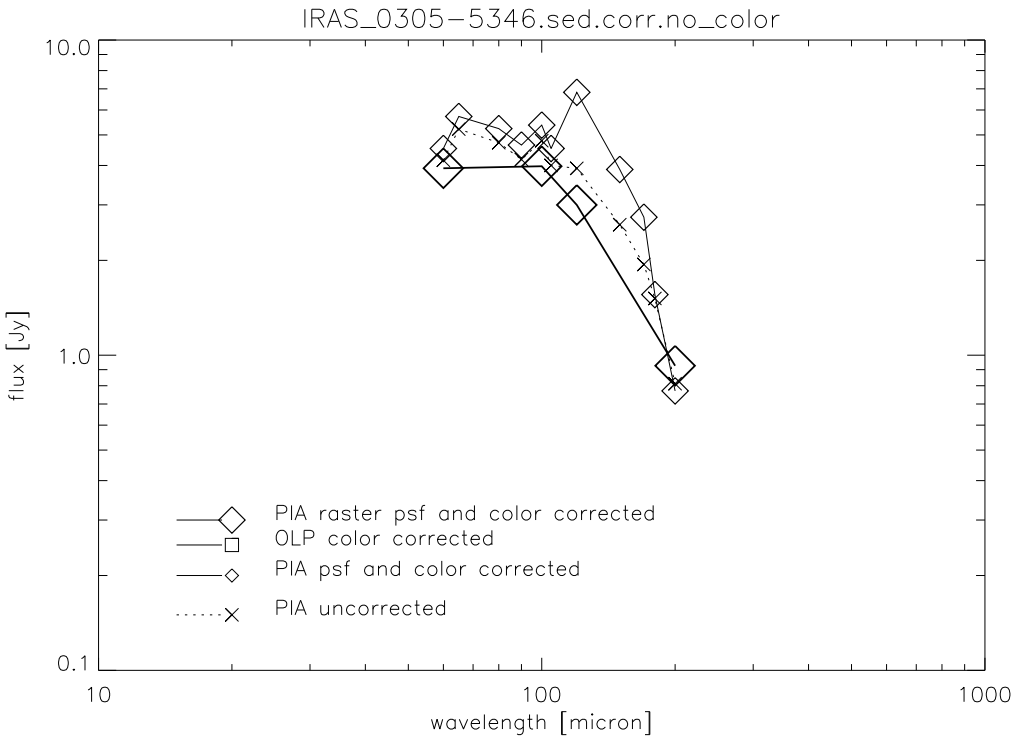

Figure 3: FIR SED of galaxy IRAS 0305-5346: comparison between nodding photometry (large symbols) and chopped photometry (small symbols). For mode detailed meaning of symbols, see legend inside figure frame.

4.2.5 Results

1) HR7001: Fig. 4
   OLP: values too high due to wrong background, will become similar to PIA after bug fixed. PIA: 120 μm (and also 150 μm) higher then expected, possible reasons:
   a) the time per chopper plateau is long 8s (4s) compared to 1s for all shorter wavelengths and the chopper frequency correction is not yet perfect (in connection with the default responsivity).
   b) the Vega disk is extended and the C2 array is larger than C1.

2) IRAS 0305-5346: Fig. 5
   OLP: SPD level similar to PIA, but AAP level different due to bug mentioned PIA: comparison between chopped and raster, again omega discrepancies/problems?

3) Alpha Bootes: Fig. 6
   again omega discrepancies/problems?

4) Arp244: See Fig. 7
   OLP: C200 values agree with those of PIA, C100 values differ more, possible reasons: detector has strong wiggles on SRD level. note: PV phase data

5) M51: qualitative/morphological check ok (elongation and companion present).

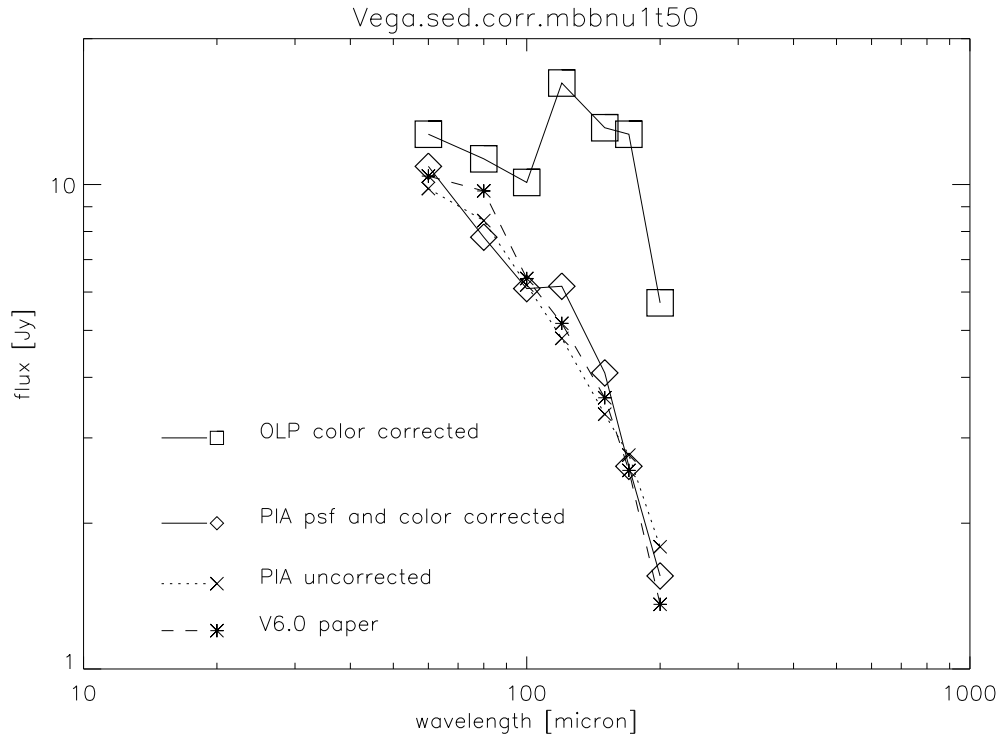

Figure 4: Derived FIR spectral energy distribution of Vega from chopped measurements. For the meaning of the various symbols associated with different evaluation modes, see legend inside figure frame. V6.0 paper is Ref.[15].

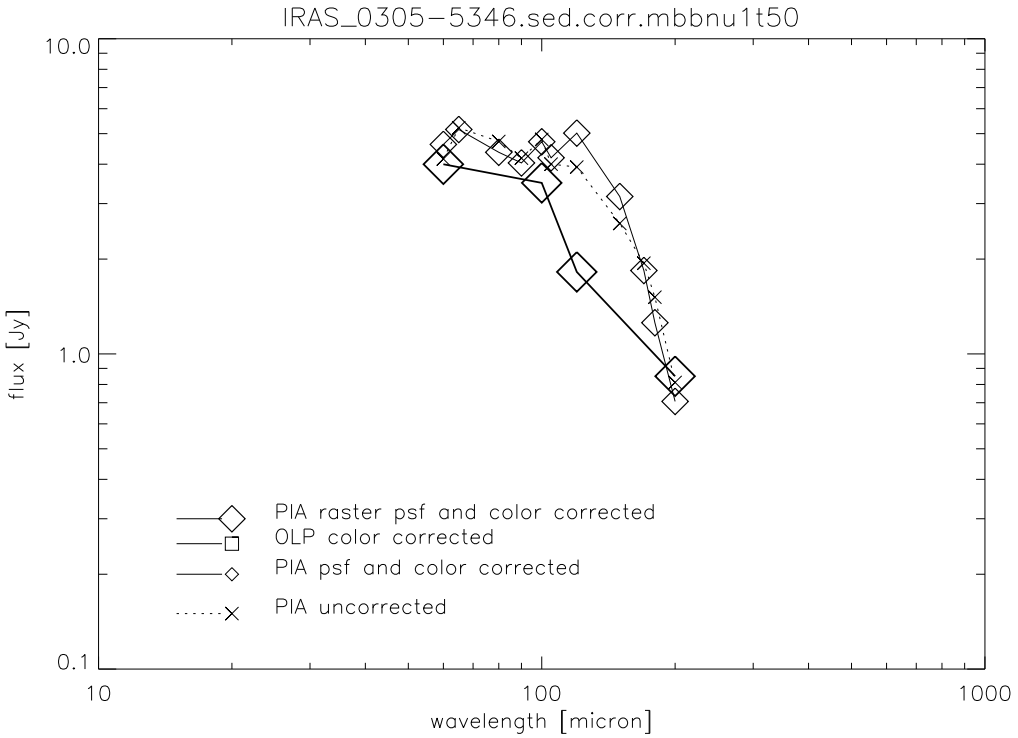

Figure 5: Derived FIR spectral energy distribution of galaxy IRAS 0305-5346 with color corrections for a modified BB of 50 K ($\varepsilon \propto \nu$) applied. Large symbols is the reference nodding photometry, smaller symbols the chopped photometry. For the meaning of the various symbols associated with different evaluation modes, see legend inside figure frame.

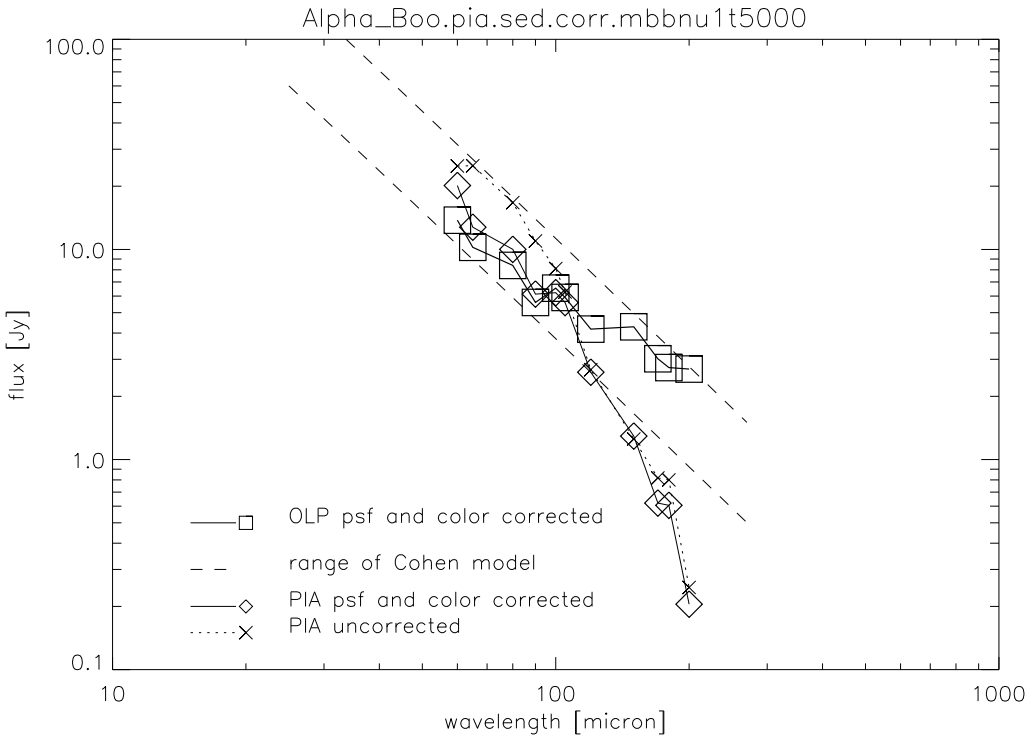

Figure 6: Derived FIR spectral energy distribution of the star α Bootes (HR 5340) with color corrections for a modified BB of 5000 K ($\varepsilon \propto \nu$) applied (staring mode validation case). For the meaning of the various symbols associated with different evaluation modes, see legend inside figure frame.

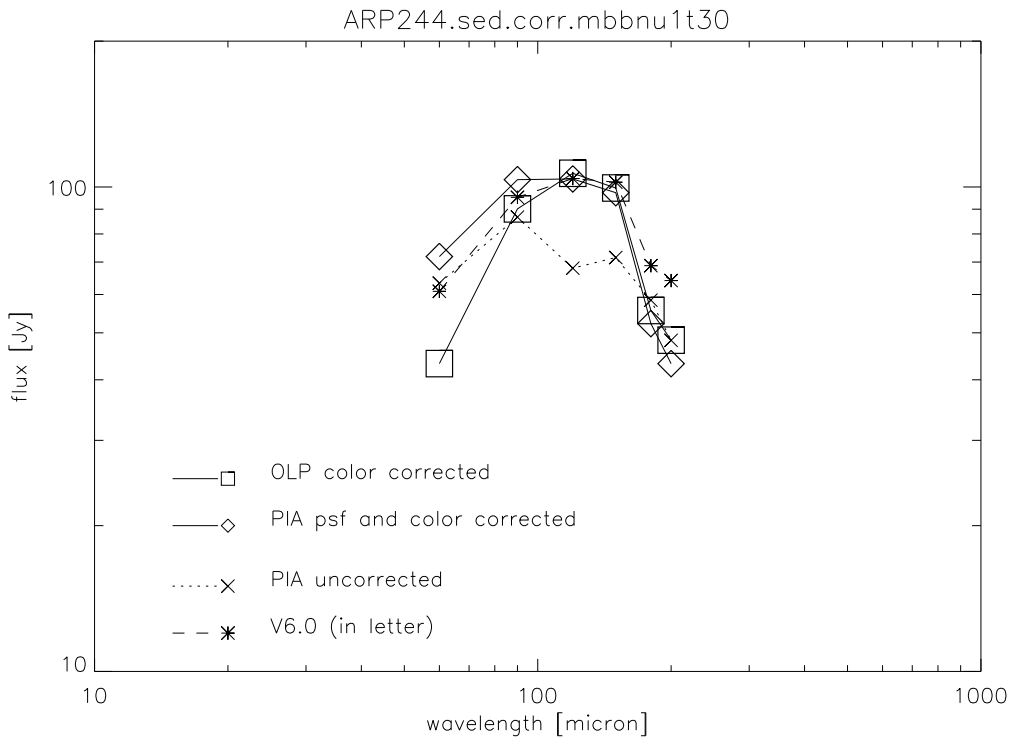

Figure 7: Derived FIR spectral energy distribution of Arp 244 with color corrections for a modified BB of 30 K ($\varepsilon \propto \nu$). For the meaning of the various symbols associated with different evaluation modes, see legend inside figure frame.

5 Revalidation Tests (Results from OLP 7 Scientific Validation Period 2)

In this section we present the results of the validation tests proving that there is no negative impact on already validated data products by the newly introduced calibration features, but rather an improvement. The subsections follow the sequence of re-validation steps as outlined in the "Plan for the PHT Scientific (Re-)Validation of OLP Version 7.0" [4].
The following table gives an overview of the changes, both in software and calibration files, after validation period 2, documented in the following SPRs:

Table 12: Change Record for OLP 7 and CAL-G 4 at the end of scientific validation period 2

Title	**SPR**
Reappearance of PBOR errors	2642
Refinement of PHT color correction cal-G files	2643
Missing FCS warning in PHT sparse maps	2644
Zero central wavelength in PHT PCAS product	2646

5.1 PHT-C Multi-filter Relative Calibration

- authors: M. Radovich, U. Klaas
- date: 07-May-1998

5.1.1 Motivation

We investigate the improvement of the final OLP data by the introduction of the relative filter-to-filter calibration including the flat-fielding of the C100 and C200 arrays, as provided by the new CAL-G files PC1FLAT and PC2FLAT. This correction is important in the case of multi-filter measurements for filters other than the one used for the FCS calibration.

5.1.2 References to Calibration Analysis and Software Change Documentation

- calibration report: Relative Filter-to-Filter Correction for C-Arrays [5]
- Software Change Request: SCREW 321

5.1.3 Method

Prerequisite is to check multi-filter measurements with C100 and C200. The effect of this calibration can be best verified using background measurements. The following checks are done:

- Compare OLP V6.x (as in the current archive) and OLP V7.0b2 test cases. As a consequence of the calibration the background SED should look smoother for OLP V7.0. It should be noted that on the surface brightness level a parallel improvement by the revised solid angle values cannot be disentangled.
- Check against COBE results for absolute sky background brightness (common with solid angle validation, cf. Sect. 5.11)
- Compare OLP V6.x and OLP V7.0b2 for the standard deviation of the individual pixel fluxes. The value of the standard deviation should have decreased.

5.1.4 Results

Fig. 8 shows a comparison of background SEDs of the following target positions:

TDT		Object	Description
35602203	*	HR6705	background (C100+C200)
39802002	*	HR6705	Background (C100)
45200203	*	Alpha Bootes	Background
47600207	*	NGC6543	Background (C100+C200)
47600511	*	NGC6240	Background

In part 1 of Sect. 5.1.6 we list the fluxes derived by OLP V6.x and OLP V7.0b2, as well as the reference fluxes from the COBE annual maps using the median over an area with 0.5deg (i.e the 8 nearest neighbours of the image pixel). We did not use the weekly maps, because there were several examples with very large errors or negative flux values at the longest wavelengths.
A graphical comparison between COBE and ISOPHOT OLP results, both for V6.x and V7.0b2 is shown in Figs. 9 and 10.
In part 2 of Sect. 5.1.6 we provide the standard deviations of the fluxes of the individual pixels. For C100 we have excluded pixel 6 from the average because it shows a somewhat anomalous behaviour due to its relatively high dark current.

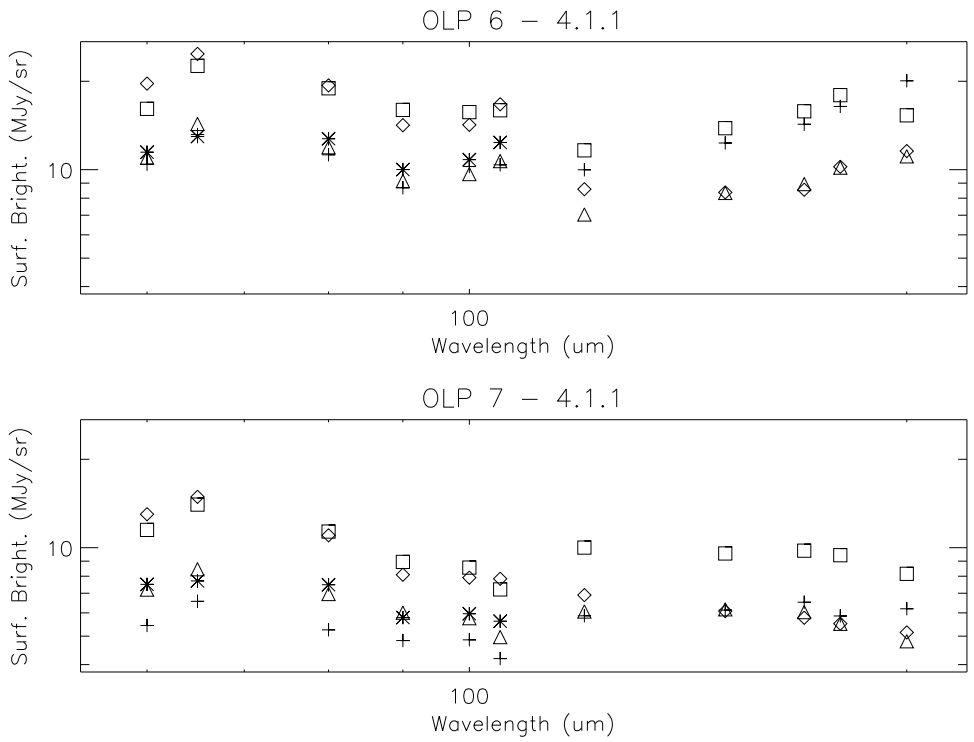

Figure 8: Comparison of OLP V6.x and OLP V7.0b2 results for the background measurements: TDT35602203 (plus), TDT39802002 (asterisk), TDT45200203 (diamond), TDT47600207 (triangle), TDT 47600511 (square).

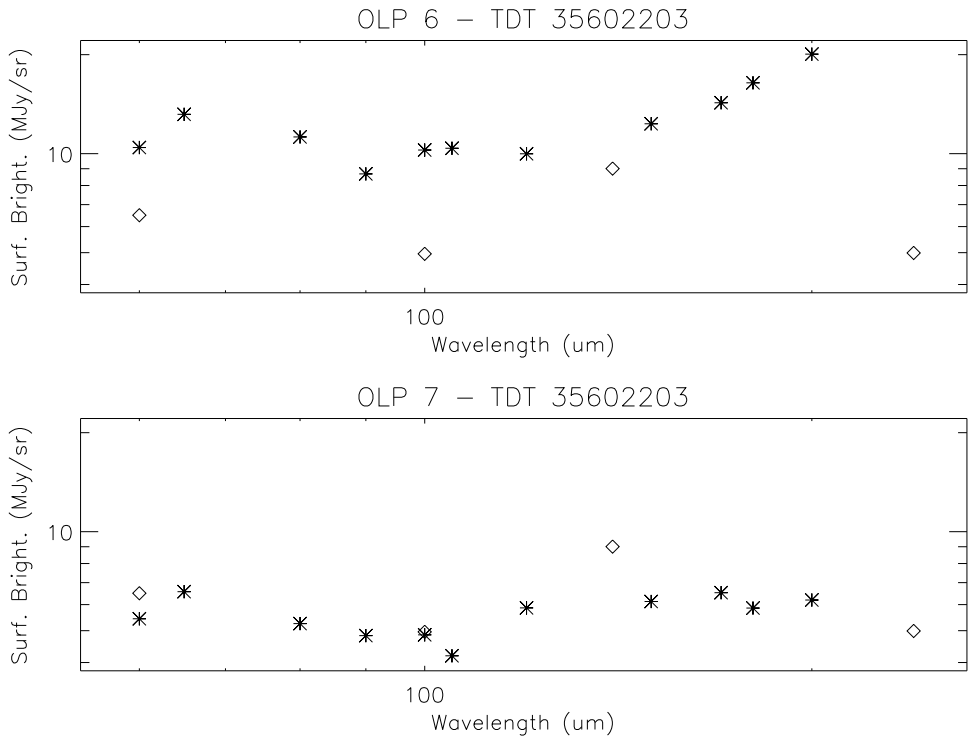

Figure 9: Comparison of OLP V6.x and OLP V7.0b2 surface brightness (asterisk) with COBE annual map fluxes (diamond).

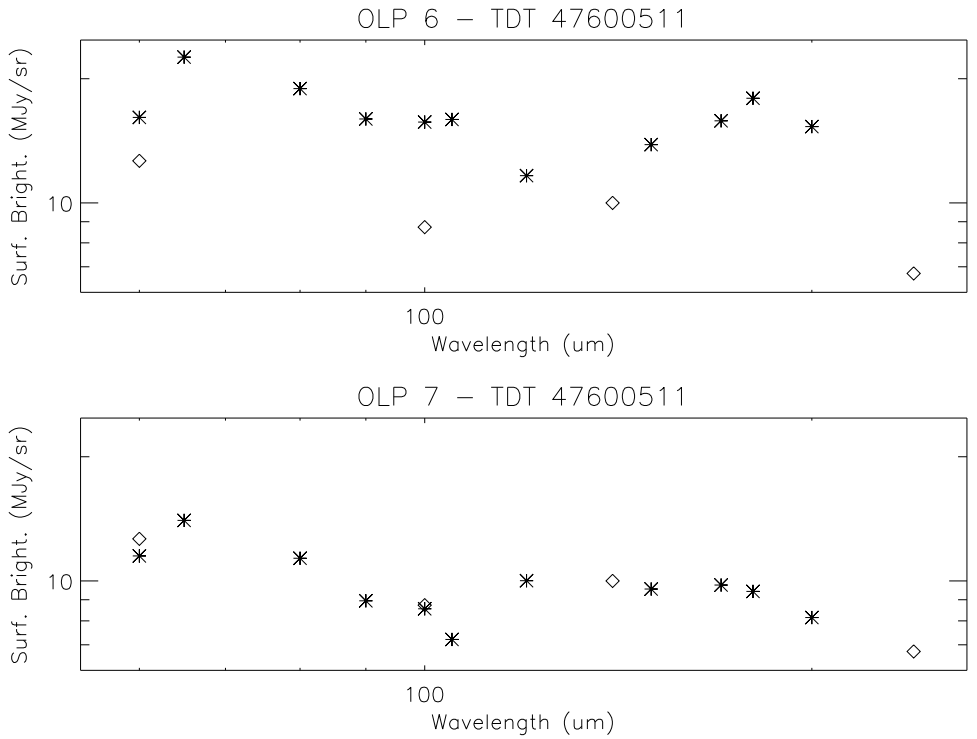

Figure 10: Comparison of OLP V6.x and OLP V7.0b2 surface brightness (asterisk) with COBE annual map fluxes (diamond).

5.1.5 Conclusions

- The background SEDs produced by OLP V7.0b2 look smoother and much more consistent than the ones produced by OLP V6.x.
- The background values are up to a factor of ~ 2 lower in OLP V7.0b2 and correspond to COBE in most cases to better than 20%. The stronger correction factor comes from the solid angle, nevertheless the filter-to-filter calibration is consistent to it.
- The strongest indication for an improvement of the relative filter-to-filter PHT-C calibration including the flat-field is given by the considerably smaller scatter of the fluxes among the individual pixels.

5.1.6 Evaluation Log

```
1) OLP V6 vs OLP V7 background fluxes and comparison with COBE annual map
   fluxes

TDT 35602203 - HR 6705
 Cwl    OLP 6.0      OLP 7.0        COBE
 [um] [MJy sr^-1]  [MJy sr^-1]  [MJy sr^-1]
-----------------------------------------------
   60    10.44         5.44         6.50
   65    13.17         6.57
   80    11.24         5.25
   90     8.68         4.83
  100    10.25         4.86         4.96
  105    10.39         4.19
  120     9.99         5.86
  150    12.33         6.13         9.00 (140um)
  170    14.28         6.52
  180    16.42         5.86
  200    20.07         6.20         4.99 (240um)
```

TDT 39802002 - HR 6705

Cwl [um]	OLP 6.0 [MJy sr^-1]	OLP 7.0 [MJy sr^-1]	COBE [MJy sr^-1]
60	11.47	7.50	6.50
65	12.97	7.71	
80	12.75	7.48	
90	10.01	5.78	
100	10.82	5.96	4.96
105	12.38	5.62	

TDT 45200203 - Alpha Bootes

Cwl [um]	OLP 6.0 [MJy sr^-1]	OLP 7.0 [MJy sr^-1]	COBE [MJy sr^-1]
60	19.64	13.00	10.83
65	24.79	14.90	
80	19.37	11.02	
90	14.17	8.09	
100	14.21	7.91	6.11
105	16.70	7.84	
120	8.58	6.90	
150	8.37	6.09	7.59 (140um)
170	8.55	5.77	
180	10.23	5.52	
200	11.58	5.15	3.64 (240um)

TDT 47600207 - NGC 6543

Cwl [um]	OLP 6.0 [MJy sr^-1]	OLP 7.0 [MJy sr^-1]	COBE [MJy sr^-1]
60	10.98	7.20	6.91
65	14.31	8.45	
80	11.92	6.96	
90	9.15	6.01	
100	9.66	5.76	5.56
105	10.70	4.96	
120	7.04	6.07	
150	8.33	6.17	5.78 (140um)
170	8.93	6.04	
180	10.16	5.51	
200	11.10	4.80	4.22 (240um)

TDT 47600511 - NGC 6240

Cwl [um]	OLP 6.0 [MJy sr^-1]	OLP 7.0 [MJy sr^-1]	COBE [MJy sr^-1]
60	16.11	11.50	12.65
65	22.57	14.02	
80	18.93	11.35	
90	15.98	8.95	
100	15.70	8.56	8.73
105	15.94	7.21	
120	11.64	10.01	
150	13.85	9.56	10.00 (140um)

```
  170    15.81         9.77
  180    17.94         9.43
  200    15.31         8.15         6.74 (240um)
-----------------------------------------------

2) Pixel standard deviations; Pixel 6 was NOT considered in PHT C100 data

TDT 35602203

  Cwl    OLP 6.0     OLP 7.0

   60    1.88156     0.83263
   65    2.02214     1.09937
   80    1.89442     1.23683
   90    0.86958     0.30470
  100    1.81761     0.63960
  105    2.16578     1.04568
  120    0.85139     0.45935
  150    1.94910     0.45132
  170    1.43985     0.43893
  180    1.78433     0.28582
  200    4.22054     1.00227

TDT 47600511

  Cwl  OLP 6.0     OLP 7.0

   60  2.75271     1.97837
   65  2.67647     1.63996
   80  1.74495     0.99638
   90  1.67586     0.69362
  100  1.72697     1.05990
  105  5.35571     3.34159
  120  1.45017     1.03177
  150  2.39852     1.03891
  170  1.93945     1.00490
  180  2.26039     0.87432
  200  2.58734     0.32844
```

5.2 Signal Dependence on Reset Interval Correction

- authors: M. Radovich, U. Klaas
- date: 08-May-1998

5.2.1 Motivation

OLP V7.0 contains a new processing feature very early in the processing chain, the correction for the dependence of the signal on the selected reset interval. Systematic variations of the signal with reset interval length have been observed and characterized. Linear calibration corrections homogenizing the signals w.r.t. a reference reset interval of 1/4 s have been established and implemented in the new CAL-G files PxxRESETI (xx = detector code). This correction has an impact on the signals of all PHT-P and PHT-C SPD products, including darks and CAL-A files, and therefore needs detailed testing. It has to be noted that a large number of CAL-G files were regenerated for CAL-G V4.0 in order to include this correction in a consistent way, too. A list of the CAL-G files and their dependence on the reset interval correction is given in Sect. 5.2.7.

5.2.2 References to Calibration Analysis and Software Change Documentation

- calibration report: CRE Signal Dependence on Reset Interval Length: C100, C200, P1, P2, and P3 [6]
- Software Change Request: SCREW 322

5.2.3 Method

As outlined in the motivation section the reset interval correction is affecting each PHT-P and PHT-C data product, and so the general re-validation checks for an overall validity of the processing with this new correction. In this subsection we describe the analysis of special OLP validation measurements varying the reset interval on the same target in order to see effects by this correction in a more systematic manner. In the following we quote the scientific justification of this OLP validation proposal (OLPVAL02) for more details on the method:
"The proposal is to use the FIR detectors as these show the largest effects under normal observing conditions. Preferentially select a source with the total flux requiring a reset interval of 1/4 s under nominal observing conditions, so that no correction will be applied. Use a factor of 2-4 longer reset interval, which should in the case of a factor of 2 not lead to serious saturation, as the saturation limits of the AOT Logic are quite conservative, but for the factor of 4 to about 50% saturation. Thus the performance of the correction under saturation is checked, too. Use a factor of 4-8 shorter reset interval in order to test the correction for a more extreme read-out configuration with small dynamic range.
Use the sparse map mode in order to minimise the number of FCS measurements, but include multi-filter mode to verify an end-to-end multi-filter photometric calibration.
Proposed target and observing mode: beta And at 60 and 100 micron with P3 and C100 and C200 at 120 micron. The target is a calibration star with a quite accurate flux prediction at 60, 100, and 120 micron:
f60 = 10.7 Jy f100 = 3.05 Jy f120 = 2.7 Jy
B60 = 16 MJysr^{-1} B100 = 11 MJysr^{-1} B120 = 12 MJysr^{-1}
For C100 the nominal reset interval in the 100 micron filter is 1/2 s. For C200 the nominal reset interval in the 120 micron filter is 4 s.
Start with the background measurement, using the nominal set-up only (for C100 and C200 measurements the flux specification values were increased by a factor of 2 in order to limit the FCS calibration duration to 128 s) and perform then a sparse map sequence with the correct flux specification in the first intermediate module and repeated in the end module. This can help to account for possible drift effects:
PHT-17 / PHT-37 background with FCS measurement
PHT-18 / PHT-38 target correct flux specification
PHT-18 / PHT-38 target with reset interval 2-4*RIideal
PHT-18 / PHT-38 target with reset interval 1/4-1/8*RIideal

PHT-19 / PHT-39 target with correct flux specification

The following reset intervals were used in the end (1/4 s is the reference reset interval with no correction taking place):
P3_60: 1/4 (ref), 1/2, 1/16 s
P3_100: 1/4 (ref), 1, 1/16 s
C100_60: 1/4 (ref), 1/2, 1/16 s
C100_100: 1/2, 1, 1/8 s
C200_120: 4, 8, 1/2 s

5.2.4 Results

The following Figs. 11 to 15 give a comparison of the HR 337 on-source fluxes between OLP V6.x and OLP V7.0b2. Note that the figures present the output of the sparse map AOT result, i.e. backgrounds are not subtracted. We present the pure source fluxes after background subtraction below.
The outcome of the P3 measurements has become very consistent, both for the 60 and 100 μm filters. The χ^2 as presented in part 1 of Sect. 5.2.6 are drastically reduced. The FCS calibration for this 2 filter sparse map measurement has been done in the 60 μm filter.
For C100 there is a general upward trend from the first to the last measurement which have both identical reset interval set-ups, the difference is 21%. The most likely reason for this trend is the interpolation between the two FCS measurements which are done with different illumination levels. The first FCS measurement is matched to the background brightness expected at 60 μm, while the second FCS measurement is matched to the target brightness at 60 μm, where the star is still considerably bright. Therefore, the second FCS measurements is expected to have a $\sim$ 6 times brighter FCS illumination than the first one. The time sequence gives a stronger weight to the first FCS measurement in the case of the first on-source measurement, while it gives a stronger weight to the second FCS measurement in the case of the last on-source measurement.
In the case of C200 the two measurements at the start and the end of the on-source sequence give fairly reproducible results, as well as the measurement with 8 s reset interval, while the measurement with 1/2 s reset interval shows an outlier. This one off points to a check of the correction parameters, or one of the caveats of the C200 reset interval correction applies.
In order to investigate the effects of the reset interval correction alone for a specific measurement we compare the signals of the four on-source measurements with PIA by switching the reset interval correction off and on. The χ^2 from a linear fit to the 4 data points as presented in part 2 of Sect. 5.2.6 are drastically reduced for P3 and C100, while slightly increased for C200. This strengthens the interpretations that

1) The trend in the resulting flux of the C100 sparse map is caused by the interpolation between the two different FCS measurements.

2) The reset interval correction parameters for the C200 need refinement. The inconsistency measured from this test case is 18%.

Figs. 16 to 20 display the comparison between switched off and switched on reset interval correction on signal level. The resulting differences in the signals with correction show systematic trends which can be explained as a consequence of signal transients which is not the case for a scattered distribution.
The final Fig. 21 gives the background subtracted source photometry in comparison with the extrapolation to 300 μm of the composite spectrum provided by M. Cohen (bet And – composite created 10-15-93 T(eff) = 3839K, wavelength range of composite matched = 10.72–11.76 um interpolated from a grid of red giant models by D. F. Carbon (NASA-Ames) and the color corrected IRAS values). Plotted are the values from the final photometric measurement, for which both the FCS power and the reset interval should be best adapted.
In part 3 of Sect. 5.2.6 we present a table of the photometry with the ranges as given by the first and the last measurement. Note that the values of the first measurement match the model flux better. We compute the following consistency of the photometry with the model:

Table 13: Consistency check of photometric results with HR 337 model

Photometry	consistency w.r.t. model [%]
PHT-P 60 μm 1st meas.	-2.7
PHT-P 60 μm last meas.	+9.6
PHT-C 60 μm 1st meas.	-4.8
PHT-C 60 μm last meas.	+33.3
IRAS 60 μm	+2.6
PHT-P 100 μm 1st meas.	+12.2
PHT-P 100 μm last meas.	+24.2
PHT-C 100 μm 1st meas.	+6.6
PHT-C 100 μm last meas.	+52.6
IRAS 100 μm	-1.8
PHT-C 120 μm 1st meas.	+32.3
PHT-C 120 μm last meas.	+46.0

For this particular measurement series we conclude that the P3 photometry is better than 25%, the C100 is on average 30%, while the C200 photometry is systematically off by $\sim$ 40%. Reason for the latter outlier could be an overcorrection by the empirical PSF factor of the C200 array. This should be followed up in the general re-validation of PHT-22.
In part 4 of Sect. 5.2.6 we give for comparison the fluxes as derived with PIA V7.1 AOT batch processing. They are consistent with the OLP V7.0b2 results. We also did the C100 photometry using the central pixel 5 only. The resulting source fluxes are presented in part 5 of Sect. 5.2.6. The fluxes are only 60% and 45%, respectively, of the ones derived using the whole array. They are too small w.r.t. the model fluxes. This behaviour points towards some inconsistency of the p_{psf} factors used for the array and the pixel, respectively.

5.2.5 Conclusions

- The reset interval correction results in a drastic homogenisation of source signals for P3 and C100 w.r.t. to tested reset interval settings, i.e. also measurements with badly matched dynamic ranges give much more consistent results now. For C200 there seems to be some inconsistency between the long (4, 8 s) reset intervals and the shorter ones (1/2 s). The difference of 18% may be reduced by refined tuning of the correction parameters, but is not an unusual residual error of this correction.

- For P3 the scatter between the first and the last on-source measurement performed with the same reset interval setting has been drastically reduced w.r.t. OLP 6 and the absolute flux values match the model prediction to within 25%. For C100 the scatter has increased which is very likely a consequence of the flux calibration, rather than of the reset interval correction, as on signal level the scatter with reset interval correction got smaller. For C200 first and last measurement coincide within 10%, but are systematically off by 40%.

- P3 and C100 photometry coincide within better than 25% for this measurement.

- As a side track result of this investigation: The FCS calibration interpolation in sparse maps has to be reviewed. The illuminations of the FCS in the start and end module can be quite different. If systematic trends in the photometric calibration introduced by this interpolation can be traced to a non-linearity of the responsivity with flux, such trends would be removed with a non-linearity correction.

- C100 photometry using the whole array and using only the central pixel does not yet give consistent results (factor of 2 difference for this test case). The issue of the p_{psf} factors for the array vs. the ones for one pixel has to be reviewed.

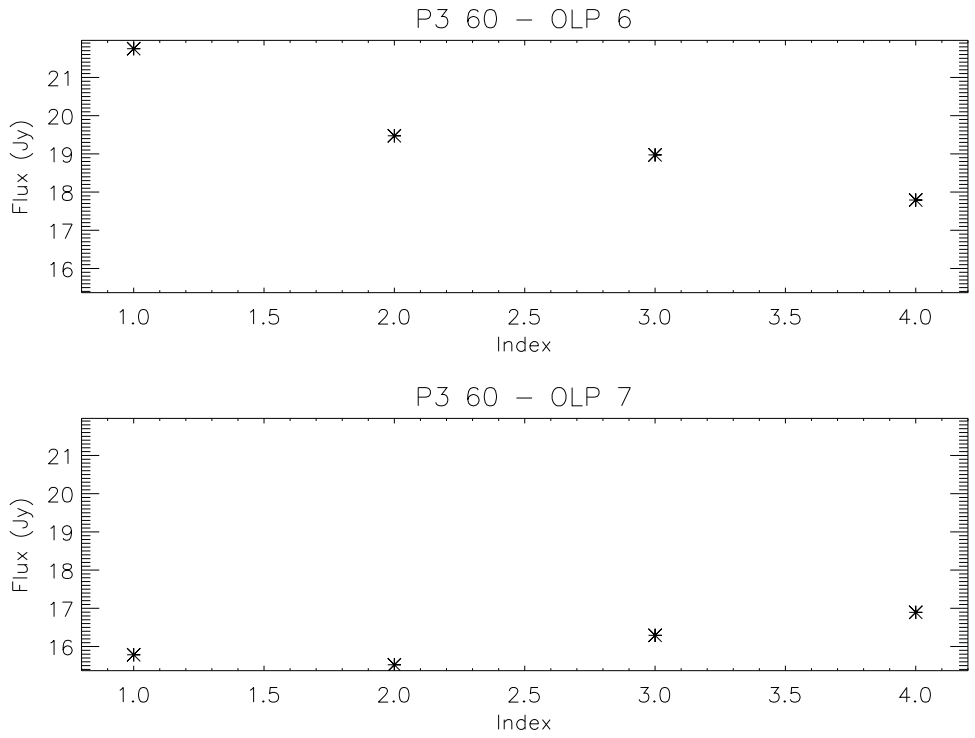

Figure 11: Comparison of OLP V6.x and OLP V7.0b2 for the P3 60 μm on-source fluxes (no background subtraction). The index for the measurements is the following: 1: 1/4, 2: 1/2, 3: 1/16, 4: 1/4 s reset interval

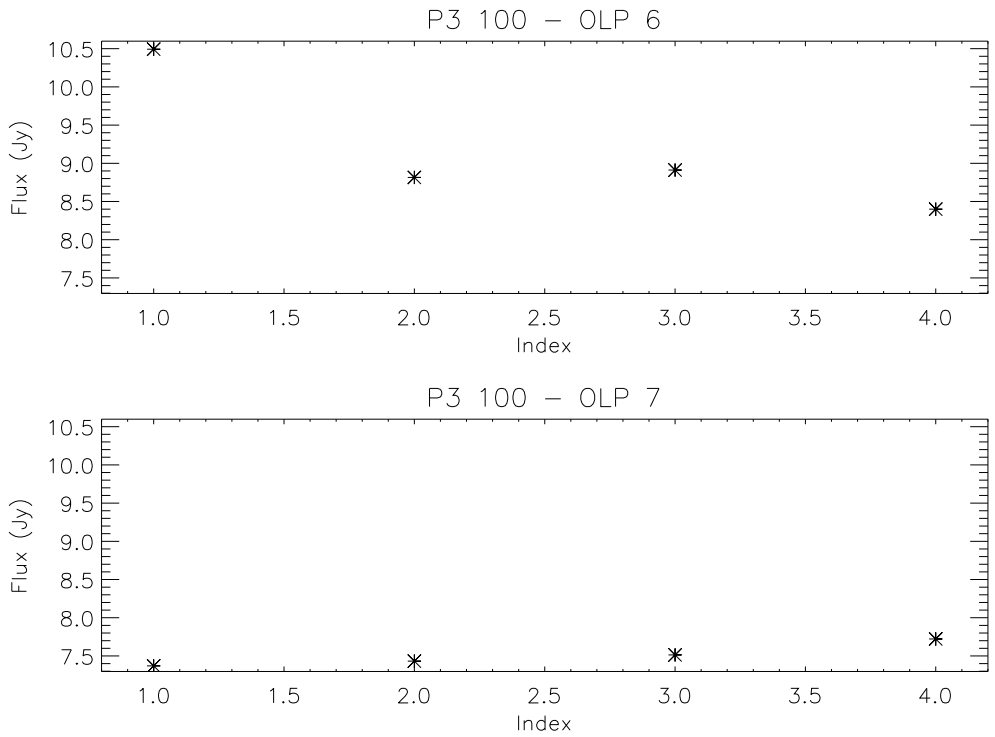

Figure 12: Comparison of OLP V6.x and OLP V7.0b2 for the P3 100 μm on-source fluxes (no background subtraction). The index for the measurements is the following: 1: 1/4, 2: 1, 3: 1/16s, 4: 1/4 s reset interval.

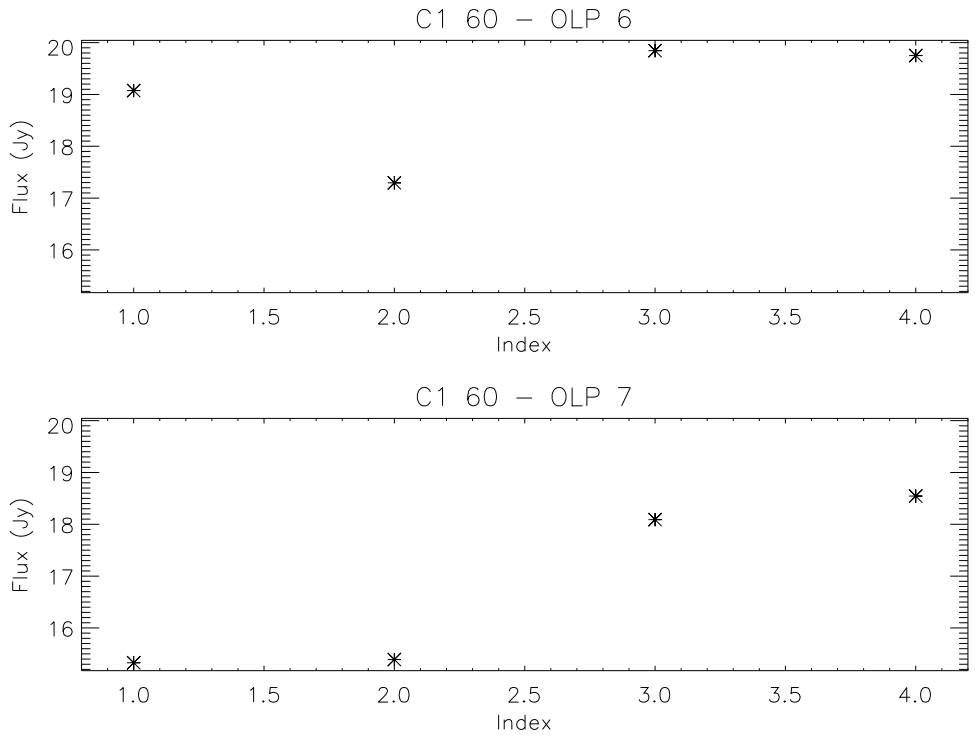

Figure 13: Comparison of OLP V6.x and OLP V7.0b2 for the C100 60 μm on-source fluxes (no background subtraction). The index for the measurements is the following: 1: 1/4, 2: 1/2, 3: 1/16, 4: 1/4 s reset interval.

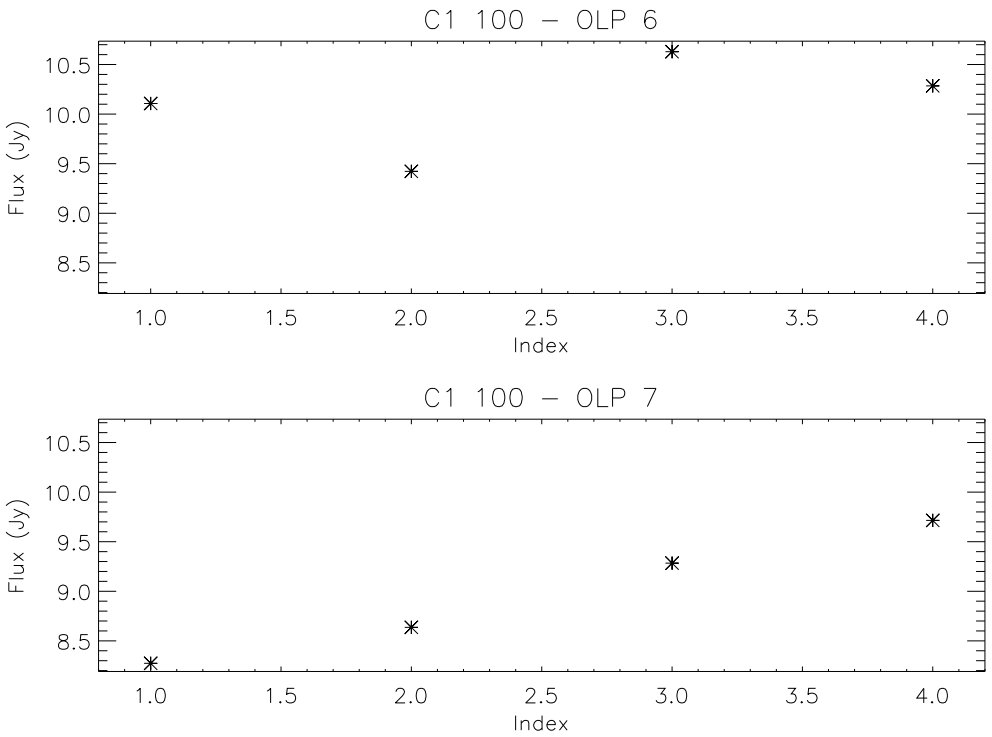

Figure 14: Comparison of OLP V6.x and OLP V7.0b2 for the C100 100 μm on-source fluxes (no background subtraction). The index for the measurements is the following: 1: 1/2, 2: 1, 3: 1/8, 4: 1/2 s reset interval.

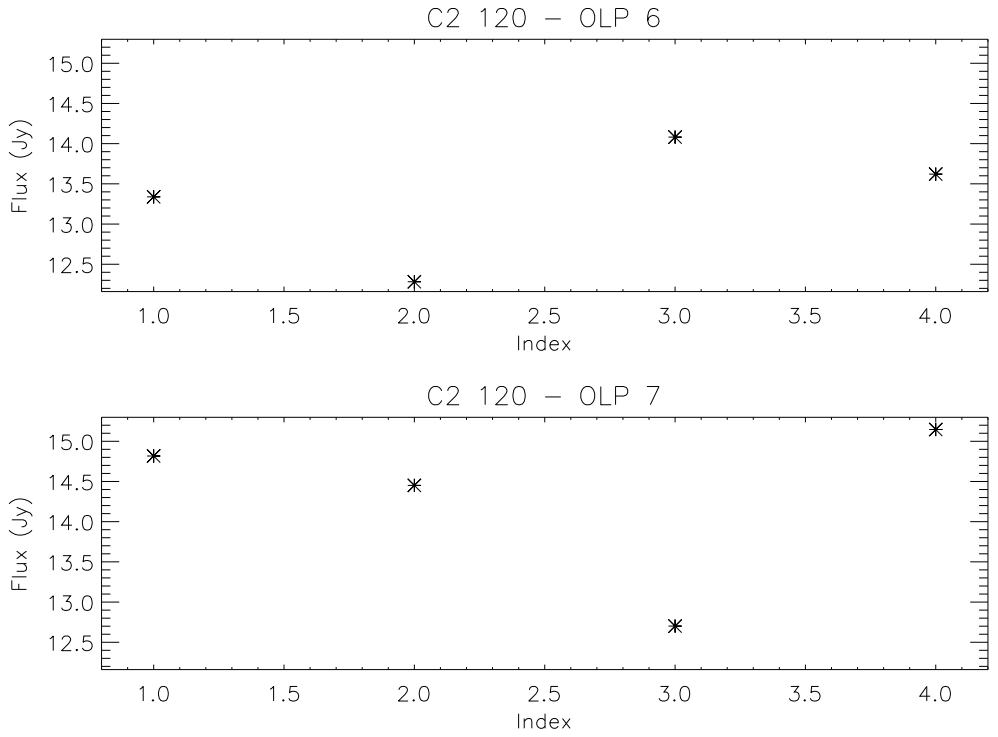

Figure 15: Comparison of OLP V6.x and OLP V7.0b2 for the C200 120 μm on-source fluxes (no background subtraction). The index for the measurements is the following: 1: 4, 2: 8, 3: 1/2, 4: 4 s reset interval

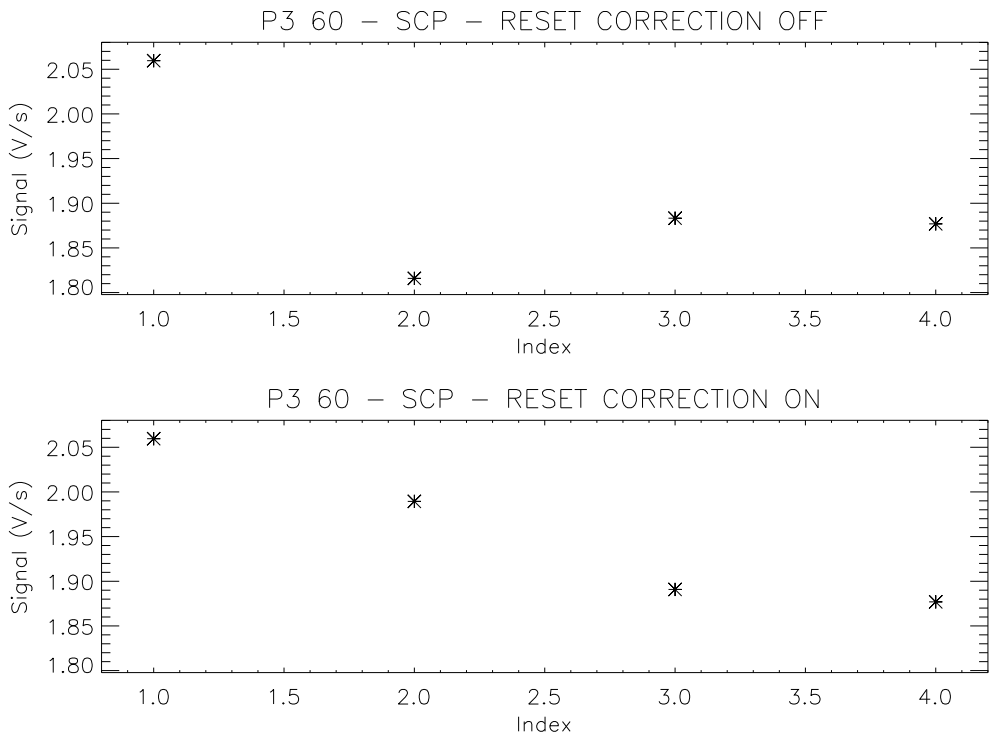

Figure 16: Comparison of signals without and with reset interval correction for the P3 60 μm filter. The index for the measurements is the following: 1: 1/4, 2: 1/2, 3: 1/16 4: 1/4 s reset interval

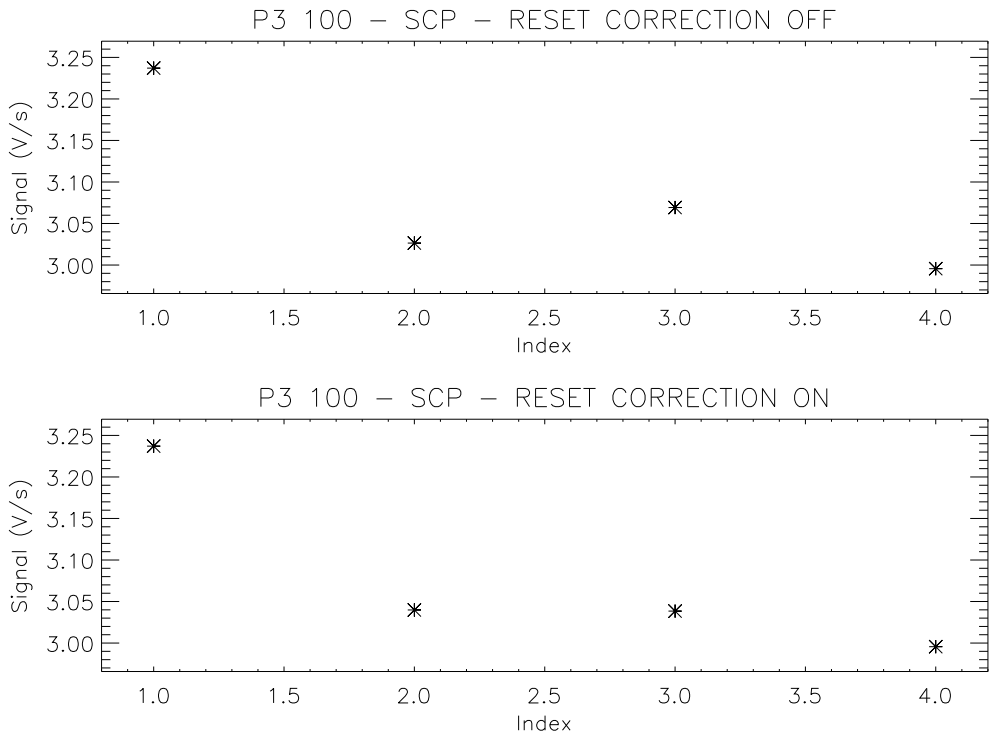

Figure 17: Comparison of signals without and with reset interval correction for the P3 100 μm filter. The index for the measurements is the following: 1: 1/4, 2: 1, 3: 1/16 4: 1/4 s reset interval

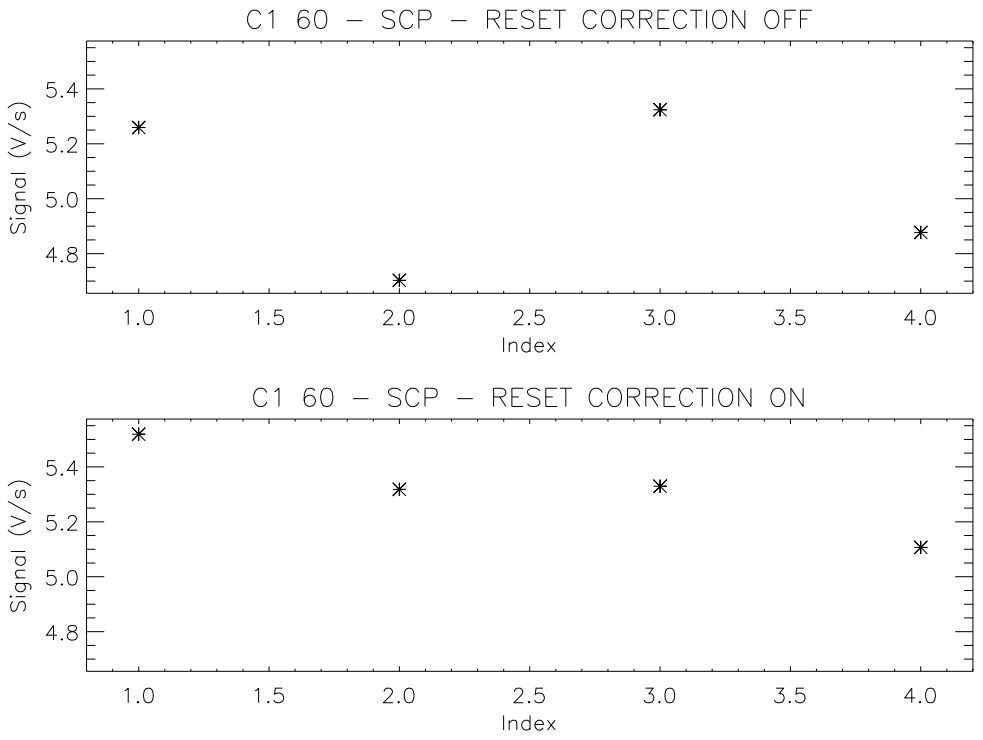

Figure 18: Comparison of signals without and with reset interval correction for the C100 60 μm filter. The index for the measurements is the following: 1: 1/4, 2: 1/2, 3: 1/16 4: 1/4 s reset interval

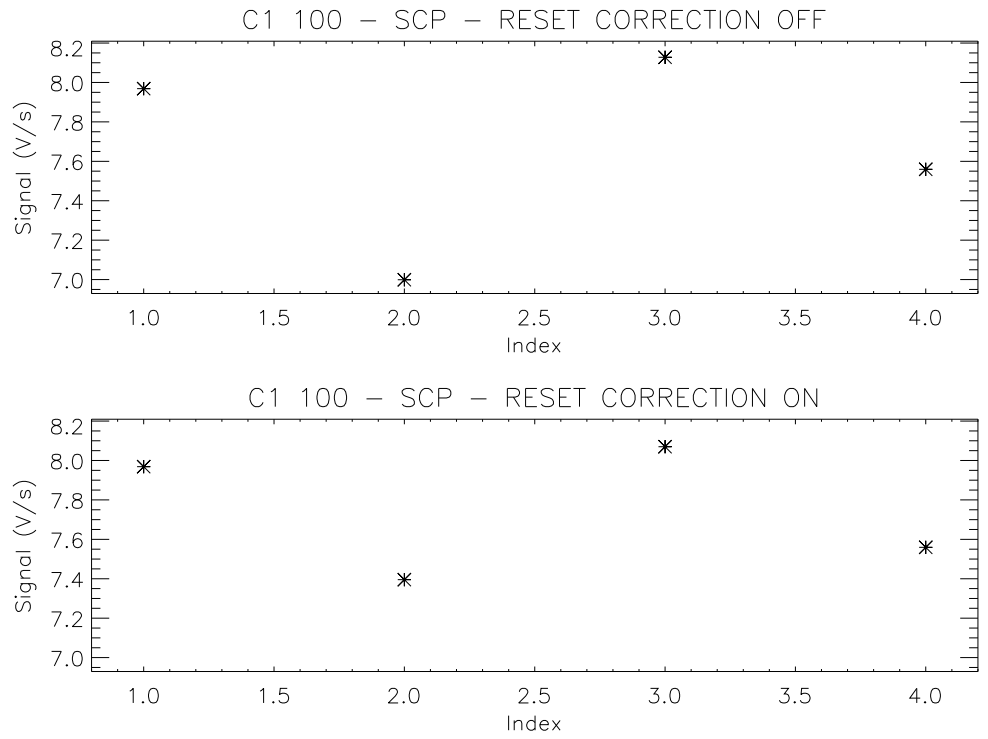

Figure 19: Comparison of signals without and with reset interval correction for the C100 100 μm filter. The index for the measurements is the following: 1: 1/2, 2: 1, 3: 1/8 4: 1/2 s reset interval

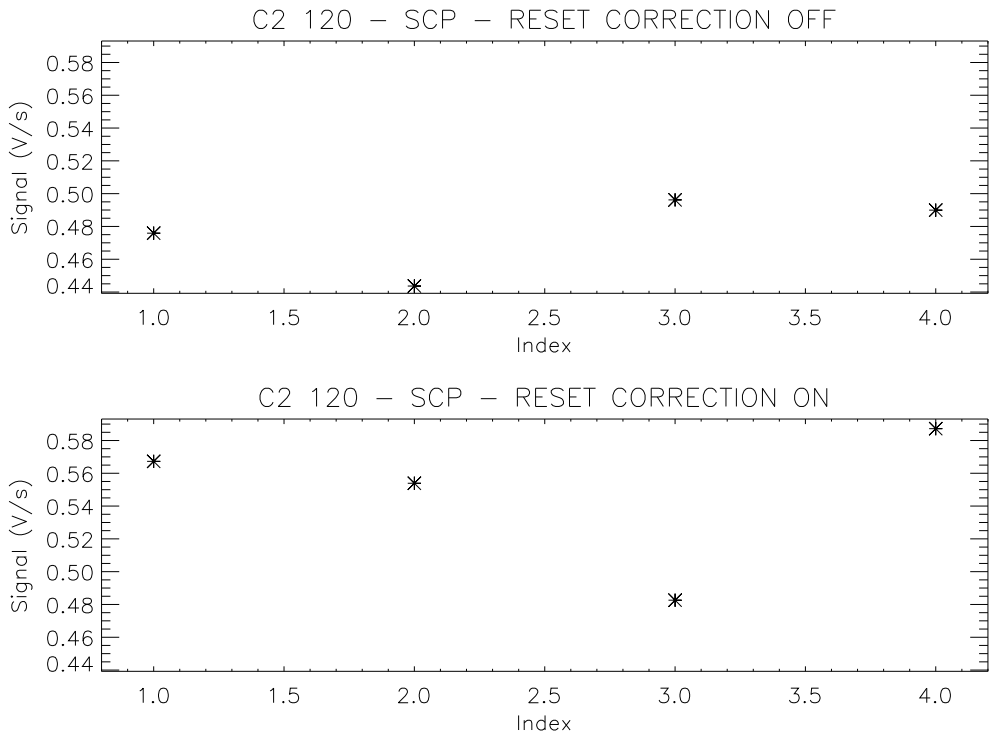

Figure 20: Comparison of signals without and with reset interval correction for the C200 120 μm filter. The index for the measurements is the following: 1: 4, 2: 8, 3: 1/2 4: 4 s reset interval

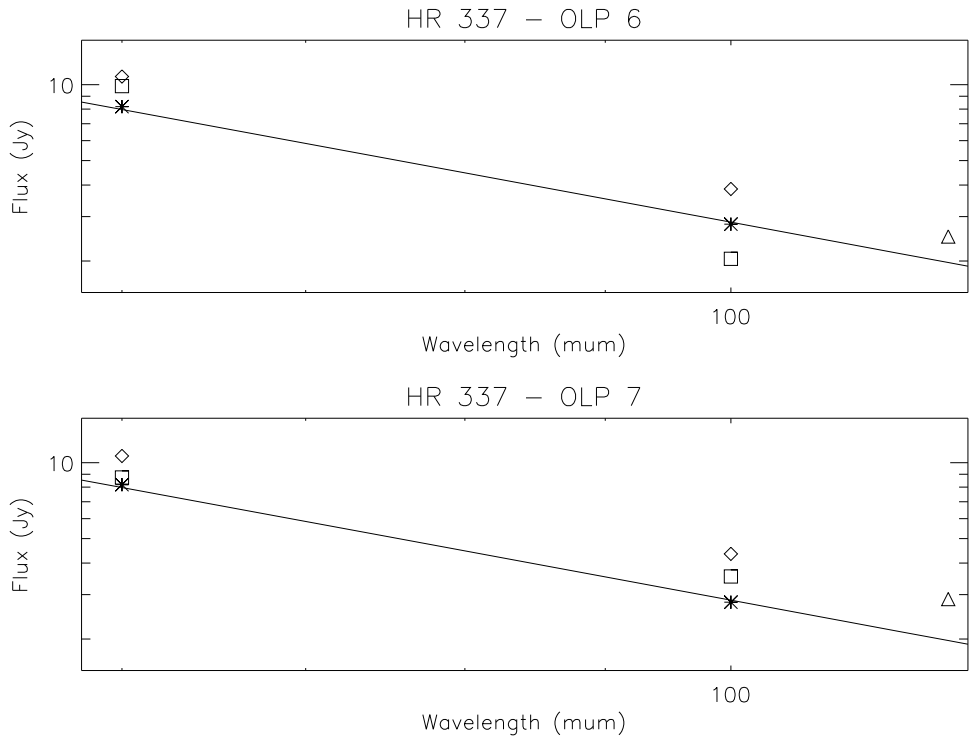

Figure 21: Comparison of P3, C100, and C200 photometry with the out to 300 μm extrapolated SED of β And (HR 337) provided by M. Cohen and IRAS photometry, both for OLP 6.x and OLP 7.0b2. All photometric points are color corrected for a 4000 K BB. The meaning of the symbols is the following: solid line: model, asterisk: IRAS, square: P3, diamond : C100, triangle: C200.

- OLP applies the point source fraction factor (f_{psf} to all data products flagged as point source type. This includes staring mode measurements performed on the on-source position and the final flux contains still the background contribution. For a consistent background subtraction it has to be taken into account, that this factor applies only to the pure point source flux and not to the fraction of the total flux which is due to the background.

5.2.6 Evaluation Log

1) CHI^2 for linear fit to the 4 data on-source measurements of HR 337
sparse map measurements
(TDT 80400602-5)

	P3 60	P3 100
OLP 6	0.604962	0.623589
OLP 7	0.258335	0.005964

2) CHI^2 for linear fit to signals of HR 337 sparse map measurements with reset interval correction switched off and on (performed with PIA V7.1)

	TDT 80400602-5		TDT 80400707-10		TDT 80400812-5
	P3 60	P3 100	C1 60	C1 100	C2 120
rc OFF	0.0215	0.0115	0.2553	0.7605	0.0012
rc ON	0.0014	0.0088	0.0101	0.2969	0.0062

3) bet And photometry from OLP

OLP 6, 7: fluxes are given in Jy, they have been background subtracted and color corrected assuming T = 4000 BB, also the IRAS fluxes have been color corrected

	Model	OLP6	OLP7	IRAS
cwl				
P3				
60	7.972	6.36 - 9.87	7.76 - 8.74	8.18
100	2.851	4.03 - 2.04	3.20 - 3.54	2.80
C1				
60	7.972	10.13 - 10.77	7.59 - 10.63	8.18
100	2.851	3.70 - 3.86	3.04 - 4.35	2.80
C2				
120	1.973	2.27 - 2.50	2.61 - 2.88	

4) bet And photometry from PIA AOT batch processing

Colour corrected fluxes, T=4000

P30180400601	60.	6.273	0.046	0.
P30180400602	60.	14.144	0.085	7.87
P30180400603	60.	13.913	0.072	7.64
P30180400604	60.	14.601	0.062	8.33
P30180400605	60.	15.152	0.043	8.88
P30080400601	100.	3.989	0.033	0.
P30080400602	100.	7.092	0.046	3.10
P30080400603	100.	7.168	0.041	3.18
P30080400604	100.	7.147	0.042	3.16
P30080400605	100.	7.459	0.03	3.47
C10180400706	60.	6.962	0.165	0.
C10180400707	60.	14.384	0.307	7.42
C10180400708	60.	14.622	0.313	7.66
C10180400709	60.	17.174	0.365	10.21
C10180400710	60.	17.613	0.374	10.65

C10080400706	100.	4.513	0.113	0.
C10080400707	100.	7.619	0.181	3.11
C10080400708	100.	7.924	0.189	3.41
C10080400709	100.	8.588	0.208	4.07
C10080400710	100.	8.915	0.212	4.40
C20080400811	120.	9.566	0.417	0.
C20080400812	120.	12.199	0.535	2.63
C20080400813	120.	11.886	0.521	2.32
C20080400814	120.	10.274	0.45	0.71
C20080400815	120.	12.488	0.548	2.92

5) beta And C100 photometry using central pixel 5 only

Colour corrected, T=4000

C10180400706	60.	0.97	0.059	0.
C10180400707	60.	6.282	0.323	5.31
C10180400708	60.	5.979	0.306	5.01
C10180400709	60.	7.293	0.372	6.32
C10180400710	60.	7.395	0.375	6.42
C10080400706	100.	0.577	0.036	0.
C10080400707	100.	2.305	0.141	1.73
C10080400708	100.	2.21	0.135	1.63
C10080400709	100.	2.428	0.148	1.85
C10080400710	100.	2.547	0.155	1.97

5.2.7 CAL-G Files Affected by Reset Interval Correction

Overview of PHT cal-G re-processing for OLP V7.0

13/10/97

column 1: cal-G file name
column 2: signal dependence on reset interval for cal-G entries (Y/N)
column 3: documented calibration file derivation procedure or at least written analysis and processing plan by responsible
column 4: stage of automatisation of deriving cal-G file numbers (if possible specify percentage)
column 5: forecast for the re-processing time including preparations (adapting programs, inclusion of signal dependence processing)
column 6: responsible person
column 7: remarks and explanations to columns 1 - 6

cal-G name	depends on RI	CFDP avail.	autom. proc.	forecast reproc. t	resp.	remarks
PC1CRELIN	N	Y(TBC)	Y(TBC)	n.a.	JA	uses ramp shape,
PC2CRELIN	N	Y(TBC)	Y(TBC)	n.a.	JA	no signals
PPCRELIN	N	Y(TBC)	Y(TBC)	n.a.	JA	
PDARKCURR	Y	Y(TBC)	Y	?	HC	reference RI !
PDIE1TRANS	N	Y?	N	n.a.	IH	dedicated meas.
PDIE2TRANS	N	Y?	N	n.a.	IH	on digital level
PC1ILLUM	Y	Y?	semi?	?	BS	linked to
PC2ILLUM	Y	Y?	semi?	?	BS	derivation of
PC1FCSPOW	Y	Y?	semi?	?	BS	P*FCSPOW and
PC2FCSPOW	Y	Y?	semi?	?	BS	PC*FLAT and
PP1FCSPOW	Y	Y?	semi?	?	BS	PFLUXCONV
PP2FCSPOW	Y	Y?	semi?	?	BS	
PP3FCSPOW	Y	Y?	semi?	?	BS	
PC1FLAT	Y	Y?	semi?	?	BS	
PC2FLAT	Y	Y?	semi?	?	BS	
PFLUXCONV	Y	Y?	semi?	?	BS	
PRESPONSE	Y	Y?	?	?	BS	default response
PSELNDR	N	n.a.	n.a.	n.a.	PIDT	proc. set-up
PP1RESETI	Y*	Y	Y	1 mD	MBr	* reference RI !
PP2RESETI	Y*	Y	Y		MBr	
PP3RESETI	Y*	Y	Y		MBr	
PC1RESETI	Y*	Y	Y		MBr	
PC2RESETI	Y*	Y	Y		MBr	
PC1VIGN	N	?	?	n.a.	MH	relative signals
PC2VIGN	N	?	?	n.a.	MH	from maps
PP1VIGN	N	?	?	n.a.	MH	
PP2VIGN	N	?	?	n.a.	MH	
PP3VIGN	N	?	?	n.a.	MH	
PPSF	N*	N	n.a.	n.a.	PIDT	* theoretical values for P1,P2,P3,C100
	N*	Y	N	n.a.	UK	* relative comp. pixel/array C200

PSPECAL	N*	Y	Y?	n.a.	JA/ThM	* PHT-S
PTIMEDEP	N	n.a.	n.a.	n.a.	PIDT	cal-G time dep.
POMEGA	N*	n.a.	n.a.	n.a.	PIDT	* theoretical values
	Y*	TBD	TBD	?	UH	* complete revision for meas. values
PP1FCSAP	Y*	Y?	Y?	?	SH	* files being established for first time
PP2FCSAP	Y*	Y?	Y?	?	SH	
PP3FCSAP	Y*	Y?	Y?	?	SH	

5.2.8 Independent Check of the Quality of the Reset Interval Correction

Another check of the reset interval correction for both C100 and C200 is provided by a consistency verification of the responsivity checks in activation. They were actually the first measurement sequences for which a systematic signal variation with reset interval length was found. Compared are the signals before and after revolution 191, as the reset interval had been shortened by a factor of 2 due to the FCS illumination change in rev. 94. The following changes were made:

- C100: 1/4 s (ref.) $\Rightarrow$ 1/8 s
- C200: 1/2 s $\Rightarrow$ 1/4 s (ref.)

Therefore, both sequences contain one part which is not affected by the reset interval correction, as the measurement is performed with the reference reset interval length.
In Figs. 22 and 23 the effect of the correction on the C100 signals can be seen. While for pixel 3 it is nearly perfect, for pixel 5 a residual error of about 15% remains. In Figs. 24 and 25 we show the result of the correction on C200 pixels 1 and 4. It is nearly perfect, as only minor systematic signal jumps can be seen. Note that the scatter of the individual signals is due to Space Weather impact on the resulting responsivity after curing.

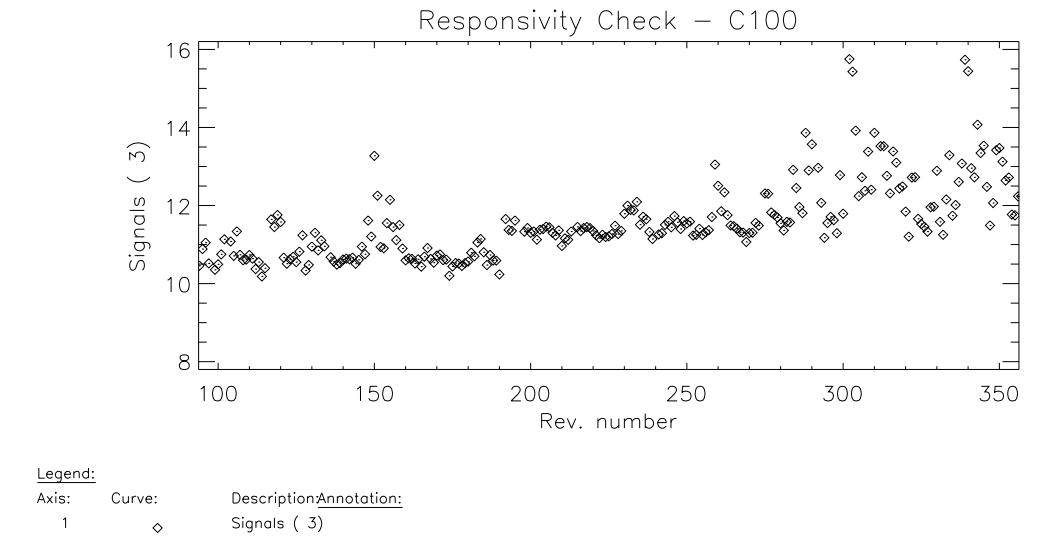

Figure 22: Signals of the responsivity checks in activation for C100 pixel 3. The modification of the reset interval became active with rev. 191.

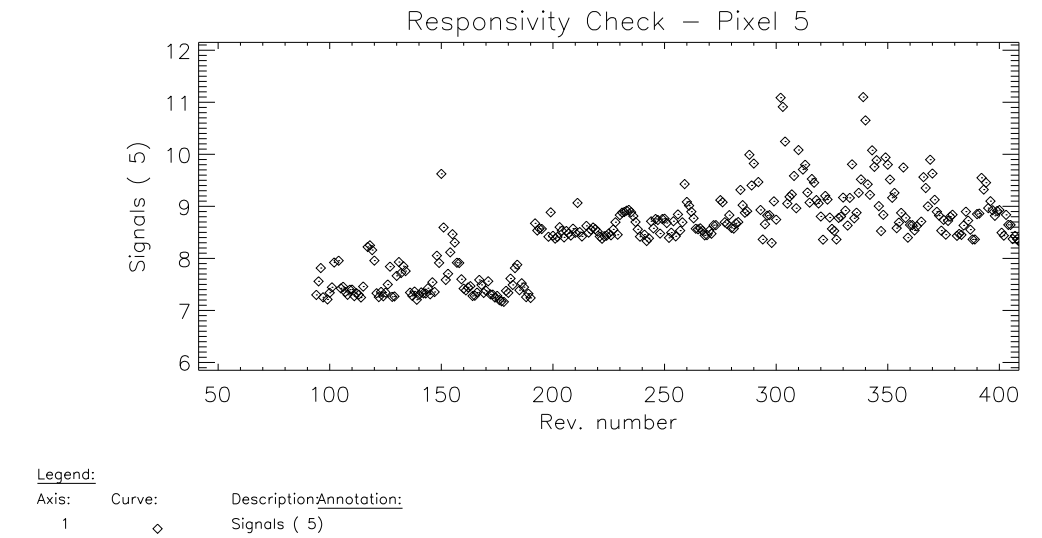

Figure 23: Signals of the responsivity checks in activation for C100 pixel 5. The modification of the reset interval became active with rev. 191.

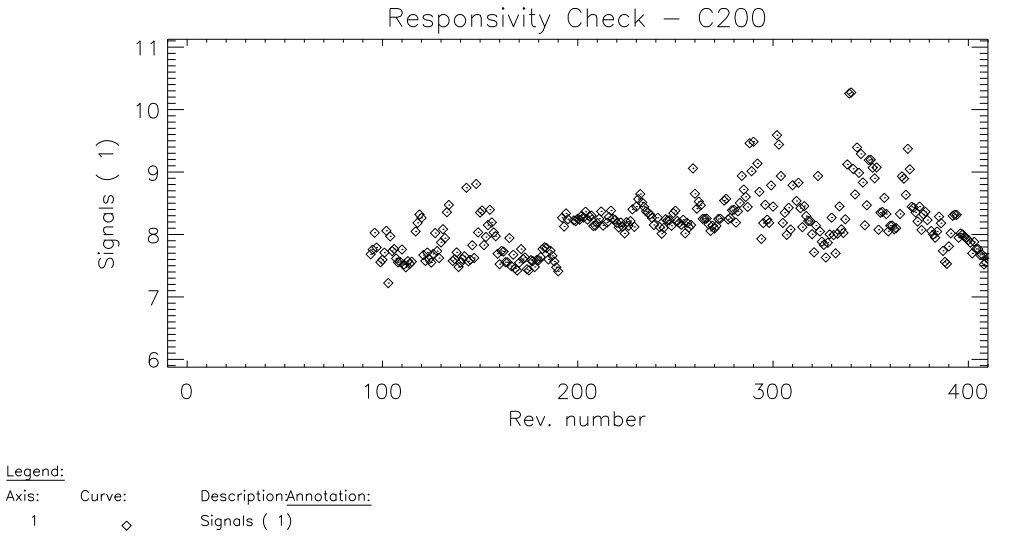

Figure 24: Signals of the responsivity checks in activation for C200 pixel 1. The modification of the reset interval became active with rev. 191.

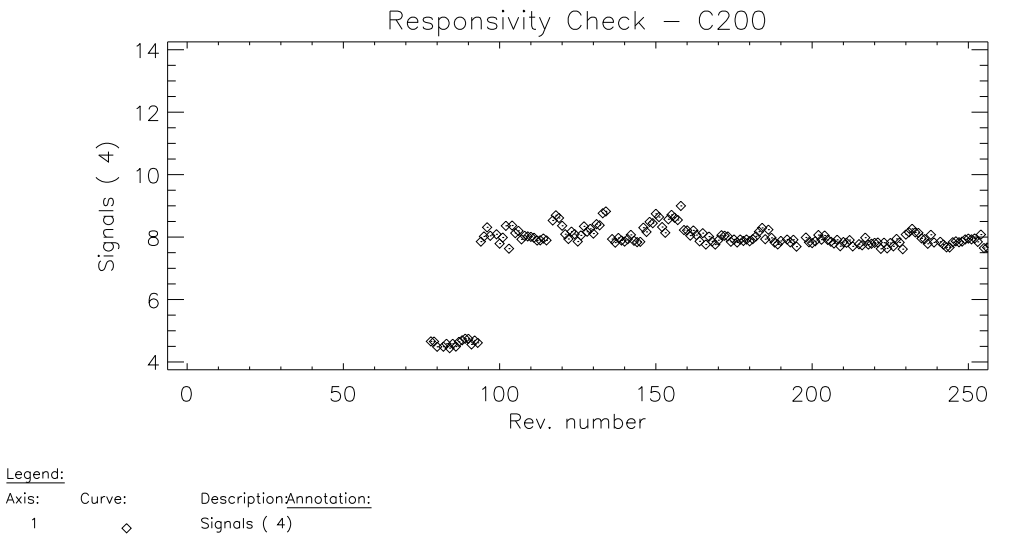

Figure 25: Signals of the responsivity checks in activation for C200 pixel 4. The modification of the reset interval became active with rev. 191. Note that the jump at rev. 94 comes from the change in illumination behaviour of the FCS (reset interval was not changed at this time, but only on rev. 191).

5.3 Extension of PHT SPD Data Records for Improved Error Handling

- authors: P.J. Richards, L. Cornwall, U. Klaas
- date: 26-May-1998

5.3.1 Motivation

An additional field is added to the records for the SPD, Cal A and dark current products to store the actual number of signals used in the calculation of the weighted means written to these files.

5.3.2 Reference to Software Change Documentation

- calibration report: n/a
- Software Change Request: SCREW 323

5.3.3 Method

The data products were examined to determine whether the number of slopes (signals) averaged were as expected. Depending on whether the drift recognition algorithm (Mann-test) flags the detection of a drift in the detector pixel on the chopper plateau, the number of slopes should correspond to the expected number per chopper plateau. A detailed check on the number of signals on a plateau would have been too time consuming. However checks were made on the number of signals per pixel against the status flag for that pixel. When no drift was detected in the signals, then all signals (with the possible exception of a few affected by glitches) were averaged and pixel status flag is set to 0. For those cases where a drift was detected, but part of the plateau was processed (i.e. the no. of signals $<$ expected no. per plateau, but > 7) then only the latter part of the data for the plateau are averaged and the status flag is set to 2. For those cases where the drift persists to the final 7 signals on the plateau, then the Mann-test cannot be carried reliably out and the status flag for the pixel is set to 4. Occasionally (for example for the dark files) the signal is negative and in these cases the pixel flag is set to 7.
The observations examined were:

TDT	Products
47600206	PP1S, PP2S, PP3S, PP1A, PP2A, PP3A
47600208	PC1S, PC2S, PC1A, PC2A
38300521	PSSS, PSLS
35300301	PP1D
35300303	PP2D
35300305	PP3D
35300307	PC1D
35300311	PC2D

5.3.4 Results

For all data products examined, the results for each plateau was as expected.
An example for the four C200 pixels in the SPD product for observation 47600208 is:

```
' No. of valid signals on the plateau          '          7          58
        31          63
' Status flags                                 '          4           0
          2           0
```

Also for the nine C100 pixels in the dark current product (PC1D) for observation 35300307:

```
' Dark current (V/s)                              ' -2.9180432E-02  7.1007319E-02
 2.9069552E-02 -2.6758071E-02  1.6284103E-03  0.2292581     -1.7635636E-02
-2.0138796E-02 -1.4403219E-02
' Uncertainty in dark current (V/s)               '  1.6964279E-02  1.2853188E-02
 1.4022420E-02  9.2920167E-03  1.4155664E-02  2.4609717E-02  1.3119154E-02
 1.0614714E-02  1.7130915E-02
' No. of valid signals on the plateau             '          31           8
         15          30          27          15          28          15
         31
' Status flag                                     '           7           2
          2           7           0           2           7           7
          7
```

5.4 Use of Improved Pointing Information for PHT Maps

- author: L. Cornwall, U. Klaas
- date: 14-May-1998

5.4.1 Motivation

With OLP 6.1 improved pointing information is provided in the product headers and the IRPH file. This was possible by refined calibrations of the Star Tracker Focal Length and the Fine Sun Sensor. For the uplink this optimised pointing became effective from rev. 452 onwards, but a posteriori it was possible to reconstruct a better actual pointing for previous revolutions. So far PHT OLP did not make any use of the improved pointing information, as an introduction requires a re-validation of the products which is only possible with a major version like the OLP V7.0 now.

5.4.2 References to Calibration Analysis and Software Change Documentation

- calibration report: n/a
- Software Change Request: SCREW 324 (changes to PHT software), SCREW 280 (update of pointing information)

5.4.3 Method

The re-validation of the map products is confined to a technical re-validation, as the data products are not yet scientifically validated. PHT mapping software works from quaternion level and the main check is whether the updated pointing information is consistent with the PHT mapping software.

- produce displays of map products as specified in the test plan both from OLP 6.x ($\geq$ 6.1) which use the old pointing information and compare with the OLP 7.0b2 data products which use the improved pointing information;
- verify by eye-check that the OLP 7.0b2 data products do not show any disrupted appearance.

5.4.4 Results

We have selected here one representative example each both from PHT-P and PHT-C mapping. Figs. 26 and 27 show a comparison of a 90 μm image of the Helix Nebula (TDT 16701405) produced with OLP V6.x and OLP V7.0b2. Figs. 28 and 29 show a comparison of a 25 μm image of a shell around a LBV (TDT 38101802). The images produced by both pipeline versions look very similar. This is expected, as the improved pointing brings only a very minor effect which should not be easily detectable by eye. We note that the OLP V7.0b2 image of the 90 μm map looks a bit sharper than the OLP V6.x one which is presumably a consequence of the better pixel-to-pixel correction in the FCS illumination matrix files. The brightest spots in the 25 μm map have a slightly different appearance. The OLP V6.x data product shows indentation at the borders of the map which is gone with the OLP V7.0b2 version.

5.4.5 Conclusions

- We verified that the usage of the improved pointing information is implemented correctly, as no distortion of the images is observed and details look like as in the previous version using the old pointing information.
- The new C100 image looks somewhat sharper than the old one, so that the overall progress in absolute calibration has given an improvement of the maps. The flat-field techniques can, however, still be improved, as some of the structures are generated by not perfect pixel-to-pixel calibration.

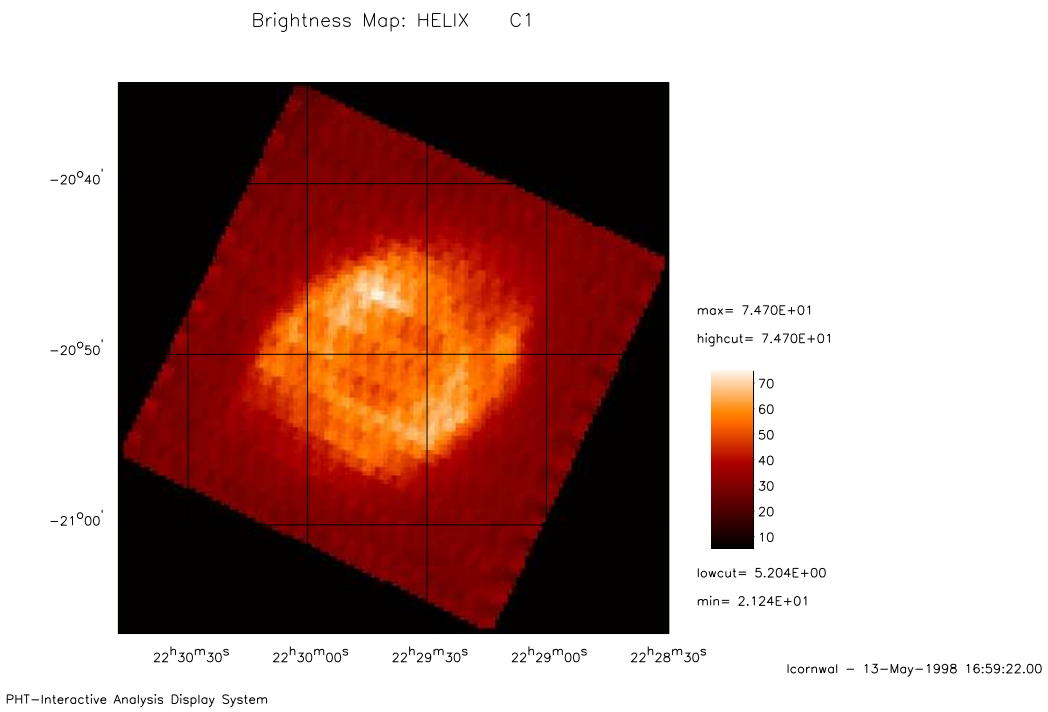

Figure 26: 90 μm image of the Helix Nebula (TDT16701405) as produced by OLP V6.x

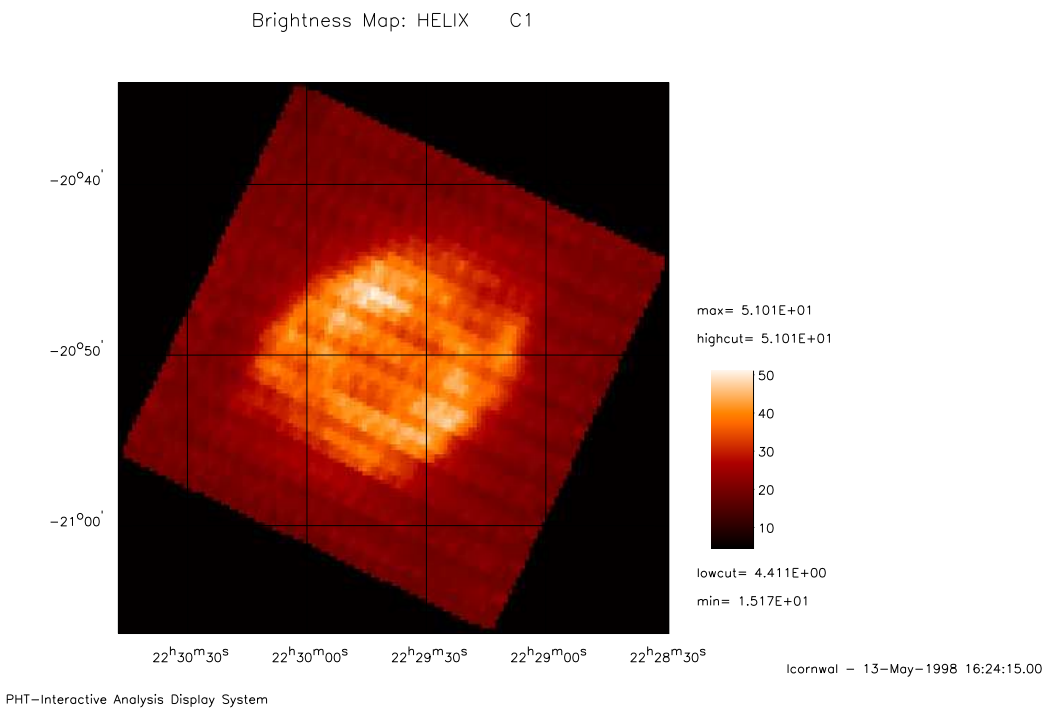

Figure 27: 90 μm image of the Helix Nebula (TDT16701405) as produced by OLP V7.0b2

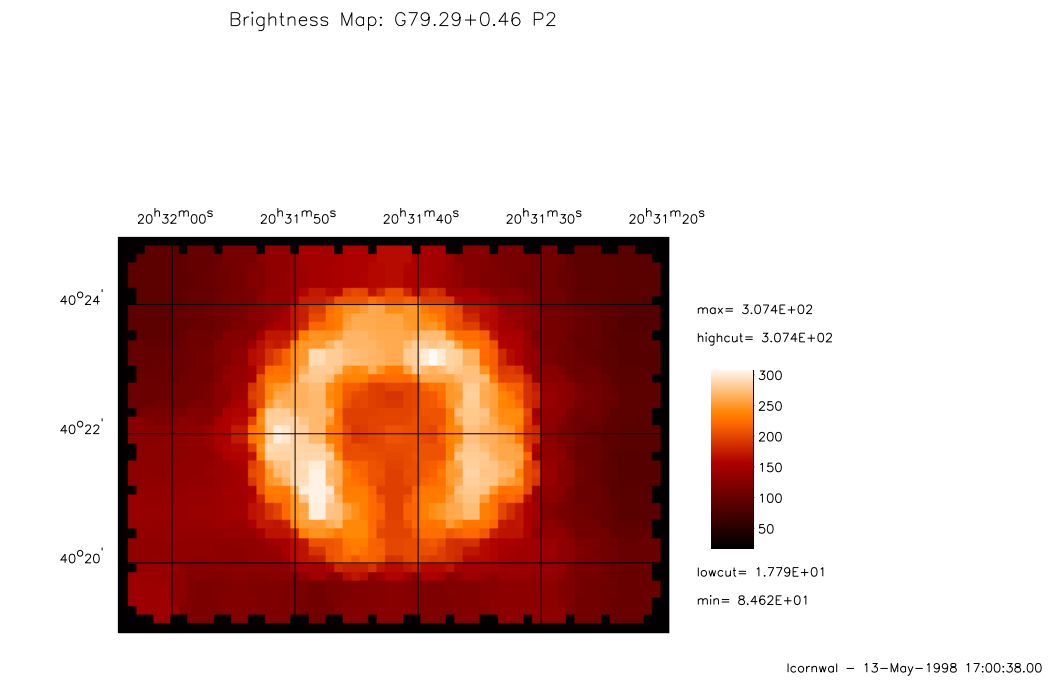

Figure 28: 25 μm image of the shell around a LBV (TDT38101802) as produced by OLP V6.x

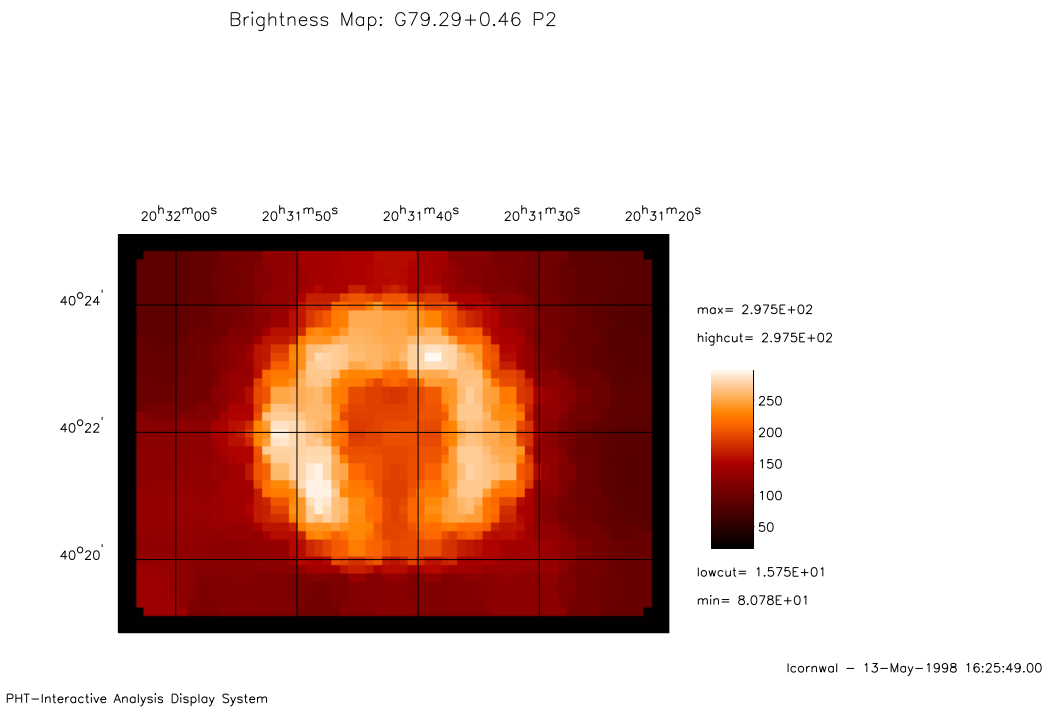

Figure 29: 25 μm image of the shell around a LBV (TDT38101802) as produced by OLP V7.0b2

5.5 Power Ranges of FCS Cal-G Files

- authors: P.J. Richards, L. Cornwall, U. Klaas
- date: 19-May-1998

5.5.1 Motivation

With the OLP V7.0 / CALG V4.0 a check for the validity ranges of the FCS power files was included. The FCS power cal-G files contain lower and upper limits (cf. Sect. 2.1) between which the curves could be established by polynomial fits to the measured data points of calibration standards. Below and above this range an extrapolation using a physical model of a grey body is done which is less accurate. Hence, the OLP shall issue a warning both in the SPD data products, if the applied electrical FCS power is outside the calibrated range. The observer has then to make sure himself how far outside the calibrated range his measurement is and whether the extrapolation is reasonable.

5.5.2 References to Calibration Analysis and Software Change Documentation

- calibration report: cf. Sect. 2.1
- Software Change Request: SCREW 351, SCREW 338
- SPR: 2510, 2544

5.5.3 Method

The "Plan for the PHT Scientific (Re-)Validation of OLP Version 7.0" [4] provides test cases for which the FCS powers are outside the calibrated range. SPD products of these TDTs shall be checked for the occurrence of the warning:

```
**************************************************
The selected FCS power was outside the calibrated range.
**************************************************
```

5.5.4 Results

TDT 05702709 did not show the expected warning message. Investigation showed that this TDT was a special case: It is the end module of a sparse map sequence. It was found that the FCS electrical power of the start module was inside the valid range and OLP only checked the start module. Sparse maps are the only cases for which the two FCS measurements at the beginning and the end can have different electrical FCS powers (as for each module the fluxes are specified individually). Consequently the SPR " Missing FCS warning in PHT sparse maps" (no. 2644) was submitted.
A fix was checked out in the PIDT test environment with positive result:

```
PC2S05702709.HDR

TRS1S2  =                    2 / Selected TRS for FCS1
POW1S2  =              2.50305 / Selected power for FCS1
POW1M2  =              2.50305 / Measured power for FCS1
CALPOW2 =             1.03E-13 / In-band power on detector for cal (Watts)
COMMENT **********************************************
COMMENT The selected FCS power was outside the calibrated range.
COMMENT **********************************************
RESPDEF =                    F / TRUE if default responsivity is used.
CALPOL2 =                   14 / Polarizer used for cal (CHW position)
CALTYP2 =                    2 / Type of processing for cal measurement
RS1P1F2 =            33.448296 / Responsivity (A/W) for first cal measurement
RU1P1F2 =             0.625224 / Uncertainty in responsivity for first cal
```

This warning is written to the header for all 9 separate observations in the sparse map. It is also written to the SPD product headers for the other two observations examined (TDTs 06507201 and 39200415).
In the original SCREW 351, reference was made to the message appearing in the Cal A header which has not been implemented. An SPR should be raised for V8.2.

5.5.5 Conclusions

- The special case of the sparse map with two different FCS powers had been overlooked in the implementation. Both powers must be checked. SPR 2644 was submitted and the provided fix worked.
- The warning message appears in the SPD product headers, if the check for a certain FCS power results in finding it outside the validated range.

5.6 Orbit Dependent Dark Current Subtraction for the PHT-S Spectrum of the Faint Star HR 6514

- authors: M. Radovich, U. Klaas
- date: 09-July-1998

5.6.1 Motivation

OLP7 has introduced the dark current subtraction from staring measurements which is orbit dependent. This includes PHT-S for which the strongest dark signal variations have been observed at the beginning of the science window when a memory of the relatively bright responsivity checks during activation mimics an increased dark current signal. The measurements of HR 6514 were performed repeatedly during revolution 57 in order to monitor the responsivity drifts of the detector. Since HR 6514 is a relatively faint star these measurements are very suitable to check for an improvement of the dark current subtraction including the orbit dependence. This was established from measurements taken on different revolutions and an improvement would demonstrate a general and hence reproducible behaviour of the PHT-S detectors.

5.6.2 References to Calibration Analysis and Software Change Documentation

- calibration report: Dependence of the Dark Signal with Orbital Position [11]
- Software Change Request: SCREW 336

5.6.3 Method

We plot the resulting fluxes of four measurements distributed over the revolution 57 both for OLP6 and OLP7 products and compare the homogeneity of the signals.

5.6.4 Results

Figs. 30 and 31 show the results both for OLP 6.x and OLP7.0b2 processing. The comparison by eye shows that

- the scatter in-between the data points is reduced. The third spectrum which shows a very poor quality for OLP 6.x processing (many points are set to zero due to the standard dark current subtraction) has been considerably improved by the OLP 7 processing.
- the spectra are closer to the expected fluxes provided by the composite of the stellar photospheric emission and the Zodiacal Light model. Inclusion of the latter one shows that the bent of the measured spectrum beyond 9 μm can be mainly explained by the background contribution.

5.6.5 Conclusions

Concerning the investigated test case, a relatively faint star on top of the Zodiacal background, a measurement which is very sensitive to background subtraction, the following results were obtained:

- the scatter in the data points is reduced with OLP7, and in some cases points, which were discarded (set to zero) due to negative signals after background subtraction previously, are recovered.
- more homogeneous spectra, also with regard to absolute accuracy, are achieved.

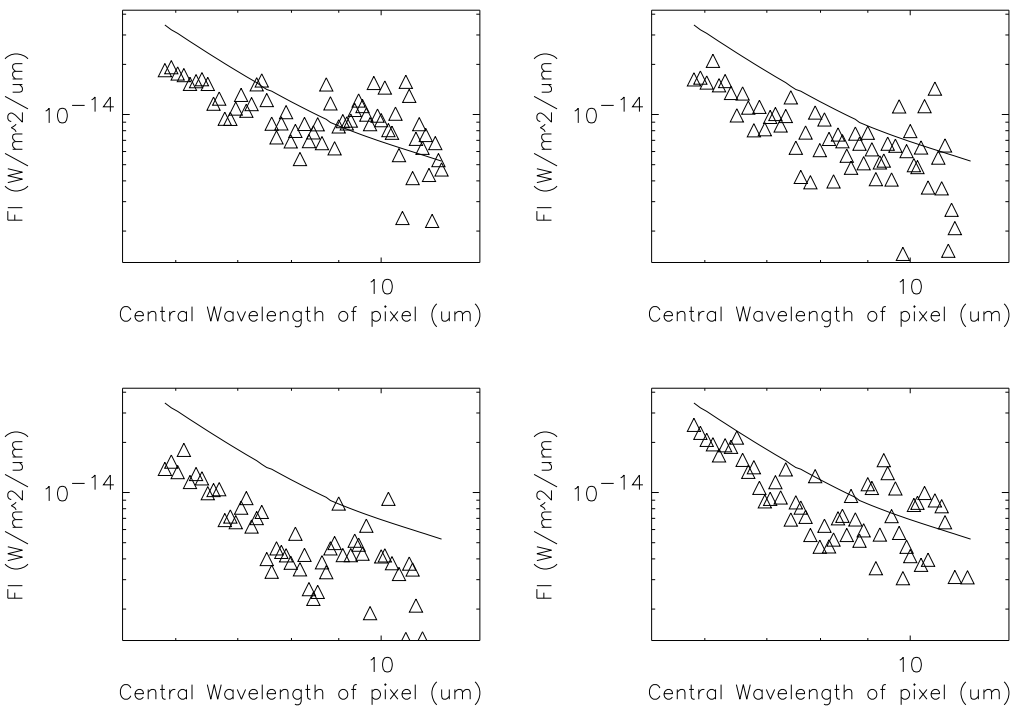

Figure 30: 4 PHT-S spectra (triangles) of the star HR6514 plus background obtained during revolution 57 and processed with OLP 6.x. The solid line gives a composite of the model of the HR 6514 photospheric emission (as provided by P. Hammersley but slightly smoothed) plus a model of the Zodical Light which becomes the dominant part of the spectrum beyond 9 μm. TDT05701101 (upper left) performed 8:03 h after perigee passage, TDT05702001 (upper right) performed 11:34 h after perigee passage, TDT05703101 (lower left) performed 16:19 h after perigee passage and TDT05704401 (lower right) performed 18:54 h after perigee passage.

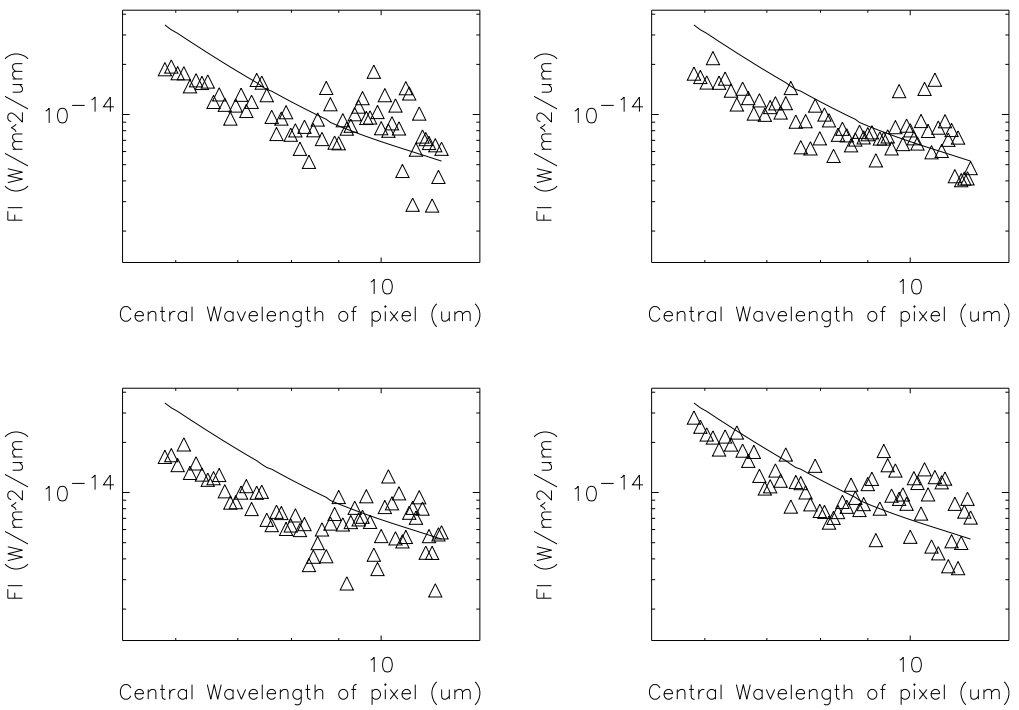

Figure 31: 4 PHT-S spectra (triangles) of the star HR6514 plus background obtained during revolution 57 and processed with OLP 7.0b2. The solid line gives a composite of the model of the HR 6514 photospheric emission (as provided by P. Hammersley but slightly smoothed) plus a model of the Zodical Light which becomes the dominant part of the spectrum beyond 9 μm. TDT05701101 (upper left) performed 8:03 h after perigee passage, TDT05702001 (upper right) performed 11:34 h after perigee passage, TDT05703101 (lower left) performed 16:19 h after perigee passage and TDT05704401 (lower right) performed 18:54 h after perigee passage.

5.7 Orbit Dependent Dark Current Subtraction for the Absolute Surface Brightness Photometry of the Earth Straylight Measurements

- authors: M. Radovich, U. Klaas
- date: 09-July-1998

5.7.1 Motivation

For the verification of the impact of the orbit dependent dark current subtraction on photometric results one needs a measurement repeated along the revolution on a not too bright source in order to see the proper dark current subtraction reflected in the homogeneity of the finally achieved fluxes. The Earth Straylight measurements performed on revolution 819 with the P2 detector in the 25 μm filter and on revolution 820 with the C200 detector in the 160 μm filter appear to form a suitable data set, though the total flux in the 180" aperture of the 25 μm filter is presumably already so high that the dark signal can be neglected.

5.7.2 References to Calibration Analysis and Software Change Documentation

- calibration report: Dependence of the Dark Signal with Orbital Position [11]
- Software Change Request: SCREW 336

5.7.3 Method

We can compare on two levels:

- As the set of Earth Straylight measurements contains an absolute photometry module with a direct dark current measurement, we can compare the measured dark current with the general prediction derived from the mission dark current data base. It has to be noted that the direct comparison between OLP6 and OLP7 in absolute terms is not possible, as the OLP6 did not contain the reset interval correction. Due to the reset interval correction, refering all signals to a 1/4 s reset interval, the dark signals measured with relatively long reset intervals of 8 s become negative for some detectors.
- We can investigate the scatter of the photometric results between OLP6 and OLP7 which are influenced by the dark current subtraction.

5.7.4 Results

Part 1 of Sect. 5.7.6 lists the measured dark signals on rev. 819 for P2 and on rev. 820 for C200, respectively. On rev. 819 the P2 detector shows the same trend as predicted by the mission dark data base, namely a steady increase by some 50%. The absolute level of the measured dark signals is about 10% lower than the average one determined from all dark measurements obtained during the mission. For rev. 820 the C200 detector shows a somewhat different trend behaviour than predicted by the general cal-G file. While there is nearly no difference in dark signal between the first two measurements, there is a drastic increase towards the last one (small negative values!). On the other hand the absolute level of the first two measurements is within 10-20% of the prediction.
Part 2 of Sect. 5.7.6 lists the measured surface brightness values for the Earth Straylight target position as monitored along the revolution. COBE fluxes are 30 MJy sr^{-1} for 25 μm and 3.5 MJy sr^{-1} for 170 micron, respectively. The comparison with COBE shows the improvement w.r.t. OLP 6 by the upgraded C200 solid angles (for P2 no changes in solid angles are implemented yet).
We did various statistical analyses to assess the scatter among the measurement sets taken at approximately the same orbit position but evaluated with different dark current subtraction methods (for the first absolute photometric measurement the measured dark current is subtracted, while for the standard photometric mode and the second absolute photometric measurement the average orbit dependent dark current is subtracted. The average values, their standard deviation and the relative scatter are given in the following tables Tab. 14 to 16.

For P2 the reproducibility of the flux per measurement set with the different AOT modes is remarkably good. The OLP 6.x version shows slightly better results here, but the relative scatter for OLP 7 is still below 2%. For C200 where the background is relatively fainter the OLP7 version gives improved results and reduces the maximum scatter from 12% to 8%. The consistency between the absolute measurements alone is even better and OLP 6.x and 7 results are quite similar so that an impact by the dark current subtraction method is hard to see. At 25 μm no big effect should be expected, as the total flux through the 180" aperture is already quite high. Also the scatter of the three measurements along the revolution is comparable for OLPs 6.x and 7. In case of a significant level of Earth Straylight some variation of the total surface brightness along the revolution would be expected introducing a systematic scatter. While P2 shows the expected downward trend (which could be an insufficient responsivity correction, too), C200 shows an unexpected upward trend which must be attributed to responsivity changes. It is beyond the scope of this report to derive accurate numbers for an assessment of the Earth Straylight - this must be done by careful interactive analysis -, however, it is worthwhile to note that the flux reproducibility of these carefully designed measurements is remarkably good for an automatic processing.

Table 14: Relative consistency of fluxes of all 3 measurements of the set P05-P03-P05 and P25-P22-P25 for the three orbit positions. $\bar{B}$ is the average flux, s_{B} is the standard deviation, $\Delta\, B/B$ the relative scatter

TDT	**OLP V6.x**			**OLP V7.0**		
	$\bar{B}$ [MJysr^{-1}]	s_{B} [MJysr^{-1}]	$\Delta\, B/B$ [%]	$\bar{B}$ [MJysr^{-1}]	s_{B} [MJysr^{-1}]	$\Delta\, B/B$ [%]
819003..	35.893	0.249	0.7	36.751	0.654	1.8
819017..	35.645	0.133	0.4	36.531	0.569	1.6
819022..	35.556	0.183	0.5	36.452	0.266	0.7
820003..	6.099	0.468	7.7	4.369	0.131	3.0
820010..	6.236	0.766	12.3	4.416	0.346	7.8
820016..	6.812	0.741	10.9	4.817	0.264	5.5

Table 15: Relative Consistency of fluxes of the two bracketing absolute measurements of the set P05-P03-P05 and P25-P22-P25 for the three orbit positions. $\bar{B}$ is the average flux, s_{B} is the standard deviation, $\Delta\, B/B$ the relative scatter

TDT	**OLP V6.x**			**OLP V7.0**		
	$\bar{B}$ [MJysr^{-1}]	s_{B} [MJysr^{-1}]	$\Delta\, B/B$ [%]	$\bar{B}$ [MJysr^{-1}]	s_{B} [MJysr^{-1}]	$\Delta\, B/B$ [%]
819003..	35.768	0.170	0.5	36.381	0.175	0.5
819017..	35.587	0.124	0.3	36.213	0.196	0.5
819022..	35.662	0.019	0.1	36.300	0.055	0.2
820003..	5.844	0.209	3.6	4.338	0.168	3.9
820010..	5.826	0.404	6.9	4.293	0.385	9.0
820016..	6.384	0.008	0.1	4.667	0.067	1.4

5.7.5 Conclusions

- The extra dark measurements of the Earth Straylight obsercations on rev. 819 and 820 show that for P2 the general orbit dependent modelling of the dark current fits within 10% for a randomly selected revolution, while for C200 a significantly different trend behaviour is observed, although the dark signal levels of the first two measurements are matched within 20% by the orbit dependent average dark current.

Table 16: Relative scatter of fluxes of the three long exposures along the revolution. $\bar{B}$ is the average flux, s_{B} is the standard deviation, $\Delta B/B$ the relative scatter

filter	OLP V6.x			OLP V7.0		
	$\bar{B}$ [MJysr^{-1}]	s_{B} [MJysr^{-1}]	$\Delta B/B$ [%]	$\bar{B}$ [MJysr^{-1}]	s_{B} [MJysr^{-1}]	$\Delta B/B$ [%]
P2_25	35.750	0.399	1.1	37.139	0.369	1.0
C200_160	7.112	0.530	7.4	4.737	0.348	7.4

- The orbit dependent dark current subtraction seems to work properly without any negative side effect, however, for the specific test case no significant improvement, which is unambiguously related to the orbit dependent dark current subtraction, could be demonstrated.

5.7.6 Evaluation Log

```
1) Dark Currents measured as part of the absolute photometric measurements
   P05 and P25 versus the prediction from the orbit dependent dark current
   modelling (based on ca. 70 calibration measurements performed during the
   whole mission). The orbit position measure orb_pos is in units of 0.24 h.

TDT       Start                orb_pos       Dark current (V/s)
                                         Tabulated   OLP6       OLP7

P2_25
81900301  11-Feb-1998 10:33:06     20 0.0060880  0.00877    0.005233
81901705  11-Feb-1998 19:06:45     56 0.0082174  0.01147    0.007739
81902209  12-Feb-1998 01:09:13     81 0.0088658  0.01198    0.008211



C2_160

82000313  12-Feb-1998 10:28:03     20  -0.0128944  0.00342   -0.010670   1
                                       -0.0119500  0.00284   -0.011502   2
                                       -0.0123935  0.00409   -0.009702   3
                                       -0.0128756  0.00363   -0.010367   4

82001018  12-Feb-1998 19:22:22     57  -0.0108251  0.00406   -0.009756   1
                                       -0.0101290  0.00369   -0.010285   2
                                       -0.0108749  0.00345   -0.010898   3
                                       -0.0111490  0.00343   -0.010648   4

82001621  13-Feb-1998 01:09:58     81  -0.0094383 -0.00088   -0.001017   1
                                       -0.0092742  0.00695   -0.005604   2
                                       -0.0097802  0.00767   -0.004564   3
                                       -0.0101602  0.00626   -0.006590   4


2) Surface Brightness for the Earth Straylight Target position as measured
   on 3 positions on the revolution (with different illumiantion angles of
   the inner sun shade by the Earth) with a set of absolute photometry -
   long exposure single filter photometry - absolute photometry. The first
   absolute photometric measurement contains a direct dark signal measurement.

TDT           Detector     cwl    Surf Brigth (MJy/sr)
                               OLP 6   OLP 7

pcae82000313  C200_160_UM  170.    5.695   4.219
```

```
pcae82000314  C200_160_UM  170.    6.612   4.432
pcae82000315  C200_160_UM  170.    5.991   4.456

pcae82001018  C200_160_UM  170.    5.540   4.021
pcae82001019  C200_160_UM  170.    7.056   4.663
pcae82001020  C200_160_UM  170.    6.112   4.565

pcae82001621  C200_160_UM  170.    6.390   4.619
pcae82001622  C200_160_UM  170.    7.667   5.117
pcae82001623  C200_160_UM  170.    6.378   4.714

ppae81900301  P2_25_UM      25.   35.647  36.257
ppae81900302  P2_25_UM      25.   36.144  37.493
ppae81900303  P2_25_UM      25.   35.888  36.504

ppae81901705  P2_25_UM      25.   35.499  36.074
ppae81901706  P2_25_UM      25.   35.760  37.168
ppae81901707  P2_25_UM      25.   35.675  36.351

ppae81902209  P2_25_UM      25.   35.675  36.261
ppae81902210  P2_25_UM      25.   35.346  36.756
ppae81902211  P2_25_UM      25.   35.648  36.339
```

5.8 PHT Photometry Color Correction Factors

- authors: U. Klaas, Th. Müller, R. Laureijs
- date: 12-May-1998

5.8.1 Motivation

In commonality with IRAS the ISOPHOT flux densities as provided in the OLP AAR data products assume a constant spectrum per logarithmic frequency interval, i.e. $\nu * F_\nu = \text{const.}$ or $F_\nu \propto \nu^{-1}$. For other SEDs sometimes significant correction factors ($\sim$ 50%) for the relative contribution of the flux density at the quoted reference wavelength to the inband power have to be applied. These color correction factors are available with CAL-G Version 4.0 associated with OLP V7.0. While they will not be applied by OLP but are a self-standing calibration item, they are also available in the PIA package, and there color corrected flux densities can be derived.

5.8.2 References to Calibration Analysis and Software Change Documentation

- calibration report: Flux Conversion and Colour Corrections for ISOPHOT P and C Filters [7]
- Software Change Request: SCREW 333

5.8.3 Method

There are various approaches to check the validity of the color correction factors:

- Two independent programs (one based on FORTRAN and one in the IDL environment) with different integration methods have been developed and the results of both are compared to each other.
- The IRAS relative system responses as provided in the IRAS Explanatory Supplement have been run through both programs and results are compared to the color correction tables given in the IRAS Explanatory Supplement.
- The ASCII versions of the CAL-G files are checked against the computation program output for all entries.
- Individual color correction values have been used for comparison of the ISOPHOT fluxes with models in many sections of this report.

5.8.4 Results

Concerning the steps outlined in the previous section, the following results have been achieved:

- Both program approaches agree now in their results. A two coarse interpolation in the IDL routine has been corrected for, which led to the update of some correction factors in the power law table. Both programs refer to the same input data files. There are some slight discrepancies in the values for the convolution of the Wien branches of cold bodies (below 200 K) with the short wavelength filters of P1 where the correction factors become very large. These discrepancies are caused by the different integration methods. A caveat on the limitation of the current color correction factors has been placed in the caveat section.
- The results of both programs for the IRAS band passes compare well to the numbers published in the Explanatory Supplement. For extreme spectra (very hot BB, very steep power laws) both programs show some discrepancy with the published results for the 12 micron IRAS filter. This could be due to a finer data grid used by the IRAS Science Team and not published in the IRAS Explanatory Supplement.
- The practical use of these correction factors has not shown any unrealistic number.

5.8.5 Final Color Correction Values for CAL-G V4.0

```
; ************************************************************************
;
; ISOPHOT colour correction table for power law functions
;
; ************************************************************************
;
alpha   -3.0  -2.0  -1.0   0.0   1.0   2.0   3.0
P1_3.29  1.00  1.00  1.00  1.00  1.00  1.00  1.00
P1_3.60  0.99  0.99  1.00  1.02  1.04  1.07  1.11
P1_4.85  1.02  1.00  1.00  1.01  1.02  1.04  1.08
P1_7.30  1.01  1.00  1.00  1.02  1.07  1.14  1.23
P1_7.70  0.99  0.99  1.00  1.01  1.02  1.02  1.03
P1_10.0  1.00  1.00  1.00  1.01  1.01  1.03  1.04
P1_11.3  1.01  1.00  1.00  1.00  0.99  0.99  0.99
P1_11.5  0.96  0.97  1.00  1.07  1.17  1.33  1.54
P1_12.8  1.00  1.00  1.00  1.00  1.01  1.02  1.03
P1_16.0  1.02  1.01  1.00  1.00  0.99  0.99  1.00
P2_20    1.09  1.03  1.00  0.99  0.99  1.01  1.06
P2_25    0.90  0.94  1.00  1.08  1.17  1.29  1.43
P3_60    1.01  1.00  1.00  1.02  1.07  1.14  1.24
P3_100   1.04  1.01  1.00  1.00  1.02  1.05  1.10
C1_50    1.06  1.00  1.00  1.05  1.15  1.29  1.50
C1_60    1.04  1.01  1.00  1.00  1.02  1.06  1.13
C1_70    0.99  0.98  1.00  1.05  1.12  1.23  1.38
C1_90    1.09  1.03  1.00  1.01  1.06  1.17  1.34
C1_100   1.03  1.01  1.00  1.01  1.05  1.10  1.19
C1_105   1.03  1.01  1.00  1.00  1.02  1.05  1.10
C2_120   0.96  0.97  1.00  1.05  1.12  1.22  1.35
C2_135   1.05  1.01  1.00  1.01  1.04  1.10  1.18
C2_160   1.00  0.99  1.00  1.04  1.10  1.20  1.36
C2_180   1.00  0.99  1.00  1.02  1.05  1.10  1.17
C2_200   1.02  1.00  1.00  1.00  1.01  1.03  1.06


; ************************************************************************
;
; ISOPHOT colour correction table for Black-body type functions
;
; ************************************************************************
;
 T      10000  5000  4000  3000  2000  1000   800   600   500   400   300
          250   220   200   180   160   140   120   100    80    60    50
           40    30    20    15    10
P1_3.29  1.00  1.00  1.00  1.00  1.00  1.00  1.00  1.01  1.01  1.02  1.04
         1.06  1.08  1.10  1.14  1.19  1.29  1.52  2.22   10    10    10
          10    10    10    10    10
P1_3.60  1.06  1.05  1.05  1.04  1.03  0.99  0.98  0.97  0.98  1.01  1.12
         1.25  1.40  1.55  1.78  2.15  2.81  4.13  7.50   10    10    10
          10    10    10    10    10
P1_4.85  1.04  1.03  1.03  1.03  1.02  0.99  0.99  0.98  0.99  1.01  1.10
         1.22  1.35  1.48  1.69  2.03  2.66  3.99  7.87   10    10    10
          10    10    10    10    10
P1_7.30  1.13  1.12  1.11  1.10  1.09  1.04  1.01  0.98  0.97  0.95  0.97
         1.01  1.07  1.13  1.23  1.38  1.65  2.14  3.23  6.41   10    10
          10    10    10    10    10
P1_7.70  1.02  1.02  1.02  1.02  1.02  1.01  1.01  1.00  1.00  0.99  0.99
         0.98  0.98  0.98  0.97  0.97  0.98  0.98  1.00  1.05  1.19  1.38
         1.91   10    10    10    10
P1_10.0  1.02  1.02  1.02  1.02  1.02  1.01  1.01  1.01  1.00  1.00  0.99
         0.99  0.99  0.99  1.00  1.00  1.02  1.04  1.09  1.20  1.51  1.93
         2.95   10    10    10    10
```

```
P1_11.3  0.99  0.99  0.99  0.99  0.99  0.99  0.99  0.99  1.00  1.00  1.00
         1.00  1.01  1.01  1.01  1.02  1.02  1.03  1.05  1.08  1.14  1.21
         1.34   10    10    10    10
P1_11.5  1.31  1.30  1.29  1.28  1.26  1.19  1.15  1.10  1.06  1.00  0.94
         0.91  0.89  0.89  0.89  0.91  0.95  1.04  1.23  1.68  3.19  5.69
          10    10    10    10    10
P1_12.8  1.02  1.02  1.02  1.02  1.02  1.01  1.01  1.01  1.00  1.00  1.00
         0.99  0.99  0.99  0.99  1.00  1.00  1.01  1.04  1.09  1.24  1.42
         1.81  3.01   10    10    10
P1_16.0  0.99  0.99  0.99  0.99  0.99  0.99  0.99  0.99  0.99  0.99  0.99
         1.00  1.00  1.00  1.00  1.01  1.02  1.04  1.07  1.13  1.29  1.48
         1.92  3.33   10    10    10    10
P2_20    1.01  1.01  1.01  1.01  1.01  1.00  0.99  0.99  0.98  0.97  0.97
         0.96  0.96  0.96  0.97  0.98  1.00  1.03  1.10  1.26  1.70  2.24
         3.59  8.68   10    10    10
P2_25    1.29  1.28  1.28  1.28  1.27  1.24  1.23  1.21  1.20  1.17  1.13
         1.09  1.07  1.05  1.02  0.99  0.96  0.92  0.87  0.82  0.79  0.80
         0.86  1.14   10    10    10
P3_60    1.13  1.13  1.13  1.13  1.13  1.12  1.12  1.11  1.11  1.10  1.09
         1.08  1.08  1.07  1.06  1.05  1.04  1.03  1.01  0.99  0.96  0.96
         0.97  1.03  1.32  1.86  4.42
P3_100   1.05  1.05  1.05  1.05  1.05  1.05  1.05  1.05  1.05  1.04  1.04
         1.04  1.04  1.03  1.03  1.03  1.03  1.02  1.01  1.01  0.99  0.98
         0.98  0.98  1.03  1.17  1.73
C1_50    1.29  1.29  1.29  1.29  1.28  1.27  1.27  1.26  1.25  1.23  1.21
         1.20  1.18  1.17  1.16  1.14  1.12  1.09  1.05  1.00  0.93  0.90
         0.89  0.97  1.75  4.80   10
C1_60    1.06  1.06  1.06  1.06  1.06  1.06  1.05  1.05  1.05  1.04  1.04
         1.03  1.03  1.02  1.02  1.01  1.01  1.00  0.99  0.98  0.97  0.98
         1.00  1.09  1.44  2.10  5.34
C1_70    1.23  1.23  1.23  1.23  1.23  1.22  1.21  1.21  1.20  1.20  1.18
         1.17  1.17  1.16  1.15  1.14  1.13  1.11  1.09  1.05  1.00  0.97
         0.93  0.92  1.04  1.44  4.51
C1_90    1.17  1.17  1.16  1.16  1.16  1.15  1.15  1.15  1.14  1.13  1.12
         1.11  1.10  1.10  1.09  1.08  1.07  1.05  1.03  1.00  0.97  0.95
         0.94  0.96  1.16  1.59  3.87
C1_100   1.10  1.10  1.10  1.10  1.10  1.10  1.09  1.09  1.09  1.09  1.08
         1.08  1.07  1.07  1.07  1.06  1.06  1.05  1.04  1.02  1.00  0.99
         0.97  0.96  1.02  1.17  1.89
C1_105   1.05  1.05  1.05  1.05  1.05  1.05  1.05  1.05  1.05  1.05  1.04
         1.04  1.04  1.03  1.03  1.03  1.03  1.02  1.02  1.01  1.00  0.99
         0.98  0.98  1.02  1.11  1.50
C2_120   1.21  1.21  1.21  1.21  1.21  1.21  1.21  1.20  1.20  1.19  1.19
         1.18  1.18  1.17  1.17  1.16  1.15  1.14  1.13  1.10  1.07  1.04
         1.01  0.96  0.92  0.94  1.10
C2_135   1.10  1.10  1.10  1.10  1.10  1.09  1.09  1.09  1.09  1.09  1.08
         1.08  1.08  1.08  1.07  1.07  1.07  1.06  1.06  1.05  1.03  1.02
         1.00  0.98  0.96  0.99  1.22
C2_160   1.20  1.20  1.20  1.20  1.20  1.20  1.20  1.19  1.19  1.19  1.18
         1.18  1.18  1.17  1.17  1.16  1.16  1.15  1.14  1.12  1.09  1.07
         1.04  1.00  0.95  0.94  1.04
C2_180   1.10  1.10  1.10  1.10  1.10  1.10  1.10  1.10  1.10  1.09  1.09
         1.09  1.09  1.09  1.09  1.08  1.08  1.08  1.07  1.07  1.05  1.04
         1.03  1.01  0.98  0.96  1.00
C2_200   1.03  1.03  1.03  1.03  1.03  1.03  1.03  1.03  1.03  1.03  1.03
         1.03  1.03  1.03  1.02  1.02  1.02  1.02  1.02  1.02  1.01  1.01
         1.01  1.00  0.99  0.99  1.01


; ***************************************************************************
;
; ISOPHOT colour correction table for modified Black-body type functions
; with an emissivity law proportional to nu^1 (or lambda^-1)
;
```

```
; ************************************************************************
;
 T        10000  5000   4000   3000   2000   1000   800    600    500    400
            300   250    220    200    180    160   140    120    100     80
             60    50     40     30     20     15    10
P1_3.29   1.000  1.000  1.000  0.999  0.999  0.998  0.998  0.999  1.001  1.005
          1.018  1.034  1.050  1.067  1.093  1.134  1.207  1.365  1.828  10.
          10.    10.    10.    10.    10.    10.    10.
P1_3.60   1.202  1.186  1.178  1.163  1.134  1.052  1.020  0.982  0.965  0.962
          1.008  1.092  1.192  1.300  1.466  1.737  2.216  3.181  5.595  10.
          10.    10.    10.    10.    10.    10.    10.
P1_4.85   1.161  1.151  1.145  1.135  1.116  1.057  1.031  0.998  0.980  0.969
          0.991  1.047  1.119  1.200  1.328  1.542  1.930  2.747  4.954  10.
          10.    10.    10.    10.    10.    10.    10.
P1_7.30   1.498  1.477  1.466  1.447  1.408  1.288  1.231  1.145  1.086  1.016
          0.946  0.927  0.933  0.951  0.991  1.067  1.210  1.497  2.146  4.040
          13.44  38.23  10.    10.    10.    10.    10.
P1_7.70   1.056  1.054  1.053  1.052  1.050  1.041  1.037  1.029  1.023  1.015
          1.002  0.993  0.987  0.983  0.979  0.975  0.973  0.974  0.983  1.015
          1.124  1.275  10.    10.    10.    10.    10.
P1_10.0   1.075  1.073  1.072  1.070  1.067  1.056  1.051  1.041  1.034  1.024
          1.008  0.999  0.993  0.989  0.986  0.985  0.988  0.998  1.026  1.099
          1.323  1.629  10.    10.    10.    10.    10.
P1_11.3   0.984  0.984  0.984  0.984  0.984  0.985  0.985  0.986  0.986  0.988
          0.990  0.992  0.994  0.996  0.999  1.002  1.007  1.015  1.028  1.051
          1.103  1.159  10.    10.    10.    10.    10.
P1_11.5   2.221  2.186  2.168  2.138  2.077  1.891  1.798  1.651  1.541  1.393
          1.195  1.078  1.006  0.959  0.916  0.881  0.862  0.873  0.948  1.190
          2.064  3.521  10.    10.    10.    10.    10.
P1_12.8   1.065  1.064  1.063  1.062  1.060  1.053  1.049  1.042  1.037  1.029
          1.017  1.009  1.003  0.999  0.994  0.990  0.988  0.989  0.998  1.029
          1.131  1.263  1.568  2.496  10.    10.    10.
P1_16.0   1.010  1.010  1.009  1.009  1.008  1.005  1.004  1.001  0.999  0.996
          0.992  0.989  0.988  0.987  0.987  0.987  0.990  0.996  1.011  1.048
          1.155  1.290  1.607  2.636  10.    10.    10.
P2_20     1.224  1.219  1.217  1.213  1.204  1.178  1.164  1.142  1.124  1.097
          1.055  1.025  1.003  0.987  0.970  0.953  0.939  0.931  0.942  1.004
          1.228  1.540  2.330  5.289  10.    10.    10.
P2_25     1.824  1.816  1.812  1.805  1.792  1.749  1.727  1.690  1.659  1.613
          1.534  1.472  1.423  1.383  1.336  1.280  1.213  1.133  1.039  0.931
          0.821  0.781  0.782  0.927  10.    10.    10.
P3_60     1.583  1.579  1.578  1.575  1.569  1.552  1.544  1.529  1.517  1.499
          1.469  1.445  1.425  1.408  1.388  1.363  1.331  1.290  1.236  1.164
          1.068  1.012  0.959  0.935  1.060  1.396  3.059
P3_100    1.266  1.265  1.264  1.264  1.262  1.258  1.255  1.252  1.249  1.244
          1.236  1.229  1.224  1.220  1.214  1.207  1.198  1.186  1.169  1.144
          1.104  1.074  1.036  0.988  0.954  0.994  1.291
C1_50     2.154  2.148  2.145  2.141  2.131  2.102  2.088  2.063  2.043  2.013
          1.962  1.920  1.886  1.858  1.823  1.780  1.725  1.652  1.555  1.420
          1.228  1.106  0.970  0.848  0.941  1.736  16.11
C1_60     1.351  1.349  1.348  1.346  1.342  1.331  1.325  1.316  1.308  1.296
          1.277  1.261  1.248  1.237  1.224  1.207  1.186  1.159  1.124  1.076
          1.014  0.979  0.951  0.957  1.131  1.537  3.587
C1_70     1.854  1.851  1.849  1.847  1.841  1.824  1.816  1.802  1.790  1.773
          1.743  1.719  1.700  1.683  1.663  1.637  1.605  1.562  1.502  1.417
          1.288  1.199  1.089  0.964  0.881  0.987  2.163
C1_90     1.993  1.989  1.986  1.982  1.974  1.950  1.938  1.918  1.901  1.876
          1.835  1.802  1.774  1.752  1.724  1.690  1.647  1.590  1.513  1.406
          1.253  1.153  1.040  0.930  0.907  1.073  2.119
C1_100    1.460  1.459  1.458  1.456  1.454  1.446  1.442  1.435  1.430  1.422
          1.408  1.397  1.388  1.380  1.370  1.358  1.343  1.323  1.294  1.252
          1.185  1.137  1.075  0.999  0.938  0.972  1.320
C1_105    1.266  1.266  1.265  1.264  1.263  1.258  1.256  1.252  1.249  1.245
          1.237  1.230  1.225  1.221  1.215  1.208  1.200  1.188  1.171  1.147
```

```
         1.108  1.079  1.042  0.996  0.960  0.984  1.192
C2_120   1.790  1.788  1.787  1.786  1.782  1.772  1.767  1.758  1.751  1.740
         1.722  1.707  1.695  1.685  1.673  1.657  1.637  1.610  1.572  1.515
         1.424  1.356  1.263  1.136  0.978  0.913  0.949
C2_135   1.446  1.445  1.444  1.443  1.442  1.437  1.434  1.430  1.426  1.421
         1.412  1.405  1.399  1.394  1.388  1.381  1.371  1.357  1.339  1.311
         1.265  1.229  1.179  1.104  0.997  0.943  0.967
C2_160   1.866  1.864  1.863  1.862  1.859  1.850  1.846  1.838  1.832  1.823
         1.807  1.795  1.785  1.776  1.766  1.753  1.735  1.713  1.681  1.632
         1.553  1.492  1.404  1.274  1.083  0.971  0.908
C2_180   1.362  1.362  1.361  1.361  1.360  1.357  1.356  1.353  1.351  1.348
         1.343  1.339  1.336  1.333  1.330  1.326  1.320  1.313  1.302  1.286
         1.258  1.236  1.203  1.151  1.064  1.002  0.948
C2_200   1.141  1.141  1.141  1.141  1.140  1.139  1.139  1.138  1.137  1.136
         1.133  1.132  1.130  1.129  1.128  1.126  1.124  1.121  1.116  1.110
         1.099  1.090  1.077  1.057  1.022  0.997  0.976


 ************************************************************************
;
; ISOPHOT colour correction table for modified Black-body type functions
; with an emissivity law proportional to nu^2 (or lambda^-2)
;
; ************************************************************************
;
 T       10000  5000   4000   3000   2000   1000   800    600    500    400
           300   250    220    200    180    160   140    120    100     80
            60    50     40     30     20     15    10
P1_3.29  1.002  1.001  1.001  1.001  1.000  0.998  0.997  0.998  0.999  1.003
         1.014  1.027  1.042  1.058  1.081  1.118  1.185  1.325  1.731  10.
         10.    10.    10.    10.    10.    10.    10.
P1_3.60  1.269  1.250  1.240  1.223  1.188  1.089  1.049  0.998  0.973  0.957
         0.985  1.053  1.139  1.234  1.382  1.625  2.057  2.927  5.093  10.
         10.    10.    10.    10.    10.    10.    10.
P1_4.85  1.224  1.211  1.204  1.193  1.169  1.097  1.065  1.020  0.994  0.970
         0.972  1.010  1.067  1.133  1.241  1.423  1.756  2.454  4.310  10.
         10.    10.    10.    10.    10.    10.    10.
P1_7.30  1.700  1.672  1.658  1.634  1.585  1.433  1.360  1.249  1.171  1.077
         0.972  0.930  0.919  0.923  0.946  1.000  1.113  1.348  1.892  3.487
         11.36  31.98  10.    10.    10.    10.    10.
P1_7.70  1.069  1.067  1.066  1.065  1.062  1.053  1.048  1.040  1.034  1.024
         1.010  1.000  0.993  0.988  0.983  0.978  0.974  0.972  0.979  1.006
         1.105  1.245  10.    10.    10.    10.    10.
P1_10.0  1.098  1.096  1.095  1.093  1.089  1.077  1.071  1.060  1.051  1.038
         1.020  1.008  0.999  0.999  0.989  0.985  0.984  0.990  1.011  1.073
         1.273  1.549  10.    10.    10.    10.    10.
P1_11.3  0.983  0.983  0.983  0.983  0.983  0.983  0.983  0.984  0.984  0.985
         0.987  0.989  0.991  0.993  0.995  0.998  1.003  1.010  1.021  1.043
         1.091  1.144  10.    10.    10.    10.    10.
P1_11.5  2.774  2.726  2.701  2.660  2.577  2.322  2.196  1.994  1.843  1.641
         1.369  1.206  1.103  1.035  0.970  0.912  0.868  0.852  0.894  1.081
         1.806  3.024  10.    10.    10.    10.    10.
P1_12.8  1.087  1.085  1.085  1.083  1.081  1.072  1.068  1.060  1.054  1.045
         1.030  1.019  1.012  1.006  1.000  0.994  0.989  0.986  0.991  1.014
         1.102  1.221  1.500  2.351  10.    10.    10.
P1_16.0  1.021  1.020  1.020  1.019  1.018  1.014  1.012  1.009  1.007  1.003
         0.997  0.993  0.990  0.988  0.986  0.985  0.986  0.989  0.999  1.029
         1.120  1.239  1.523  2.449  10.    10.    10.
P2_20    1.356  1.349  1.346  1.341  1.330  1.295  1.277  1.247  1.223  1.187
         1.130  1.089  1.058  1.034  1.009  0.982  0.955  0.932  0.923  0.955
         1.125  1.380  2.039  4.514  10.    10.    10.
P2_25    2.090  2.080  2.075  2.067  2.050  1.998  1.972  1.926  1.888  1.831
         1.735  1.660  1.599  1.550  1.493  1.424  1.342  1.244  1.128  0.994
         0.852  0.793  0.771  0.878  10.    10.    10.
```

P3_60	1.856	1.852	1.850	1.846	1.838	1.815	1.803	1.783	1.767	1.743
	1.702	1.669	1.642	1.619	1.592	1.558	1.514	1.459	1.385	1.285
	1.151	1.071	0.990	0.930	1.004	1.282	2.720			
P3_100	1.387	1.386	1.386	1.385	1.383	1.377	1.374	1.369	1.365	1.359
	1.349	1.341	1.334	1.328	1.321	1.312	1.300	1.285	1.263	1.230
	1.178	1.139	1.087	1.019	0.952	0.963	1.193			
C1_50	2.656	2.648	2.645	2.638	2.626	2.587	2.567	2.534	2.508	2.467
	2.399	2.343	2.298	2.260	2.213	2.156	2.082	1.986	1.856	1.676
	1.421	1.257	1.070	0.883	0.848	1.344	10.38			
C1_60	1.529	1.526	1.525	1.523	1.518	1.503	1.495	1.482	1.472	1.456
	1.429	1.408	1.390	1.375	1.357	1.335	1.307	1.270	1.221	1.155
	1.067	1.014	0.964	0.939	1.061	1.399	3.160			
C1_70	2.215	2.210	2.208	2.205	2.197	2.175	2.163	2.144	2.129	2.106
	2.066	2.034	2.008	1.986	1.959	1.925	1.882	1.824	1.746	1.632
	1.462	1.344	1.198	1.027	0.877	0.917	1.765			
C1_90	2.585	2.578	2.574	2.568	2.556	2.520	2.502	2.471	2.446	2.409
	2.347	2.298	2.257	2.223	2.182	2.131	2.066	1.981	1.867	1.708
	1.480	1.331	1.160	0.982	0.878	0.976	1.782			
C1_100	1.673	1.671	1.670	1.668	1.665	1.654	1.649	1.640	1.633	1.622
	1.604	1.589	1.576	1.566	1.553	1.537	1.517	1.489	1.451	1.395
	1.306	1.241	1.157	1.050	0.942	0.940	1.200			
C1_105	1.394	1.393	1.392	1.391	1.389	1.384	1.381	1.376	1.372	1.365
	1.355	1.347	1.340	1.334	1.327	1.318	1.306	1.290	1.268	1.236
	1.184	1.145	1.094	1.028	0.961	0.962	1.122			
C2_120	2.130	2.127	2.126	2.123	2.119	2.105	2.098	2.086	2.076	2.062
	2.038	2.018	2.002	1.988	1.971	1.950	1.923	1.887	1.835	1.759
	1.637	1.545	1.420	1.249	1.031	0.928	0.919			
C2_135	1.656	1.654	1.654	1.653	1.650	1.643	1.640	1.634	1.629	1.622
	1.610	1.600	1.592	1.586	1.577	1.567	1.554	1.536	1.510	1.473
	1.410	1.363	1.295	1.195	1.048	0.962	0.932			
C2_160	2.284	2.281	2.280	2.278	2.274	2.261	2.255	2.244	2.236	2.223
	2.202	2.184	2.170	2.158	2.143	2.125	2.101	2.069	2.024	1.957
	1.846	1.761	1.639	1.459	1.191	1.027	0.901			
C2_180	1.503	1.502	1.502	1.501	1.500	1.497	1.495	1.492	1.489	1.486
	1.479	1.474	1.470	1.466	1.462	1.457	1.450	1.440	1.427	1.406
	1.371	1.343	1.302	1.235	1.122	1.039	0.953			
C2_200	1.208	1.207	1.207	1.207	1.206	1.205	1.204	1.202	1.201	1.200
	1.197	1.195	1.193	1.191	1.189	1.187	1.184	1.179	1.173	1.165
	1.150	1.138	1.121	1.094	1.048	1.014	0.977			

5.9 Converting PHT OLP to Run on the DEC Alpha Platform

- authors: P. Richards, H. Morris, L. Cornwall, U. Klaas
- date: 06-May-1998

5.9.1 Motivation

With the start of the ISO Post Mission Phase and the build-up of the Post Mission Archive it was decided to move from the VAX platforms to the DEC Alphas/Open VMS in order to improve processing power and enable On-the-Fly Re-Processing. This meant that the software had to be checked for VAX specific features and to be adapted to the Alpha requirements. Beside the PHT specific software also the general software, in particular the so-called MC package, had to be adapted to the new hardware platform.

5.9.2 Summary of Software Changes for Port to Alpha Platform

In general the required changes for PHT software can be grouped into the following areas:

1) format items ⇒ SCREW 334, SCREW 342, SCREW 349
2) compilation flags ⇒ SCREW 334, SCREW 349
3) modification of archive configuration table (ACT) ⇒ SPR 2525, SPR 2544, SPR 2609

The software changes and affected modules are described in detail in the following SCREWs and SPRs:

Table 17: Change Record for OLP 7 Port to Alpha Platform

Title	**SPR**	**SCREW**
Converting PHT OLP to run on the DEC Alpha platform		334
Porting non-instrument specific OLP software modules to Alpha		342
Port OLP onto Alpha / OpenVMS, issue of compilation flags		349
SPP failure during OLP v7.0b1 integration	2525	
OLP 7.0 beta wrong record length of PPSF in ACT	2544	
ACT discrepancies for PHT Cal G files	2609	

5.9.3 Results

In particular the modifications to the archive configuration table (ACT) were not considered in the beginning which caused OLP crashes and bad data products. It should be noted that the requirement for the /D_FLOAT compilation flag in SCREW 334 was superseded by the requirement for the /G_FLOAT flag in SCREW 349. From OLP V7.0b2 on the transfer to the Alpha platform was successfully completed.
In the context of the move to Alpha the PIDT test environment was successfully ported to an Alpha platform and upgraded modules could be tested there under the same environment as the operational version. The description and documentation of this test environment which will be the basis for future OLP improvement check-outs at the RAL UK National ISO Data Centre is outside the scope of this document and will be described elsewhere.

5.10 Error Message Log and Ramp Statistics in PHT SPD and Cal-A Headers

- authors: P.J. Richards, L. Cornwall, U. Klaas
- date: 27-May-1998

5.10.1 Motivation

These modifications were made to:

a) provide the observer with useful statistics on data discarded during the processing, and

b) reduce the number of error messages logged while processing.

5.10.2 References to Calibration Analysis and Software Change Documentation

- calibration report: n/a
- Software Change Request: SCREW 337

5.10.3 Method

A visual inspection of the SPD and Cal A product headers was carried out for the following observations:

TDT	Products
47600206	PP1S, PP2S, PP3S, PP1A, PP2A, PP3A
47600208	PC1S, PC2S, PC1A, PC2A
38300521	PSSS, PSLS
08500342	PP1S, PP2S, PP3S, PP1A, PP2A, PP3A
10601101	PC1S, PC2S, PC1A, PC2A
42800903	PSSS, PSLS

5.10.4 Results

The additional statistics provided in the headers are associated with the following keywords:

```
READSUSP  Readouts flagged as suspicious
RAMPINVD  Bad cycle
RAMPFROP  First ramps ignored
RAMPZSG   Zero (or negative) average signals
PLATNORP  Plateaux with no good ramps
```

Note that the keyword RAMPZSG is only written to the header if the value is greater than zero.
The results for the SPD products for each observation are as follows:

TDT 47600206

	READSUSP	RAMPINVD	RAMPFROP	RAMPZSG	PLATNORP
PP1S	0	0	10	(0)	0
PP2S	0	0	2	(0)	0
PP3S	0	0	2	(0)	0

TDT 47600208

	READSUSP	RAMPINVD	RAMPFROP	RAMPZSG	PLATNORP
PC1S	0	0	6	(0)	0

```
PC2S     0          0          5          (0)          0

TDT 38300521
------------
      READSUSP   RAMPINVD   RAMPFROP   RAMPZSG   PLATNORP
PSSS     0          0          2          29          0
PSLS     0          0          2          29          0
```

All the above statistics were as expected. The statistics in the Cal A product headers were also as expected. However, for the chopped observations, the following was found:

```
TDT 08500342
------------
      READSUSP   RAMPINVD   RAMPFROP   RAMPZSG   PLATNORP
PP1S     0          0          0          (0)          0
PP2S     0          0          0          (0)          0
PP3S     0          0          0          (0)          0

TDT 10601101
------------
      READSUSP   RAMPINVD   RAMPFROP   RAMPZSG   PLATNORP
PC1S     0          0         189         (0)         27
PC2S     0          0          0          (0)          0

TDT 42800903
------------
      READSUSP   RAMPINVD   RAMPFROP   RAMPZSG   PLATNORP
PSSS     0          0          1          283          0
PSLS     0          0          1          283          0
```

As these are chopped observations, values significantly greater than zero for the RAMPFROP keyword are expected in all cases, which indicates an error in the accumulation of this statistic. A fix for V7.0 was considered to be too risky, given that these data are only for information and do not affect the interpretation, so a fix has been deferred to V8.2.

5.10.5 Conclusions

- An SPR should be raised for V8.2 to correct the RAMPFROP (first ramps ignored) statistics.

5.11 Wavelength Dependent Solid Angles of PHT-C Arrays

- authors: M. Radovich, U. Klaas
- date: 17-May-1998

5.11.1 Motivation

For OLP V7.0 / CALG V4.0 refined and wavelength dependent solid angles derived from the theoretical footprint model instead of the ones derived from the physical size of the pixels have been introduced. The resulting surface brightness values in the background measurements shall be checked.

5.11.2 References to Calibration Analysis and Software Change Documentation

- calibration report:
  - ISOPHOT Footprints: C100 - Comparison between modelled and measured footprints - the derived parameters[9]
  - ISOPHOT Footprints: C200 - Comparison between modelled and measured footprints - the derived parameters[10]
- Software Change Request: SCREW 345

5.11.3 Method

We check the resulting background surface brightness values against COBE results. When doing this the following limitations have to be taken into consideration:

- Ideally the weekly COBE/DIRBE maps should be used in order to take into account the variation in brightness of the Zodiacal Light. However, since not always the weekly maps are available and sometimes, especially for 140 and 240 μm, the COBE values are highly uncertain, we use in the following the annual maps. Typical errors quoted for the COBE fluxes are $\leq$ 1% for both 60 and 100 μm, 22% for 140 μm and 17% for 240 μm.
- We compare the 3 arcmin ISOPHOT beam with the 0.7 deg COBE beam. For a direct comparison a COBE beam should be covered by an ISOPHOT map and the integrated background brightness be compared. This is not done here (but such measurements are available). Therefore, local fluctuations can easily account for a certain level of discrepancy between COBE and ISOPHOT.

Therefore, the comparison between COBE and ISOPHOT is more of qualitative nature.

5.11.4 Results

In Sect. 5.11.6 we list the fluxes from both OLP V6.x and OLP V7.0b2 surface brightness processing and the COBE/DIRBE fluxes from the annual maps. Surface brightness values are between 5 and 15 MJy sr^{-1}. In Figs. 32 to 34 we plot several examples in order to show the shape and smoothness of the background SEDs.
In Table 18 we check the relative consistency with the COBE photometry. Note that for simplicity 140 μm COBE photometry is compared with 150 μm ISOPHOT photometry and 240 μm COBE photometry with 200 μm ISOPHOT photometry. For the latter one the consistency is less good, as the wavelength shift introduces a positive bias for the ISOPHOT flux due to the declining energy distribution in the background SEDs.
We see that for OLP V6.x the usage of the solid angles yielded systematically considerably too high background fluxes. For OLP V7.0b2 they are consistent within 20–30%.

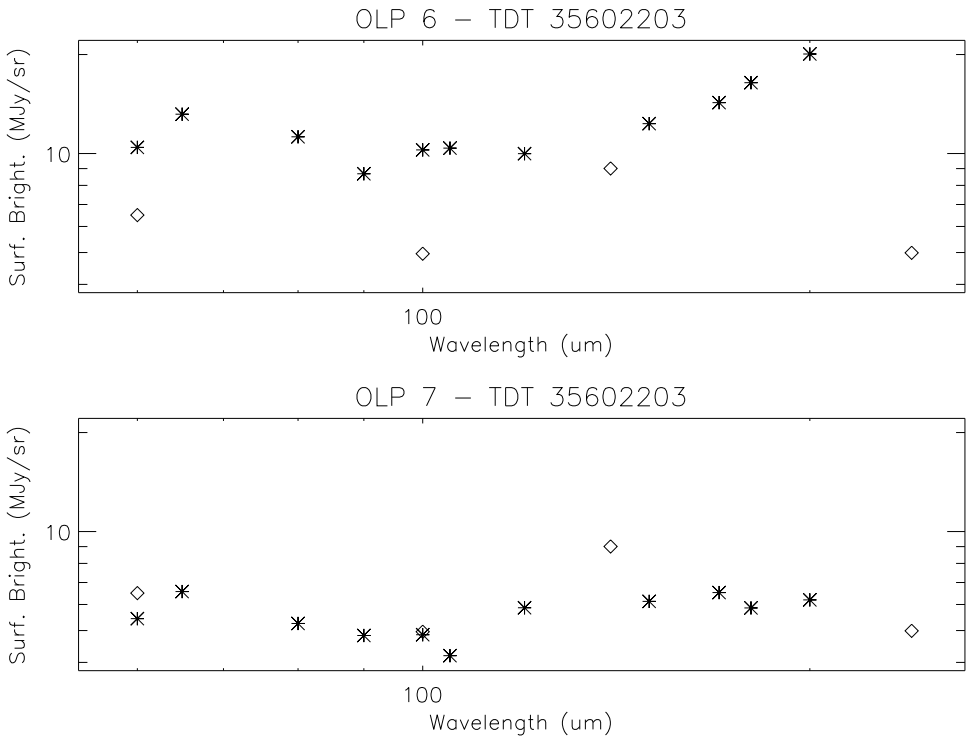

Figure 32: Comparison of OLP V6.x and OLP V7.0b2 surface brightness (asterisk) with COBE annual map fluxes (diamond).

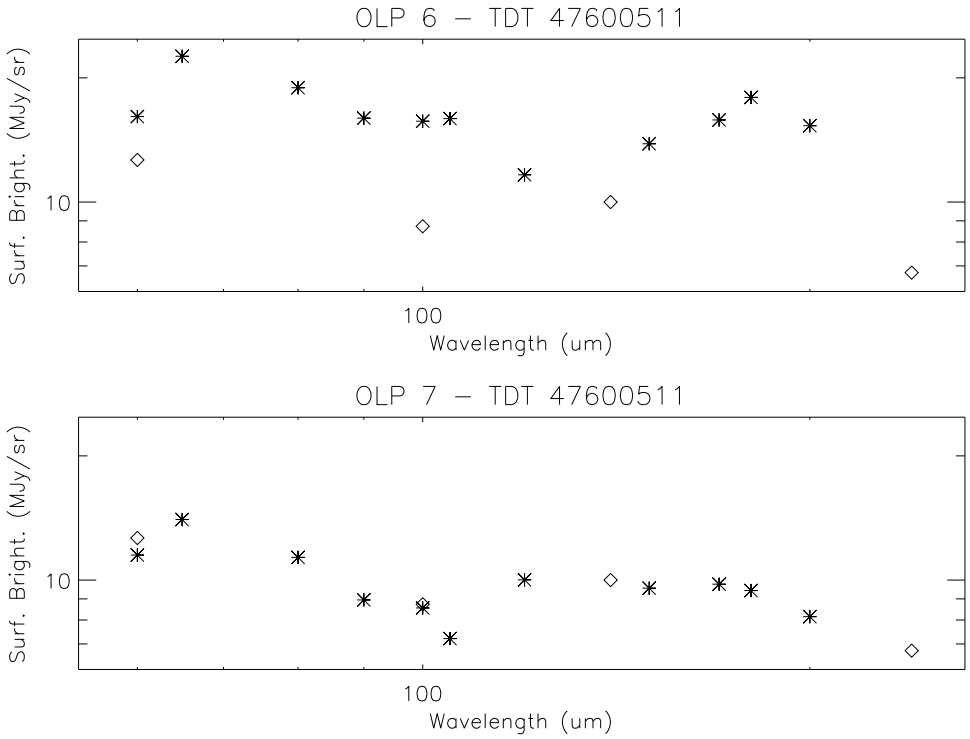

Figure 33: Comparison of OLP V6.x and OLP V7.0b2 surface brightness (asterisk) with COBE annual map fluxes (diamond).

Table 18: Consistency check of surface brightness results with COBE/DIRBE annual maps

TDT	**target name**	**wavelength** [μm]	**consistency w.r.t. COBE OLP V6.x** [%]	**consistency w.r.t. COBE OLP V7.0b2** [%]
35602203	HR 6705 background	60	+60.6	-16.3
		100	+107	-2.0
		150	+37.0	-31.9
		200	+302	+24.2
39802002	HR 6705 background	60	+76.5	+15.4
		100	+118	+20.2
45200203	HR 5340 background	60	+81.3	+20.0
		100	+133	+29.5
		150	+10.3	-19.8
		200	+218	+41.4
47600207	NGC 6543 background	60	+58.9	+4.2
		100	+73.7	+3.6
		150	+44.1	+6.7
		200	+163	+13.7
47600511	NGC 6240 background	60	+27.4	-9.1
		100	+79.8	-1.9
		150	+38.5	-4.4
		200	+127	+20.9

5.11.5 Conclusions

- We find a very good consistency between COBE and ISOPHOT background surface brightness values between 60 and 240 μm for all our test cases.
- The PHT22 AOT extended source photometry can therefore be declared scientifically validated with an absolute accuracy of better than 30% and a relative filter-to-filter accuracy of 20%.

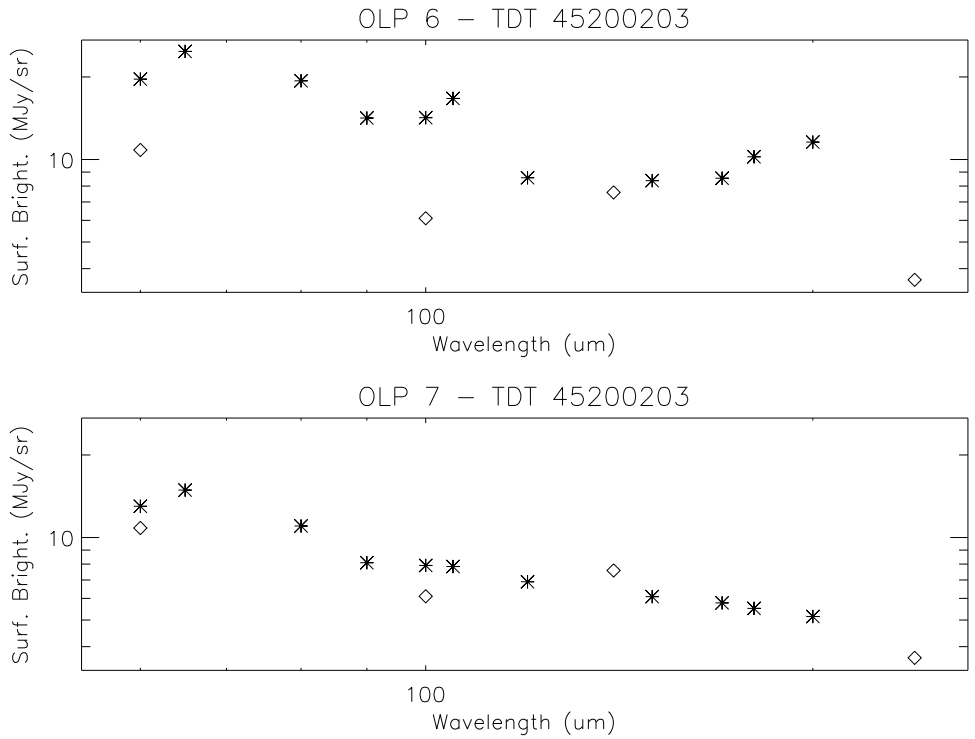

Figure 34: Comparison of PHT-C surface brightness photometry with COBE, both for OLP 6.x and OLP 7.0b2. Asterisk: PHT-C100 and C200 photometry, diamond: COBE.

5.11.6 Evaluation Log

```
1) OLP V6 vs OLP V7 background fluxes and comparison with COBE annual map
   fluxes

TDT 35602203 - HR 6705
 Cwl    OLP 6.0      OLP 7.0        COBE
 [um] [MJy sr^-1]  [MJy sr^-1]  [MJy sr^-1]
-------------------------------------------------
   60    10.44         5.44         6.50
   65    13.17         6.57
   80    11.24         5.25
   90     8.68         4.83
  100    10.25         4.86         4.96
  105    10.39         4.19
  120     9.99         5.86
  150    12.33         6.13         9.00 (140um)
  170    14.28         6.52
  180    16.42         5.86
  200    20.07         6.20         4.99 (240um)
-------------------------------------------------


TDT 39802002 - HR 6705
 Cwl    OLP 6.0      OLP 7.0        COBE
 [um] [MJy sr^-1]  [MJy sr^-1]  [MJy sr^-1]
-------------------------------------------------
   60    11.47         7.50         6.50
   65    12.97         7.71
   80    12.75         7.48
   90    10.01         5.78
  100    10.82         5.96         4.96
  105    12.38         5.62
```

TDT 45200203 - Alpha Bootes

Cwl [um]	OLP 6.0 [MJy sr^-1]	OLP 7.0 [MJy sr^-1]	COBE [MJy sr^-1]
60	19.64	13.00	10.83
65	24.79	14.90	
80	19.37	11.02	
90	14.17	8.09	
100	14.21	7.91	6.11
105	16.70	7.84	
120	8.58	6.90	
150	8.37	6.09	7.59 (140um)
170	8.55	5.77	
180	10.23	5.52	
200	11.58	5.15	3.64 (240um)

TDT 47600207 - NGC 6543

Cwl [um]	OLP 6.0 [MJy sr^-1]	OLP 7.0 [MJy sr^-1]	COBE [MJy sr^-1]
60	10.98	7.20	6.91
65	14.31	8.45	
80	11.92	6.96	
90	9.15	6.01	
100	9.66	5.76	5.56
105	10.70	4.96	
120	7.04	6.07	
150	8.33	6.17	5.78 (140um)
170	8.93	6.04	
180	10.16	5.51	
200	11.10	4.80	4.22 (240um)

TDT 47600511 - NGC 6240

Cwl [um]	OLP 6.0 [MJy sr^-1]	OLP 7.0 [MJy sr^-1]	COBE [MJy sr^-1]
60	16.11	11.50	12.65
65	22.57	14.02	
80	18.93	11.35	
90	15.98	8.95	
100	15.70	8.56	8.73
105	15.94	7.21	
120	11.64	10.01	
150	13.85	9.56	10.00 (140um)
170	15.81	9.77	
180	17.94	9.43	
200	15.31	8.15	6.74 (240um)

5.12 Subtracted Source Flux for Chopped PHT AA Products

- authors: M. Radovich, U. Klaas
- date: 28-May-1998

5.12.1 Motivation

From OLP V7.0b2 onwards chopped Auto-Analysis Results contain as an additional information the background subtracted source flux. This allows to avoid reading the data records or calculating the source flux from the header information of source+background minus background flux including a conversion from MJy sr^{-1} to Jy with wavelength dependent solid angles.

5.12.2 References to Calibration Analysis and Software Change Documentation

- calibration report: n/a
- Software Change Request: SCREW 353

5.12.3 Method

A check of the new implementation is included in the normal scientific evaluation of chopped data products by extracting the differential (source) fluxes from the headers. We concentrate here therefore on the formal aspects whether the implementation is according to the SCREW specification, by inspecting one randomly picked example.
We also check that the contents of the header correspond to the contents of the data records.

5.12.4 Results

Below we list the header of a chopped PHT-P (PPAP) data product. Below the comment fields that it was processed using the default responsivity, as requested by SCREW 341, the field
"SOURCE1 6.17093E+00 Flux density (source) (Jy)"
contains the information of the background subtracted source flux.

```
#  Table PPAP78300901.fits[1]  Wed 09:54:32 27-May-98

XTENSION 'BINTABLE'  Binary table FITS extension
BITPIX   8  8 BITS character format
NAXIS    2  Tables are 2-d character array
NAXIS1   64  Characters in a row
NAXIS2   1  Number of rows in a table
PCOUNT   0  Parameter count always 0
GCOUNT   1  Group count always 1
TFIELDS  16  No of columns in table
TFORM1   1J
TTYPE1   'PPAPFILT'  Filter ID (CHW3 position)
TFORM2   1J
TTYPE2   'PPAPAPER'  Aperture ID (CHW2 position)
TFORM3   1J
TTYPE3   'PPAPNBCK'  Number of background reference positions
TFORM4   1E
TTYPE4   'PPAPSRCE'  Source flux
TUNIT4   Jy
TFORM5   1E
TTYPE5   'PPAPSRCU'  Uncertainty in source flux
TUNIT5   Jy
TFORM6   1E
TTYPE6   'PPAPBACK'  Background for given aperture
TUNIT6   Jy
TFORM7   1E
TTYPE7   'PPAPBCKU'  Uncertainty in background
```

```
TUNIT7   Jy
TFORM8   1E
TTYPE8   'PPAPSPB'  Source plus background
TUNIT8   Jy
TFORM9   1E
TTYPE9   'PPAPSPBU'  Uncertainty in source plus background
TUNIT9   Jy
TFORM10  1E
TTYPE10  'PPAPBCK1'  Background at reference position 1
TUNIT10  Jy
TFORM11  1E
TTYPE11  'PPAPBK1U'  Uncertainty in background 1
TUNIT11  Jy
TFORM12  1E
TTYPE12  'PPAPBCK2'  Background at reference position 2
TUNIT12  Jy
TFORM13  1E
TTYPE13  'PPAPBK2U'  Uncertainty in background 2
TUNIT13  Jy
TFORM14  1E
TTYPE14  'PPAPBINT'  Mean background intensity
TUNIT14  MJy/ster
TFORM15  1E
TTYPE15  'PPAPBINU'  Uncertainty in background intensity
TUNIT15  MJy/ster
TFORM16  1J
TTYPE16  'PPAPNCYC'  Number of accepted chopper cycles
FPCMODE  'TR'  Chopper mode
COMMENT  ************************************************
COMMENT  !!!WARNING!!!
COMMENT  The DEFAULT responsivity has been used in the processing.
COMMENT  ************************************************
FILTER1  'P1_3P29_UM'  Filter
LAMBDA1  3.30000E-06  Central Wavelength of filter (m)
EXFLUX1  1.02901E+01  Expected source flux (Jy)
UNCFLX1  5.00000E-01  Uncertainty in expected flux (Jy)
MXBACK1  2.10000E-01  Max expected background (MJy/ster)
APER1    '52" = 2.3mm'  Aperture
SOURCE1  6.17093E+00  Flux density (source) (Jy)
SOURCU1  6.07273E-02  Uncertainty in flux (source)(Jy)
SBACK1   6.87130E+00  Flux density (source + background) (Jy)
SBACKU1  3.03070E-02  Uncertainty in flux (source + background)(Jy)
BACK1    1.41792E+01  Measured background (MJy/ster)
```

In the following we compare the flux values in the headers and in the data records for one P1 and one C100 data product, respectively. For both products header and data records contain identical information.

```
P1 HEADER

#  Table PPAP78300901.tab  Thu 16:02:33 28-May-98
# row         PPAPSPB        PPAPSPBU        PPAPSRCE        PPAPSRCU
    1        6.871299      0.03030703        6.170926      0.06072726

P1 DATA RECORDS

SBACK1   6.87130E+00  Flux density (source + background) (Jy)
SOURCE1  6.17093E+00  Flux density (source) (Jy)

-------------------------------------------------------------------------

C100 HEADER

- Source + background
```

```
SBACK1   9.34711E+00  Flux density (source + background)(Jy)
SBACK2   9.89216E+00  Flux density (source + background)(Jy)
SBACK3   9.03772E+00  Flux density (source + background)(Jy)
SBACK1   8.66223E+00  Flux density (source + background)(Jy)
SBACK2   8.77608E+00  Flux density (source + background)(Jy)
SBACK3   8.52525E+00  Flux density (source + background)(Jy)

- Source

SOURCE1  2.84999E+00  Flux density (source)(Jy)
SOURCE2  3.60451E+00  Flux density (source)(Jy)
SOURCE3  4.25641E+00  Flux density (source)(Jy)
SOURCE1  2.91988E+00  Flux density (source)(Jy)
SOURCE2  2.43603E+00  Flux density (source)(Jy)
SOURCE3  3.12672E+00  Flux density (source)(Jy)

----------------------------------------

C100 DATA RECORDS

- Source+background

>>> PCAP67100803_r0001.txt
 Total flux (Jy) = 9.3471068  +/- 0.010063918
>>> PCAP67100803_r0002.txt
 Total flux (Jy) = 9.8921561  +/- 0.0031216757666667
>>> PCAP67100803_r0003.txt
 Total flux (Jy) = 9.0377189  +/- 0.0032129293033333
>>> PCAP67100912_r0001.txt
 Total flux (Jy) = 8.662229  +/- 9.2619246333333E-4
>>> PCAP67100912_r0002.txt
 Total flux (Jy) = 8.7760789  +/- 0.0010043964533333
>>> PCAP67100912_r0003.txt
 Total flux (Jy) = 8.5252506  +/- 0.0014333879209333

- Source

>>> PCAP67100803_r0001.txt
    Total flux (Jy) = 2.84999135  +/- 0.030774144333333
>>> PCAP67100803_r0002.txt
    Total flux (Jy) = 3.60451213  +/- 0.0089204704
>>> PCAP67100803_r0003.txt
    Total flux (Jy) = 4.256406754  +/- 0.0088661397
>>> PCAP67100912_r0001.txt
    Total flux (Jy) = 2.91988056  +/- 0.01420567
>>> PCAP67100912_r0002.txt
    Total flux (Jy) = 2.436029276  +/- 0.0058666241
>>> PCAP67100912_r0003.txt
    Total flux (Jy) = 3.126718057  +/- 0.005436922
```

5.12.5 Conclusions

- The header structure is as requested by SCREW 353 and contains the additional keyword with the background subtracted source flux.
- Values in the headers and in the data records have been proven to be identical.
- Having the information of the background subtracted source flux in the header makes the scientific validation tests and inspections of the data products much handier. This will also serve the observer.

5.13 Change in Error Handling for PHT OLP

- authors: L. Cornwall, U. Klaas
- date: 28-May-1998

5.13.1 Motivation

With the current design of error handling and propagation in OLP the processing of uncertainties had to be restricted to statistical errors from signal processing, as the inclusion of systematic errors did not produce any meaningful results anymore. Several error terms put in into earlier OLP Versions and into the first OLP 7 delivery had to be disabled. We check here that there is no impact on the scientific results (fluxes) obtained with OLP V7.0b2.

5.13.2 References to Calibration Analysis and Software Change Documentation

- calibration report: Flow of Corrections Made During Processing [3]
- Software Change Request: SCREW 356

5.13.3 Method

For the test we have selected representative cases of all 3 PHT subsystems PHT-P, PHT-C, and PHT-S. We have selected point source and extended source data products. We compared the flux and uncertainty values from official OLP V7.0b2 processing with OLP V7.0b2+'Deltas in PIDT test environment'.

5.13.4 Results

1) PCAE47600415 (PHT-C)

   a) Comparison of the brightness and brigthness uncertainty in the headers showed that the brightness are similar, but not exactly the same. The differences are of the order of 1%. The uncertainty is consistently less for the processing with the Deltas.
   The reason for this slight difference is that the surface brightness in the headers are derived values from the individual pixel values in the records. They are calculated by taking the weighted mean (with the weight being one over the variance of the uncertainties of the pixel fluxes). That means that one should expect a slight change, as the uncertainties of the individual pixels will not change 1:1 when taking out the remaining systematic uncertainties.

   b) A direct check of the values in the data records directly gives the following (expected) result:
   Comparison of the source plus background and errors from the .DAT files from b2 processing and b2+deltas added for PCAE47600415 and check of all pixels from 3 filters shows that the source plus background is always the same, and the errors are lower for the version with the deltas.

2) PPAP47600413 (PHT-P)
   Comparison of the brightness and brightness uncertainty in the headers shows no differences at all.

3) PLAP38300521 (PHT-S)
   Comparison of the brightness and brightness uncertainty in the data, for a few randomly selected pixels shows no differences at all.

5.13.5 Conclusions

- The delta changes do exactly what is expected. The validity of the product fluxes is not touched.

- The clean separation of statistical errors provided by OLP and systematic errors to be provided by an extra document (cf. Ref. [3]) has been achieved on the OLP side.

5.14 General Re-validation of PHT03 and PHT22 Staring Mode: The SED of α Bootes (HR 5340)

- authors: M. Radovich, U. Klaas
- date: 13-May-1998

5.14.1 Motivation

TDTs 45200201(background, PHT-P), 45200202(α Boo, PHT-P), 45200203(background, PHT-C), 45200204(α Boo, PHT-C) is one of the key OLP V6.0 validation cases [1]. The staring mode AOTs PHT-03 and PHT-22 use all available PHT filters (but the 3.6 and 4.85 μm filters had to be excluded from the analysis, because the source saturates the measurement) on a stellar (declining) SED. α Bootes is one of the most important stellar PHT calibration standards and there are detailed models available from M. Cohen (composite spectrum from 1 to 35 μm and extrapolations to 300 μm). This test case is very suitable for a test of both the absolute calibration and the relative filter-to-filter calibration. It should be noted that this multi-filter measurement was not used for the establishment of the FCS calibration curve.

5.14.2 Method

We compare the background subtracted flux values of both OLP V6.x and OLP V7.0b2 results against the model prediction.

5.14.3 Results

In the following Tab. 19 we compare the photometry from part 1 of Sect. 5.14.5 with the model. We estimate the absolute photometric accuracy per detector assembly for this target as the deviation from the model flux in the filter in which the FCS calibration was done, and the relative filter-to-filter accuracy as the peak-to-peak variation of the other filters around this offset. Note that for P1 the FCS calibration was actually done in the 3.6 μm filter, but for this filter the sky measurement is heavily saturated. The photometric accuracies are presented in Tab. 20. Fig. 35 shows the PHT photometric data points in comparison to the model and IRAS photometry (color corrected) from 3.3 to 200 μm. The C200 photometry does not give any reasonable results. It shows a negative photometric bias with a relative overestimate of the individually calibrated background flux. This was already noted during the OLP 6 validation [1]. Currently it can be excluded that the bad photometry is due to

- a mis-pointing, as the C200 data were obtained by the same AO as the C100 data;
- a R/T problem: there is no mentioning of any problem (star tracker) in the R/T reports;
- a peculiar behaviour of the sky background (steeply rising) at the background position, see Fig. 36;
- a detection limitation. The expected source flux is between 6.8 and 1.85 Jy between 120 and 200 μm;
- cirrus confusion noise is expected to be less than 250 mJy and cannot explain the full discrepancy.

In order to characterize the negative photometric bias (background overestimate) better we derived in Table 21 the source-to-background contrast (background flux in Jy is calculated according to the following formula: $F(Jy)_{back} = 1/f_{psf} * I(MJy/sr) * (1 - \varepsilon^2) * Omega * n_{pix}$). At 105 μm the source flux is comparable with the background flux (1:1.3). From 120 to 200 μm the background becomes more and more dominant (from 1.9:1 to 5.1:1). The settings for the off-source and on-source FCS measurements were different, see Table 22.
PIA AOT batch processing gives the same results, also for C200, as OLP. Again, the background data give very nice consistency with the wide beam COBE data, see part 2 of Sect. 5.14.5 and Fig. 36.

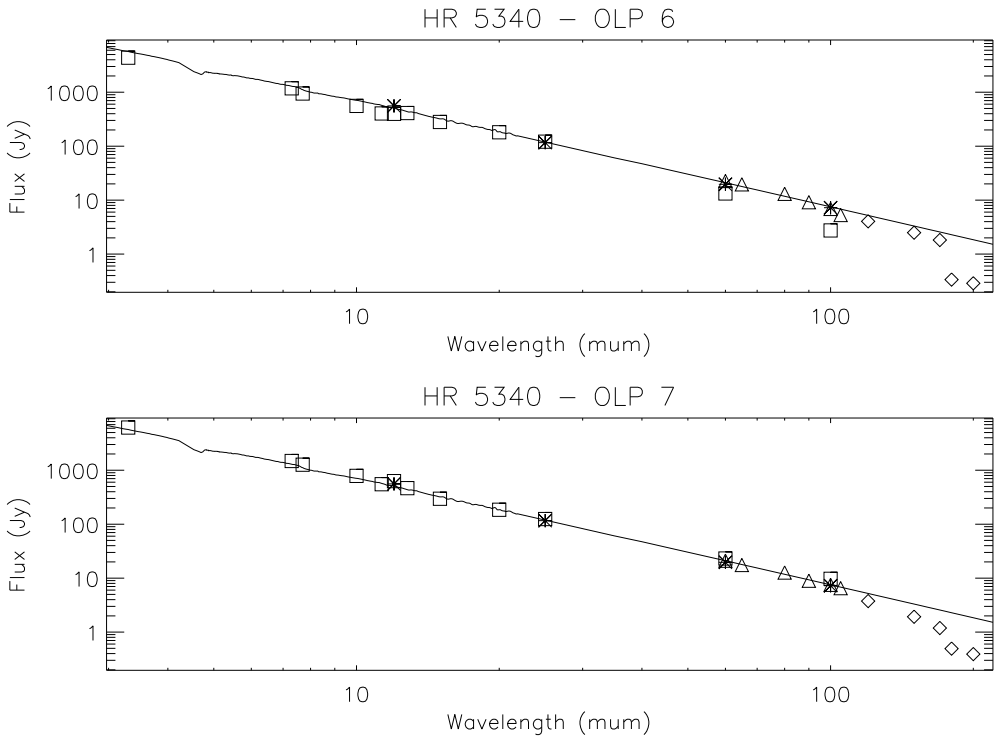

Figure 35: Comparison of PHT-P and PHT-C photometry, using the full ISOPHOT filter set, with the composite spectrum and out to 300 μm extrapolated SED of α Boo (HR 5340) provided by M. Cohen and with IRAS photometry. Upper panel for OLP 6.x and lower panel for OLP 7.0b2. All photometric points are color corrected for a 4000 K BB. The meaning of the symbols is the following: solid line: model, asterisk: IRAS, square: PHT-P (P03 AOT), triangle: C100 (P22 AOT), diamond: C200 (P22 AOT).

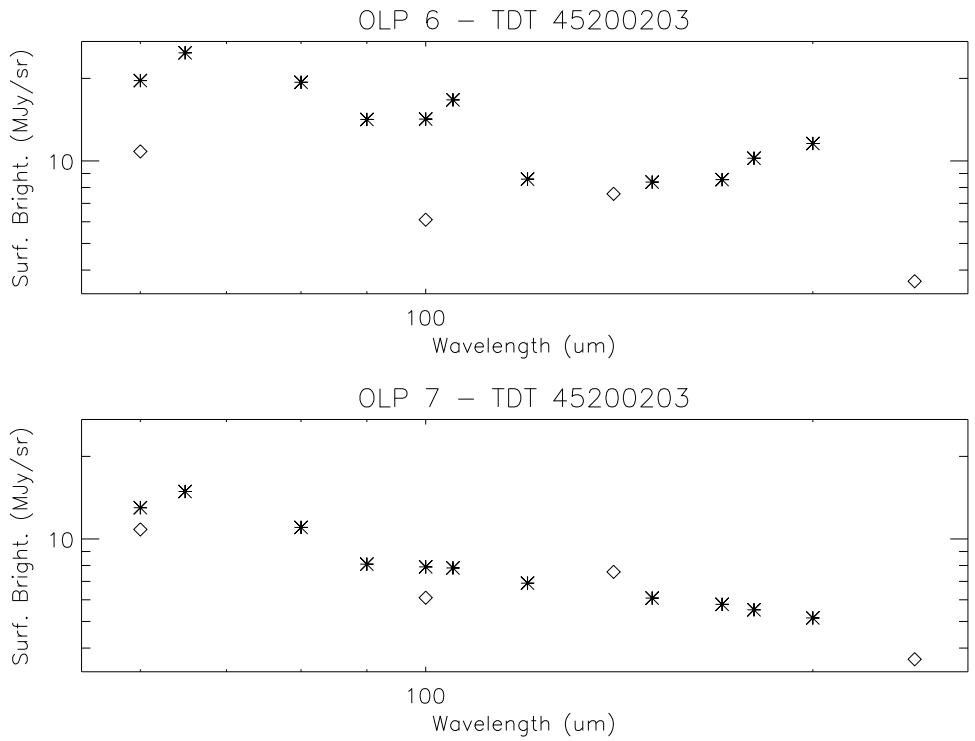

Figure 36: Comparison of PHT-C surface brightness photometry with COBE, both for OLP 6.x and OLP 7.0b2. Asterisk: PHT-C100 and C200 photometry, diamond: COBE.

Table 19: Consistency check of photometric results with HR 5340 model

Filter	**consistency w.r.t. model OLP V6.x** [%]	**consistency w.r.t. model OLP V7.0b2** [%]
3.3	-23.3	+8.6
7.3	-7.8	+15.9
7.7	-15.1	+13.8
10	-21.1	+11.2
11.3	-29.1	-3.3
12	-21.6	+24.1
12 IRAS	+10.1	+10.1
12.8	-5.4	+6.9
16	-12.5	+7.5
20	-2.4	-0.1
25	+1.8	+4.5
25 IRAS	-2.3	-2.3
60 PHT-P	-36.7	+9.9
60 PHT-C	+7.6	+0.2
60 IRAS	-6.6	-6.6
65	+9.4	-2.0
80	+10.8	+7.6
90	-1.5	-3.7
100 PHT-P	-63.5	+29.3
100 PHT-C	-8.6	-0.04
100 IRAS	-3.6	-3.6
105	-22.2	-4.3
120	-22.2	-27.8
150	-24.8	-41.9
170	-28.9	-53.6
180	-85.3	-78.4
200	-84.4	-78.8

5.14.4 Conclusions

- For α Boo absolute calibration for both P1 and P3 have been considerably improved with OLP V7.0.
- PHT photometry gives a good representation of the SED from 3.3 to 105 μm.
- C200 multi-filter photometry shows a negative photometric bias in that respect that the individually calibrated background is relatively too high, yielding a too low source flux. The source-to-background contrast suggests that staring off/on photometry becomes unreliable for source-to-background ratios below 1:1.3 (0.75). This issue needs follow-up in the context of the responsivity non-linearity with flux investigations.

Table 20: Absolute and relative calibration accuracies per detector achieved for HR 5340 observation with OLP V7.0b2

detector	**absolute accuracy** [%]	**relative accuracy** [%]
P1	10 at 3.3 μm	15
P2	1 at 20 μm	5
P3	10 at 60 μm	20
C100	5 at 90 μm	10

Table 21: Source-to-background contrast for α Bootes in FIR filters. The expected source flux is the model flux, the background flux is from the background measurement converted to Jy as decribed in the text.

λ_c [μm]	**background flux** [Jy]	**expected source flux** [Jy]	**source-to-backgr. contrast**
105	8.89	6.81	0.77 (1:1.3)
120	9.63	5.20	0.54 (1:1.9)
150	9.23	3.31	0.36 (1:2.8)
170	8.96	2.57	0.29 (1:3.5)
180	9.60	2.29	0.24 (1:4.2)
200	9.41	1.85	0.20 (1:5.1)

Table 22: Electrical power settings of FCS1/TRS2 and filters used for α Bootes PHT-C on-source and off-source FCS measurements.

pointing	**filter**	**electrical FCS power** [mW]
off-source	C100_90_UM	0.36
	C200_160_UM	0.16
on-source	C100_60_UM	1.60
	C200_160_UM	0.20

5.14.5 Evaluation Log

1) Point source photometry for Alpha Bootes (TDTs 45200201, 45200202, 45200203, and 45200204) in comparison with IRAS and Cohen model.

Filter	cwl	cc_olp6	cc_olp7	IRAS	Model	PIA
P1_3P29_UM	3.3	4367.974	6185.493	0.	5695.47	6183.832
P1_7P3_UM	7.3	1179.945	1483.791	0.	1279.82	1482.971
P1_7P7_UM	7.7	946.0117	1267.99	0.	1114.00	1268.580
P1_10_UM	10.	557.5679	785.8817	0.	706.819	782.239
P1_11P3_UM	11.3	404.3626	551.4589	0.	570.349	551.728
P1_11P5_UM	12.	397.8398	629.4504	558.5	507.360	621.850
P1_12P8_UM	12.8	411.7902	465.6441	0.	435.541	460.485
P1_16P0_UM	15.	280.6255	296.6608	0.	320.700	294.877
P2_20_UM	20.	181.0318	185.2973	0.	185.467	185.517
P2_25_UM	25.	121.3267	124.5598	116.4	119.146	124.743
P3_60_UM	60.	13.30304	23.10966	0.	21.03	23.11
P3_100_UM	100.	2.745338	9.723714	0.	7.521	9.82
C100_60_UM	60.	22.62992	21.06331	19.65	21.03	21.07
C100_50_UM	65.	19.59962	17.54877	0.	17.91	17.73
C100_70_UM	80.	13.0765	12.69519	0.	11.80	12.81
C100_90_UM	90.	9.159431	8.956803	0.	9.303	9.03
C100_100_UM	100.	6.871119	7.517926	7.25	7.521	7.58
C100_105_UM	105.	5.301021	6.52084	0.	6.814	6.66
C200_120_UM	120.	4.04716	3.75622	0.	5.201	3.74
C200_135_UM	150.	2.488855	1.922364	0.	3.31	1.81
C200_160_UM	170.	1.824815	1.190747	0.	2.568	1.11
C200_180_UM	180.	0.3364218	0.494190	0.	2.286	0.86
C200_200_UM	200.	0.2877184	0.391382	0.	1.845	0.40

2) Surface brightness photometry at the background position of alpha Boo and comparison with COBE

	Cwl [um]	OLP 7.0 [MJy/sr]	COBE [MJy/sr]
C100_60_UM	60	1.30016E+01	10.83
C100_50_UM	65	1.48969E+01	
C100_70_UM	80	1.10188E+01	
C100_90_UM	90	8.09316E+00	
C100_100_UM	100	7.90832E+00	6.11
C100_105_UM	105	7.83832E+00	
C200_120_UM	120	6.89752E+00	
C200_135_UM	150	6.08553E+00	7.59 (140um)
C200_160_UM	170	5.77478E+00	
C200_180_UM	180	5.51525E+00	
C200_200_UM	200	5.15002E+00	3.64 (240um)

5.15 General Re-validation of PHT03 and PHT22 Staring Mode: The SED of Arp 220

- authors: M. Radovich, U. Klaas
- date: 13-May-1998

5.15.1 Motivation

TDTs 47600413(background, PHT-P), 47600414(Arp 220, PHT-P), 47600415(background, PHT-C), 47600416(Arp 220, PHT-C) is one of the key OLP V6.0 validation cases [1]. The staring mode AOTs PHT-03 and PHT-22 in all PHT filters measure a galaxy SED which is steeply rising between 10 and 60 μm and gradually declining beyond 100 μm, hence has a very different shape than a stellar atmosphere SED. It can therefore be used for a check of the robustness of the relative filter-to-filter calibration and the color correction factors applied to modified Black Bodies in the temperature range 50 – 120 K. Arp 220 is significantly bright over the full wavelength range from 3.3 to 200 μm. Its photometric properties are discussed in detail in "Infrared spectral energy distributions of the interacting galaxies Arp 244, NGC 6240 and Arp 220" [8].

5.15.2 Method

We compare the background subtracted flux values of both OLP V6.x and OLP V7.0b2 results against the IRAS photometry and a model fit based on the OLP V6.x calibration.

5.15.3 Results

Fig. 37 shows the derived SED for Arp 220. The model fit from [8] is plotted as a guide line to easier recognize the changes w.r.t. OLP V6.x. Note that this fit cannot serve as reference photometry.
We have color corrected the photometry w.r.t. modified blackbodies with emissivities $\propto \nu$ for the 12.8 to 200 μm range (for details, see part 2 of Sect. 5.15.5). This color corrected SED shows a smooth behaviour.
The transition between C100_105 and C200_120 photometry is smooth which proves the good cross-calibration between the two arrays.
The 12 μm photometry is now consistent with IRAS and the full short wavelength branch is lower in flux than previously. The kind of excess emission at 12.8 and 16 μm has disappeared. The relatively low fluxes at 10 and 11.3 μm can be a consequence of the strong extinction still present in the NIR.
The PHT-P3 photometry is in general too high both w.r.t. C100 and IRAS.
The C100 photometry is now 10% higher than IRAS, for OLP V6.x both PHT and IRAS photometry were more or less consistent. The 90 μm photometric point introduces a dip in the SED. This filter is the one used for the FCS calibration of the C100 filters. It provides therefore the absolute calibration for C100. With the recently established non-linearity of responsivity with in-band power (decreasing responsivity with in-band power) the dip could at least be partly understood by the explanation that for the 90 μm filter the responsivity is lower than for the other filters. Hence the other filters would have to be corrected with a higher responsivity, scaling the fluxes somewhat down and diluting the dip.
There appears to be still a slight inconsistency between the results in the C_160 and C_180 filters, but the color correction makes the 170 μm flux more consistent with the other C200 fluxes. The color corrected C200 photometry would now need a somewhat steeper fall-off of the BB emission, possibly the indication for an emissivity $\propto \nu^2$.
Fig. 39 provides the comparison of the background fluxes with COBE both for PHT-P and PHT-C from 3.5 to 200 μm. Both PHT-P and PHT-C surface brightness values of OLP V7.0b2 are consistent with the COBE DIRBE results from 3.5 to 240 μm. The only significant outlier is the 3.3 μm point, however, the photometry of the faint Zodiacal Background in a narrow band filter using only a 52" aperture cannot provide any meaningful result. The PHT-P3 surface brightness values are smaller than the C100 ones which match with COBE.

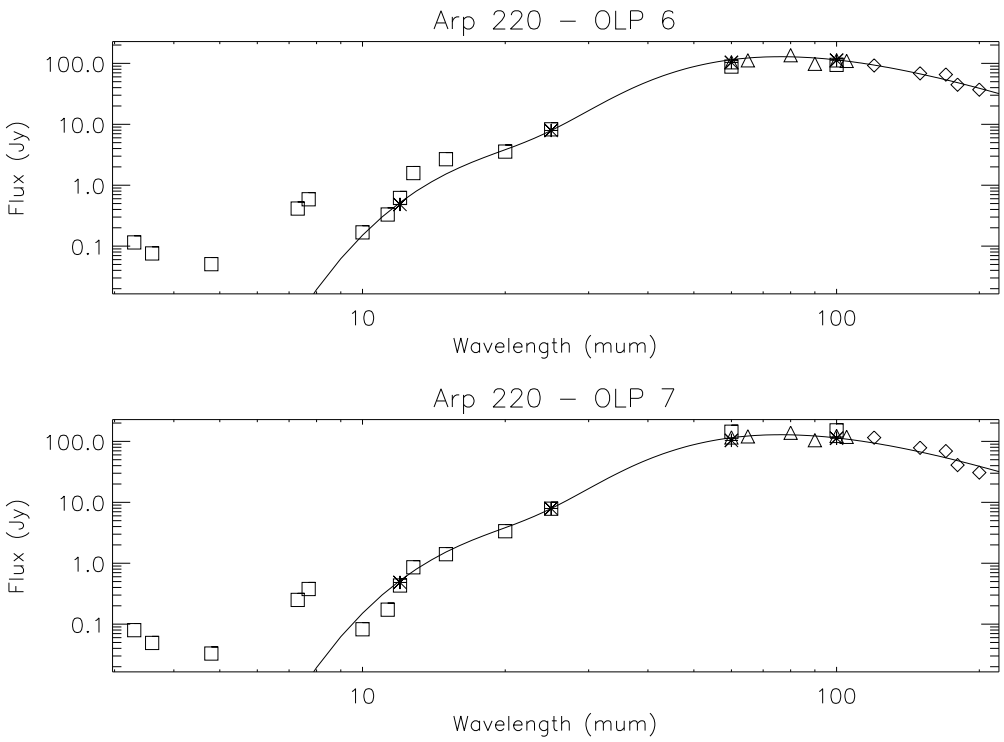

Figure 37: Comparison of PHT-P and PHT-C photometry, using the full ISOPHOT filter set, with IRAS photometry and the model fit as described in [8]. Note that this model fit only serves as a guide for the eye to recognize more easily the changes between the two versions. It is not an absolute photometric reference. No color correction has been applied. The meaning of the symbols is the following: solid line: model, asterisk: IRAS, square: PHT-P (P03 AOT), triangle: C100 (P22 AOT), diamond: C200 (P22 AOT).

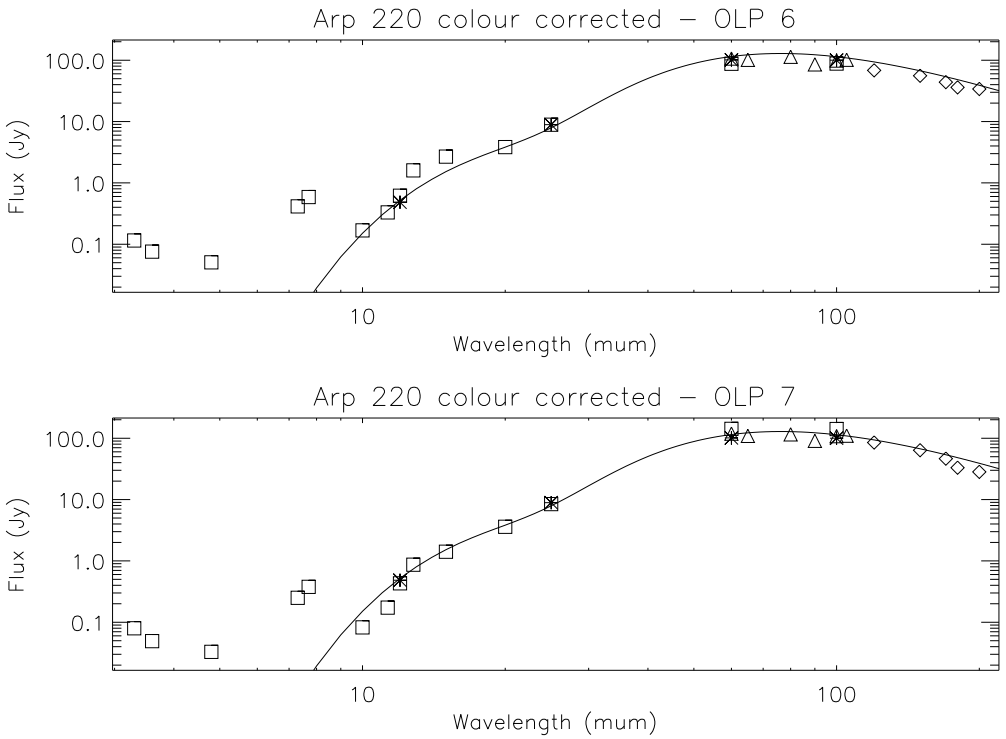

Figure 38: Color corrected PHT-P and PHT-C photometry as provided in part 2 of Sect. 5.15.5. The IRAS photometry has been color corrected, too. The model fit as described in Fig. 37 is plotted. Note that this model fit only serves as a guide for the eye to recognize more easily the changes between the two versions. It is not an absolute photometric reference. The meaning of the symbols is the following: solid line: model, asterisk: IRAS, square: PHT-P (P03 AOT), triangle: C100 (P22 AOT), diamond: C200 (P22 AOT).

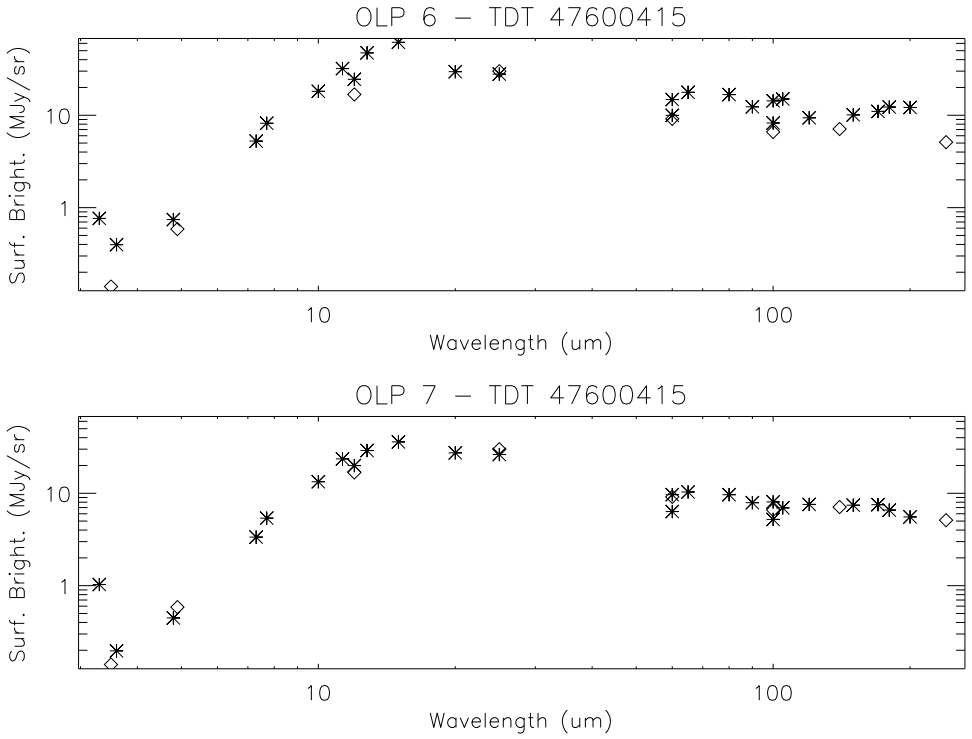

Figure 39: Comparison of PHT surface brightness photometry with COBE, both for OLP 6.x and OLP 7.0b2. Asterisk: PHT-P and PHT-C photometry, diamond: COBE.

5.15.4 Conclusions

- The 12 μm photometry is now very consistent with IRAS. In general the flux values in the short wavelength region have decreased by some 30 to 40% w.r.t. OLP 6.
- The SED in the 12 to 25 μm region fits now very well the 120 K modified BB and does not show anymore the excess peaking at around 16 μm.
- In the 60 to 100 μm region the flux is in general 10% higher than previously and also 10% higher than IRAS.
- The P3 photometry gives about 25% too high fluxes w.r.t. C100 and 40% too high fluxes w.r.t. IRAS.
- The transition between C100 and C200 photometry is very smooth after color correction. The larger correction to the C_160 filter data point brings it well in line with the shorter wavelength C200 photometry. The 180 μm data point lies relatively low.
- A model fit to the data may need a modified BB $\propto \nu^2$ now in order to fit the relatively steep decline at the longest wavelengths.
- PHT-P1, PHT-P2, PHT-C100, and PHT-C200 surface brightness values derived for the background position are very consistent with COBE DIRBE results. The PHT-P3 surface brightness values are too low.

5.15.5 Evaluation Log

1) point source photometry of Arp 220 (not colour corrected)

Filter	Cwl	OLP6	OLP7	IRAS	PIA
P1_3P29_UM	3.3	0.1150295	0.0796712	0.	0.07
P1_3P6_UM	3.6	0.0757821	0.0491831	0.	0.03
P1_4P85_UM	4.8	0.0506276	0.0328892	0.	0.04
P1_7P3_UM	7.3	0.4142557	0.250238	0.	0.24
P1_7P7_UM	7.7	0.5883092	0.3774157	0.	0.38
P1_10_UM	10.	0.168159	0.0824959	0.	0.07
P1_11P3_UM	11.3	0.330425	0.172965	0.	0.19
P1_11P5_UM	12.	0.617082	0.4312	0.4837	0.43
P1_12P8_UM	12.8	1.580775	0.857934	0.	0.87
P1_16P0_UM	15.	2.672868	1.407122	0.	1.40
P2_20_UM	20.	3.567332	3.354951	0.	3.33
P2_25_UM	25.	8.27045	7.84971	7.92	7.83
P3_60_UM	60.	88.58941	143.9594	0.	144.01
P3_100_UM	100.	94.63771	151.8657	0.	153.10
C100_60_UM	60.	104.1478	116.1116	103.8	116.79
C100_50_UM	65.	112.2574	120.9544	0.	120.56
C100_70_UM	80.	136.3292	138.5939	0.	138.56
C100_90_UM	90.	98.48979	104.7533	0.	104.86
C100_100_UM	100.	111.9964	122.9243	112.4	123.40
C100_105_UM	105.	109.7524	118.7288	0.	120.91
C200_120_UM	120.	92.55816	115.413	0.	115.24
C200_135_UM	150.	68.51204	78.4187	0.	78.13
C200_160_UM	170.	65.55658	69.31552	0.	69.12
C200_180_UM	180.	44.5738	40.8519	0.	40.58
C200_200_UM	200.	37.01015	30.78647	0.	30.80

2) point source photometry of Arp 220 colour corrected from 12.8 to 200 micron

Filter	Cwl	OLP6	OLP7	IRAS	TBB
P1_3P29_UM	3.3	0.1150295	0.0796712	0.	n/a
P1_3P6_UM	3.6	0.0757821	0.0491831	0.	n/a
P1_4P85_UM	4.8	0.0506276	0.0328892	0.	n/a
P1_7P3_UM	7.3	0.4142557	0.250238	0.	n/a
P1_7P7_UM	7.7	0.5883092	0.3774157	0.	n/a
P1_10_UM	10.	0.168159	0.0824959	0.	n/a
P1_11P3_UM	11.3	0.330425	0.172965	0.	n/a
P1_11P5_UM	12.	0.617082	0.4312	0.4837	n/a
P1_12P8_UM	12.8	1.598357	0.867476	0.	120
P1_16P0_UM	15.	2.683602	1.412773	0.	120
P2_20_UM	20.	3.831721	3.603599	0.	120
P2_25_UM	25.	8.883405	8.431482	8.909	80
P3_60_UM	60.	87.53894	142.2524	0.	50
P3_100_UM	100.	88.11705	141.4020	0.	50
C100_60_UM	60.	106.3818	118.6022	101.17	50
C100_50_UM	65.	101.4986	109.3620	0.	50
C100_70_UM	80.	113.7024	115.5912	0.	50
C100_90_UM	90.	85.42046	90.85282	0.	50
C100_100_UM	100.	98.50167	108.1128	100.18	50
C100_105_UM	105.	101.7168	110.0360	0.	50
C200_120_UM	120.	68.25823	85.11283	0.	50
C200_135_UM	150.	55.74617	63.80692	0.	50
C200_160_UM	170.	43.93873	46.45812	0.	50
C200_180_UM	180.	36.06295	33.05170	0.	50
C200_200_UM	200.	33.95427	28.24447	0.	50

5.16 General Re-validation of PHT Multi-filter (PHT03/PHT22) and PHT Absolute (PHT05/PHT25) Staring Mode Photometry: The SED of γ Draconis (HR 6705)

- authors: M. Radovich, U. Klaas
- date: 15-May-1998

5.16.1 Motivation

γ Dra (HR 6705) is a key calibration standard in ISOPHOT calibration. It is about five times fainter than α Bootes. It was observed in multi-filter staring mode from 3.3 out to 200 μm, as well as for some selected filters in absolute photometric mode (commissioning case of PHT05/25). Beside the check of the absolute photometric accuracy and the relative filter-to-filter calibration the results from two different types of AOTs (multi-filter simple photometry versus absolute photometry) can be compared with each other.

5.16.2 Method

We compare the background subtracted flux values of both OLP V6.x and OLP V7.0b2 results against the model prediction and IRAS, both for the multi-filter and the absolute photometry, respectively. We compare the results of the multi-filter photometry against the ones from the absolute photometry in common filters.

5.16.3 Results

In Table 23 we compare the photometry from parts 1 and 3 (multi-filter) and part 2 (absolute) of Sect. 5.16.5 with the model by Cohen (composite spectrum out to 35 μm and extrapolation out to 300 μm. From the results it can be seen that the photometry beyond 60 μm (fluxes below 4 Jy) is unreliable for the single pointing staring mode. Reasons may be a combination of effects by signal evaluation, background subtraction from an individually calibrated background measurement, background confusion, non-linearities in responsivities, etc. (note that the 170 μm absolute photometry gives still a reasonable flux, while multi-filter photometry gives negative fluxes; FCS measurement is done in this filter) This has to be investigated in further detail. Like in the case of α Bootes it is related to the source-to-background contrast falling below 0.75 (1:1.3), as can be seen from Tab. 25. The settings used for the off-source and on-source FCS measurements are given in Table 26.
We therefore restrict the following analysis on the wavelength range from 3.6 to 60 μm:

- The P1 photometry gives very consistent results with the model except for 10, 12.8 and 16 μm. In these three wide band filters the in-band power is already fairly low compared to the in-band powers encountered in the 3.6 μm filter, for which the FCS calibration is done. The 16 μm filter measurement suffers a significant transient effect. For that reason the measurement had been repeated at 16 and 3.6 μm with longer measurement times. The second 16 μm measurement is consistent with the relative filter-to-filter accuracy found for the shorter wavelengths filters. The reproducibility of the measurement in the 3.6 μm filter is remarkable (0.2% !). Overall, the results found for α Boo are more or less reproduced (slightly less good relative filter-to-filter calibration). Multi-filter and absolute photometry at 12 μm yield the same results.
- The P2 photometry gives very consistent results with the model and among the two AOT modes. Accuracies are 10% absolute and 10% relative.
- The P3 60 μm photometry turns out to be very accurate, better than 10%.
- The C100 60 μm photometry has the same accuarcy for the multi-filter mode, but is systematically off (+35%) in two repeated measurements in absolute mode.

One remarkable point concerning the impact of signal evaluation is a discrepancy of 1 Jy at 170 μm between OLP and PIA (nominal flux of the source at this wavelength: 0.566 Jy !). As can be seen from the investigation in part 4 of Sect. 5.16.5 the discrepancy comes from systematically lower (one outlier) background fluxes for 3 C200 pixels in PIA.

Table 23: Consistency check of results from both multi-filter and absolute photometry with with HR 6705 model

Filter	**mode**	**consistency w.r.t. model OLP V6.x** [%]	**consistency w.r.t. model OLP V7.0b2** [%]
3.3	multf	-27.3	+2.9
3.6	multf 1	-16.7	+10.7
3.6	multf 2	-16.6	+10.9
4.8	multf	-17.1	+16.1
7.3	multf	-16.3	+5.0
7.7	multf	-10.5	+12.9
10	multf	-38.1	-17.5
11.3	multf	-18.0	+6.3
12	multf	-36.6	-4.7
12	abs	-16.3	-6.3
12 IRAS		-7.5	-7.5
12.8	multf	-20.4	-13.7
16	multf 1	+32.8	+35.6
16	multf 2	+1.3	+3.7
20	multf	-1.4	-2.9
25	multf	+7.0	+5.8
25	abs	-2.0	-7.1
25 IRAS		+7.1	+7.1
60 PHT-P	multf	+22.8	-7.4
60 PHT-P	abs	+24.7	-0.2
60 PHT-C	multf	–	-6.6
60 PHT-C	abs 1	+22.5	+28.2
60 PHT-C	abs 2	+24.1	+33.5
60 IRAS		-0.8	-0.8
65	multf	–	+55.3
80	multf	–	+31.9
90	multf	–	+27.1
100 PHT-P	multf	-51.2	-39.9
100 PHT-C	multf	–	+16.3
100 IRAS		+0.4	+0.4
105	multf	–	-31.3
120	multf	–	-86.1
150	multf	–	-86.2
170	multf	–	-155
170	abs	+10.7	-29.1
180	multf	–	-263
200	multf	–	-140

Table 24: Absolute and relative calibration accuracies per detector achieved for HR 6705 observation with OLP V7.0b2

detector	**absolute accuracy** [%]	**relative accuracy** [%]
P1	10 at 3.6 μm	20
P2	10 at 20 μm	10
P3	10 at 60 μm	–
C100	10 at 60 μm	–

Table 25: Source-to-background contrast for γ Draconis in FIR filters. The expected source flux is the model flux, the background flux is from the background measurement converted to Jy.

λ_c [μm]	**background flux** [Jy]	**expected source flux** [Jy]	**source-to-backgr. contrast**
60	5.89	4.55	0.77 (1:1.3)
65	6.26	3.87	0.62 (1:1.6)
80	6.40	2.55	0.40 (1:2.5)
90	5.10	2.01	0.40 (1:2.5)
100	6.13	1.63	0.27 (1:3.8)
105	6.37	1.47	0.23 (1:4.3)
120	8.19	1.13	0.14 (1:7.3)
150	9.30	0.72	0.08 (1:13)
170	10.12	0.56	0.05 (1:18)
180	10.20	0.50	0.05 (1:21)
200	11.33	0.40	0.04 (1:28)

Table 26: Electrical power settings of FCS1/TRS2 and filters used for γ Draconis PHT-C on-source and off-source measurements.

pointing	**mode**	**filter**	**electrical FCS power** [mW]
off-source	multi-filter	C100_90_UM	0.30
on-source	multi-filter	C100_60_UM	1.13
off-source	multi-filter	C200_160_UM	0.13
on-source	multi-filter	C200_160_UM	0.13
off-source	absolute	C100_60_UM	0.55
on-source	absolute	C100_60_UM	1.13
off-source	absolute	C200_160_UM	0.13
on-source	absolute	C200_160_UM	0.13

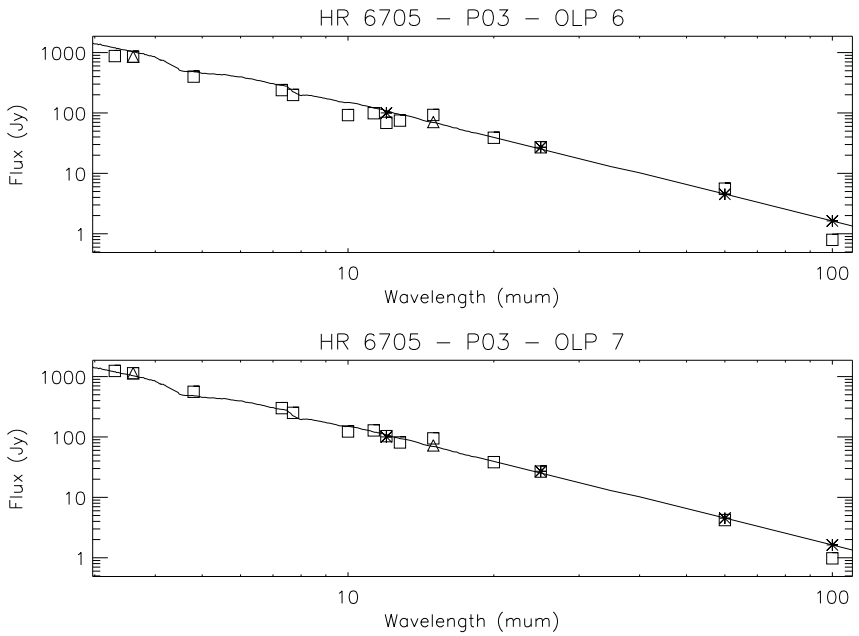

Figure 40: Comparison of PHT-P photometry, using the full ISOPHOT-P filter set, with the composite spectrum and out to 300 μm extrapolated SED of γ Dra (HR 6705) provided by M. Cohen and with IRAS photometry. Upper panel for OLP 6.x and lower panel for OLP 7.0b2. All photometric points are color corrected for a 4000 K BB. The meaning of the symbols is the following: solid line: model, asterisk: IRAS, square: PHT-P (P03 AOT) on rev. 356, triangle: repetition of 3.6 and 16 μm photometry on rev. 398.

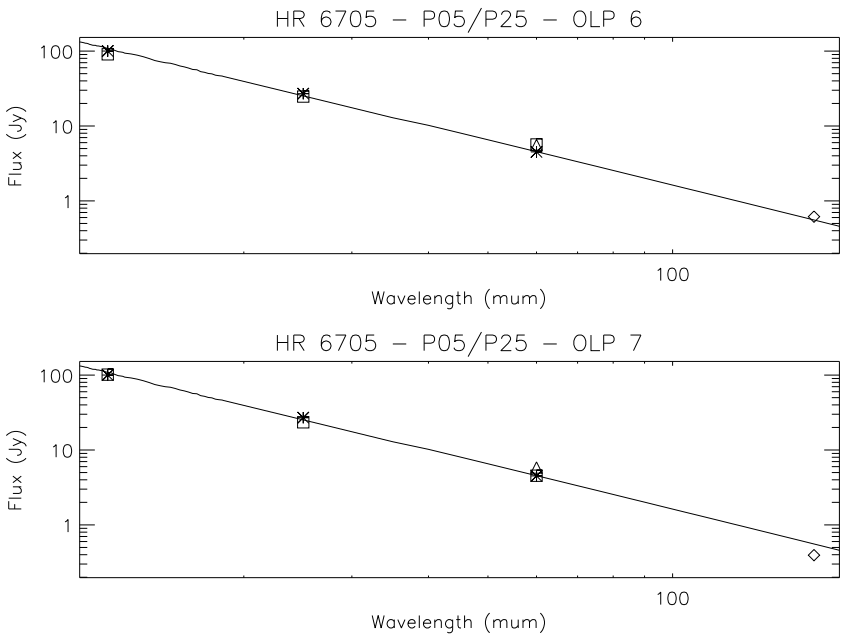

Figure 41: Comparison of PHT-P and PHT-C absolute photometry at 12, 25, 60 (P3 and C100) and 160 μm with the composite spectrum and out to 300 μm extrapolated SED of γ Dra (HR 6705) provided by M. Cohen and with IRAS photometry. Upper panel for OLP 6.x and lower panel for OLP 7.0b2. All photometric points are color corrected for a 4000 K BB. The meaning of the symbols is the following: solid line: model, asterisk: IRAS, square: PHT-P (P05 AOT), triangle: C100 (P25 AOT), diamond: C200 (P25 AOT).

5.16.4 Conclusions

- For γ Dra absolute calibration for both P1 and P3 have been considerably improved with OLP V7.0b2.
- The multi-filter photometry for P1 has been improved, too.
- PHT photometry gives a good representation of the SED from 3.3 to 105 μm.
- The C100 absolute photometry is slightly worse with OLP V7.0b2 and is systematically too high by about 35%.
- Detailed explanations for the unreliable photometry beyond 60 μm for this simple staring off/on mode have to be worked out. The source-to-background contrast suggests that multi-filter staring off/on photometry becomes unreliable for source-to-background ratios below 1:1.3 (0.75). Absolute photometry is more stable but shows a similar trend of negative photometric bias for low source-to-background contrasts. This issue needs follow-up in the context of the responsivity non-linearity with flux investigations.

5.16.5 Evaluation Log

```
1) multi-filter point source photometry of HR 6705
  (TDTs 35602101 (background), 35602102, and 39801901(!))
  (color corrected for T = 4000 K BB)

Filter          Cwl           OLP6          OLP7        IRAS      Cohen model
P1_3P29_UM      3.3          875.1927      1240.16       0.        1204.81
P1_3P6_UM       3.6          853.0809      1134.352      0.        1024.29
P1_4P85_UM      4.8          399.9616      559.9567      0.        482.322
P1_7P3_UM       7.3          239.1871      299.9805      0.        285.770
P1_7P7_UM       7.7          198.647       250.5493      0.        221.993
P1_10_UM       10.           92.26231      123.1164      0.        149.162
P1_11P3_UM     11.3          98.98927      128.291       0.        120.679
P1_11P5_UM     12.           68.60023      103.2155    100.16      108.251
P1_12P8_UM     12.8          74.77631      81.03918      0.        93.9518
P1_16P0_UM     15.           92.78841      94.79015      0.        69.8961
P2_20_UM       20.           38.84711      38.2479       0.        39.3867
P2_25_UM       25.           27.00178      26.69118     27.03      25.2292
P3_60_UM       60.           5.582195      4.208035      4.51      4.545
P3_100_UM     100.           0.7932419     0.9779581     1.633     1.627
C1_3P6_UM  #    3.6          854.4516      1136.092      0.        1204.81
C1_16P0_UM #   15.           70.81024      72.46912      0.        69.8961

#just a trick: last 2 meas. are NOT C meas. , but P (m398 !!)


2) absolute point source photometry of HR 6705
   (TDTs 35300301..06 for PHT-P, 35300308..12 for PHT-C)
   (color corrected for T = 4000 K BB)

Filter          Cwl         OLP6        OLP7       IRAS    Cohen model      PIA
P1_11P5_UM      12.       90.64442    101.4209    100.16     108.251       100.53
P2_25_UM        25.       24.73496    23.43052    27.03      25.2292       23.63
P3_60_UM        60.       5.668673    4.532713    4.51       4.545         4.47
C100_60_UM      60.       5.566906    5.825477    0.         4.545         6.40   *)
C100_60_UM      60.       5.639548    6.0665      0.         4.545          -     **)
C200_160_UM     170.      0.615834    0.394695    0.         5.563E-01     1.39

*)  photometry from TDT 35300310 (35300308 background)
**) photometry from TDT 35300309 (35300308 background)


3) C100 and C200 multi-filter point source photometry of HR 6705
```

(TDTs 35602203/4 for C200, TDTs 39802002/3 for C100)

Filter	Cwl	OLP 7 (color corrected)	Cohen model
C100_60_UM	60.	4.246181	4.545
C100_50_UM	65.	6.014968	3.872
C100_70_UM	80.	3.364533	2.550
C100_90_UM	90.	2.55722	2.012
C100_100_UM	100.	1.891809	1.627
C100_105_UM	105.	1.013118	1.474
C200_120_UM	120.	0.1562826	1.126
C200_135_UM	150.	0.09913819	7.169E-01
C200_160_UM	170.	-0.3054825	5.563E-01
C200_180_UM	180.	-0.8051882	4.954E-01
C200_200_UM	200.	-0.1590631	3.999E-01

4) investigation of discrepancy between OLP7 and PIA 170 um photometry discrepancy

Pix	S+B (C20135300312)		Back (C20235300311)	
	OLP 7	PIA 7.1	OLP 7	PIA 7.1
1	2.27	2.53	2.15	2.10
2	2.79	2.25	2.54	1.92
3	2.55	2.79	2.47	2.20
4	2.52	2.52	2.50	2.19
Total	10.13	10.09	9.66	8.42

Background subtracted flux (not col. corrected)	0.47	(OLP)
	1.67	(PIA)

5.17 General Re-validation of PHT Staring, Nodding and Mini-map Modes: The SED of Sirius (HR 2491)

- authors: M. Radovich, U. Klaas
- date: 22-May-1998

5.17.1 Motivation

Beside Vega (HR 7001), Sirius is the main primary stellar standard with a model provided by M. Cohen (1-300 mic, R = 4000 up to 35 mic, delivered 12-Jan-96). Therefore, a dedicated cross-calibration program has been performed on this star using absolute photometry complemented by multi-filter photometry out to 25 μm and for the longer wavelengths using the nodding and mini-map technique in order to obtain a proper background subtraction.

5.17.2 Method

We compare the background subtracted flux values of both OLP V6.x and OLP V7.0b2 results against the model and IRAS fluxes.

5.17.3 Results

In the following Tab. 27 we compare both the multi-filter and the absolute photometry of Sect. 5.17.5 with the model. We estimate the absolute photometric accuracy per detector assembly for this target as the deviation from the model flux in the filter in which the FCS calibration was done and the relative filter-to-filter accuracy as the peak-to-peak variation of the other filters around this offset. The resulting photometric accuracies are presented in Tab. 28. Fig. 42 shows the PHT photometric data points in comparison to the model and IRAS photometry (color corrected) from 3.3 to 100 μm.

Table 27: Consistency check of photometric results with Sirius model

Filter	**mode**	**consistency w.r.t. model OLP V6.x** [%]	**consistency w.r.t. model OLP V7.0b2** [%]
3.3	multf	–	+8.7
3.3	abs	–	+1.0
7.7	multf	–	+1.4
11.3	multf	-26.3	-6.2
12	multf	-3.9	+14.7
12	abs	–	+7.2
12 IRAS		+5.9	+5.9
12.8	multf	-10.3	-3.8
16	multf	+2.2	+1.5
25	abs	+23.5	+15.2
25 IRAS		+11.8	+11.8
60 P3	nodding	–	+14.7
60 C100	nodding	–	-17.0
60 C100	minimap	–	-13.3
60 IRAS		+1.4	+1.4
100 C100	minimap	–	-32.1
100 IRAS		+69.8	+69.8

5.17.4 Conclusions

- For P1 the photometry has improved for OLP V7.0b2. Absolute photometry in two filters (3.3 and 12 μm) gave results better than 7%. Also the relative filter-to-filter

Table 28: Absolute and relative calibration accuracies per detector achieved for Sirius observation with OLP V7.0b2

detector	**absolute accuracy** [%]	**relative accuracy** [%]
P1	1 at 3.3 μm (abs. phot)	–
P1	10 at 3.3 μm	8
P1	7 at 12 μm (abs. phot)	–
P1	4 at 12.8 μm	5
P2	15 at 25 μm	–
P3	15 at 60 μm	–
C100	17 at 60 μm	–
C100	32 at 100 μm	–

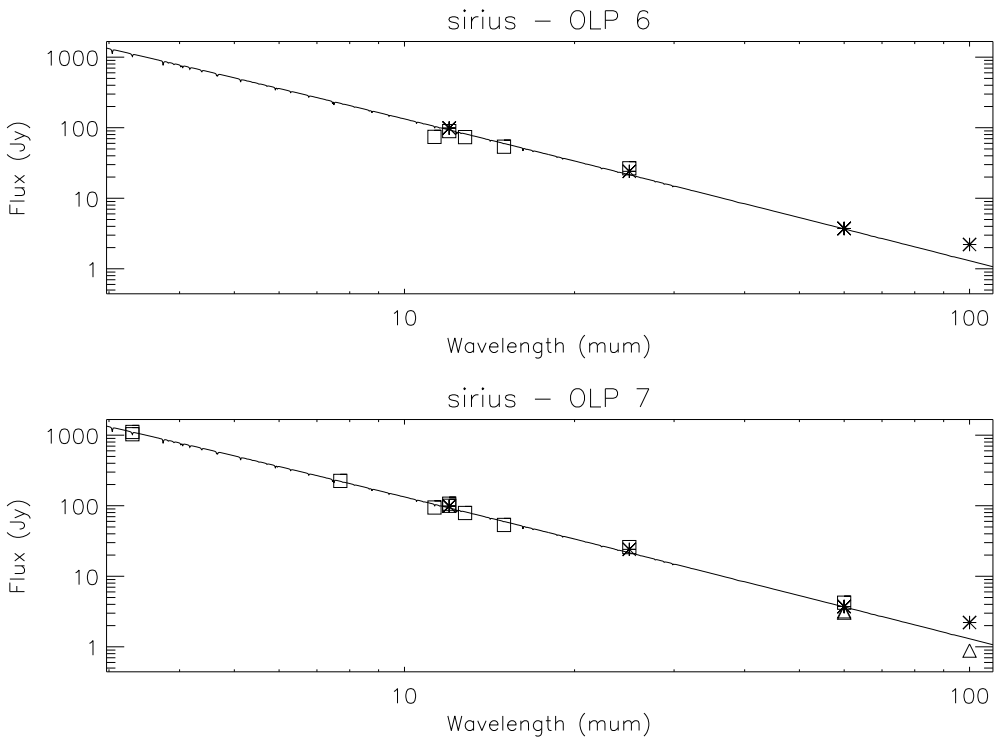

Figure 42: Comparison of PHT-P1 multi-filter, PHT-P1 and P2 absolute photometry, P3 and C100 nodding and C100 minimap photometry with the model spectrum of Sirius provided by M. Cohen and with IRAS photometry. Upper panel for OLP 6.x and lower panel for OLP 7.0b2 (For V6 some measurements were not processed by OLP or not evaluated for this report). All photometric points are color corrected for a 10000 K BB. The meaning of the symbols is the following: solid line: model, asterisk: IRAS, square: PHT-P multi-filter or nodding (P03 AOT) and absolute (P05 AOT), triangle: PHT-C nodding and mini-map (P22 AOT).

calibration is better than 10%. Of some help may have been the splitting up of the observations into a short and long wavelength part avoiding too large flux steps with only one absolute FCS calibration. The absolute photometry is relative to the multi-filter photometry more accurate.

- For P2 the absolute photometry has improved to 15%.
- For P3 the nodding technique gives an absolute accuracy of 15% for a flux of approximately 4 Jy.
- For C100 nodding and mini-map give consistent results with an absolute accuarcy of $\sim$ 15% at 60 μm. At 100 μm the derived flux is 30% below the model flux; note that IRAS gives a flux value which is 70% above the model. As for HR 5430 and HR 6705 the photometric bias w.r.t. the model is again negative.
- Two AOTs which crashed for OLP V6.2.2 are processed without any problem with OLP V7.0b2. The likely explanation for the crash is the FCS power in the P1_3P29_UM filter being at the margin of the CALG power file with a value of 49.99 mW. With the new CALG V4.0 the margin is now at 50.00 mW.

5.17.5 Evaluation Log

```
1) P1 multi-filter point source photometry of HR 2491
   (TDTs 70705301, 70705302)
   Color corrected fluxes (T=10000 K)

 Filter         cwl     OLP6        OLP7       IRAS      Cohen model

P1_3P29_UM      3.3     0.*)      1110.84      0.          1021.90
P1_7P7_UM       7.7     0.*)      225.0382     0.          222.038
P1_11P3_UM     11.3    74.20546   94.39465     0.          100.654
P1_11P5_UM      12.    89.55344   106.8664     98.69       93.1571
P1_12P8_UM     12.8    73.55049   78.87461     0.          82.0013
P1_16P0_UM      15.    53.79828   53.44737     0.          52.6472

*) OLP 6 data not available due to processing error:
   arithmetic trap, subscript out of range

2) P1 and P2 absolute photometry of HR 2491
   (TDTs 70705310, 70705313, 70705707)
   Color corrected fluxes (T=10000 K)

 Filter         cwl     OLP6        OLP7       IRAS      Cohen model

P1_3P29_UM      3.3     0.*)      1032.6       0.          1021.90
P1_11P5_UM      12.     0.*)      99.9084      98.69       93.1571
P2_25_UM        25.    26.59477   25.9193      24.09       21.5411

*) OLP 6 data not available due to processing error:
   arithmetic trap, subscript out of range

3) P3 60 um nodding, C100 60 um nodding, C100 60 um and 100 um mini-map
   (TDTs 70705606, 70705605, 70705603, 70705604)
   (OLP 6 data not evaluated)
   Color corrected fluxes (T=10000 K)

 Filter         cwl     OLP6        OLP7       IRAS      Cohen model

P3_60_UM        60.    0.        4.22042      3.73        3.67960
C100_60_UM      60.    0.        3.053216     3.73        3.67960   nodding
C100_60_UM      60.    0.        3.188838     3.73        3.67960   mini-map
C100_100_UM    100.    0.        0.8841559    2.21        1.30191
```

5.18 General Re-validation of PHT03 Staring Mode: Photometric Reproducibility Aspects in the Case of the SED of Vega (HR 7001)

- authors: M. Radovich, U. Klaas
- date: 22-May-1998

5.18.1 Motivation

We investigate here the photometric accuracy of PHT-P multi-filter aperture photometry for an observation of Vega from a general observer program which was repeated several times as part of a variability monitoring project. From 3.3 to 100 μm it used the typical exposure time of 32 s per filter and non-standard apertures. The absolute calibration via the FCS of the on-source measurement was performed in the 3.6, 20, and 100 μm filter, respectively. The absoloute calibration of the off-source measurement was performed in the 7.3, 25, and 100 μm filter, respectively. We selected 3 measurements out of this program from rev. 85 (TDT 08500106; before rev. 94 FCS change!), rev. 558 (TDT 55800419) and rev. 865 (TDT 86500706). The used apertures w.r.t. the standard apertures for point source calibration are listed in the following Table 29:

Table 29: Apertures used in the Vega variability monitoring program versus standard apertures

filter	**program aperture** ["]	**standard aperture** ["]
P1_3P29_UM	18	23
P1_3P6_UM	18	23
P1_4P85_UM	18	23
P1_7P3_UM	18	23
P1_10_UM	18	52
P1_11P5_UM	18	52
P1_12P8_UM	18	52
P1_16P0_UM	18	52
P2_20_UM	52	79
P2_25_UM	52	79
P3_60_UM	120	180
P3_100_UM	120	180

5.18.2 Method

Vega is one of the primary photometric stellar standards. However, due to its IR excess, the photospheric models, e.g. by Cohen, are valid only out to approximately 15 μm. Beyond 15 μm we solely compare with the available IRAS photometry. The investigation of the flux reproducibility is restricted to the OLP V7.0b2 results and does not include OLP V6.x results.
The color correction was dependent on the relative contribution by the stellar photosphere and the IR disc, and hence on the wavelength. We followed the description as given in Ref.[15]:

- from 3.3 to 16 μm the SED behaves like a 10000 K Black Body,
- from 60 to 100 μm the SED behaves like an 80 K modified BB, $\varepsilon \propto \nu$
- from 20 to 25 μm the SED is a mixture of a 10000 K BB and an 80 K modified BB with a ratio 2:1.

5.18.3 Results

In Sect. 5.18.5 we give the background subtracted and color corrected photometry for the three epochs. In Table 30 we compare these fluxes against Cohen's Vega model up to 15 μm and against IRAS beyond. For illustration the resulting SEDs are plotted in Figs. 43 to 45. From the table we can conclude the following:

- The absolute calibration of P1 w.r.t. the model is as accurate as $\pm$ 10%. The relative filter-to-filter calibration is $\pm$ 20% out to 10 μm. For longer wavelengths the uncertainties become much larger which can be traced to signatures of severe transient effects for the low in-band power filters during the 32 s lasting measurement (cf. Report on HR 6705 staring photometry).

- The absolute calibration of P2 w.r.t. IRAS is systematically above the IRAS flux by 35%. No relative filter-to-filter accuracy can be derived due to the lack of a reference measurement. However, it should be noted that the color correction is tricky in this range due to a mixture of a very hot SED with a relatively cold one and the respective correction factors for IRAS and ISOPHOT 25 μm are different (the color correction factors are 1.41/0.889 for IRAS and 1.285/0.931 for ISOPHOT).

- The absolute calibration of P3 w.r.t. IRAS is as accurate as $\pm$ 7%. The relative filter-to-filter calibration is as good as 15%.

- The reproducibility of the relative shape of the SED is remarkably high, with a scatter of $\simeq$ 10%, including the filters with the transient features with a scatter of up to $\simeq$ 20%. This can be seen from Table 31 where the fluxes normalized to 3.3 μm and the 1 σ values of the flux scatter are given.

Table 30: Consistency check of photometric results with Vega model and IRAS photometry for the three epochs on revs. 085, 558, and 865. The values in each second column per revolution give the offset relative to the FCS calibration filter.

filter	**ref.**	**consistency w.r.t. model or IRAS**					
		rev. 085 [%]		**rev. 558** [%]		**rev. 865** [%]	
3.3	model	-11.1	-5.5	+3.6	-6.3	+0.3	-9.9
3.6	model	-5.6	0.00	+9.9	0.00	+10.2	0.00
4.8	model	+6.7	+12.3	+22.4	+12.5	+22.0	+11.8
7.3	model	-1.8	+3.8	+11.9	+2.0	+12.2	+2.0
10	model	-20.5	-14.9	+4.7	-5.2	-13.7	-22.9
12	model	-34.5	-28.9	-20.1	-30.0	-30.5	-40.7
12	IRAS	-38.4	–	-24.8	–	-34.6	–
12.8	model	+12.3	+17.9	+55.8	+45.9	+25.0	+14.8
16	model	+60.7	+66.3	+111	+101	+80.6	+70.4
25	IRAS	+38.2	0.00	+31.6	0.00	+31.9	0.00
60	IRAS	+9.1	+3.9	-0.4	+4.1	+20.0	+13.7
100	IRAS	+5.2	0.00	-4.5	0.00	+6.3	0.00

5.18.4 Conclusions

- PHT-P photometry with the minimum recommended exposure time of 32 s and in non standard apertures yields about $\pm$ 10% absolute accuracy for P1 and P3. The relative filter-to-filter calibration is better than 20%.

- The P2 accuracy is difficult to estimate for the selected target, due to an unknown mixture of highly different temperature components which involve different ratios of color correction factors for ISOPHOT and the reference photometry.

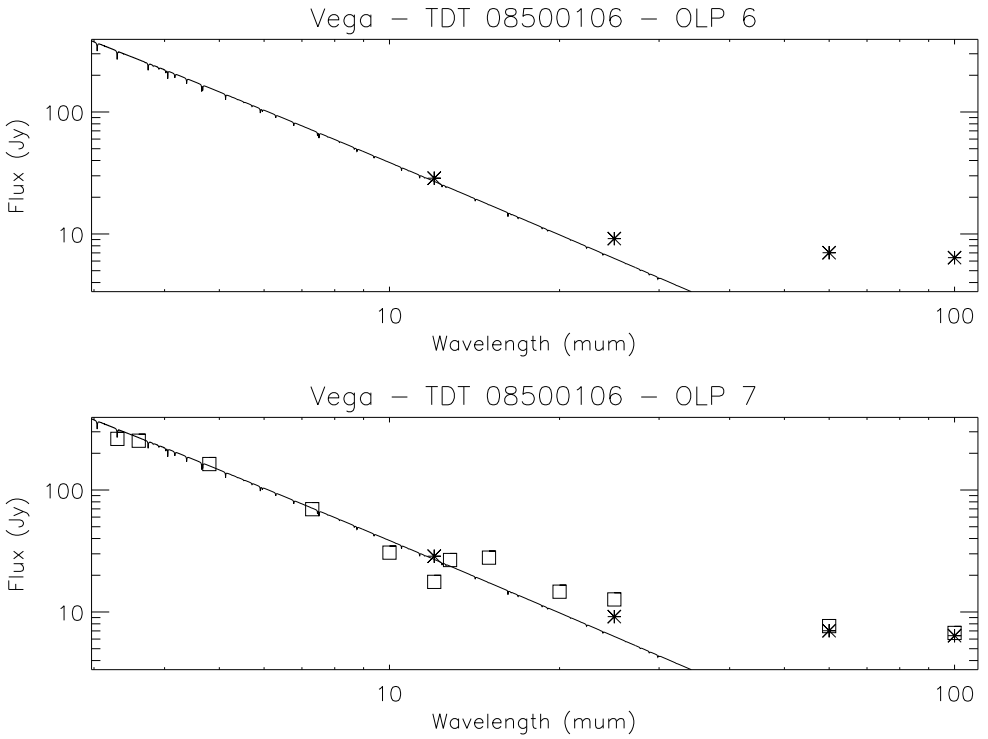

Figure 43: Comparison of PHT-P Vega photometry from rev. 085 with the Cohen Vega spectrum and with IRAS photometry. Only OLP 7.0b2 results are plotted. All photometric points are color corrected as described in section Method. The meaning of the symbols is the following: solid line: model, asterisk: IRAS, square: PHT-P (P03 AOT).

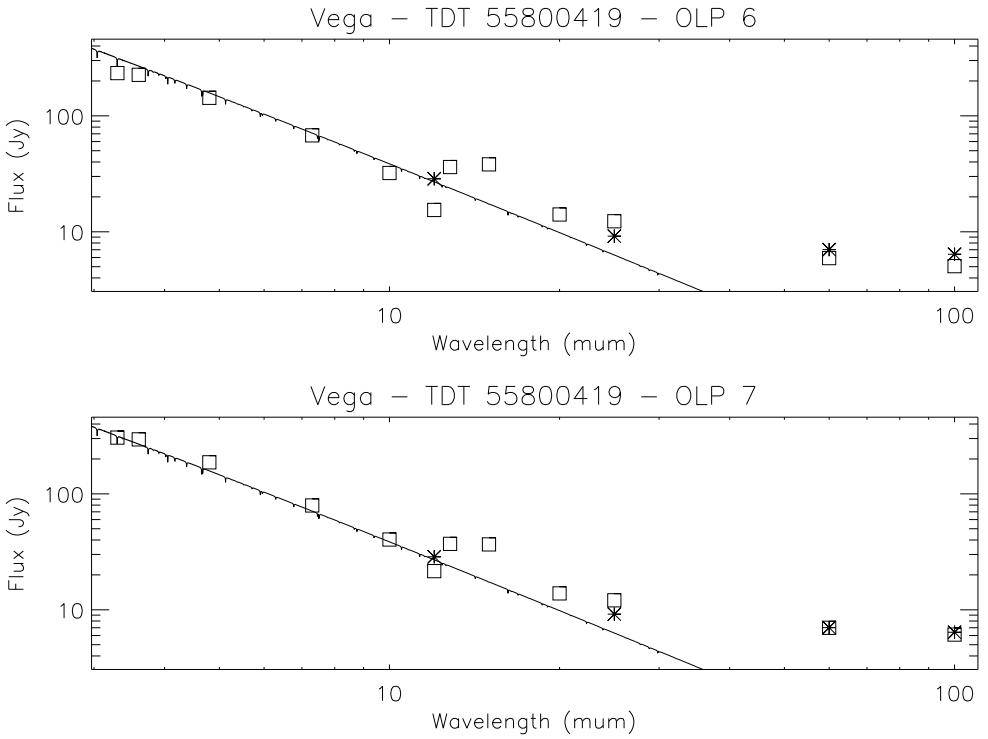

Figure 44: Comparison of PHT-P Vega photometry from rev. 558 with the Cohen Vega spectrum and with IRAS photometry. Only OLP 7.0b2 results are plotted. All photometric points are color corrected as described in section Method. The meaning of the symbols is the following: solid line: model, asterisk: IRAS, square: PHT-P (P03 AOT).

Table 31: Normalized fluxes w.r.t. flux in the 3.3 μm filter and relative variation (1 σ) of the flux for the revolutions 085, 558, and 865.

Filter	**normalized flux**			**relative variation of flux** [%]
	rev. 085	**rev. 558**	**rev. 865**	
3.3	1.0000	1.0000	1.0000	7.9
3.6	0.9664	0.9655	1.0001	8.6
4.8	0.6221	0.6128	0.6307	7.6
7.3	0.2655	0.2598	0.2691	7.5
10	0.1169	0.1322	0.1125	14.4
12	0.0673	0.0705	0.0634	10.4
12.8	0.1017	0.1212	0.1004	17.1
16	0.1064	0.1200	0.1060	13.8
20	0.0560	0.0453	0.0472	3.2
25	0.0483	0.0395	0.0409	2.8
60	0.0292	0.0229	0.0285	9.3
100	0.0257	0.0200	0.0230	5.8

- Although the parts of the SED refering to the same absolute calibration scale up and down due to the absolute calibration accuracy achievable with a 32 s FCS measurement, the relative shape of the SED is reproducible within approximately 10%.
- The accuracy in several filters of this measurement sequence is currently limited by the accuracy of the signal evaluation due to signal transients.
- The measurement belong to a project for source variability monitoring. From the reproducibility of the measurements due to current absolute and relative measurement scatter, variability below 30% cannot be recognized on a 2 σ level.

5.18.5 Evaluation Log

```
1) Vega PHT-P aperture photometry from 3.3 to 100 um
   (color corrected: 3.3 - 16 um: 10000 K BB
                     60 - 100 um: 80 K modified BB propto nu
                     20 -  25 um: mixture of 10000 K BB and 80 K modified BB
                                  with ratio 2:1

a) rev. 085

# Filter        cwl   cc_flx_olp7    IRAS     Cohen model
P1_3P29_UM      3.3     262.3633      0.        294.972
P1_3P6_UM       3.6     253.5429      0.        268.460
P1_4P85_UM      4.8     163.2152      0.        152.911
P1_7P3_UM       7.3     69.65817      0.        70.9460
P1_10_UM        10.     30.68213      0.        38.5701
P1_11P5_UM      12.     17.65871     28.66      26.9774
P1_12P8_UM      12.8    26.67884      0.        23.7636
P1_16P0_UM      15.     27.90421      0.        17.3640
P2_20_UM        20.     14.6799       0.          --
P2_25_UM        25.     12.67361      9.17        --
P3_60_UM        60.     7.661637      7.02        --
P3_100_UM      100.     6.733053      6.40        --

b) rev. 585

# Filter        cwl   cc_flx_olp7    IRAS     Cohen model
P1_3P29_UM      3.3     305.4923      0.        294.972
```

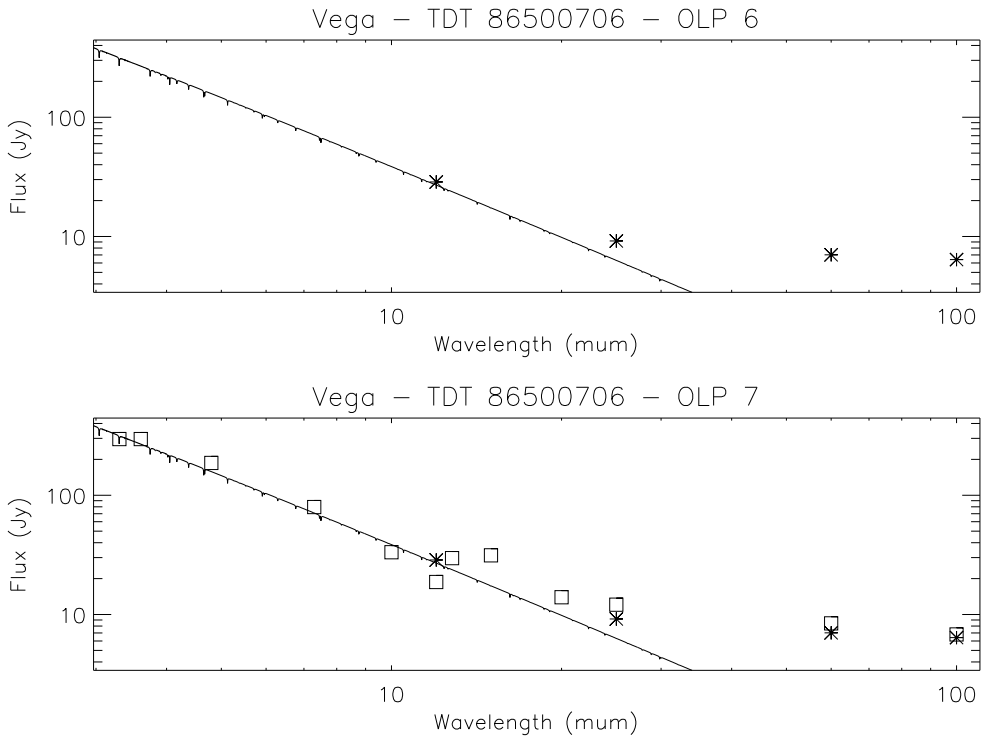

Figure 45: Comparison of PHT-P Vega photometry from rev. 865 with the Cohen Vega spectrum and with IRAS photometry. Only OLP 7.0b2 results are plotted. All photometric points are color corrected as described in section method. The meaning of the symbols is the following: solid line: model, asterisk: IRAS, square: PHT-P (P03 AOT).

```
P1_3P6_UM       3.6     294.9571      0.        268.460
P1_4P85_UM      4.8     187.2034      0.        152.911
P1_7P3_UM       7.3     79.36838      0.        70.9460
P1_10_UM        10.     40.37111      0.        38.5701
P1_11P5_UM      12.     21.54255     28.66      26.9774
P1_12P8_UM      12.8    37.0346       0.        23.7636
P1_16P0_UM      15.     36.64511      0.        17.3640
P2_20_UM        20.     13.85091      0.          --
P2_25_UM        25.     12.07224      9.17        --
P3_60_UM        60.     6.990124      7.02        --
P3_100_UM      100.     6.110443      6.40        --

c) rev. 865

# Filter        cwl   cc_flx_olp7    IRAS     Cohen model
P1_3P29_UM      3.3     295.7858      0.        294.972
P1_3P6_UM       3.6     295.8083      0.        268.460
P1_4P85_UM      4.8     186.5487      0.        152.911
P1_7P3_UM       7.3     79.60626      0.        70.9460
P1_10_UM        10.     33.28211      0.        38.5701
P1_11P5_UM      12.     18.74165     28.66      26.9774
P1_12P8_UM      12.8    29.70022      0.        23.7636
P1_16P0_UM      15.     31.36514      0.        17.3640
P2_20_UM        20.     13.96321      0.          --
P2_25_UM        25.     12.09636      9.17        --
P3_60_UM        60.     8.424611      7.02        --
P3_100_UM      100.     6.80208       6.40        --
```

5.19 General Re-validation of C200 Absolute and Mapping Photometry of Ceres

- authors: M. Radovich, U. Klaas
- date: 05-June-1998

5.19.1 Motivation

As the stellar standards are relatively faint with significant contribution by the background in the C200 range, we investigate here the photometry of the bright primary asteroid standard Ceres. We compare absolute photometry, including an independent background measurement, with mapping photometry in order to derive the achieved photometric accuracy for a bright C200 point source.

5.19.2 Method

We compare both the absolute and the mapping photometry against the prediction of the thermophysical model by Lagerros calculated for the specific revolutions.

5.19.3 Results

In Figs. 46 and 47 we plot the absolute photometry (PHT25) and mini-map photometry (PHT22), respectively against the flux prediction from the thermophysical model by Lagerros.
While the fluxes in the first three filters are matching quite well for the PHT25 mode, the last two filters show a considerably negative offset of up to 40%. This time this cannot be explained by the background subtraction, as the source is at least five times brighter than the background. Comparison with the PHT22 mode results leads to the suggestion that the empirical f_{psf} factor for the C_180 and C_200 filter is incorrect by about 20% - 30%. Re-analysis of other test cases, like the ones from Arp 220 and α Bootes, under this aspect confirm this suggestion. Also for those a systematic drop of the photometric flux at 180 and 200 μm is observed (but for α Bootes there is an additional effect due to the relatively strong background flux superimposed).
In Table 32 we perform the consistency check w.r.t. the thermophysical model flux calculated for the respective revolution. It can be seen that the mapping photometry is now as accurate as 25% for all C200 filters. The absolute mode shows a split in wavelength range concerning the achieved accuracy: below 170 μm the photometry is better than 15%, while for the longer wavelengths the insufficient (too large) empirical point source fraction correction factor leads to less reliable photometry. This empirical correction factor needs re-analysis,as the current ones are based only on a small set of measurements [20]. The validation results suggest that the values of f_{psf} for C_180 and C_200 must be 20 - 30% smaller, which rises the photometric fluxes by the same percentage.

5.19.4 Conclusions

- PHT22 C200 mapping photometry of Ceres could be successfully validated for OLP 7 with an accuracy of better than 25%.
- The consistency check with the model suggests that in the case of this object which is considerably brighter (at least 5x) than the background the negative photometric bias for the two longest wavelength filters C_180 and C_200 is introduced by too large empirical point spread function correction factors when centering the source on the array. Comparison with other test cases points towards a 20 - 30% correction of the factors in both filters. A caveat on this subject will be issued and a refined calibration analysis be initiated.

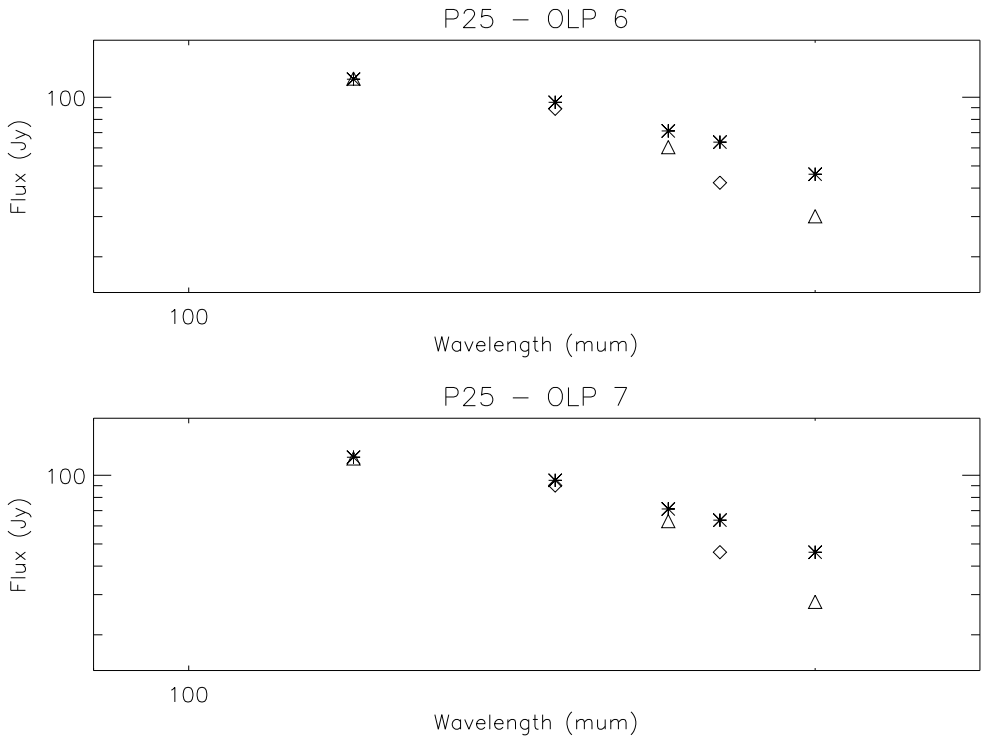

Figure 46: Comparison of C200 absolute photometry (AOT PHT25) in all 5 filters obtained at two different epochs (revs. 579 and 594) with the thermophysical model by Lagerros. All photometric points are color corrected for a 240 K BB. The meaning of the symbols is the following: asterisk: Lagerros model, triangle: rev. 579 photometry, diamond: rev. 594 photometry.

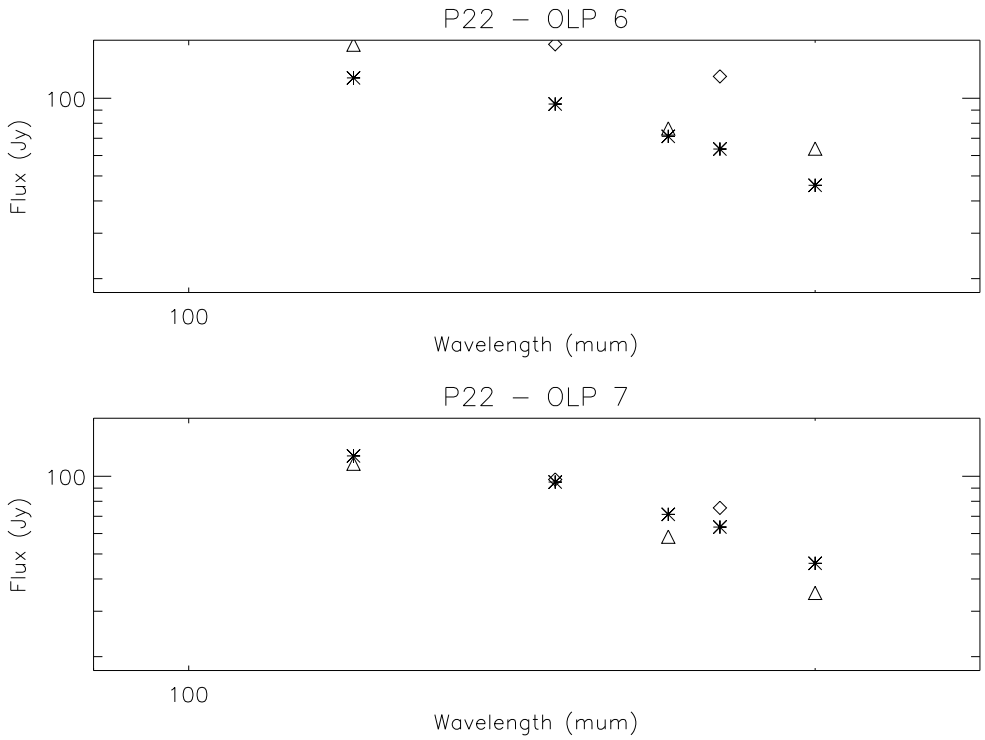

Figure 47: Comparison of C200 mapping photometry (AOT PHT22) in all 5 filters obtained at two different epochs (revs. 579 and 594) with the thermophysical model by Lagerros. All photometric points are color corrected for a 240 K BB. The meaning of the symbols is the following: asterisk: Lagerros model, triangle: rev. 579 photometry, diamond: rev. 594 photometry.

Table 32: Consistency check of C200 absolute (PHT25) and mini-map (PHT22) photometric results with the thermophysical model by Lagerros.

Filter	**AOT**	**consistency w.r.t. model OLP V6.x** [%]	**consistency w.r.t. model OLP V7.0b2** [%]
120	PHT25	+0.6	-1.2
120	PHT22	+34.5	-6.7
150	PHT25	-6.3	-5.1
150	PHT22	+70.4	+2.3
170	PHT25	-15.1	-11.5
170	PHT22	+7.3	-18.1
180	PHT25	-33.6	-27.6
180	PHT22	+91.2	+18.7
200	PHT25	-34.6	-39.4
200	PHT22	+38.7	-23.2

5.19.5 Evaluation Log

```
Ceres C200 photometry in absolute mode (P25) and mapping Mode (P22)

Fluxes have been color corrected (BB with T = 240 K)


OLP 6

# Detector       cwl      model        P25        P22     P25/model   P22/model

Rev. 579
C200_200_UM      200.      45.99      30.10      63.80       0.65       1.39
C200_120_UM      120.     119.96     120.73     161.31       1.01       1.34
C200_160_UM      170.      71.18      60.46     76.36        0.85       1.07

Rev. 594
C200_180_UM      180.      63.57      42.21     121.57       0.66       1.91
C200_135_UM      150.      95.00      89.00     161.84       0.94       1.70


OLP 7

# Detector       cwl      model        P25        P22    P25/model   P22/model

Rev. 579
C200_200_UM      200.      45.99      27.88      35.33       0.61       0.77
C200_120_UM      120.     119.96     118.50     111.90       0.99       0.93
C200_160_UM      170.      71.18      62.98      58.32       0.88       0.82

Rev. 594
C200_180_UM      180.      63.57      46.03      75.44       0.72       1.19
C200_135_UM      150.      95.00      90.19      97.14       0.95       1.02
```

5.20 General Re-validation of C200 Absolute and Mapping Photometry of Uranus

- authors: M. Radovich, U. Klaas
- date: 09-July-1998

5.20.1 Motivation

As the stellar standards are relatively faint with significant contribution by the background in the C200 range, we investigate here the photometry of the bright primary planetary standard Uranus. We compare absolute photometry, including an independent background measurement, with mapping photometry in order to derive the achieved photometric accuracy for a bright C200 point source.

5.20.2 Method

We compare both the absolute and the mapping photometry against the prediction of the model by M. Abbas calculated for the specific revolution.

5.20.3 Results

In Figs. 48 and 49 we plot the absolute photometry (PHT25) and mini-map photometry (PHT22), respectively against the flux prediction from the model by Abbas.
While the C_120 filter gives consistent photometry with the model within 10% for the PHT25 mode, the C_200 filter shows a considerably negative offset of 30%. This time this cannot be explained by the background subtraction, as the source is significantly brighter than the background. Comparison with the PHT22 mode results leads to the suggestion that the empirical f_{psf} factor for the C_200 filter is too large by about 20% - 30%, confirming the results obtained for Ceres.

Table 33: Consistency check of C200 absolute (PHT25) and mini-map (PHT22) photometric results with the flux model of the planet Uranus by M. Abbas.

Filter	**AOT**	**consistency w.r.t. model OLP V6.x** [%]	**consistency w.r.t. model OLP V7.0b2** [%]
120	PHT25	+4.5	+1.4
120	PHT22	+36.0	-10.3
200	PHT25	-21.8	-27.3
200	PHT22	+88.5	-7.5

5.20.4 Conclusions

- PHT22 C200 mapping photometry of Uranus could be successfully validated for OLP 7 with an accuracy of better than 10%.
- The consistency check with the model suggests, that in the case of this object, which is considerably brighter than the background, the negative photometric bias for the longest wavelength filter C_200 is introduced by a too large empirical point spread function correction factor when centering the source on the array. This confirms the results found for the Ceres observations. Comparison with other test cases points towards a 20 - 30% correction of the factor in this filter. A caveat on this subject will be issued and a refined calibration analysis be initiated.

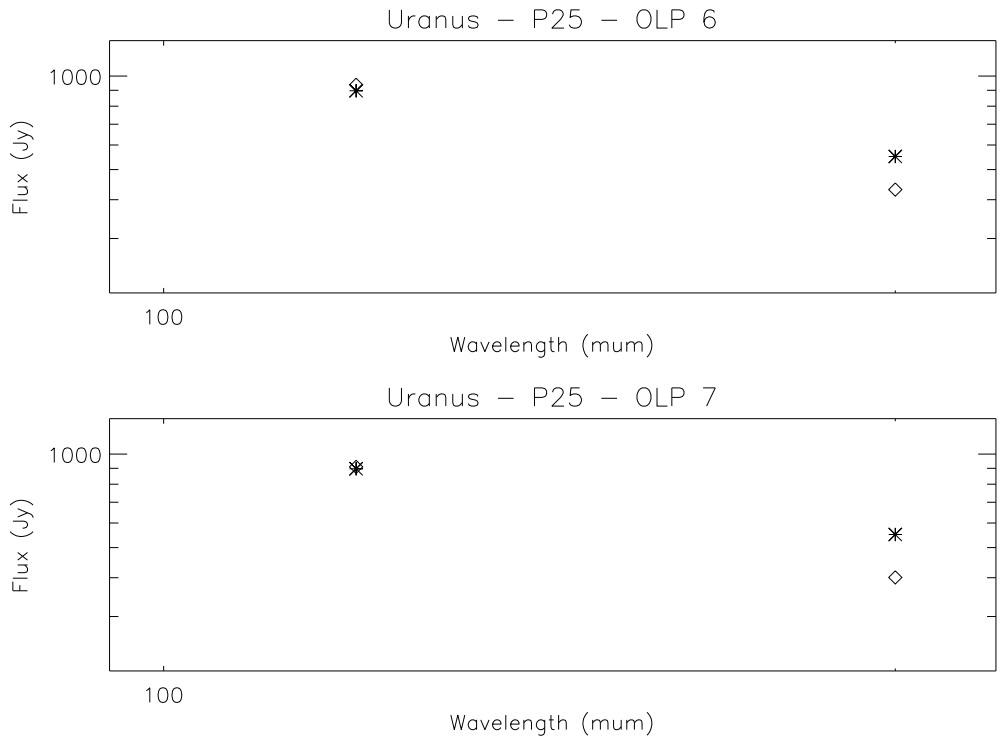

Figure 48: Comparison of C200 absolute photometry (AOT PHT25) in the 120 and 200 μm filters with the flux model of Uranus by Abbas. All photometric points are color corrected for a 60 K BB. The meaning of the symbols is the following: asterisk: Abbas model, diamond: C200 photometry.

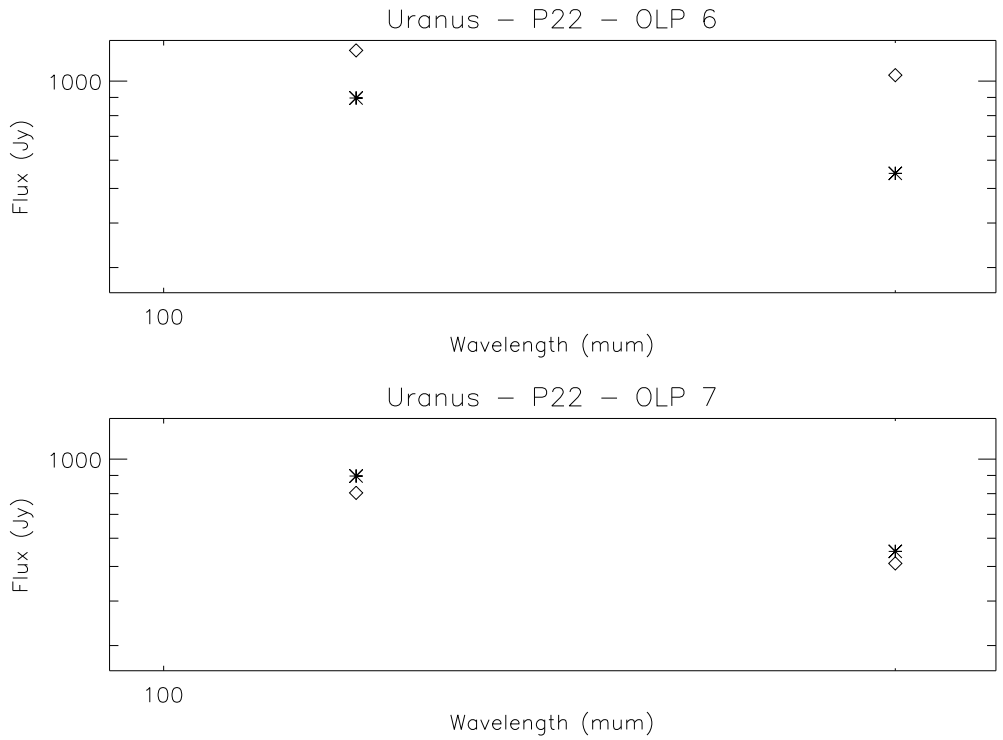

Figure 49: Comparison of C200 mapping photometry (AOT PHT22) in the 120 and 200 μm filters with the flux model of Uranus by Abbas. All photometric points are color corrected for a 60 K BB. The meaning of the symbols is the following: asterisk: Abbas model, diamond: C200 photometry.

5.20.5 Evaluation Log

Uranus C200 photometry in absolute mode (P25) and mapping Mode (P22)

Fluxes have been color corrected (BB with T = 60 K)

P25

# Detector	cwl	P25_OLP6	P25_OLP7	model
C2_200	200	431.098	400.8142	551.13
C2_120	120	937.1589	909.4031	896.66

P22

# Detector	cwl	P22_OLP6	P22_OLP7	model
C2_200	200	1039.092	509.8673	551.13
C2_120	120	1219.457	804.1442	896.66

5.21 C200 Mini-map Photometry of the Faint Star ε Lep (HR 1654)

- authors: M. Radovich, U. Klaas
- date: 20-July-1998

5.21.1 Motivation

Due to the difficulties in getting reasonable C200 photometry for stars out of multi-filter staring off/on photometry we investigate here measurements of one star which had been observed in absolute photometric mode as well as in mini-map mode.

5.21.2 Method

We compare the absolute photometry with the mini-map mode photometry and the results of both photometric modes with the predictions of the Cohen model.

5.21.3 Results

In part 1 of Sect. 5.21.5 we present the background subtracted flux values for both the absolute and mini-map photometry. As no separate background measurement in absolute mode was taken, the background as derived from the mini-map was used for background subtraction in the absolute photometry. In Table 34 we perform the consistency check with the Cohen model. The result is that the absolute photometry does not yield reasonable fluxes. For the two shorter wavelength filters the derived fluxes are considerably too high, while for the longest wavelength (170 μm) again, as for other stars, the systematic negative bias is observed. In the case of OLP 6.x an even negative netto flux of the star is derived, while the one for OLP 7.0b2 is slightly positive, but considerably too low.
The mini-map mode in itself is much more consistent and reasonable photometric results are produced. OLP 7.0b2 achieves an accuracy of better than 30% which is in line with the findings on the somewhat brighter star γ Dra. For this target OLP 6.x gave results closer to the model prediction with a consistency of better than 15%.

Table 34: Consistency check of C200 absolute (PHT25) and mini-map (PHT22) photometric results with the model of ε Lep by M. Cohen.

Filter	**AOT**	**consistency w.r.t. model OLP V6.x** [%]	**consistency w.r.t. model OLP V7.0b2** [%]
120	PHT25	+92.7	+131
120	PHT22	+3.4	-7.2
150	PHT25	+82.3	+95.1
150	PHT22	-8.5	-29.6
170	PHT25	-463	-89.3
170	PHT22	+12.5	-20.3

5.21.4 Conclusions

- The absolute photometry in off/on mode is not reliable for this very faint source and gives strong deviations from the model. It confirms earlier results, e.g. on γ Dra, however, this time not showing an always negative photometric bias (too low fluxes), but in two out of three cases too high fluxes. The background values have been taken this time from the mini-map and not from a dedicated off-measurement, since a measurement of the latter type was lacking.
- The mini-map mode yields photometric results with an accuracy of better than 30% for OLP 7.0b2. For this target the OLP 6.x had given photometric accuracies of better than 15%.

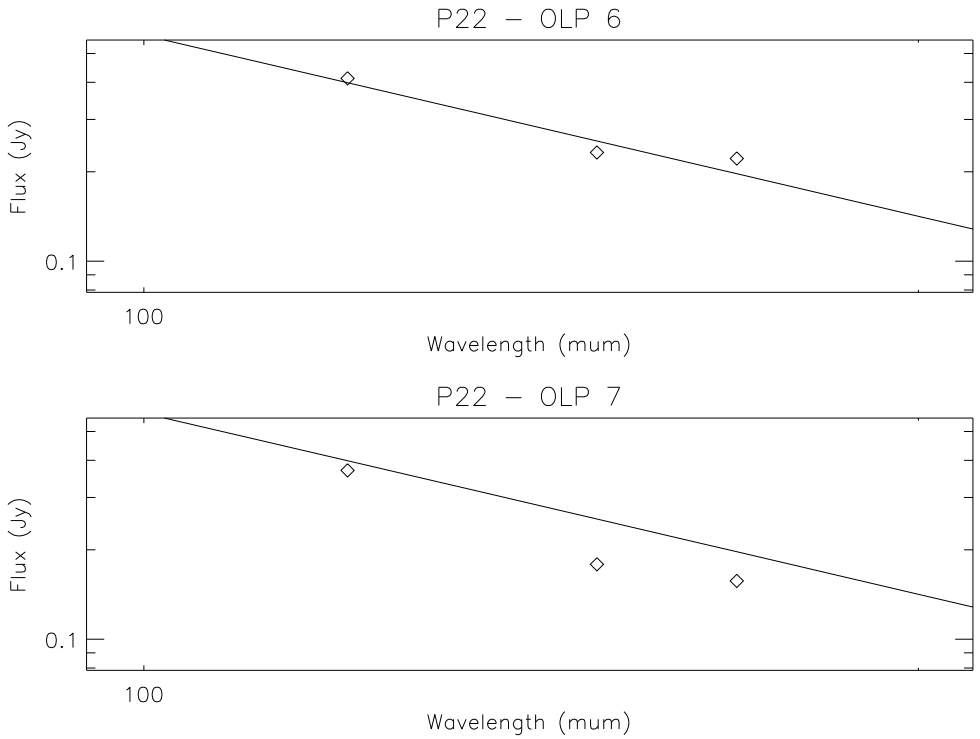

Figure 50: Comparison of C200 mini-map photometry (AOT PHT22) of ε Lep (HR 1654) with the model provided by M. Cohen. Upper panel for OLP 6.x and lower panel for OLP 7.0b2. All photometric points are color corrected for a 4000 K BB. The meaning of the symbols is the following: solid line: Cohen model, diamond: C200 photometry.

5.21.5 Evaluation Log

```
1) Photometric Results of eps Lep (HR 1654) absolute photometry and mini-map
   evaluation. The background values for background subtraction in the case
   of the absolute photometry have been taken from the mini-maps.

   Fluxes are color corrected for T = 4000 K BB.

#Detector      cwl        P22_OLP6   P22_OLP7     P25_OLP6       P25_OLP7     Cohen
C200_135_UM    150.     0.232174    0.1786587    0.462754618     0.4950518   0.2538
C200_160_UM    170.     0.2216832   0.1571082    -0.71526717     0.0209833   0.1970
C200_120_UM    120.     0.4122941   0.3699558    0.768631876     0.9208736   0.3988
```

5.22 Reproducibility of Photometry Processed by OLP for the C200 MFAINT Program on γ Dra (HR 6705)

- authors: M. Radovich, U. Klaas
- date: 20-July-1998

5.22.1 Motivation

In Sect. 1.2, Table 3 we provide the measurement reproducibilities obtained from the monitoring programs. These data were evaluated semi-automatically with the PHT Interactive Analysis. We investigate here a subset of measurements of the C200 faint source monitoring performed on γ Dra and processed with OLP and compare with the general results.

5.22.2 Method

The P22 mini-map photometry of γ Dra from 5 different revolutions is compiled and the standard deviation of the photometric fluxes w.r.t. the model by Cohen are derived.

5.22.3 Results

In part 1 of Sect. 5.22.5 we provide the photometric fluxes derived for the 5 different revolutions both processed with OLP 6.x and OLP 7.0b2. In Table 35 we compare the measured fluxes with the flux prediction by the Cohen model. It can be seen that for OLP 6.x the fluxes of 3 measurements match the model flux very well, while the fluxes for 2 measurements are completely off (too low flux values). For OLP 7.0b2 there is a systematic deviation from the model flux in so far that the measured stellar fluxes are always too small. However, one of the bad measurements of OLP 6.x could be recovered and the most heavily effected one from rev. 650 also has a much better quality. In Table 36 we give the average of the consistency with the model flux and the standard deviation for the 5 measurements. This shows clearly that the good consistency achieved for three measurements in the case of OLP 6.x is destroyed by the large scatter introduced by the two bad results. For OLP 7.0b2 a systematic negative deviation of -30% (too low fluxes) is derived with a standard deviation of only $\pm$8%, which is consistent with the global assessment of the reproducilbility in Table 3. This result can be supplemented by the finding that for the measurement on rev. 748 the derived photometric flux is only -15% off as presented in Sect. 6.8.
We looked for some reason why on average the derived 170 μm flux is systematically by 30% too low w.r.t. the model, in particular as these measurements went into the establishment of the FCS calibration for this filter. Some hints we found are the values for the in-band power and the responsivity as provided by OLPs 6 and 7, respectively. These are listed in parts 2 and 3 of Sect. 5.22.5. While the difference in in-band power for the calibration measurement is only 5% between the two OLP versions, responsivities are different by 30–60%. Therefore, the derivation of the various photometric factors, including cal-G file reading, should be looked at in more detail and they should be compared with a detailed interactive analysis.

Table 35: Consistency check of P22 mini-map photometric results of the monitoring program MFAINT with the model from Cohen.

TDT no.	**consistency w.r.t. model OLP 6** [%]	**consistency w.r.t. model OLP 7** [%]
55206105	+1.6	-29.4
57903105	+3.5	-23.8
59403105	-42.5	-27.9
65001005	-81.1	-45.0
83200605	+2.3	-30.6

Table 36: Reproducibility of P22 mini-map photometric results of monitoring program MFAINT (average of 5 randomly selected measurements.

OLP6		**OLP7**	
aver. consistency [%]	**1 σ** [%]	**aver. consistency** [%]	**1 σ** [%]
-23.2	$\pm$ 37.8	-31.3	$\pm$ 8.0

5.22.4 Conclusion

- OLP 7.0b2 shows a much better homogeneity of the fluxes for the C200 faint source monitoring of γ Dra than OLP 6.x. This appears to be a consequence of improved signal processing, like reset interval correction and orbit dependent dark current subtraction. The derived standard deviation for the selected sample of 5 measurements is $\pm$8% and is consistent with the global reproducibility assessment.
- The OLP 7.0b2 photometry achieves an accuracy of $\sim$ 30% which is, however, not statistical but determined by a photometric bias giving always too low fluxes. Whether this is an effect introduced by the FCS cal-G file or by one stage in the OLP processing needs further investigation. Some hints which need to be followed up are given by this report.

5.22.5 Evaluation Log

```
1) Results of Monitoring of Photometry of Gamma Dra in P22 mini-map mode

fluxes are color corrected, T=4000, Cohen model: 0.5563 Jy

OLP6

# File          Detector      cwl       src
PGAI55206105    C200_160      170      0.565
PGAI57903105    C200_160      170      0.576
PGAI59403105(*) C200_160      170      0.320
PGAI65001005(*) C200_160      170      0.105
PGAI83200605    C200_160      170      0.569

(*):  something wrong in the processing of the data


OLP7

# File          Detector      cwl  src
PGAI55206105    C200_160      170      0.393
PGAI57903105    C200_160      170      0.424
PGAI59403105    C200_160      170      0.401
PGAI65001005(*) C200_160      170      0.306
PGAI83200605    C200_160      170      0.386

(*): the source+background flux is lower than in the other measurements,
     whereas the background does not vary: a too low source flux is therefore
     produced


2) Derived in-band power and responsivities for OLP 6 SPD processing

pc2s55206105
#K POW1M1   0.15873  Measured power for FCS1
#K CALPOW1  1.77E-15  In-band power on detector for cal (Watts)
#K DARKP1   0.00400  dark current
```

```
#K DARKP2   0.00330  dark current
#K DARKP3   0.00267  dark current
#K DARKP4   0.00349  dark current
#K RS1P1F1  16.601526  Responsivity (A/W) for first cal measurement
#K RS1P2F1  11.864943  Responsivity (A/W) for first cal measurement
#K RS1P3F1  17.539597  Responsivity (A/W) for first cal measurement
#K RS1P4F1  15.837438  Responsivity (A/W) for first cal measurement

pc2s57903105
#K POW1M1   0.15873  Measured power for FCS1
#K CALPOW1  1.77E-15  In-band power on detector for cal (Watts)
#K DARKP1   0.00400  dark current
#K DARKP2   0.00330  dark current
#K DARKP3   0.00267  dark current
#K DARKP4   0.00349  dark current
#K RS1P1F1  16.012510  Responsivity (A/W) for first cal measurement
#K RS1P2F1  12.081531  Responsivity (A/W) for first cal measurement
#K RS1P3F1  16.846119  Responsivity (A/W) for first cal measurement
#K RS1P4F1  15.137811  Responsivity (A/W) for first cal measurement

pc2s59403105
#K POW1M1   0.15873  Measured power for FCS1
#K CALPOW1  1.77E-15  In-band power on detector for cal (Watts)
#K DARKP1   0.00400  dark current
#K DARKP2   0.00330  dark current
#K DARKP3   0.00267  dark current
#K DARKP4   0.00349  dark current
#K RS1P1F1  15.833005  Responsivity (A/W) for first cal measurement
#K RS1P2F1  11.719931  Responsivity (A/W) for first cal measurement
#K RS1P3F1  16.357132  Responsivity (A/W) for first cal measurement
#K RS1P4F1  15.319472  Responsivity (A/W) for first cal measurement

pc2s65001005
#K POW1M1   0.15873  Measured power for FCS1
#K CALPOW1  1.77E-15  In-band power on detector for cal (Watts)
#K DARKP1   0.00400  dark current
#K DARKP2   0.00330  dark current
#K DARKP3   0.00267  dark current
#K DARKP4   0.00349  dark current
#K RS1P1F1  16.748831  Responsivity (A/W) for first cal measurement
#K RS1P2F1  12.632421  Responsivity (A/W) for first cal measurement
#K RS1P3F1  16.915501  Responsivity (A/W) for first cal measurement
#K RS1P4F1  16.110954  Responsivity (A/W) for first cal measurement

pc2s83200605
#K POW1M1   0.15873  Measured power for FCS1
#K CALPOW1  1.77E-15  In-band power on detector for cal (Watts)
#K DARKP1   0.00400  dark current
#K DARKP2   0.00330  dark current
#K DARKP3   0.00267  dark current
#K DARKP4   0.00349  dark current
#K RS1P1F1  17.804678  Responsivity (A/W) for first cal measurement
#K RS1P2F1  12.870892  Responsivity (A/W) for first cal measurement
#K RS1P3F1  26.743835  Responsivity (A/W) for first cal measurement
#K RS1P4F1  16.688055  Responsivity (A/W) for first cal measurement


3) Derived in-band power and responsivities for OLP 7 SPD processing

PC2S55206105
#K POW1M1   0.15873  Measured power for FCS1
#K CALPOW1  1.86E-15  In-band power on detector for cal (Watts)
#K DARKP1   -0.00955  dark current
#K DARKP2   -0.01019  dark current
```

```
#K DARKP3   -0.00994  dark current
#K DARKP4   -0.01051  dark current
#K RS1P1F1  25.341311  Responsivity (A/W) for first cal measurement
#K RS1P2F1  19.523727  Responsivity (A/W) for first cal measurement
#K RS1P3F1  22.749744  Responsivity (A/W) for first cal measurement
#K RS1P4F1  23.159332  Responsivity (A/W) for first cal measurement

PC2S57903105
#K POW1M1   0.15873  Measured power for FCS1
#K CALPOW1  1.86E-15  In-band power on detector for cal (Watts)
#K DARKP1   -0.00977  dark current
#K DARKP2   -0.01046  dark current
#K DARKP3   -0.01029  dark current
#K DARKP4   -0.01075  dark current
#K RS1P1F1  24.441042  Responsivity (A/W) for first cal measurement
#K RS1P2F1  19.910069  Responsivity (A/W) for first cal measurement
#K RS1P3F1  21.853630  Responsivity (A/W) for first cal measurement
#K RS1P4F1  22.133749  Responsivity (A/W) for first cal measurement

PC2S59403105
#K POW1M1   0.15873  Measured power for FCS1
#K CALPOW1  1.86E-15  In-band power on detector for cal (Watts)
#K DARKP1   -0.00994  dark current
#K DARKP2   -0.01066  dark current
#K DARKP3   -0.01055  dark current
#K DARKP4   -0.01094  dark current
#K RS1P1F1  24.175545  Responsivity (A/W) for first cal measurement
#K RS1P2F1  19.314714  Responsivity (A/W) for first cal measurement
#K RS1P3F1  21.223074  Responsivity (A/W) for first cal measurement
#K RS1P4F1  22.425205  Responsivity (A/W) for first cal measurement

PC2S65001005
#K POW1M1   0.15873  Measured power for FCS1
#K CALPOW1  1.86E-15  In-band power on detector for cal (Watts)
#K DARKP1   -0.01074  dark current
#K DARKP2   -0.01147  dark current
#K DARKP3   -0.01161  dark current
#K DARKP4   -0.01177  dark current
#K RS1P1F1  25.672153  Responsivity (A/W) for first cal measurement
#K RS1P2F1  20.916573  Responsivity (A/W) for first cal measurement
#K RS1P3F1  22.075151  Responsivity (A/W) for first cal measurement
#K RS1P4F1  23.695784  Responsivity (A/W) for first cal measurement

PC2S83200605
#K POW1M1   0.15873  Measured power for FCS1
#K CALPOW1  1.86E-15  In-band power on detector for cal (Watts)
#K DARKP1   -0.01137  dark current
#K DARKP2   -0.01198  dark current
#K DARKP3   -0.01231  dark current
#K DARKP4   -0.01236  dark current
#K RS1P1F1  27.371964  Responsivity (A/W) for first cal measurement
#K RS1P2F1  21.357862  Responsivity (A/W) for first cal measurement
#K RS1P3F1  35.319710  Responsivity (A/W) for first cal measurement
#K RS1P4F1  24.620787  Responsivity (A/W) for first cal measurement
```

5.23 General Re-validation of PHT-40: Spectra of Line and Continuum Sources (HR 6705, HR 6817, NGC 7023, NGC 6543)

- authors: M. Radovich, U. Klaas
- date: 20-May-1998

5.23.1 Motivation

The spectral response functions of PHT-S have not been updated for OLP V7. The only changes expected in the spectra are those from the orbit dependent dark current correction which should show up for sources with low continuum level.

5.23.2 References to Calibration Analysis and Software Change Documentation

- calibration report: Dependence of the Dark Signal on Orbital Position [11]
- Software Change Request: SCREW 336

5.23.3 Method

We compare the results from OLP V6.x and OLP V7.0b2 and determine the difference in percent. The stellar continua of HR 6705 and HR 6817 are compared with the model predictions by Cohen (COMPOSITE OF OBSERVED SPECTRA OF GAMMA DRA Assembled 12-22-95) and P. Hammersley (GBPP, DATE = 26/11/1995, HR6817, K1III, TABLES = Kurucz 1991, VEGAMOD = Cohen 1992), respectively.

5.23.4 Results

In Sect. 5.23.6 we perform a direct comparison of the OLP output fluxes from Versions V6.x versus V7.0b2:
For HR 6705 the changes are below the 1% level. The continuum level never falls below 10^{-12} W m^2 μm^{-1}.
For HR 6817 the differences are below 2% for the short wavelength part (pixel 64 shows a very unstable behaviour of the dark current which is a factor of 10 higher than for all the other pixels of this array). In the long wavelength channel the orbit dependent dark signal subtraction becomes noticeable. Significant changes of F_λ occur below a continuum level of 4 10^{-14} W m^2 μm^{-1}. For both stars the comparison with the model spectra shows the limitations of the averaged spectral response function to cope with the different signal transient times depending on the flux level. While the spectrum of HR 6705 is quite well reproduced including the broad features, cf. Fig. 51, the measured PHT-S spectrum of HR 6817 is systematically below the model spectrum for nearly all pixels and shows some continuum features, in particular the one at 3 μm, which cannot be real, as HR 6817 is a K giant like HR 6705, cf. Fig. 52. Beyond 10 μm the OLP 7 results match the model better.
NGC 7023 shows a considerably weaker continuum in the short wavelength part. From the analysis of this spectrum we conclude that significant changes in flux occur below a continuum level of 6 10^{-14} W m^2 μm^{-1}. Changes of the continuum level w.r.t. OLP 6 are in the order of $\pm$ 20%. From Fig. 53 we see that the continuum between 4 and 5 μm looks now somewhat smoother and flatter, better matching the long wavelength part.
For NGC 6543 we find significant changes in the continuum level. For the OLP 7 spectrum the continuum in the SL range is around 50% lower than for OLP 6, while the peak flux in the strongest lines (at 9 and 10.5 μm) is nearly preserved. The continuum is very low (a few hundreds of mJy) and therefore hard to measure accurately. In order to check the impact on the scientific validation we compare the continuum flux at 3 wavelengths with IRAS LRS [12] and CAM-CVF scan data summed over a 24x24 arcsec^2 area, corresponding to the PHT-S entrance aperture area (by courtesy of B. Altieri, CIDT) in Table 37. The continuum levels of the IRAS LRS spectrum have been measured with a ruler out of Fig. 1a in Ref. [12] and should be considered only as approximate values. Nevertheless, the OLP 7 data match the IRAS LRS better than the OLP 6 ones. CAM-CVF is consistent with the OLP 6 result for 6.1 μm, but consistent with the OLP 7 result at 11.55 μm. In between, at

9.7 μm, the CAM-CVF continuum level is approximately a factor of 2 above both the OLP 6 and the OLP 7 results. For SWS the derived continuum level close to the [ArIII] line is 6.3 10^{-14} W m^{-2} μm^{-1} (with a scatter between 3.7 and 9.3, H. Feuchtgruber, SIDT, private communication).
The comparison of all continuum level references is therefore not conclusive at the moment, and an uncertainty of 50% in the continuum level at this faint flux has to be accepted until refined (cross) calibration may bring some more coherent results. As NGC 6543 is a slightly extended source, a correction towards somewhat higher fluxes appears necessary for PHT-S, as the source was calibrated like a point source. This is, however, less than 50% which is the correction factor for a source fully extended over the PHT-S aperture, cf. Ref. [13]. Transient correction on the CAM CVF data scales the continuum at 6.1 μm down by 16% and at 9.7 μm down by 20%, respectively (B. Altieri, private communication). At 11.6 μm there is no change.
We also determined the line intensities of the [ArIII] and [SIV] lines (for integration details, see part 5 of sect. 5.23.6) and compare them with IRAS LRS [12] and SWS [14] results in Table 38. The [NaIII] line intensity which is given in [14], too, could not be determined, as for PHT-S the feature is a blend of the [NaIII] line with a hydrogen line. The [ArIII] line intensities of PHT-S and IRAS LRS coincide within 10%, while the [SIV] line intensity of PHT-S is larger by 40% w.r.t. IRAS LRS and a factor of 2 w.r.t. SWS. The latter discrepancy may be explained by the smaller SWS entrance aperture, which does not cover the elliptically shaped emission line source completely. From a monitoring program of NGC 6543 SIDT derives an [ArIII] line flux between 5.2 and 6.1 10^{-14} W m^2 and a [SIV] line flux between 29.3 and 32.4 10^{-14} W m^2 (H. Feuchtgruber, SIDT, private communication). It can be seen that for the strong lines the discrepancy between OLP 6 and OLP 7 results is less than 0.1%, so that the uncertainty of the continuum level affects only more than 10 times weaker lines.
We conclude therefore, that in the context of the available reference data the discrepancy in the continuum level between the OLP 6 and OLP 7 PHT-S spectrum of NGC 6543 is not contradictory, but within the relatively high uncertainties set by the references. We trust the OLP 7 dark current subtraction more, as it is based on a considerably larger dark data base.

Table 37: Comparison of continuum levels of NGC 6543 from PHT-S (OLP V6.x and OLP 7), IRAS LRS and CAM CVF

wavelength	**OLP 6**	**OLP 7**	**IRAS LRS**	**CAM CVF**
[μm]	[10^{-14} W m^2 μm^{-1}]			
6.1	2.0	1.3	–	1.9
9.7	4.9	3.5	~ 2	8.0
11.55	7.8	4.6	~ 4.4	4.6

Table 38: Comparison of line intensities of NGC 6543 from PHT-S (OLP V6.x and OLP 7, IRAS LRS and SWS

line	**OLP 6**	**OLP 7**	**IRAS LRS**	**SWS**
	[10^{-14} W m^2]			
[ArIII 9.0]	9.84	9.86	9	–
[SIV 10.5]	60.83	60.77	43	29.3

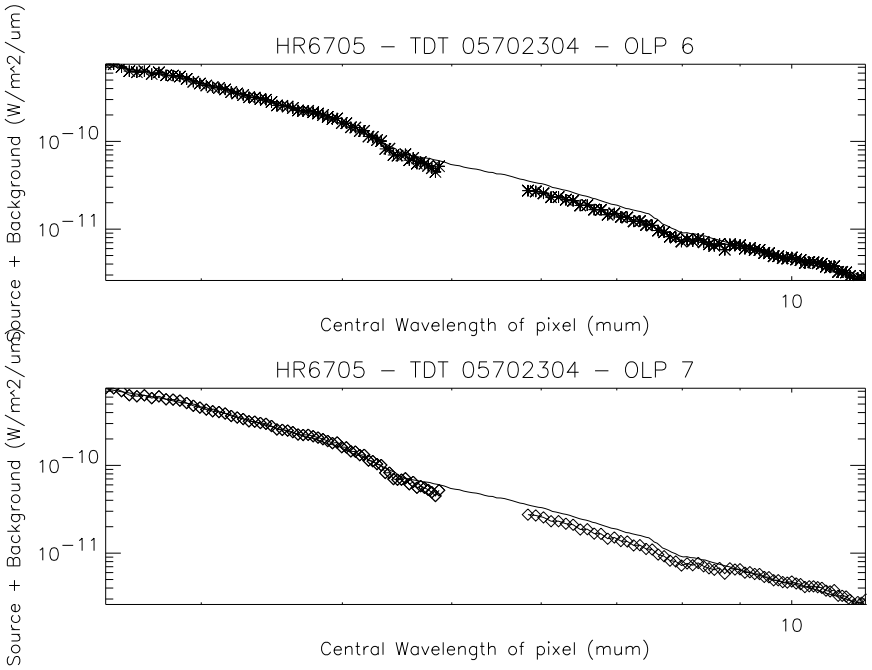

Figure 51: Spectrum of the K giant HR 6705 (γ Dra) as derived with OLP V6.x (upper panel) and with OLP V7.0b2 (lower panel). The solid line shows the composite model by Cohen.

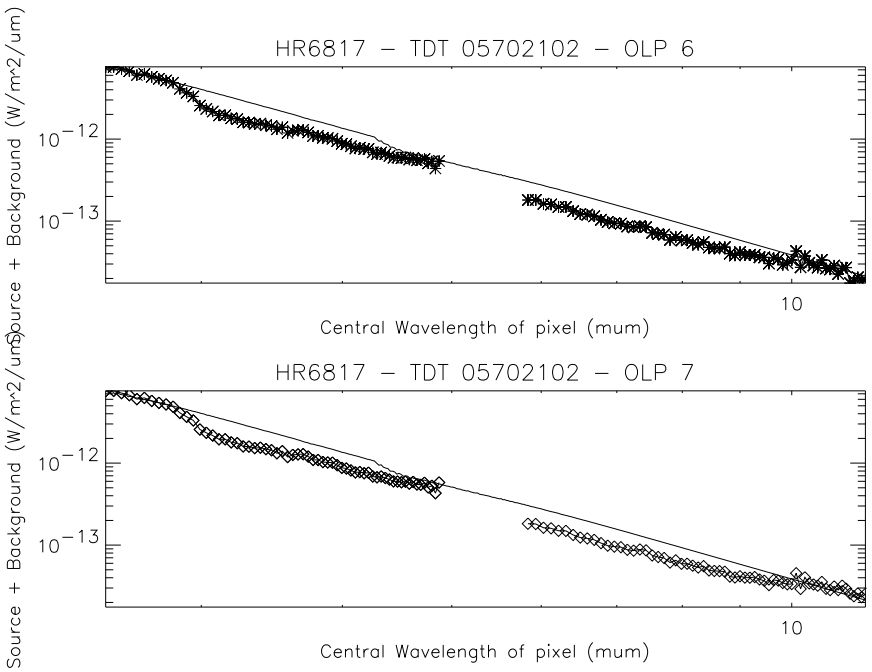

Figure 52: Spectrum of the K giant HR 6817 as derived with OLP V6.x (upper panel) and with OLP V7.0b2 (lower panel). The solid line shows the model by Hammersley (GBPP).

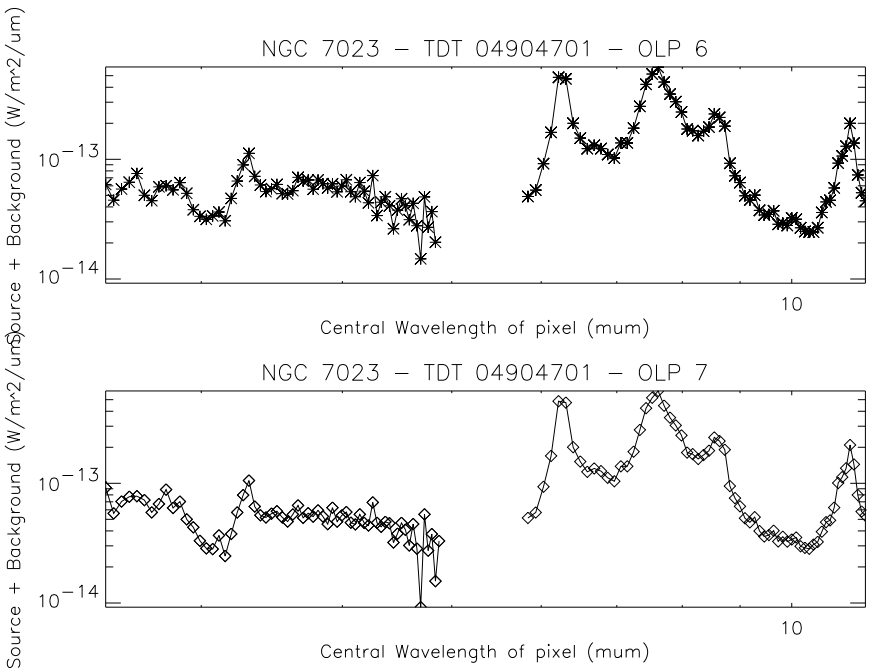

Figure 53: Spectrum of the Reflection Nebula (RN) NGC 7023 as derived with OLP V6.x (upper panel) and with OLP V7.0b2 (lower panel). The spectrum is a mixture of continuum with broad dust features (PAHs) superimposed.

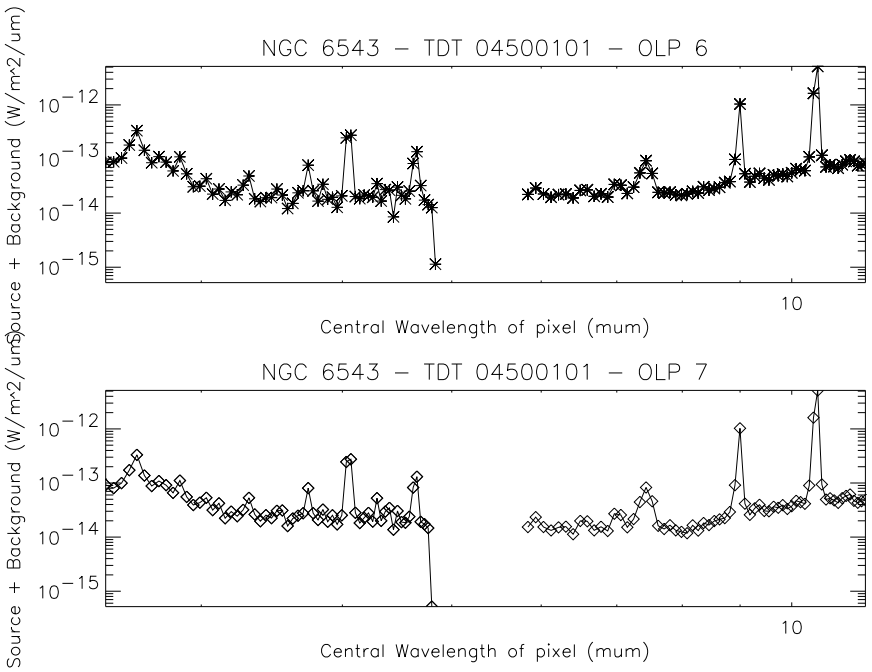

Figure 54: Spectrum of the Planetary Nebula (PN) NGC 6543 as derived with OLP V6.x (upper panel) and with OLP V7.0b2 (lower panel). The spectrum is a mixture of a weak continuum with narrow atomic and ionic emission lines superimposed. The flux in pixel 64 of SS is not reliable due to high and variable dark current.

5.23.5 Conclusions

- PHT40 OLP processing has been successfully revalidated. Spectral shapes and features are maintained.
- The newly introcuded orbit dependent dark signal subtraction shows noticeable differences in the resulting fluxes for continuum levels below 6 10^{-14} W m^2 μm^{-1} for SS and 4 10^{-14} W m^2 μm^{-1} for SL, respectively (for staring mode observations).
- For NGC 6543, a weak continuum source with strong emission lines, a discrepancy of about 50% between OLP 6 and OLP 7 is found. Cross calibration with IRAS LRS and CAM-CVF is not conclusive which PHT data set is more accurate. We trust the OLP 7 data set more, as the dark current subtraction is based on a considerably larger dark current data base. Line fluxes are not affected significantly by the difference in the continuum level.

5.23.6 Evaluation Log

```
diff = (OLP7 - OLP6) / OLP7

1)  HR6705 - TDT 05702304: F(lambda)
```

wl	olp6_FL	olp7_FL	diff
2.46870	7.56494e-10	7.56514e-10	0
2.50950	7.57043e-10	7.57046e-10	0
2.55010	7.02603e-10	7.02610e-10	0
2.59070	6.32421e-10	6.32424e-10	0
2.63110	6.13859e-10	6.13859e-10	0
2.67150	6.30172e-10	6.30182e-10	0
2.71180	5.84707e-10	5.84715e-10	0
2.75210	6.13417e-10	6.13421e-10	0
2.79220	5.66945e-10	5.66963e-10	0
2.83230	5.62669e-10	5.62676e-10	0
2.87220	5.48713e-10	5.48718e-10	0
2.91210	5.14132e-10	5.14132e-10	0
2.95190	4.78592e-10	4.78599e-10	0
2.99170	4.56796e-10	4.56801e-10	0
3.03130	4.33274e-10	4.33277e-10	0
3.07090	4.14427e-10	4.14428e-10	0
3.11030	4.05601e-10	4.05607e-10	0
3.14970	3.90670e-10	3.90669e-10	0
3.18900	3.66002e-10	3.65999e-10	0
3.22830	3.51590e-10	3.51586e-10	0
3.26740	3.37839e-10	3.37833e-10	0
3.30650	3.18327e-10	3.18325e-10	0
3.34550	3.15366e-10	3.15365e-10	0
3.38430	3.04625e-10	3.04622e-10	0
3.42320	2.98159e-10	2.98160e-10	0
3.46190	2.81505e-10	2.81506e-10	0
3.50050	2.57189e-10	2.57189e-10	0
3.53910	2.54458e-10	2.54462e-10	0
3.57760	2.49718e-10	2.49717e-10	0
3.61600	2.39812e-10	2.39815e-10	0
3.65430	2.25233e-10	2.25230e-10	0
3.69250	2.22212e-10	2.22205e-10	0
3.73070	2.23388e-10	2.23383e-10	0
3.76870	2.15231e-10	2.15229e-10	0
3.80670	2.07793e-10	2.07790e-10	0
3.84460	1.99364e-10	1.99358e-10	0
3.88240	1.89965e-10	1.89958e-10	0
3.92010	1.79475e-10	1.79478e-10	0
3.95780	1.82629e-10	1.82628e-10	0
3.99540	1.61575e-10	1.61573e-10	0

4.03280	1.60836e-10	1.60831e-10	0
4.07020	1.44774e-10	1.44770e-10	0
4.10760	1.43760e-10	1.43761e-10	0
4.14480	1.31068e-10	1.31062e-10	0
4.18190	1.31975e-10	1.31971e-10	0
4.21900	1.13510e-10	1.13514e-10	0
4.25600	1.11974e-10	1.11972e-10	0
4.29290	1.03550e-10	1.03565e-10	0
4.32970	1.00932e-10	1.00933e-10	0
4.36640	8.21538e-11	8.21543e-11	0
4.40310	8.27409e-11	8.27475e-11	0
4.43970	6.99325e-11	6.99381e-11	0
4.47610	6.87738e-11	6.87740e-11	0
4.51250	6.89241e-11	6.89230e-11	0
4.54890	7.13823e-11	7.13824e-11	0
4.58510	6.10551e-11	6.10539e-11	0
4.62120	6.47789e-11	6.47805e-11	0
4.65730	5.57218e-11	5.57199e-11	0
4.69330	5.81043e-11	5.80956e-11	0
4.72920	5.57023e-11	5.57061e-11	0
4.76500	5.27343e-11	5.27347e-11	0
4.80080	4.94242e-11	4.94197e-11	0
4.83640	4.48480e-11	4.48401e-11	0
4.87200	5.20468e-11	5.20861e-11	0
5.83960	2.74826e-11	2.74841e-11	0
5.93380	2.68996e-11	2.68998e-11	0
6.02800	2.55658e-11	2.55658e-11	0
6.12200	2.30964e-11	2.30972e-11	0
6.21600	2.31495e-11	2.31502e-11	0
6.30990	2.16335e-11	2.16341e-11	0
6.40380	2.10653e-11	2.10659e-11	0
6.49750	1.85965e-11	1.85983e-11	0
6.59120	1.87406e-11	1.87416e-11	0
6.68480	1.67000e-11	1.67016e-11	0
6.77830	1.65939e-11	1.65960e-11	0
6.87170	1.46034e-11	1.46045e-11	0
6.96500	1.50697e-11	1.50716e-11	0
7.05830	1.37423e-11	1.37438e-11	0
7.15150	1.35765e-11	1.35782e-11	0
7.24460	1.22499e-11	1.22516e-11	0
7.33760	1.23374e-11	1.23394e-11	0
7.43060	1.11611e-11	1.11631e-11	0
7.52350	1.10250e-11	1.10278e-11	0
7.61630	9.63634e-12	9.63855e-12	0
7.70900	9.22375e-12	9.22518e-12	0
7.80160	8.20960e-12	8.21207e-12	0
7.89420	8.04179e-12	8.04291e-12	0
7.98660	7.22637e-12	7.22751e-12	0
8.07900	7.63685e-12	7.63762e-12	0
8.17140	7.28316e-12	7.28540e-12	0
8.26360	7.74085e-12	7.74269e-12	0
8.35580	7.08064e-12	7.08079e-12	0
8.44780	6.72634e-12	6.72773e-12	0
8.53980	6.46513e-12	6.46709e-12	0
8.63180	6.77934e-12	6.78124e-12	0
8.72360	5.82859e-12	5.82798e-12	0
8.81540	6.71766e-12	6.71890e-12	0
8.90700	6.51263e-12	6.51490e-12	0
8.99860	6.55798e-12	6.55798e-12	0
9.09020	5.99309e-12	5.99490e-12	0
9.18160	6.06422e-12	6.06555e-12	0
9.27300	5.79143e-12	5.79363e-12	0
9.36430	5.78502e-12	5.78708e-12	0
9.45550	5.35905e-12	5.35992e-12	0

9.54660	5.31499e-12	5.31731e-12	0
9.63760	4.90951e-12	4.91156e-12	0
9.72860	4.91436e-12	4.91726e-12	0
9.81950	4.67142e-12	4.67688e-12	0
9.91030	4.62138e-12	4.62405e-12	0
10.0010	4.75013e-12	4.75023e-12	0
10.0917	4.51300e-12	4.51548e-12	0
10.1823	4.43330e-12	4.43532e-12	0
10.2727	4.10567e-12	4.10877e-12	0
10.3632	4.19034e-12	4.19360e-12	0
10.4535	4.18202e-12	4.18657e-12	0
10.5437	4.08571e-12	4.09076e-12	0
10.6339	4.02250e-12	4.02469e-12	0
10.7240	3.73545e-12	3.73846e-12	0
10.8140	3.66264e-12	3.66544e-12	0
10.9040	3.78930e-12	3.79212e-12	0
10.9938	3.25989e-12	3.26578e-12	0
11.0836	3.25943e-12	3.26510e-12	0
11.1733	3.20935e-12	3.21183e-12	0
11.2629	2.92756e-12	2.93596e-12	0
11.3524	2.59692e-12	2.60221e-12	0
11.4419	2.77109e-12	2.77632e-12	0
11.5313	2.72128e-12	2.72608e-12	0
11.6206	2.92248e-12	2.92896e-12	0

2) HR6817 - TDT 05702102: F(lambda)

wl	olp6_FL	olp7_FL	diff
2.46870	7.53231e-12	7.55189e-12	0
2.50950	7.60043e-12	7.60276e-12	0
2.55010	7.13785e-12	7.14375e-12	0
2.59070	6.74550e-12	6.74919e-12	0
2.63110	6.03030e-12	6.03038e-12	0
2.67150	6.23065e-12	6.24005e-12	0
2.71180	5.72608e-12	5.73401e-12	0
2.75210	5.42983e-12	5.43375e-12	0
2.79220	5.18112e-12	5.19879e-12	0
2.83230	4.86720e-12	4.87341e-12	0
2.87220	4.09173e-12	4.09604e-12	0
2.91210	3.66758e-12	3.66747e-12	0
2.95190	3.31238e-12	3.31894e-12	0
2.99170	2.56542e-12	2.57045e-12	0
3.03130	2.33856e-12	2.34139e-12	0
3.07090	2.17048e-12	2.17140e-12	0
3.11030	1.94593e-12	1.95237e-12	0
3.14970	1.95319e-12	1.95206e-12	0
3.18900	1.79477e-12	1.79172e-12	0
3.22830	1.75650e-12	1.75267e-12	0
3.26740	1.60404e-12	1.59799e-12	0
3.30650	1.59203e-12	1.59031e-12	0
3.34550	1.52659e-12	1.52549e-12	0
3.38430	1.54673e-12	1.54425e-12	0
3.42320	1.47906e-12	1.48070e-12	0
3.46190	1.43670e-12	1.43752e-12	0
3.50050	1.31919e-12	1.31862e-12	0
3.53910	1.39506e-12	1.39935e-12	0
3.57760	1.18860e-12	1.18843e-12	0
3.61600	1.25709e-12	1.26029e-12	0
3.65430	1.27979e-12	1.27730e-12	0
3.69250	1.29381e-12	1.28661e-12	0
3.73070	1.20752e-12	1.20289e-12	0
3.76870	1.09540e-12	1.09420e-12	0
3.80670	1.09670e-12	1.09411e-12	0
3.84460	1.03701e-12	1.03084e-12	0

3.88240	1.02589e-12	1.01967e-12	0
3.92010	1.01028e-12	1.01286e-12	0
3.95780	9.46125e-13	9.44841e-13	0
3.99540	8.77761e-13	8.76446e-13	0
4.03280	8.66462e-13	8.60605e-13	0
4.07020	8.18087e-13	8.14534e-13	0
4.10760	7.68888e-13	7.70472e-13	0
4.14480	7.83870e-13	7.78762e-13	0
4.18190	7.56868e-13	7.53149e-13	0
4.21900	7.60737e-13	7.64496e-13	0
4.25600	6.89365e-13	6.87109e-13	0
4.29290	6.56745e-13	6.71610e-13	2
4.32970	6.85903e-13	6.87093e-13	0
4.36640	6.58206e-13	6.58728e-13	0
4.40310	6.25151e-13	6.31799e-13	1
4.43970	5.93436e-13	5.98938e-13	0
4.47610	5.96588e-13	5.96789e-13	0
4.51250	5.85655e-13	5.84565e-13	0
4.54890	5.95631e-13	5.95719e-13	0
4.58510	5.63579e-13	5.62280e-13	0
4.62120	5.88855e-13	5.90322e-13	0
4.65730	5.51389e-13	5.49342e-13	0
4.69330	5.53825e-13	5.45011e-13	-1
4.72920	5.71391e-13	5.75077e-13	0
4.76500	5.06334e-13	5.06702e-13	0
4.80080	5.34556e-13	5.29883e-13	0
4.83640	4.38014e-13	4.30089e-13	-1
4.87200	5.41406e-13	5.80296e-13	6
5.83960	1.80902e-13	1.82299e-13	0
5.93380	1.80829e-13	1.80961e-13	0
6.02800	1.62886e-13	1.62908e-13	0
6.12200	1.59439e-13	1.60229e-13	0
6.21600	1.49025e-13	1.49611e-13	0
6.30990	1.48625e-13	1.49177e-13	0
6.40380	1.32515e-13	1.32982e-13	0
6.49750	1.22044e-13	1.23697e-13	1
6.59120	1.19786e-13	1.20719e-13	0
6.68480	1.14406e-13	1.15966e-13	1
6.77830	1.03645e-13	1.05743e-13	1
6.87170	9.74195e-14	9.84825e-14	1
6.96500	9.40211e-14	9.58740e-14	1
7.05830	9.29708e-14	9.44114e-14	1
7.15150	8.60318e-14	8.76549e-14	1
7.24460	8.40283e-14	8.57274e-14	1
7.33760	8.66621e-14	8.86094e-14	2
7.43060	8.45981e-14	8.64296e-14	2
7.52350	7.19894e-14	7.47675e-14	3
7.61630	6.94572e-14	7.16206e-14	3
7.70900	6.83182e-14	6.96747e-14	1
7.80160	5.89146e-14	6.12983e-14	3
7.89420	6.42202e-14	6.52888e-14	1
7.98660	5.81014e-14	5.92000e-14	1
8.07900	5.86137e-14	5.93118e-14	1
8.17140	5.40119e-14	5.61517e-14	3
8.26360	5.16183e-14	5.33530e-14	3
8.35580	5.54032e-14	5.54416e-14	0
8.44780	4.77875e-14	4.91216e-14	2
8.53980	4.66061e-14	4.84870e-14	3
8.63180	4.63667e-14	4.81649e-14	3
8.72360	4.80573e-14	4.74498e-14	-1
8.81540	4.01320e-14	4.13399e-14	2
8.90700	3.81472e-14	4.03695e-14	5
8.99860	4.18534e-14	4.17510e-14	0
9.09020	3.84844e-14	4.01810e-14	4

9.18160	3.88236e-14	4.00828e-14	3
9.27300	3.86957e-14	4.07842e-14	5
9.36430	3.61969e-14	3.81477e-14	5
9.45550	3.60618e-14	3.68265e-14	2
9.54660	3.03503e-14	3.25805e-14	6
9.63760	3.55805e-14	3.75358e-14	5
9.72860	3.42546e-14	3.69812e-14	7
9.81950	2.92963e-14	3.45858e-14	15
9.91030	3.06504e-14	3.32375e-14	7
10.0010	3.35096e-14	3.35912e-14	0
10.0917	4.31115e-14	4.54343e-14	5
10.1823	2.72950e-14	2.92091e-14	6
10.2727	3.74913e-14	4.03956e-14	7
10.3632	3.09802e-14	3.40931e-14	9
10.4535	2.87577e-14	3.31546e-14	13
10.5437	2.71133e-14	3.20491e-14	15
10.6339	3.35880e-14	3.55774e-14	5
10.7240	2.64647e-14	2.93595e-14	9
10.8140	2.57514e-14	2.83191e-14	9
10.9040	2.86255e-14	3.12992e-14	8
10.9938	2.26645e-14	2.83201e-14	19
11.0836	2.65767e-14	3.20655e-14	17
11.1733	2.71448e-14	2.94238e-14	7
11.2629	1.75383e-14	2.55987e-14	31
11.3524	1.87343e-14	2.38079e-14	21
11.4419	2.06381e-14	2.57593e-14	19
11.5313	1.86343e-14	2.32188e-14	19
11.6206	1.92745e-14	2.54791e-14	24

3) NGC 7023 - TDT 04904701: F(lambda)

wl	olp6_FL	olp7_FL	diff
2.46870	6.16621e-14	9.18640e-14	32
2.50950	4.55521e-14	5.61078e-14	18
2.55010	5.64377e-14	7.04091e-14	19
2.59070	6.42931e-14	7.72771e-14	16
2.63110	7.61072e-14	7.80618e-14	2
2.67150	5.00045e-14	7.24404e-14	30
2.71180	4.51070e-14	5.71731e-14	21
2.75210	5.88797e-14	6.71940e-14	12
2.79220	6.00919e-14	8.86721e-14	32
2.83230	5.55227e-14	6.22330e-14	10
2.87220	6.38765e-14	7.03734e-14	9
2.91210	5.19521e-14	4.99946e-14	-3
2.95190	3.79003e-14	4.29179e-14	11
2.99170	3.33870e-14	3.30942e-14	0
3.03130	3.14842e-14	2.86009e-14	-10
3.07090	3.36337e-14	2.82024e-14	-19
3.11030	3.62923e-14	3.66950e-14	1
3.14970	3.06350e-14	2.46941e-14	-24
3.18900	4.70796e-14	3.77811e-14	-24
3.22830	6.58343e-14	5.70914e-14	-15
3.26740	8.97695e-14	7.97452e-14	-12
3.30650	1.12191e-13	1.05493e-13	-6
3.34550	7.20732e-14	6.39791e-14	-12
3.38430	6.10172e-14	5.40714e-14	-12
3.42320	5.37419e-14	5.18473e-14	-3
3.46190	5.67962e-14	5.58292e-14	-1
3.50050	6.17051e-14	5.84618e-14	-5
3.53910	5.16928e-14	5.18986e-14	0
3.57760	5.12549e-14	4.79620e-14	-6
3.61600	5.46702e-14	5.49380e-14	0
3.65430	7.07208e-14	6.53596e-14	-8

3.69250	6.56640e-14	5.14989e-14	-27
3.73070	6.72258e-14	5.62677e-14	-19
3.76870	5.62553e-14	5.26680e-14	-6
3.80670	6.72126e-14	5.94469e-14	-13
3.84460	6.24624e-14	5.28581e-14	-18
3.88240	5.76033e-14	4.55858e-14	-26
3.92010	6.24478e-14	6.25499e-14	0
3.95780	5.35278e-14	4.78462e-14	-11
3.99540	5.97673e-14	5.39368e-14	-10
4.03280	6.74830e-14	5.75451e-14	-17
4.07020	5.35575e-14	4.69043e-14	-14
4.10760	4.87232e-14	4.53717e-14	-7
4.14480	6.39435e-14	5.50657e-14	-16
4.18190	5.41834e-14	4.67287e-14	-15
4.21900	4.33325e-14	4.44330e-14	2
4.25600	7.30938e-14	6.92699e-14	-5
4.29290	3.38697e-14	4.67892e-14	27
4.32970	4.37792e-14	4.33377e-14	-1
4.36640	4.86587e-14	4.76231e-14	-2
4.40310	4.08582e-14	4.64214e-14	11
4.43970	2.62868e-14	3.20332e-14	17
4.47610	3.76583e-14	3.78996e-14	0
4.51250	4.68084e-14	4.66941e-14	0
4.54890	4.09010e-14	4.09437e-14	0
4.58510	3.12992e-14	3.02559e-14	-3
4.62120	4.29203e-14	4.57070e-14	6
4.65730	2.78458e-14	2.84627e-14	2
4.69330	1.47272e-14	9.21827e-15	-59
4.72920	4.84907e-14	5.50650e-14	11
4.76500	2.70119e-14	2.73848e-14	1
4.80080	3.65556e-14	3.76524e-14	2
4.83640	2.02707e-14	1.52338e-14	-33
4.87200	0.00000	3.29805e-14	100
5.83960	4.89108e-14	5.13716e-14	4
5.93380	5.52521e-14	5.70467e-14	3
6.02800	9.20267e-14	9.35997e-14	1
6.12200	1.67823e-13	1.69426e-13	0
6.21600	4.83954e-13	4.85287e-13	0
6.30990	4.70086e-13	4.72426e-13	0
6.40380	1.99989e-13	2.00396e-13	0
6.49750	1.50303e-13	1.51895e-13	1
6.59120	1.22800e-13	1.24770e-13	1
6.68480	1.30857e-13	1.33132e-13	1
6.77830	1.22955e-13	1.26401e-13	2
6.87170	1.09639e-13	1.11202e-13	1
6.96500	1.02386e-13	1.04030e-13	1
7.05830	1.37094e-13	1.38746e-13	1
7.15150	1.37089e-13	1.38733e-13	1
7.24460	1.82068e-13	1.83906e-13	0
7.33760	2.76730e-13	2.79487e-13	0
7.43060	4.23099e-13	4.24754e-13	0
7.52350	5.15875e-13	5.18491e-13	0
7.61630	5.87869e-13	5.90996e-13	0
7.70900	4.42075e-13	4.45213e-13	0
7.80160	3.50873e-13	3.53808e-13	0
7.89420	3.02939e-13	3.04741e-13	0
7.98660	2.48599e-13	2.51393e-13	1
8.07900	1.79260e-13	1.80586e-13	0
8.17140	1.73539e-13	1.75392e-13	1
8.26360	1.57943e-13	1.59732e-13	1
8.35580	1.71826e-13	1.72419e-13	0
8.44780	1.85897e-13	1.87414e-13	0
8.53980	2.39446e-13	2.41635e-13	0
8.63180	2.23772e-13	2.25372e-13	0

8.72360	1.89252e-13	1.90757e-13	0
8.81540	9.26194e-14	9.48273e-14	2
8.90700	7.28340e-14	7.52383e-14	3
8.99860	6.38994e-14	6.42400e-14	0
9.09020	4.95699e-14	5.11193e-14	3
9.18160	4.56735e-14	4.72136e-14	3
9.27300	5.01793e-14	5.21657e-14	3
9.36430	3.74399e-14	3.99502e-14	6
9.45550	3.42820e-14	3.59565e-14	4
9.54660	3.45954e-14	3.69688e-14	6
9.63760	3.71436e-14	4.02246e-14	7
9.72860	2.86476e-14	3.27009e-14	12
9.81950	2.93028e-14	3.58245e-14	18
9.91030	2.79983e-14	3.25706e-14	14
10.0010	3.23792e-14	3.39369e-14	4
10.0917	3.15135e-14	3.52773e-14	10
10.1823	2.67808e-14	2.97658e-14	10
10.2727	2.49532e-14	2.88818e-14	13
10.3632	2.47553e-14	2.83845e-14	12
10.4535	2.46739e-14	3.08044e-14	19
10.5437	2.68089e-14	3.24135e-14	17
10.6339	3.59557e-14	3.94368e-14	8
10.7240	4.40702e-14	4.73805e-14	6
10.8140	4.54003e-14	4.90493e-14	7
10.9040	5.76389e-14	6.26980e-14	8
10.9938	9.29341e-14	1.00575e-13	7
11.0836	1.06445e-13	1.12645e-13	5
11.1733	1.28582e-13	1.33722e-13	3
11.2629	1.99900e-13	2.09023e-13	4
11.3524	1.36516e-13	1.43914e-13	5
11.4419	7.40856e-14	7.98991e-14	7
11.5313	5.25702e-14	5.81011e-14	9
11.6206	4.50342e-14	5.36401e-14	16

4) NGC 6543 - TDT 04500101: F(lambda)

wl	olp6_FL	olp7_FL	diff
2.46870	8.63459e-14	9.22417e-14	6
2.50950	8.87386e-14	8.04632e-14	-10
2.55010	1.03975e-13	9.94745e-14	-4
2.59070	1.80992e-13	1.72708e-13	-4
2.63110	3.33682e-13	3.31348e-13	0
2.67150	1.44941e-13	1.37554e-13	-5
2.71180	8.53366e-14	8.79461e-14	2
2.75210	1.10496e-13	1.08731e-13	-1
2.79220	8.76186e-14	9.12402e-14	3
2.83230	6.02143e-14	6.57904e-14	8
2.87220	1.09517e-13	1.11005e-13	1
2.91210	5.31018e-14	5.53717e-14	4
2.95190	3.06832e-14	3.92190e-14	21
2.99170	3.15196e-14	4.34135e-14	27
3.03130	4.31632e-14	5.33508e-14	19
3.07090	2.24214e-14	3.15320e-14	28
3.11030	2.78853e-14	4.20912e-14	33
3.14970	1.71859e-14	2.22738e-14	22
3.18900	2.46231e-14	2.96224e-14	16
3.22830	2.18240e-14	2.43389e-14	10
3.26740	3.28570e-14	3.19333e-14	-2
3.30650	4.85492e-14	5.32431e-14	8
3.34550	1.83919e-14	2.63020e-14	30
3.38430	1.63584e-14	1.96376e-14	16
3.42320	1.92540e-14	2.54552e-14	24
3.46190	1.93294e-14	2.24607e-14	13

3.50050	2.78400e-14	3.07120e-14	9
3.53910	2.15911e-14	3.11481e-14	30
3.57760	1.21451e-14	1.60121e-14	24
3.61600	1.51136e-14	2.20963e-14	31
3.65430	2.37121e-14	2.49187e-14	4
3.69250	2.58811e-14	2.76745e-14	6
3.73070	7.69184e-14	8.04426e-14	4
3.76870	2.58389e-14	2.77142e-14	6
3.80670	1.66782e-14	2.07590e-14	19
3.84460	3.40997e-14	3.23555e-14	-5
3.88240	1.79770e-14	1.92311e-14	6
3.92010	1.96036e-14	2.53730e-14	22
3.95780	1.27914e-14	1.71767e-14	25
3.99540	2.08048e-14	2.53110e-14	17
4.03280	2.46417e-13	2.45820e-13	0
4.07020	2.74856e-13	2.75301e-13	0
4.10760	2.02408e-14	2.81877e-14	28
4.14480	1.84765e-14	1.82294e-14	-1
4.18190	2.15990e-14	2.26951e-14	4
4.21900	2.07993e-14	2.79849e-14	25
4.25600	1.96068e-14	1.93726e-14	-1
4.29290	3.50473e-14	5.24187e-14	33
4.32970	1.67046e-14	1.99972e-14	16
4.36640	2.71613e-14	2.96909e-14	8
4.40310	2.65848e-14	3.46309e-14	23
4.43970	8.52417e-15	1.37123e-14	37
4.47610	3.02437e-14	3.03929e-14	0
4.51250	2.13246e-14	1.89784e-14	-12
4.54890	1.83224e-14	1.84676e-14	0
4.58510	2.54989e-14	2.38708e-14	-6
4.62120	8.26798e-14	8.24464e-14	0
4.65730	1.36349e-13	1.30867e-13	-4
4.69330	3.22551e-14	1.91818e-14	-68
4.72920	1.73820e-14	1.73437e-14	0
4.76500	1.43510e-14	1.47107e-14	2
4.80080	1.26289e-14	5.17983e-16	-2338
4.83640	1.13612e-15	0.00000	0
4.87200	0.00000	0.00000	0
5.83960	2.21447e-14	1.53623e-14	-44
5.93380	2.90831e-14	2.33957e-14	-24
6.02800	2.25251e-14	1.53874e-14	-46
6.12200	1.96592e-14	1.33023e-14	-47
6.21600	2.19828e-14	1.51645e-14	-44
6.30990	2.24789e-14	1.56329e-14	-43
6.40380	1.90910e-14	1.12951e-14	-69
6.49750	2.62293e-14	1.99167e-14	-31
6.59120	2.69805e-14	1.96135e-14	-37
6.68480	2.04338e-14	1.33367e-14	-53
6.77830	2.27037e-14	1.55232e-14	-46
6.87170	1.97939e-14	1.29870e-14	-52
6.96500	3.38757e-14	2.70482e-14	-25
7.05830	3.26685e-14	2.55971e-14	-27
7.15150	2.31096e-14	1.51863e-14	-52
7.24460	3.01292e-14	2.15488e-14	-39
7.33760	5.54404e-14	4.44783e-14	-24
7.43060	9.30053e-14	8.27787e-14	-12
7.52350	5.40288e-14	4.60945e-14	-17
7.61630	2.41901e-14	1.61656e-14	-49
7.70900	2.35640e-14	1.41290e-14	-66
7.80160	2.43714e-14	1.65818e-14	-46
7.89420	2.18468e-14	1.33329e-14	-63
7.98660	2.12387e-14	1.25074e-14	-69
8.07900	2.26471e-14	1.18035e-14	-91
8.17140	2.51904e-14	1.65195e-14	-52

```
      8.26360  2.34690e-14  1.31941e-14     -77
      8.35580  3.06273e-14  1.82210e-14     -68
      8.44780  2.65747e-14  1.66992e-14     -59
      8.53980  2.84928e-14  1.98211e-14     -43
      8.63180  3.00007e-14  2.12890e-14     -40
      8.72360  3.65368e-14  2.24421e-14     -62
      8.81540  3.82385e-14  2.91358e-14     -31
      8.90700  9.80125e-14  9.13007e-14      -7
      8.99860  1.03716e-12  1.02615e-12      -1
      9.09020  5.34141e-14  4.14769e-14     -28
      9.18160  3.74931e-14  2.57706e-14     -45
      9.27300  4.79587e-14  3.40477e-14     -40
      9.36430  5.39764e-14  3.96596e-14     -36
      9.45550  4.43123e-14  3.04911e-14     -45
      9.54660  4.10790e-14  3.00556e-14     -36
      9.63760  5.07643e-14  3.64323e-14     -39
      9.72860  4.90109e-14  3.49088e-14     -40
      9.81950  5.28590e-14  3.90141e-14     -35
      9.91030  4.74454e-14  3.31544e-14     -43
      10.0010  5.54517e-14  3.73019e-14     -48
      10.0917  6.60601e-14  4.68151e-14     -41
      10.1823  6.22181e-14  4.42731e-14     -40
      10.2727  6.09709e-14  4.13365e-14     -47
      10.3632  1.09498e-13  8.98470e-14     -21
      10.4535  1.63629e-12  1.61387e-12      -1
      10.5437  5.14480e-12  5.12503e-12       0
      10.6339  1.16835e-13  9.40025e-14     -24
      10.7240  7.14197e-14  4.96033e-14     -43
      10.8140  7.82104e-14  5.22332e-14     -49
      10.9040  7.26034e-14  4.77770e-14     -51
      10.9938  6.76631e-14  4.29536e-14     -57
      11.0836  7.82293e-14  5.24606e-14     -49
      11.1733  9.05763e-14  5.78866e-14     -56
      11.2629  9.62597e-14  6.14761e-14     -56
      11.3524  9.02439e-14  4.69104e-14     -92
      11.4419  7.55975e-14  4.31494e-14     -75
      11.5313  7.81318e-14  4.61285e-14     -69
      11.6206  8.30081e-14  4.79455e-14     -73


5) Determination of line intensities of NGC 6543

continuum level = average of short and long wavelength continuum
band width per pixel = (l_n - l_n-1)/2 + (l_n+1 - l_n)/2

[ArIII 9.0]

      8.81540  3.82385e-14  2.91358e-14     -31
      8.90700  9.80125e-14  9.13007e-14      -7
      8.99860  1.03716e-12  1.02615e-12      -1
      9.09020  5.34141e-14  4.14769e-14     -28
      9.18160  3.74931e-14  2.57706e-14     -45

OLP 7 continuum level: 2.75e-14
OLP 6 continuum level: 3.79e-14

OLP 7 line integration:
      6.38e-14 * 0.0916
     99.85e-14 * 0.0916
      1.40e-14 * 0.0906
     ------------------
      9.86e-14

OLP 6 line integration:
```

```
      6.01e-14 * 0.0916
     99.91e-14 * 0.0916
      1.55e-14 * 0.0906
     ------------------
      9.84e-14

[SIV 10.5]

      10.2727  6.09709e-14  4.13365e-14     -47
      10.3632  1.09498e-13  8.98470e-14     -21
      10.4535  1.63629e-12  1.61387e-12      -1
      10.5437  5.14480e-12  5.12503e-12       0
      10.6339  1.16835e-13  9.40025e-14     -24
      10.7240  7.14197e-14  4.96033e-14     -43

OLP 7 continuum level: 4.55e-14
OLP 6 continuum level: 6.62e-14

OLP 7 line integration:
      4.44e-14 * 0.0904
    156.39e-14 * 0.09025
    507.95e-14 * 0.0902
      4.85e-14 * 0.09015
    --------------------
     60.77e-14

OLP 6 line integration:
      4.33e-14 * 0.0904
    157.00e-14 * 0.09025
    507.86e-14 * 0.0902
      5.06e-14 * 0.09015
    --------------------
     60.83e-14
```

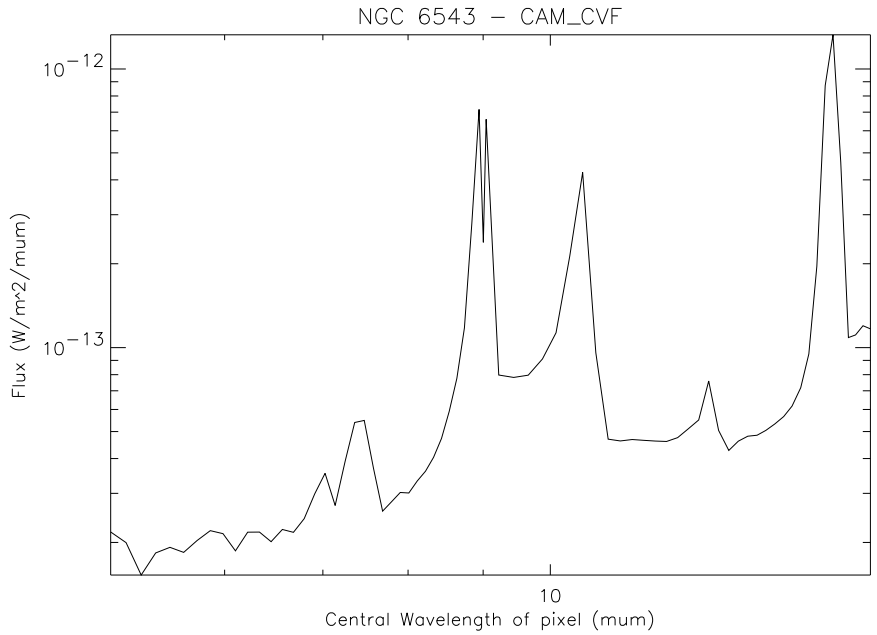

Figure 55: Spectrum of the Planetary Nebula (PN) NGC 6543 taken with CAM-CVF. The camera pixel size used was 1.5 arcsec. The spectrum displays the total flux inside a 24 x 24 arcsec^2 box aperture (comparable to the ISOPHOT-S entrance aperture). The data are not transient corrected. Data courtesy by B. Altieri, CIDT

6) CAM-CVF data of NGC 6543 used for the comparison with PHT-S (kindly provided by B. Altieri, CIDT)

Flux in Jy

10.6331	10.6589	9.65271	9.23247	38.3069	107.364
68.8881	15.0799	7.12427	5.25466	4.39320	3.92466
3.59090	3.30841	3.09401	2.98118	2.77823	2.49730
2.85436	4.16182	2.92215	2.62178	2.36429	2.21280
2.14330	2.07988	2.01830	1.92183	1.87730	3.68873
15.7028	7.55306	3.84026	2.96406	2.47934	2.32512
2.26293	6.45312	0.000000	17.9995	19.0997	7.26623
2.99989	1.93158	1.43485	1.12008	0.934569	0.812269
0.730113	0.644007	0.629571	0.567070	0.510518	0.707556
1.01994	0.973221	0.684411	0.461051	0.582847	0.476434
0.375236	0.323940	0.320409	0.279672	0.291886	0.281053
0.231758	0.256921	0.253091	0.223940	0.194558	0.194288
0.177388	0.141175	0.176058	0.183169		

Corresponding wavelengths in microns :

16.5200	16.3300	16.1400	15.9600	15.7700	15.5800
15.3900	15.1900	15.0000	14.8100	14.6100	14.4200
14.2200	14.0200	13.8300	13.6300	13.4300	13.2300
13.0200	12.8200	12.6200	12.4100	12.2100	12.0000
11.7900	11.5800	11.3700	11.1600	10.9500	10.7400
10.5200	10.3100	10.0900	9.87800	9.66000	9.44200
9.22300	9.00300	9.00300	9.04300	8.94300	8.84200
8.74000	8.63700	8.53400	8.43100	8.32700	8.22200
8.11600	8.01000	7.90300	7.79500	7.68700	7.57800
7.46900	7.35800	7.24800	7.13600	7.02400	6.91100
6.79800	6.68400	6.56900	6.45400	6.33700	6.22100
6.10300	5.98500	5.86700	5.74700	5.62700	5.50700
5.38500	5.26400	5.14100	5.01800		

6 Validation of the Chopped Point Source Photometry

6.1 Motivation

For OLP V7 a completely new approach has been developed for the processing and calibration of chopped photometry. As the absolute calibration with the FCS is solely based on staring and mini-map observations and chopped measurements have usually smaller signal differences than the corresponding staring off/on measurement, a consistent calibration of the signal losses and the detector responsivity had to be found. The following combination of calibration has been chosen:

- Signal losses in chopped measurements are empirically corrected for dependence on the chopper frequency. The empirical correction factors have been determined from a set of chopped AOT calibration measurements. P3 and C100 show the largest loss factors of 50% and 70%, respectively. For the other detectors the loss factors are $\leq$ 20%.
- As the chopped FCS measurement is not necessarily reliable in the sense that the average chopped FCS1 signal corresponds to the equivalent staring FCS1 signal, it was decided not to rely on the actual FCS measurement for this OLP version, but to use default responsivities established as an averaged value of each detector from the FCS vs. celestial standard measurements, including its orbit dependent variation established from a large subset of all availabe FCS measurements (Cal-A) in scientific AOs.

6.2 References to Calibration Analysis and Software Change Documentation

- calibration reports:
  - Correction of Signal Losses in Chopped Measurements [16]
  - Responsivity Variation vs. Orbit Position [17]
- Software Change Requests: SCREW 340, SCREW 341, SCREW 353

6.3 Method

In the following sections we investigate chopped photometry of several special validation but also of general observers' programs for which staring ISOPHOT reference photometry, IRAS photometry or model photometry are available. We establish the consistency of the chopped photometry with this reference photometry and derive the achieved accuracy of the new method.

6.4 Validation of PHT03 and PHT22 Chopped Mode: The SED of IRAS 03068-5346

- authors: M. Radovich, U. Klaas
- data: 25-May-1998

6.4.1 Motivation

We quote here the scientific justification as given in the proposal OLPVAL03: "OLP V7.0 introduces the empirical photometric correction of chopped measurements. The correction factors were established by comparing chopped measurements against staring measurements. For stability arguments these calibration measurements were restricted to one filter each. Furthermore the chopped photometric correction introduces the concept of orbit dependent default responsivities. As there are no multi-filter reference measurements both in staring and chopped mode available, this proposals closes the gap.
For a full validation of the proper functioning of all correction factors in multi-filter chopped photometry dedicated test cases in which nearly the full set of all PHT filters are applied are needed. As good test cases covering the full wavelength range with reasonable SEDs the IR active galaxies were good test cases for the check out of the staring modes. They are as well good cases for the chopped mode, but fainter objects have to be selected for a realistic application.
Such an object is ULIRG 0306-5346 observed in the GT program by U. Klaas. In the 60 to 200 micron range its flux ranges from 2 to 4 Jy. It is not too faint so that one needs to be concerned of no detection due to cirrus. It is not too bright to fall out of the contrast range used for establishment of the empirical signal loss correction factors. In the range 10 to 25 micron it has flux levels between 20 and 200 mJy. The source is very well visible with more than 50000 s per revolution between revs. 780 and 850.
Do a (nearly) full filter scan between 7.3 and 200 micron in chopped mode and verify the fluxes for a subset of filters with the nodding mode".

6.4.2 Method

We compare the OLP V7.0b2 results with the OLP V6.x results. OLP V6.x applied neither the empirical signal correction nor the orbit dependent default responsivity. It uses the actual chopped FCS measurement in order to derive the absolute calibration. Furthermore we compare with the IRAS photometry and in a subset of filters with the nodding mode photometry.

6.4.3 Results

Fig. 56 shows the derived spectral energy distribution for IRAS 03068-5346 chopped photometry in comparison with the IRAS photometry and with the results of nodding photometry. From the plot it can be seen that, although results for OLP V7.0b2 chopped FIR photometry look relatively consistent in comparison to OLP V6.x results, the chopped photometry gives too high fluxes w.r.t. the reference photometry. This is quantitatively determined in Table 39. OLP V6.x results using the actual response are not more reliable. They look better for C100, but worse for C200.
The P1 fluxes are below 30 mJy. Beside some relatively good coincidence with the nodding photometry, there is also a major outlier due to a non-detection (negative flux) in the 16 μm filter. This is likely solely caused by the signal evaluation rather than by the final flux calibration.
For P2 mixed results are achieved. While 25 μm photometry is fine both with IRAS and nodding mode photometry, the 20 μm photometry shows a large positive deviation.
As a further investigation we have checked the consistency of the background photometry from the nodding observations with COBE/DIRBE. The fluxes are given in part 3 of Sect. 6.4.5 and the resulting overall good consistency is displayed in Fig. 57, being another support case for the validation of the PHT22 extended source photometry (for PHT03 the issue of the dependence on the aperture size is not yet clarified).
We also did a similar check with the background values for the chopped photometry. This is displayed in Fig. 58 showing a considerably less good correlation. This is on the one

Table 39: Consistency check of chopped photometric results with IRAS and ISOPHOT nodding photometry

Filter	**reference**	**consistency w.r.t. reference photometry OLP V6.x** [%]	**consistency w.r.t. reference photometry OLP V7.0b2** [%]
P1_7P3	nodding	+22.8	+26.9
P1_11P5	nodding	-67.8	-41.5
P1_16P0	nodding	-72.7	-195
P2_20	nodding	+52.2	+87.3
P2_25	nodding	-35.3	-5.3
P2_25	IRAS	-43.7	-17.7
P3_60	nodding	+15.6	+84.3
P3_60	IRAS	-7.8	+47.1
P3_100	nodding	-16.1	+49.5
P3_100	IRAS	-42.2	+3.0
C100_60	nodding	+54.4	+126
C100_60	IRAS	+28.8	+88.1
C100_100	nodding	+35.1	+104
C100_100	IRAS	+3.3	+56.0
C200_120	nodding	+384	+190
C200_200	nodding	+173	-7.4

hand an indicator of the limitation by using a constant default responsivity, but on the other hand it must be clearly noted that the empirical chopper correction is only working for the signal difference, but is not correcting the absolute levels. Therefore, background values derived from chopped photometry are currently not reliable, but are not intended to be by the design of the processing and correction. In the table of part 4 of Sect. 6.4.5 we also give the range of the values of the OLP keyword RESPRi which gives the ratio of the derived actual responsivity from the chopped FCS measurement and the constant default responsivity used for the calibration. It can be seen that in some cases adjustment of the default responsivity value to the actual one can explain the ratio between staring and chopped background photometry, but in some cases not.

6.4.4 Conclusions

- The P1 photometry is performed on a very faint flux level ($\leq$ 30 mJy). For some filters good consistency with the nodding photometry is found, but also at least one outlier (the 12.8 μm point which has no staring reference photometry might include a strong Ne emission line?), a non-detection at 16 μm occurs. This seems to be mainly related to the signal evaluation, and clearly, an automatic processing is inferior to careful interactive analysis.

- P2 25 μm chopped photometry coincides well with IRAS photometry (within 20%) and the nodding photometry (within 5%). However, the 20 μm point leaves the decision about the quality of the chopped P2 photometry open. IRAS and nodding photometry are consistent within 12%.

- P3 chopped photometry is on the spot with nodding photometry for the 100 μm point, but too high by nearly a factor of 2 for the 60 μm filter. It coincides with IRAS photometry within 50%. It should be noted that IRAS and nodding photometry themselves are consistent to each other only within $\sim$ 40%.

- C100 chopped photometry yields in general between 50% and a factor of 2 higher photometric values than IRAS and nodding photometry for OLP V7.0b2. OLP V6.x results were closer to the reference photometry for this detector.

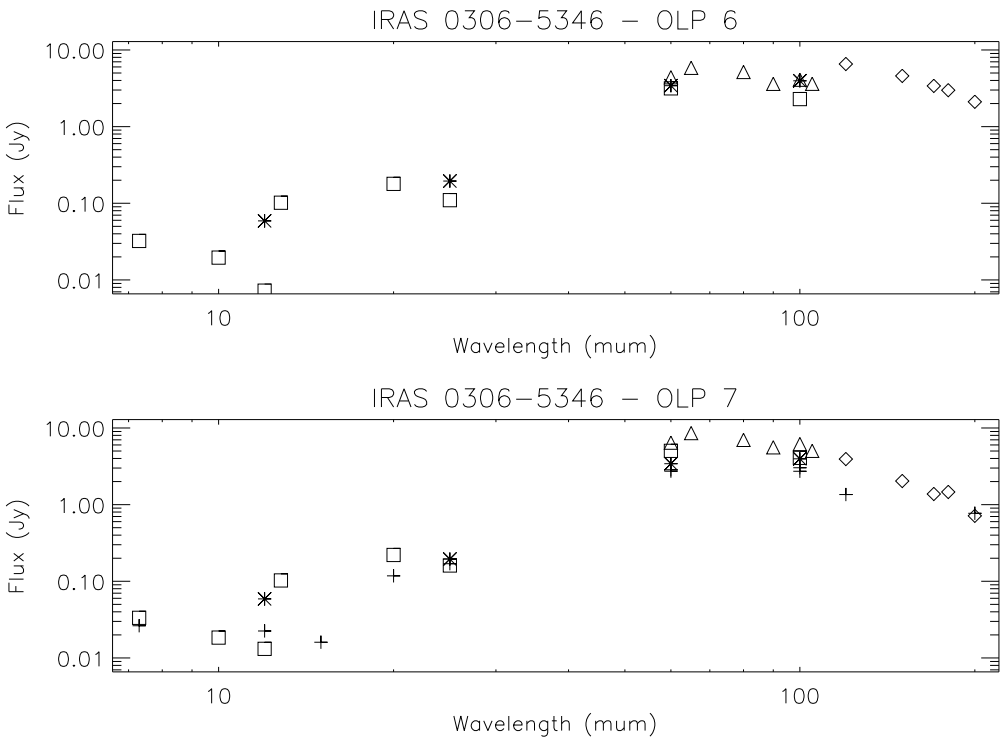

Figure 56: Comparison of PHT-P and PHT-C chopped photometry, using the ISOPHOT filter set from 7.3 to 200 μm (except feature filters), with ISOPHOT nodding (in subset of filters) and IRAS photometry. No color correction has been applied. The meaning of the symbols is the following: asterisk: IRAS (12 μm is upper limit), plus: ISOPHOT nodding photometry, square: PHT-P (P03 AOT), triangle: C100 (P22 AOT), diamond: C200 (P22 AOT).

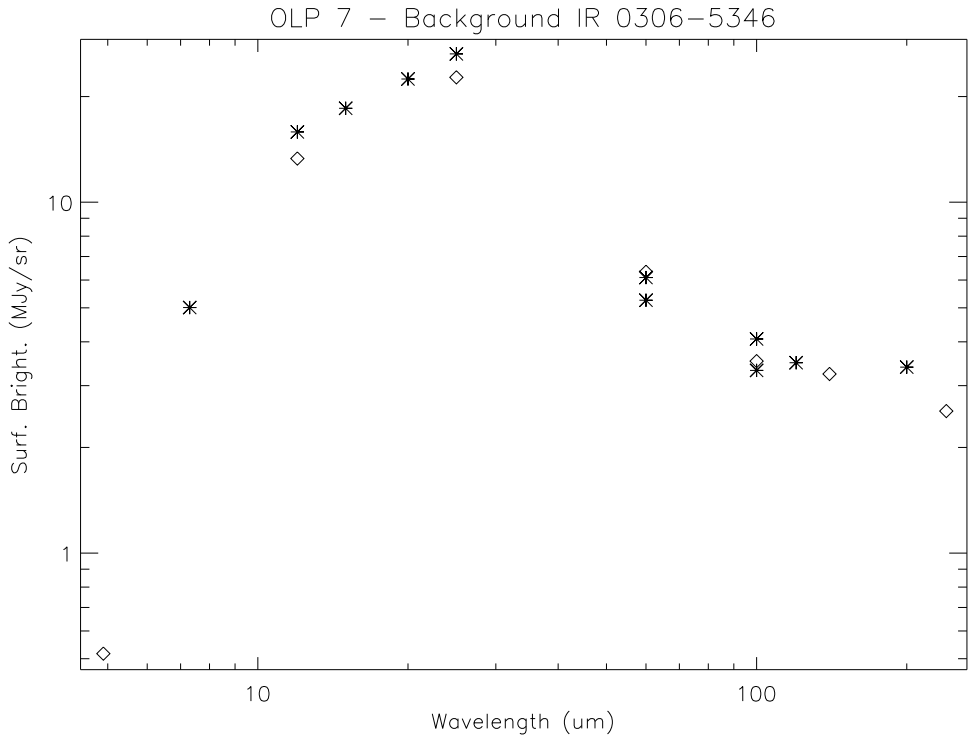

Figure 57: Comparison of the background surface brightness obtained with PHT-P and PHT-C nodding photometry with COBE/DIRBE results. No color correction has been applied. The meaning of the symbols is the following: asterisk: ISOPHOT photometry, diamond : COBE/DIRBE photometry.

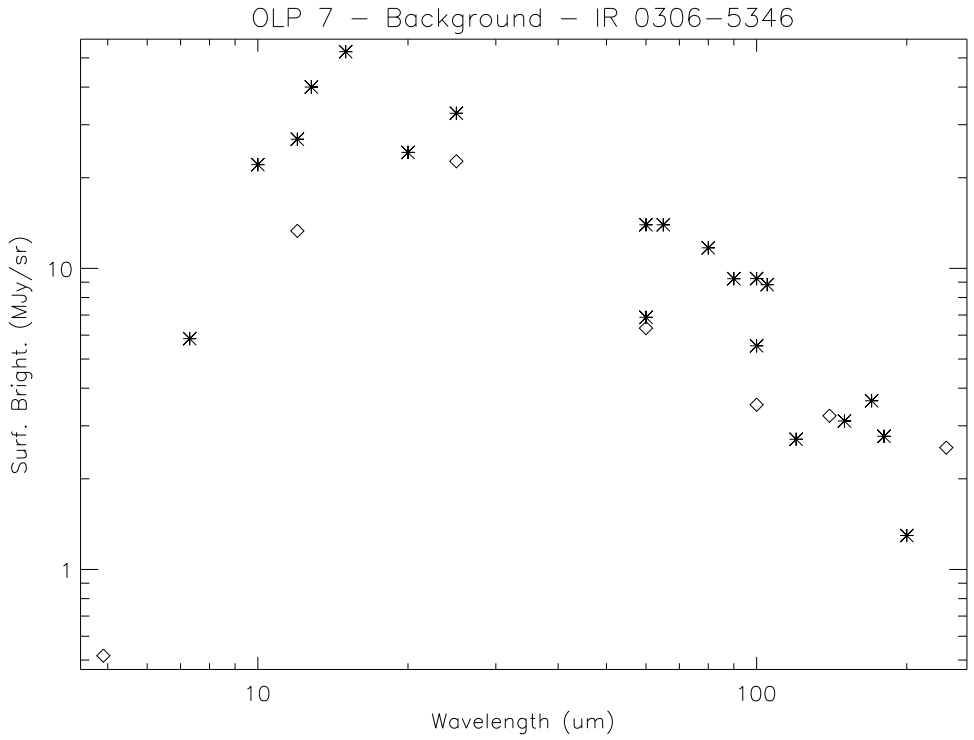

Figure 58: Comparison of the background surface brightness obtained with PHT-P and PHT-C chopped photometry with COBE/DIRBE results. No color correction has been applied. The meaning of the symbols is the following: asterisk: ISOPHOT photometry, diamond : COBE/DIRBE photometry.

- The contrary is the case for C200: The OLP V7.0b2 results are much closer and more consistent with the C100/P3 photometry for OLP V7.0b2 than for OLP V6.x.
- Overall we conclude that the chopped photometry does not yet give reliable results over the full wavelength range which achieve the implementation goal of 30% photometric accuracy. Also the consistency of the reference photometry in the FIR (IRAS vs. ISOPHOT nodding) must be checked in some more detail in order to explain the weak consistency of only $\sim$ 40%.
- Background values from nodding photometry give a good consistency with COBE DIRBE photometry. Chopped photometry gives in most cases too high background values, however, by design of the correction it is not intended to calibrate the absolute levels correctly, the correction is only working for the signal difference. Background values from chopped photometry are therefore not reliable.

6.4.5 Evaluation Log

1) chopped point source photometry results

# Filter	cwl	OLP6	OLP7	IRAS
P1_7P3_UM	7.3	0.03229433	0.0333713	0.
P1_10_UM	10.	0.0195555	0.0184598	0.
P1_11P5_UM	12.	0.007250439	0.0131614	< 5.899E-02
P1_12P8_UM	12.8	0.1016304	0.102611	0.
P1_16P0_UM	15.	0.004378796	-0.0151585	0.
P2_20_UM	20.	0.1792294	0.220583	0.
P2_25_UM	25.	0.1097912	0.160611	1.951E-01
P3_60_UM	60.	3.151688	5.02542	3.417
P3_100_UM	100.	2.286276	4.07237	3.955
C100_60_UM	60.	4.400512924	6.42881	3.417
C100_50_UM	65.	5.84085052	8.56521	0.
C100_70_UM	80.	5.1610432	6.99005	0.
C100_90_UM	90.	3.61345364	5.58736	0.
C100_100_UM	100.	4.0867529	6.17109	3.9550
C100_105_UM	105.	3.61856088	5.02906	0.
C200_120_UM	120.	6.558009	3.92809	0.
C200_135_UM	150.	4.5848026	2.03339	0.
C200_160_UM	170.	3.391446222	1.37579	0.
C200_180_UM	180.	2.9815656	1.46279	0.
C200_200_UM	200.	2.1048933	0.714194	0.

2) nodding photometry results (only OLP 7 evaluated)

# Filter	cwl	OLP6	OLP7	IRAS
P1_7P3_UM	7.3	--	0.02630773	0.
P1_11P5_UM	12.	--	0.02249053	< 5.899E-02
P1_16P0_UM	15.	--	0.01604105	0.
P2_20_UM	20.	--	0.1177684	0.
P2_25_UM	25.	--	0.1696383	1.951E-01
P3_60_UM	60.	--	2.727016	3.417
P3_100_UM	100.	--	2.72335	3.955
C100_60_UM	60.	--	2.849328	3.417
C100_100_UM	100.	--	3.026011	3.955
C200_120_UM	120.	--	1.353891	0.
C200_200_UM	200.	--	0.7713137	0.

3) background photometry from nodding observations and comparison with COBE

Filter	cwl	<MJy/sr>	COBE/DIRBE

```
P1_7P3_UM          7.3      5.009565
P1_11P5_UM        12.      15.8576          13.317
P1_16P0_UM        15.      18.51348
P2_20_UM          20.      22.43735
P2_25_UM          25.      26.45644         22.688
P3_60_UM          60.      6.099393          6.331
P3_100_UM        100.      3.3154            3.524
C100_60_UM        60.      5.256541          6.331
C100_100_UM      100.      4.075162          3.524
C200_120_UM      120.      3.487375          3.239 +- 0.506 (140 um)
C200_200_UM      200.      3.387625          2.539 +- 0.115 (240 um)
```

4) background photometry from chopped observations and comparison with nodding and COBE
(Act/Def = Ratio of actual response from chopped FCS measurement to default response;
C/S = Ratio of chopped vs. staring surface brightness photometry)

# Filter	cwl	Surf Bright (MJy/sr)		COBE/DIRBE	Act/Def Respons. Min	Max	C/S
		Staring	Chopped				
C100_50_UM	65.		13.959		0.574	1.090	
C100_105_UM	105.		8.8277				
C100_70_UM	80.		11.703				
C100_100_UM	100.	4.0752	9.2485	3.524			2.269
C100_60_UM	60.	5.2565	13.956	6.331			2.655
C100_90_UM	90.		9.2404				
C200_200_UM	200.	3.3876	1.2961	2.539	0.839	0.917	0.383
C200_120_UM	120.	3.4874	2.7062				0.776
C200_180_UM	180.		2.7685				
C200_135_UM	150.		3.1117	3.239			
C200_160_UM	170.		3.6337				
P1_16P0_UM	15.	18.513	52.451		1.264	1.264	2.833
P1_10_UM	10.		22.106				
P1_12P8_UM	12.8		40.012				
P1_7P3_UM	7.3	5.0096	5.8403				1.166
P1_11P5_UM	12.	15.858	26.845	13.317			1.693
P2_20_UM	20.	22.437	24.275		1.234	1.234	1.082
P2_25_UM	25.	26.456	32.737	22.688			1.237
P3_60_UM	60.	6.0994	6.8797	6.331	1.226	1.226	1.128
P3_100_UM	100.	3.3154	5.5304	3.524			1.668

6.5 Validation of PHT03 and PHT22 Chopped Mode: The FIR Excess SED of Vega

- authors: M. Radovich, U. Klaas
- data: 25-May-1998

6.5.1 Motivation

We investigate here observations of a general observer's program for which photometry using Interactive Analysis has been published, cf. Ref. [15]. In addition, IRAS photometry at 25, 60, and 100 μm is available.

6.5.2 Method

We compare the OLP V7.0b2 results with the OLP V6.x results. OLP V6.x applied neither the empirical signal correction nor the orbit dependent default responsivity. It uses the actual chopped FCS measurement in order to derive the absolute calibration. Furthermore, we compare with the IRAS photometry and the reference photometry established with PIA as published in Ref. [15].

6.5.3 Results

Fig. 59 shows the results of the chopped photometry. The P2 photometry gives consistent results. Obvious is a discontinuity between the C100 and the C200 photometry. While in the case of OLP V7.0 this argues for a mismatch of the default responsivities used for both detectors - the reference photometry suggests that the C200 photometry is off - in the case of the OLP V6.x either the FCS measurement (C200) or the signal losses (C100) do not give reliable photometry (see section Data Reduction of Ref.[15] for details of the problems encountered). However, Fig. 60 shows in comparison the results obtained with PIA V7.1. They do not show the discontinuity, but P3, C100, and C200 data fit together.
Tab. 40 gives the consistency of the chopped PHT photometry with the IRAS and the published reference photometry (hereafter HWK). The color corrected fluxes are given in Sect. 6.5.5). It should be noted that the IRAS photometry and the HWK photometry themselves are consistent with each other only within 20%. While the OLP V7 C100 photometry is consistent with IRAS at 60 μm and considerably below at 100 μm, the PIA results show just the opposite behaviour: at 60 μm the resulting flux is considerably too high, while at 100 μm it matches the IRAS result. This behaviour cannot be explained by just a wrong value of the default responsivity, because then the photometry in both filters should show a similar offset. Anyhow, the C200 measurements together with KAO and submm photometry suggest that the IRAS 100 μm point is less trustful than the IRAS 60 μm point.
The discontinuity in the SED of Vega produced by OLP from the chopped measurements and the discrepancy with the PIA results which gives a smooth SED needs follow-up investigation. On the other hand, the PIA results are overcorrected w.r.t. the reference photometry.

6.5.4 Conclusions

- The P2 chopped photometry is very consistent with IRAS and the published reference photometry.
- The P3 chopped photometry gives too high fluxes both w.r.t. IRAS and HWK. Possible reason is that the default responsivity does not match the actual one. The OLP V6.x result was in better agreement with the expectations.
- The chopped C100 photometry is in relatively good agreement ($\leq$ 15%) with the interactively processed and published reference photometry. Both suggest a steeper shape of the SED than IRAS.
- The chopped C200 photometry gives too high fluxes suggesting that the default responsivity used was too low. This gives a discontinuity in the SED. On the other hand the photometry would match to the color corrected IRAS 100 μm data point.

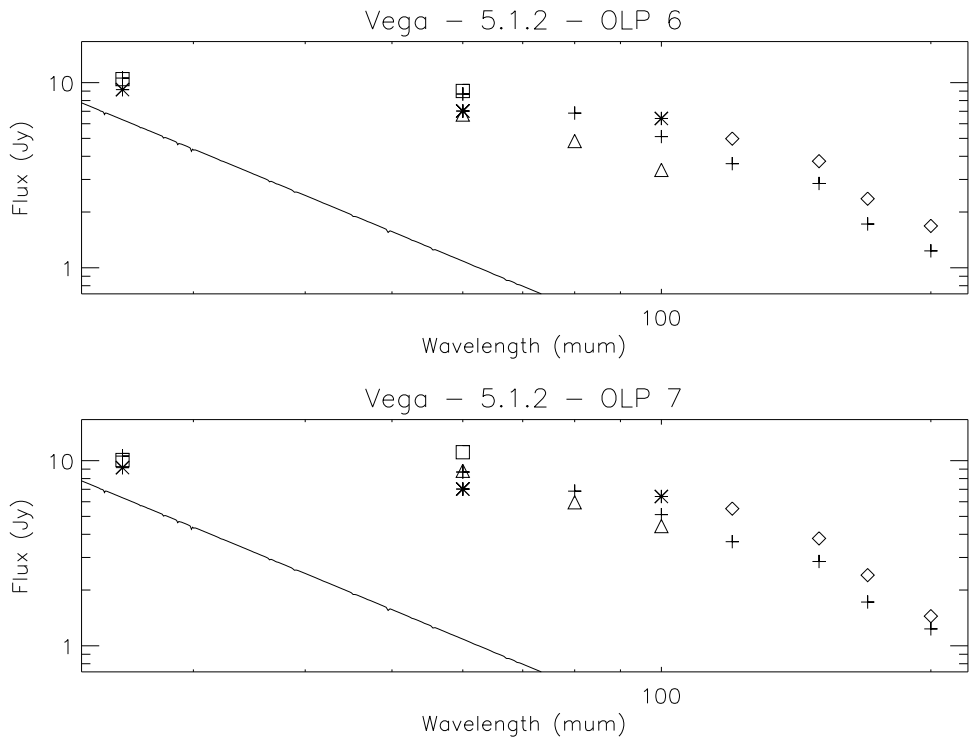

Figure 59: Comparison of PHT-P and PHT-C chopped photometry of Vega with published ISOPHOT photometry evaluated with Interactive Analysis as described in Ref. [15] and IRAS photometry. Color correction as described in Sect. 6.5.5 has been applied. The meaning of the symbols is the following: solid line: photospheric model by Cohen (to show the size of the IR excess), asterisk: IRAS, plus: ISOPHOT reference photometry (HWK), square: PHT-P (P03 AOT), triangle: C100 (P22 AOT), diamond: C200 (P22 AOT).

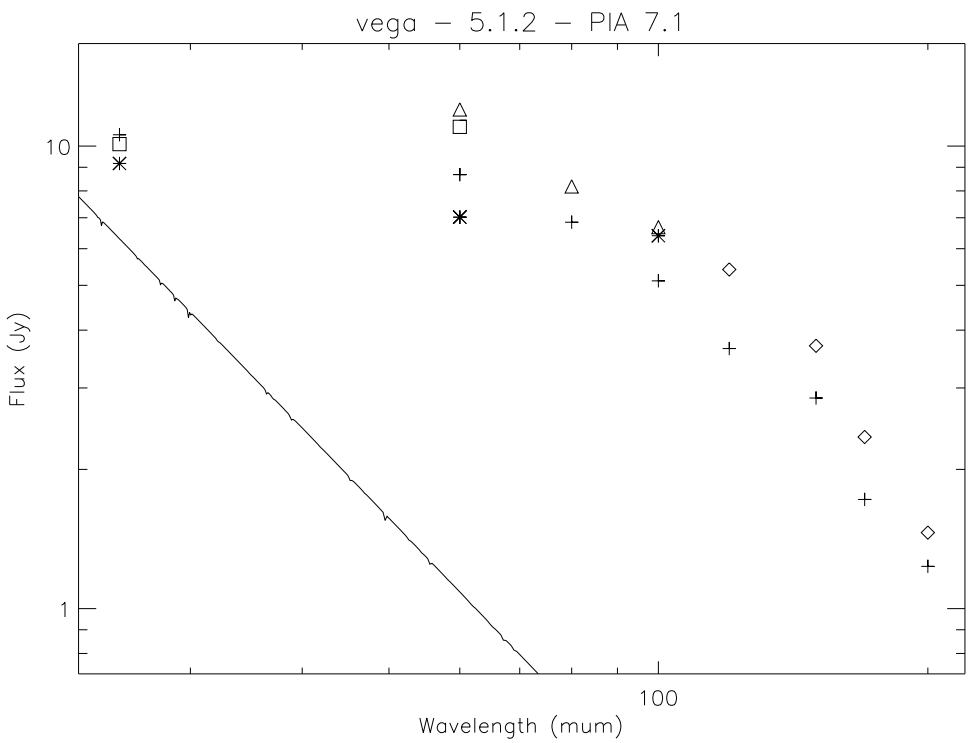

Figure 60: Comparison of PHT-P and PHT-C chopped photometry of Vega, evaluated with PIA V 7.1, with published ISOPHOT photometry evaluated with Interactive Analysis as described in Ref. [15] and IRAS photometry. Color correction as described in Sect. 6.5.5 has been applied. The meaning of the symbols is the following: solid line: photospheric model by Cohen (to show the size of the IR excess), asterisk: IRAS, plus: ISOPHOT reference photometry (HWK), square: PHT-P (P03 AOT), triangle : C100 (P22 AOT), diamond: C200 (P22 AOT).

Table 40: Consistency check of chopped photometric results with IRAS and HWK photometry

Filter	**reference**	**consistency w.r.t. reference photometry**		
		OLP V6.x [%]	**OLP V7.0b2** [%]	**PIA V7.1** [%]
P2_25_UM	IRAS	+13.9	+9.9	+10.1
P2_25_UM	HWK	-1.3	-4.7	-4.5
P3_60_UM	IRAS	+28.4	+58.2	+56.7
P3_60_UM	HWK	+3.9	+28.0	+26.8
C100_60_UM	IRAS	-4.3	+25.6	+70.9
C100_60_UM	HWK	-22.5	+1.6	+38.3
C100_70_UM	HWK	-29.4	-13.0	+19.5
C100_100_UM	IRAS	-47.2	-30.8	+4.4
C100_100_UM	HWK	-33.9	-13.3	+30.7
C200_120_UM	HWK	+36.4	+50.8	+48.2
C200_135_UM	HWK	+32.0	+33.2	+29.7
C200_160_UM	HWK	+37.0	+39.8	+36.5
C200_200_UM	HWK	+36.3	+17.1	+18.3
HWK 25	IRAS	+15.4	+15.4	+15.4
HWK 60	IRAS	+23.6	+23.6	+23.6
HWK 100	IRAS	-20.1	-20.1	-20.1

- Overall the chopped FIR photometry appears to be only as accurate as 30 to 50% which is above the goal expected for OLP 7.
- The discontinuity between the C100 and the C200 part of the SED is restricted to the OLP results. PIA V7.1 results do not show this discontinuity, but a considerably raised C100 SED branch which fits on the one side to the C200 and on the other side to the P3 photometry. However, all three chopped photometries are systematically too high.

6.5.5 Evaluation Log

```
1) results of chopped FIR photometry on Vega

Fluxes are color corrected (beyond 60 um with modified BB
                           (eps propto nu) of 80 K,
                           at 25 for a mixture of 60% BB of T = 10000 K
                           and 40% modified BB (eps propto nu) of 80 K)
The color correction for the fluxes as given in paper HWK (Heinrichsen, Walker,
Klaas, ref. 15) was re-done according to the color correction described above.


Filter          cwl      OLP6         OLP7     IRAS   PIA7  HWK photom.
P2_25_UM        25.    10.44462    10.08107    9.17   10.1   10.58
P3_60_UM        60.    9.011438    11.10448    7.02   11.0   8.677
C100_60_UM      60.    6.721669    8.814398    7.02   12.0   8.677
C100_70_UM      80.    4.836243    5.958574    0.     8.18   6.845
C100_100_UM    100.    3.37683     4.431378    6.40   6.68   5.112
C200_120_UM    120.    4.979102    5.50299     0.     5.41   3.650
C200_135_UM    150.    3.766084    3.800487    0.     3.70   2.853
C200_160_UM    170.    2.359226    2.407068    0.     2.35   1.722
C200_200_UM    200.    1.682093    1.445075    0.     1.46   1.234
```

6.6 Comparison of Chopped and Staring Mode Photometry of Standard Stars from the Empirical Signal Correction Calibration Program

- authors: M. Radovich, U. Klaas
- date: 29-May-1998

6.6.1 Motivation

A large calibration program had been set up to establish the empirical signal loss correction factors in chopped measurements from a comparison of chopped and nodding/staring photometry in the same instrumental set-up, on the same source and on the same revolution (as one block of measurements, to minimize differences in detector responsivities.) We have selected a few of these measurements to verify the end product of the chopped photometric calibration, as produced by OLP. This does not only include the signal correction, but also the signal derivation itself and the application of the default responsivity. We have selected test cases with more than one filter per detector in order to see the relative wavelength behaviour of the correction.

6.6.2 Method

All targets are standard stars for which flux models are available. In all cases ISOPHOT reference photometry, either in simple staring mode or in nodding technique are available. This allows to determine the absolute accuracy w.r.t. the model and in case of a discrepancy to cross-check how the consolidated staring mode photometry behaves.

6.6.3 Results

In Fig. 61 we show the resulting chopped and staring/nodding photometry in comparison with the parts of the SED of the respective standard star in the investigated wavelength range. In Table 41 we assess quantitatively the consistency with the model.
The results for the individual detectors are:

P1: Both chopped and nodding photometry show a similar accuracy in the order 20 to 40%. The 3.3 μm nodding measurement is a significant outlier (+ 364%) and the reason for this must be investigated in detail.

P2: The accuracy of both chopped and nodding photometry is comparable (in the range 5 – 25%). No dramatic dependence of the photometric accuracy on the aperture size (which is not the standard aperture size of 79") can be recognized.

P3: Both chopping and nodding photometry give quite good accuracy (better than $\sim$ 15%) for this flux range between 6 and 20 Jy.

C100: The chopped photometry is systematically overcorrected, between about 50% and a factor of 2. The staring photometry gives very good results (better than 10%), except of the 105 μm filter (up to 45%).

C200: Both chopped and staring photometric results are very consistent in themselves (within 10%). The 120 μm point coincides well with the model, while the 180 μm point shows again this kind of negative photometric bias with a significant underestimate of the resulting source flux, as also reported in Sect. 5.14, but less severe.

6.6.4 Conclusions

- P2 and P3 chopped photometry of the standard stars HR 6132 (3.5 – 6 Jy at 20 – 25 μm) and HR 1457 (α Tau; 7 – 20 Jy at 60 – 100 μm) shows a satisfying accuracy w.r.t. model fluxes and is consistent with the nodding photometry.

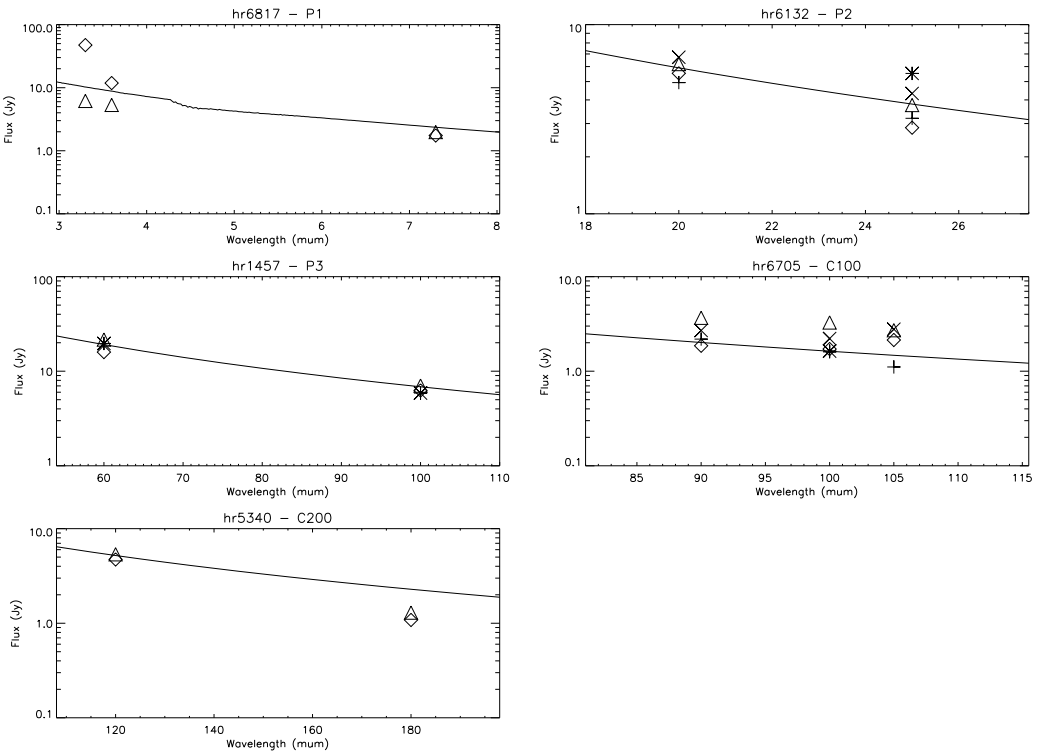

Figure 61: Comparison of PHT-P and PHT-C chopped photometry of various standard stars from the empirical signal correction calibration programme with the staring reference photometry and the models provided by Hammersley (Ground Based Preparatory Programme) and Cohen. Fluxes are color corrected according to the spectral type of the star. The meaning of the symbols is the following: solid line: photospheric model by Hammersley or Cohen, asterisk: IRAS, triangle: chopped ISOPHOT photometry, cross: chopped photometry in the same filter with a different chopper frequency, diamond: ISOPHOT nodding (P1, P2, P3) or staring off/on (C100, C200) photometry, plus: staring photometry in a different aperture.

Table 41: Consistency check of chopped and staring photometric results of standard stars with models from Hammersley and Cohen

Filter	**Mode**	**consistency w.r.t. reference photometry**	
		chopped mode [%]	**staring/nodding mode** [%]
P1_3P29_UM	–	-39.6	+364
P1_3P6_UM	–	-39.2	+34.7
P1_7P3_UM	–	-16.1	-26.1
P2_20_UM	120" aper. f_{chop} = 0.0625 Hz	+4.7	-6.4
P2_20_UM	180" aper. f_{chop} = 0.0625 Hz	+13.8	-16.4
P2_25_UM	120" aper. f_{chop} = 0.0625 Hz	-1.2	-25.1
P2_25_UM	180" aper f_{chop} = 0.0625 Hz	+13.7	-15.9
IRAS 25	–	+45.2	+45.2
P3_60_UM	–	+13.0	-16.7
IRAS 60	–	+2.8	+2.8
P3_100_UM	–	+2.8	-8.6
IRAS 100	–	-14.2	-14.2
C100_90_UM	f_{chop} = 0.250 Hz	+82.4	-7.7
C100_90_UM	f_{chop} = 0.500 Hz	+34.0	+8.6
C100_100_UM	f_{chop} = 0.125 Hz	+101	+5.5
C100_100_UM	f_{chop} = 0.250 Hz	+36.1	-1.7
IRAS 100	–	+0.2	+0.2
C100_105_UM	f_{chop} = 0.0625 Hz	+84.1	+45.1
C100_105_UM	f_{chop} = 0.125 Hz	+88.7	-24.7
C200_120_UM	–	+3.0	-9.2
C200_180_UM	–	-43.4	-52.7

- P1 chopped photometry of the standard star HR 6817 (2.5 – 10 Jy at 3 to 7.5 μm) achieves only an accuracy of 40%. In this case also the nodding photometry is not very accurate and one significant outlier was encountered (3.3 μm) which needs detailed follow-up.
- C100 chopped photometry is systematically overcorrected by 50% to a factor of 2.
- C200 chopped photometry is consistent with the staring photometry. At 180 μm where the source-to-background contrast is 1:4.2 an underestimate of the source flux occurs for both types of photometry. This behaviour is reported, too, from independent measurements on α Boo (HR 5340), cf. Sect. 5.14.

6.6.5 Evaluation Log

```
Results of chopped and staring reference photometry from calibration program
for establishment of empirical signal correction factors.

Fluxes are color corrected according to the spectral type of the star

models: H = Hammersley (Ground Based Preparatory Program)
        C = Cohen
```

Star	Filter	Cwl	Flux (Jy)		Model		IRAS
			Chopped	Staring			
HR 6817 (T = 5000 K)							
	P1_3P29_UM	3.3	6.17093	47.35837	10.216	H	
	P1_3P6_UM	3.6	5.335391	11.82415	8.780		
	P1_7P3_UM	7.3	1.979036	1.742748	2.358		
HR 6132 (T = 5000 K)							
	P2_20_UM	20.	6.188495	5.529422	5.909	H	
	P2_20_UM	20.	6.722445	4.939584	5.909		
	P2_25_UM	25.	3.756719	2.850183	3.803		5.52
	P2_25_UM	25.	4.324078	3.198051	3.803		
HR 1457 (T = 4000 K)							
	P3_60_UM	60.	21.60345	15.93567	19.12	C	19.65
	P3_100_UM	100.	7.03337	6.256239	6.842		5.87
HR 6705 (T = 4000 K)							
	C100_90_UM	90.	3.669319	1.857785	2.012	C	
	C100_90_UM	90.	2.695448	2.185172	2.012		
	C100_100_UM	100.	3.276827	1.7158	1.627		1.63
	C100_100_UM	100.	2.214573	1.599855	1.627		
	C100_105_UM	105.	2.714276	2.139333	1.474		
	C100_105_UM	105.	2.780838	1.109648	1.474		
HR 5340 (T = 4000 K)							
	C200_120_UM	120.	5.354198	4.723388	5.201	C	
	C200_180_UM	180.	1.293918	1.082191	2.286		

```
TDT Numbers:

P1 chopped photometry
TDT 78300901   HR 6817     P03    3.3 um chopping
    78300902   HR 6817     P03    3.3 um nodding
    78301005   HR 6817     P03    7.3 um chopping
    78301006   HR 6817     P03    7.3 um nodding
    78301107   HR 6817     P03    12 um chopping
    78301108   HR 6817     P03    12 um nodding

P2 chopped photometry
TDT 76901901   HR 6132     P03    20 um nodding
    76901902   HR 6132     P03    20 um chopping
    76902010   HR 6132     P03    20 um nodding (diff. aperture)
    76902011   HR 6132     P03    20 um chopping (diff. chop freq.)
    76902105   HR 6132     P03    25 um nodding
    76902106   HR 6132     P03    25 um chopping
    76902215   HR 6132     P03    25 um nodding (diff. aperture)
    76902216   HR 6132     P03    25 um chopping (diff. chop freq.)

P3 chopped photometry
TDT 86101201   HR 1457     P03    100 um nodding
    86101202   HR 1457     P03    100 um chopping
    86101305   HR 1457     P03    60 um nodding
    86101306   HR 1457     P03    60 um chopping
```

```
C100 chopped photometry
TDT 67100801   HR 6705     P22    background
    67100802   HR 6705     P22    90, 100, 105 um staring
    67100803   HR 6705     P22    90, 100, 105 um chopping
    67100910   HR 6705     P22    background
    67100911   HR 6705     P22    90, 100, 105 um staring (diff. reset interv.)
    67100912   HR 6705     P22    90, 100, 105 um chopping (diff. chop freq.)

C200 chopped photometry
TDT 62900720   HR 5340     P22    background
    62900721   HR 5340     P22    120, 180 um staring
    62900722   HR 5340     P22    120, 180 um chopping
```

6.7 OLP Chopped and Staring Mode Photometric Results for the Faint Point Source Detection Limit Program

- authors: M. Radovich, U. Klaas
- Date: 24-May-1998

6.7.1 Motivation

In order to determine the optimal observing strategies for faint point sources a dedicated engineering program had been performed. This resulted in recommendations for the most sensitive and photometrically accurate faint source observation modes [18]. This program was largely done using AOTs so that the resulting OLP fluxes can be checked for their accuracies.

6.7.2 Method

Both chopped and staring (sparse map, nodding mode was not yet available at that time) mode OLP 6 and OLP 7 results are compared with each other. All targets are faint standard stars for which M. Cohen has provided extensions of the SED out to 300 μm, so that comparison with the model prediction is possible. All observations had been evaluated interactively for an assessment report [19] using PIA V5.5. In the following table we list the results as they were presented in this assessment report:

Filter	Target	Obs. mode	t(meas) (on-source)	PHT flux [mJy]	S/N	Bgd [MJy/sr]	Flux [mJy]	Detlimit [mJy]
P_60	HR5981	staring	256 s	146 +- 17	8.6	5.5	130	15.1
P_60	HR5981	TriChop	256 s	85 +- 11*	7.7	4.6	130	16.9*
P_60	HR5981	raster	256 s	152 +- 12	12.7	5.3	130	10.2
C_60	HR5981	staring	256 s	104 +- 10	10.3	6.9	130	12.6
C_60	HR5981	TriChop	256 s	39 +- 9	4.5	6.8	130	29.0
C_60	HR5981	raster	256 s	104 +- 10	10.3	8.6	130	12.6
C_60	HR5981	P32	256 s	74 +- 11	6.7	8.6	130	19.3
C_90	IRC+60228	staring	256 s	87 +- 7	12.8	4.7	75	5.9
C_90	IRC+60228	TriChop	128 s	20 +- 12	1.6	4.5	75	46.8
C_90	IRC+60228	raster	256 s	48 +- 7	6.9	5.3	75	10.9
C_90	IRC+60228	P32	256 s	49 +- 10	5.1	5.8	75	14.7
C_90	SAO248381	staring	256 s	80 +- 9	9.0	5.7	79	8.8
C_90	SAO248381	chopping	128 s	32 +- 5	6.3	5.1	79	12.6
C_90	SAO248381	staring	256 s	73 +- 19	3.9	5.6	79	20.3

In April 1997 the sparse map staring sequence gave the most accurate photometric results. Chopped and PHT32 mode gave in general always too low fluxes which was explained with the signal losses due to the chopper signal modulation.
Note, that in this report we do not address the mapping observations done in raster or PHT32 mode.

6.7.3 Results

In part 1 of Sect. 6.7.5 we provide the OLP results of the chopped photometry. We can see that the new approach in OLP 7 does not improve the photometry. In the contrary, the OLP 6 results which use the chopped FCS measurement match the model expectations much better. In one case OLP 7 even fails to detect the source. In the other cases the resulting fluxes are by far too high. Reasons for this performance may be:

- The default responsivity seems to be too low, resulting in too high fluxes. This can be explained, like recent calibrations results imply, if the responsivity is not constant with flux.

- The failure of detection of the C100 60 μm measurement can be due to the fact that the differential source signal is determined from all C100 pixels (as in staring mode). Applying the correction factor (times 3 for C100 !) to the very small differential signals in the corner pixels may only boost the noise. Therefore, evaluation of the central pixel only should be considered in the future.

It should, however, be noted that there may be other unknown reasons. Evaluating these measurements of faint sources interactively results in the best de-selection of bad or doubtful data points. This may not be the case for the automatic processing. Therefore, the automatic processing is currently not comparable to a careful interactive analysis.
The sparse map staring observations were performed like a slow forward and backward telescope nod. We therefore combined always one on-source measurement with the two bracketing off-source measurements to subtract an averaged background in order to account for possible drift effects.
From the tables in part 2 of Sect. 6.7.5 it can be seen that in the case of SAO248381 both OLP 6 and OLP 7 results suggest that we are at the detection limit of this measurement with an expected source flux of 88 mJy. The source is not unambiguously detected.
For IRC+60228 there is a clear and consistent detection. The average flux is 105 $\pm$ 9 mJy which is within 25% of the model expectation of 84 mJy. OLP 6 gave with 94 $\pm$ 8 mJy a slightly better correspondence with the model.
For HR 5981 the C100 photometry has remained stable between both OLP versions, giving 187 $\pm$ 69 mJy as the average which is within 32% of the model expectation of 142 mJy. The P3 photometry has improved for OLP V7 yielding an average of 149 $\pm$ 39 mJy flux which is close to the model expectations.
In part 3 of of Sect. 6.7.5 we perform a comparison of the background photometry from chopped and staring modes with COBE/DIRBE results. The background surface brightness derived from the staring mode photometry is always somewhat higher than COBE, in the order of 20 – 30%. The background value derived from the chopped observations is always higher than the staring value by a factor of 1.4 to 2.3. The actual to default responsivity ratio derived by the OLP suggests that in most cases this offset might be explained by a too low default responsivity value. It has to be kept in mind, however, that the correction method does not try to get the absolute levels corrected, but only the differential flux. We only consider the background flux values in order to get some hints where to finetune the correction parameters for the source flux derivation.

6.7.4 Conclusions

- The empirical chopper correction cannot be declared scientifically valid for FIR fluxes below 200 mJy.

- The empirical chopped photometry correction was proven to give in general too high fluxes (by factor 2 - 4) for the faintest point sources. This may be explained by a too small default responsivity for the low total flux.

- The signal correction of all pixels of the C100 array (signal of pixel 6 is not considered for the end result) may boost too much the noise for the faintest sources. Restriction to the central pixel may give better results.

- Sparse map staring mode P3 and C100 photometry of faint sources gives reliable results with photometric accuracies in the order of $\sim$ 30% for sources in the 100 to 200 mJy flux range.

- Background values derived from the staring mode observations are in in general agreement with COBE fluxes within 20 – 30%. The background values derived from the chopped measurements suggest that the default responsivity values need some re-adjustment.

6.7.5 Evaluation Log

All fluxes are color corrected

1) Chopped measurements

TDT	Object	Detector	cwl	OLP6	OLP7	Model
25000801	SAO248381	C100_90_UM	90	0.227	0.353	0.08818
25202408	IRC+60228	C100_90_UM	90	0.230	0.407	0.08406
39200413	HR5981	C100_60_UM	60	0.208	-0.137	0.14212
39200626	HR5981	P3_60_UM	60	0.152	0.392	0.14212

2) Staring measurements
(The source flux is determined as the differential flux from the sparse map on-source measurement w.r.t. the preceding and succeeding sparse map off-source measurement:
source= (S+B)-avg(Back1,Back2))

a) For OLP 6

TDT	Object	Detector	Cwl	S+B	Back1	Back2	OLP6
25000703/5	SAO	C100_90_UM	90	3.718	3.714	3.628	0.041
25000705/8	SAO	C100_90_UM	90	3.607	3.628	3.641	-0.024
25202510/2	IRC	C100_90_UM	90	3.355	3.288	3.219	0.088
25202512/4	IRC	C100_90_UM	90	3.282	3.219	3.115	0.099
39200304/6	HR5981	C100_60_UM	60	5.067	4.796	4.776	0.265
39200306/8	HR5981	C100_60_UM	60	4.948	4.776	4.916	0.096
39200309/10	HR5981	C100_60_UM	60	4.984	4.916	4.619	0.204
39200310/12	HR5981	C100_60_UM	60	4.818	4.619	4.615	0.189
39200517/9	HR5981	P3_60_UM	60	0.789	0.550	0.507	0.231
39200519/21	HR5981	P3_60_UM	60	0.796	0.507	0.523	0.248
39200521/3	HR5981	P3_60_UM	60	0.836	0.523	0.622	0.234
39200523/5	HR5981	P3_60_UM	60	0.768	0.622	0.627	0.127

b) For OLP 7

TDT	Object	Detector	Cwl	S+B	Back1	Back2	OLP7
25000703/5	SAO	C100_90_UM	90	3.563	3.561	3.473	0.040
25000705/8	SAO	C100_90_UM	90	3.450	3.473	3.475	-0.021
25202510/2	IRC	C100_90_UM	90	3.129	3.053	2.977	0.099
25202512/4	IRC	C100_90_UM	90	3.042	2.977	2.849	0.111
39200304/6	HR5981	C100_60_UM	60	4.801	4.530	4.517	0.262
39200306/8	HR5981	C100_60_UM	60	4.693	4.517	4.663	0.097
39200309/10	HR5981	C100_60_UM	60	4.737	4.663	4.377	0.205
39200310/12	HR5981	C100_60_UM	60	4.575	4.377	4.387	0.182
39200517/9	HR5981	P3_60_UM	60	0.570	0.400	0.371	0.163
39200519/21	HR5981	P3_60_UM	60	0.575	0.371	0.382	0.176
39200521/3	HR5981	P3_60_UM	60	0.604	0.382	0.452	0.165
39200523/5	HR5981	P3_60_UM	60	0.556	0.452	0.457	0.090

3) background photometry and comparison with COBE

Background Surface Brightness (MJy/sr)
S: staring
C: chopped

				Surf Bright (My/sr)	C/S	Actual/Default Responsivity Min	Max
SAO248381							
25000703	S	C100_90_UM	90	5.9505			
25000801	C	C100_90_UM	90	8.3734	1.407	1.174	1.822
COBE Annual Map			60	6.478			
COBE Annual Map			100	3.909			
linear interpolation							
60-100			90	4.55			
IRC+60228							
25202510	S	C100_90_UM	90	5.1007			
25202408	C	C100_90_UM	90	6.9622	1.365	1.016	1.636
COBE Annual Map			60	6.508			
COBE Annual Map			100	3.580			
linear interpolation							
60-100			90	4.31			
HR 5981							
39200413	C	C100_60_UM	60	18.8604	2.329	1.877	2.668
39200517	S	P3_60_UM	60	8.0978			
39200626	C	P3_60_UM	60	13.6712	1.688	3.235	
COBE Annual Map			60	6.248			

6.8 Comparison of Chopped and Staring Mode Photometry of Stars Observed by the MFAINT and CFAINT Programs

- authors: M. Radovich, U. Klaas
- date: 17-July-1998

6.8.1 Motivation

The faint stars observed repeatedly by the monitoring program MFAINT have also been observed several times in chopped mode by the program CFAINT. MFAINT used the most recommended observation modes (nodding for P1, P2, and P3 and mini-map for C100 and C200). We compare here the results of the measurement set performed on revolution 748.

6.8.2 Method

Both staring (nodding/mini-map) and chopped photometry are compared with each other and against the model predictions by Cohen or Hammersley.

6.8.3 Results

In Figs. 62 and 64 we show the resulting chopped and in Figs. 63 and 65 the resulting staring/nodding photometry, respectively in comparison with the models of the SED of the respective standard star in the investigated wavelength range. In Table 42 we assess quantitatively the consistency with the model.
The results for the individual detectors are:

P1: For both stars the chopped photometry gives satisfying results for both OLP versions. On average OLP 6 gives the better results. The nodding photometry gives satisfying results for OLP V7. Albeit HR 5986 is the brighter source the accuracy is somewhat less good than for HD 172323. The reason may be a baseline drift.

P2: For both stars OLP 6 gives excellent results in chopped mode. OLP 7 gives mixed results with a too high flux for the fainter star HR 5986. This may be due to a too low value for the responsivity. The OLP 7 nodding photometric results are excellent for both stars.

P3: Both chopped and nodding photometry of both OLP versions gives accuracies better than 20%. While OLP 6 slightly undercorrected the chopped photometry, OLP 7 slightly overcorrects it.

C100: For the chopped photometry we observe again the strong overcorrection by more than a factor of 2 in the case of OLP 7. OLP 6 gives excellent chopped photometric results. For the mini-map photometry the OLP 7 photometry is better than 5% in both filters!

C200: Both OLP 6 and OLP 7 chopped photometry significantly underestimate the source flux. In the case of OLP 6 two pixels yielded negative fluxes. The C200 mini-map gives a good photometry in OLP 7. The mini-map shows a second point source in its corner. This may contaminate the background flux in the chopped measurement (exact geometry in chopped mode TBD).

6.8.4 Conclusions

- In nearly all cases OLP 6 gives the better results for chopped photometry. OLP 7 PHT-P chopped photometry can be classified as accurate as 40%. OLP 7 C100 chopped photometry shows again the strong overcorrection by more than a factor of 2. In the case of HR 6705 there may be contamination by another point source which can be seen in the corner of the mini-map, leading to a too high background flux.
- The OLP 7 nodding/mini-map photometry gives with the exception of one case very good results ($\leq$ 15%).

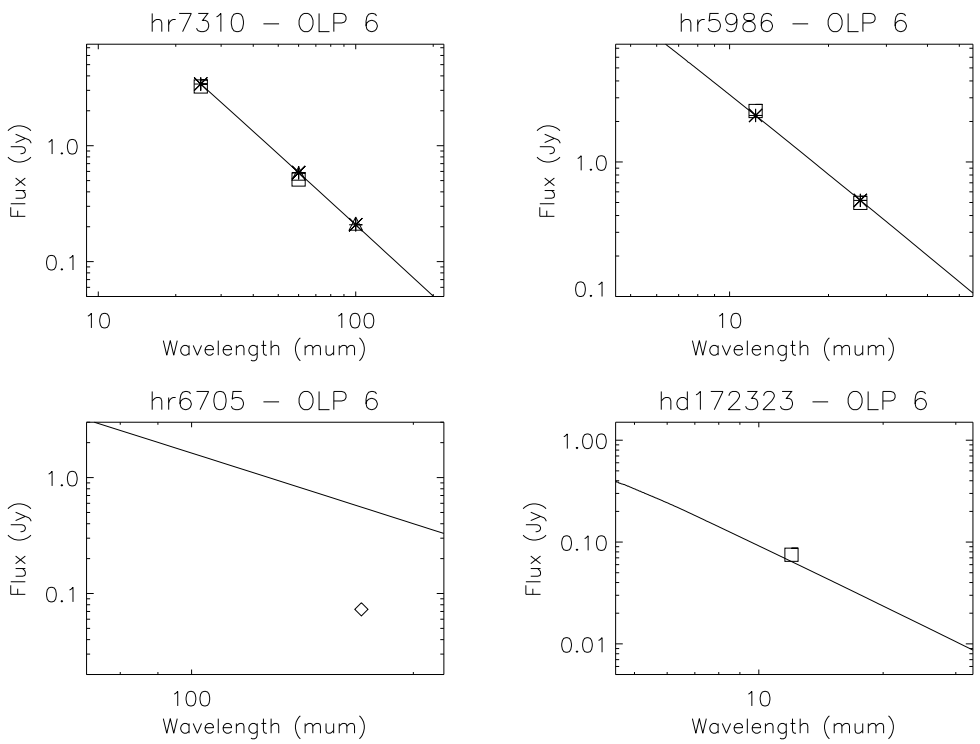

Figure 62: Comparison of PHT-P and PHT-C chopped OLP 6.x photometry of various standard stars from the CFAINT monitoring program for the epoch of rev. 748 with the models provided by Hammersley (Ground Based Preparatory Programme), for HD 172323 and HR 5986, and Cohen, for HR 7310 and HR 6705. Fluxes are color corrected according to the spectral type of the star. The meaning of the symbols is the following: solid line: photospheric model by Hammersley or Cohen, asterisk: IRAS, square: PHT-P photometry, triangle: C100 photometry, diamond: C200 photometry.

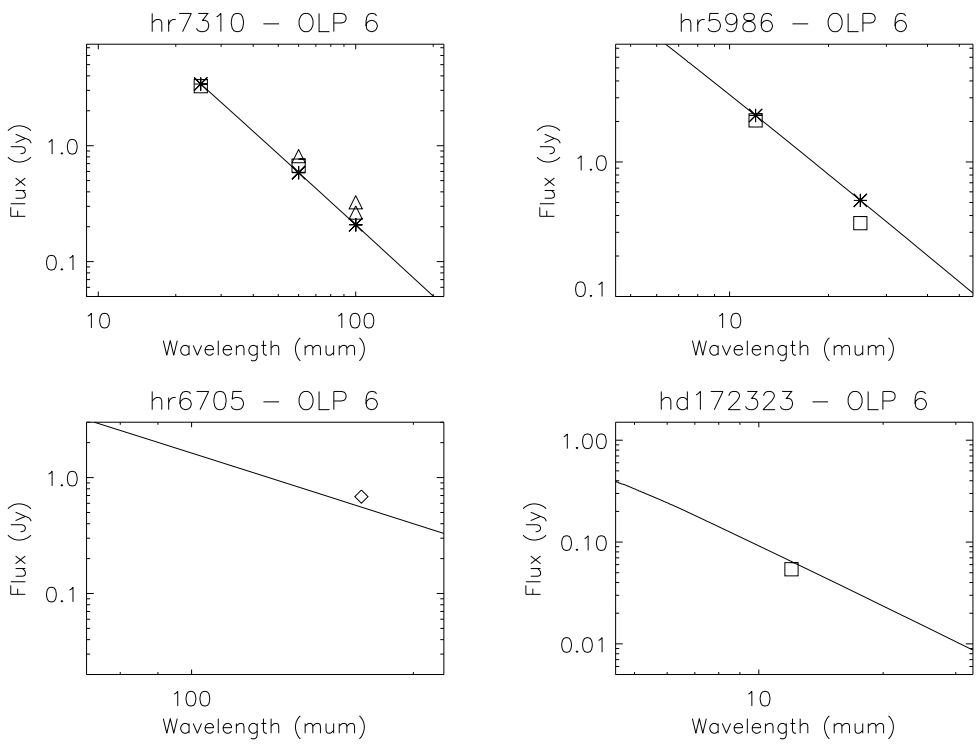

Figure 63: Comparison of PHT-P and PHT-C nodding/mini-map OLP 6.x photometry of various standard stars from the MFAINT monitoring program for the epoch of rev. 748 with the models provided by Hammersley (Ground Based Preparatory Programme), for HD 172323 and HR 5986, and Cohen, for HR 7310 and HR 6705. Fluxes are color corrected according to the spectral type of the star. The meaning of the symbols is the following: solid line: photospheric model by Hammersley or Cohen, asterisk: IRAS, square: PHT-P photometry, triangle: C100 photometry, diamond: C200 photometry.

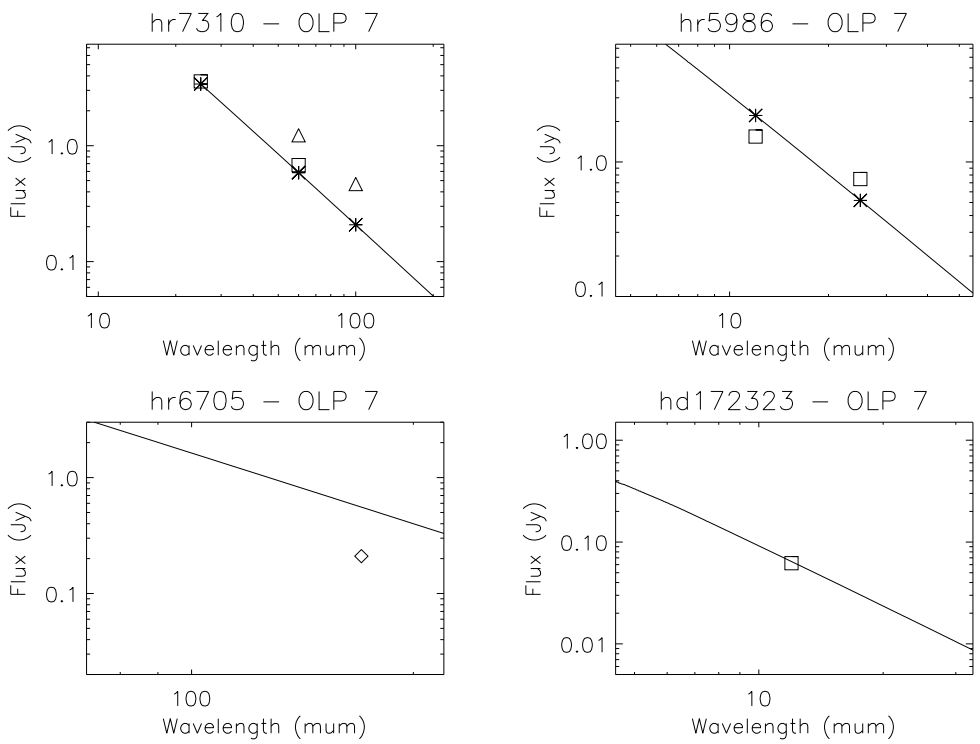

Figure 64: Comparison of PHT-P and PHT-C chopped OLP 7.0b2 photometry of various standard stars from the CFAINT monitoring program for the epoch of rev. 748 with the models provided by Hammersley (Ground Based Preparatory Programme), for HD 172323 and HR 5986, and Cohen, for HR 7310 and HR 6705. Fluxes are color corrected according to the spectral type of the star. The meaning of the symbols is the following: solid line: photospheric model by Hammersley or Cohen, asterisk: IRAS, square: PHT-P photometry, triangle: C100 photometry, diamond: C200 photometry.

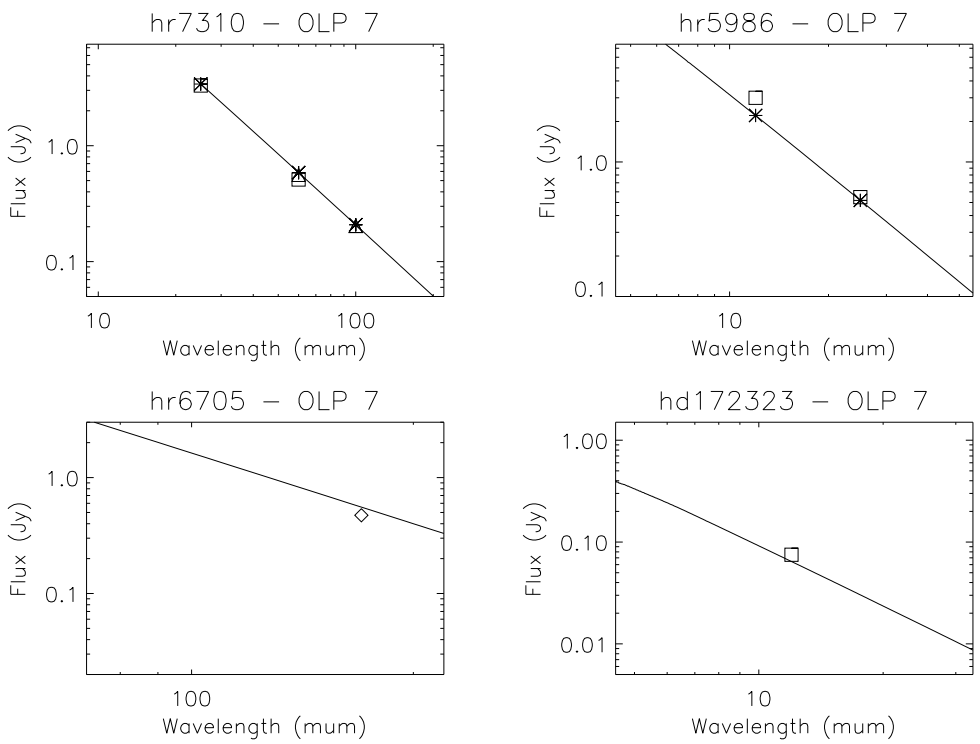

Figure 65: Comparison of PHT-P and PHT-C nodding/mini-map OLP 7.0b2 photometry of various standard stars from the MFAINT monitoring program for the epoch of rev. 748 with the models provided by Hammersley (Ground Based Preparatory Programme), for HD 172323 and HR 5986, and Cohen, for HR 7310 and HR 6705. Fluxes are color corrected according to the spectral type of the star. The meaning of the symbols is the following: solid line: photospheric model by Hammersley or Cohen, asterisk: IRAS, square: PHT-P photometry, triangle: C100 photometry, diamond: C200 photometry.

Table 42: Consistency check of chopped and staring photometric results of standard stars observed by MFAINT and CFAINT programs with models from Hammersley and Cohen

Target	**Filter**	**consistency w.r.t. reference photometry**			
		OLP 6		**OLP 7**	
		chopped mode [%]	**staring mode** [%]	**chopped mode** [%]	**staring mode** [%]
HD172323	P1_11P5	+17.2	-15.6	-3.1	+17.2
HR 5986	P1_11P5	+8.0	-8.1	-30.2	+35.4
HR 5986	P2_25	-4.1	-32.2	+44.2	+5.8
HR 7310	P2_25	-4.7	-4.2	+5.3	-2.9
HR 7310	P3_60	-12.8	+14.8	+16.0	-12.8
HR 7310	C100_60	-1.9	+38.7	+110	-4.4
HR 7310	C100_100	+2.4	+27.4	+125	-2.4
HR 6705	C200_160	-86.9	+23.2	-62.2	-14.9

6.8.5 Evaluation Log

```
Photometric Results from Monitoring Programs CFAINT (chopped mode)
and MFAINT (nodding/mini-map) performed on rev. 748

Detector    cwl    OLP6     OLP 7    Model    IRAS

#HR 7310 Te=4852  (Cohen's model)

Chopped
P3_60        60     0.511    0.680    0.586   0.629
C100_100    100     0.213    0.467    0.208   1.000L
C100_60      60     0.575    1.229    0.586   0.629
P2_25        25     3.242    3.583    3.403   3.707

Nodding
P3_60        60     0.673    0.511    0.586   0.629
P2_25        25     3.260    3.305    3.403   3.707
C100_100    100     0.265    0.203    0.208   1.000L
C100_60      60     0.813    0.560    0.586   0.629

Map
C100_100    100     0.325    0.203    0.208   1.000L


#HD 172323 Te=5719  (Hammersley's model)

Chopped
P1_11P5      12     0.075    0.062    0.064     ---

Nodding
P1_11P5      12     0.054    0.075    0.064     ---

#HR 5986  Te=6084  (Hammersley's model)

Chopped
P2_25        25     0.497    0.747    0.518    0.589
P1_11P5      12     2.393    1.546    2.216    2.362

Nodding
P2_25        25     0.351    0.548    0.518    0.589
P1_11P5      12     2.036    3.001    2.216    2.362
```

#HR 6705 Te=4000   (Cohen's model)

Chopped
C200_160   170   0.073*   0.210   0.556   ---

Map
C200_160   170   0.685   0.473   0.556   ---

* Pixels 3 and 4 have negative fluxes

6.9 General Conclusions from Chopped Photometry Analysis

- On the basis of the investigated test cases the chopped photometry of AOTs PHT03 and PHT22 can not yet be declared scientifically valid for the following reasons:
  - In particular for P3 and C100 for which the largest signal losses were stated, hence the largest corrections are needed, a general over-correction of the chopped photometric fluxes w.r.t. reference photometry from the literature or ISOPHOT staring mode photometry is observed.
  - In multi-filter modes the scatter of the photometric data points, including non-detection of the source, or discontinuitites in the resulting SEDS larger than 30% are found which do not yet allow a sound scientific analysis.
- Reasons for this behaviour which need follow-up investigations are supposed to be:
  - Limitations in the usage of an average default responsivity (the orbit dependence alone appears to be too weak to account for the variation of the responsivity values).
  - A not yet sufficient signal evaluation for chopped measurements. In particular for C100 the restriction to use the central pixel only in the case of chopped point source photometry seems to be mandatory after the tests.
  - Not yet final signal correction factors. Here, more calibration data have been acquired.

7 Conclusions and Outlook

The Scientific Validation of the OLP 7.0 beta version has demonstrated and achieved the following:

- The reset interval correction, which is performed for PHT-P and PHT-C observing modes relatively early in the processing chain, has been implemented consistently.
- The staring mode observing modes have been further consolidated with improved photometric accuarcy. This includes faint source photometry.
- The photometric accuracy of absolute and multi-filter staring modes has been assessed.
- The extended source photometry with PHT-C has been scientifically validated.
- A refined orbit dependent dark current subtraction for staring modes, including PHT-S, has been implemented.
- Color correction factors for various source SEDs have been established. These have to be consequently applied for achievement of accurate photometric flux values.
- The best available pointing information is used now in the processing.
- The empirical correction and calibration of the chopped modes is not yet accurate enough.

For the next PHT specific OLP Version 8.2, to be validated during spring 1999, the following items will be considered for inclusion:

- ultimate FCS power tables from the full data set of calibration standards obtained during the mission;
- PHT-P FCS aperture correction factors;
- correction for non-linearity of responsivity with in-band power;
- non-geometric aperture beam size scaling and calibration of multi-aperture mode;
- solid angles for all apertures of PHT-P and calibration of PHT-P extended source photometry;
- improvement and validation of the chopped photometry calibration.

A basic schedule is outlined in the following Table 43:

Table 43: Schedule for PHT OLP 8.2 Upgrades

May 98	start of analysis of multi-aperture measurements on extended and point sources for PHT-P flux dependence of the PHT-P and PHT-C detector responsivity (non-linearity) assessment report
June 98	**Version 1.0 of Scientific Validation Report of OLP7**
July 98	PHT-P FCS aperture dependence assessed (CAL-12) PHT-P multi aperture calibration assessed (CAL-06I) **Version 2.0 of Scientific Validation Report of OLP7**
Sep. 98	decision on calibration strategy w.r.t. R non-linearity (affects PHT-P FCS aperture, beam calibration and default responsivity)
Oct. 98	**1st OLP 8.2 requirements definition meeting**
Nov. 98	calibration strategy w.r.t. PHT-P beam and FCS aperture **2nd OLP 8.2 requirements definition meeting**
Dec. 98	upgrades of empirical chopped photometry
Jan. 99	**3rd and final OLP 8.2 requirements definition meeting** refined cal-G files for FCS and non-linearity responsivity, and other calibration files available for check-out in PIA **1st version of PHT OLP 8.2 test plan**
Feb. 99	**delivery of code and cal-G files for OLP V8.2**
Mar. 99	1st OLP beta version installed test cases for NDC processed **start scientific validation period 1**
Apr. 99	end of validation period 1, software re-delivery 2nd version of PHT OLP 8.2 test plan 2nd OLP beta version installed test cases for NDC re-processed start scientific validation period 2
May 99	**end of validation period 2, software re-delivery** **OLP 8.2 release** **OLP 8.2 Scientific Validation Report**

References

[1] I. Heinrichsen, L. Cornwall, M. Haas, U. Herbstmeier, H. Morris, P. Richards, and R. Saxton, "Report on the Scientific Validation of PHT OLP 6.0", Issue 1.0, 06-May-1997.

[2] R. Laureijs et al., "ISO Data User Manual (IDUM)", Version 3.0, August 1998

[3] R. Laureijs, "Flow of corrections made during processing", first version, 05-May-1998

[4] I. Heinrichsen and U. Klaas, "Plan for the PHT Scientific (Re-)Validation of OLP Version 7.0", Version 2.0, 04-May-1998

[5] B. Schulz, "Relative Filter-to-Filter Correction for C-Arrays", Version 1.0, PIDT Calibration Report, 03-September-1997

[6] M. Braun, "CRE Signal Dependence on Reset Interval Length: C100, C200, P1, P2, and P3", Version 1.0, PIDT Calibration Report, 16-December-1997

[7] U. Klaas, "Flux Conversion and Colour Corrections for ISOPHOT P and C Filters", Version 1.2, PIDT Calibration Report, 18-June-1996

[8] U. Klaas, M. Haas, I. Heinrichsen, B. Schulz, "Infrared spectral energy distributions of the interacting galaxies Arp 244, NGC 6240 and Arp 220", 1997, A&A 325, L21

[9] U. Herbstmeier, "ISOPHOT Footprints: C100 - Comparison between modelled and measured footprints - the derived parameters", Version 2.0, PHT/MPIA Calibration Report, 03-March-1998

[10] U. Herbstmeier, "ISOPHOT Footprints: C200 - Comparison between modelled and measured footprints - the derived parameters", Version 2.0, PHT/MPIA Calibration Report, 03-March-1998

[11] H. Castañeda & J. Acosta, "Dependence of the Dark Signal with Orbital Position; Proposal for Implementation Requirements of OLPv7", PIDT Calibration Report, 05-November-1997

[12] S.R. Pottash, A. Preite–Martinez, F.M. Olnon, Mo Jing–Er, S. Kingma, "IRAS spectra of planetary nebulae. III", A&A 161, 363, 1986

[13] U. Klaas, J.A. Acosta–Pulido, P. Ábrahám, H.O. Castañeda, L. Cornwall, F. Garzon, P. Hammersley, I. Heinrichsen, U. Kinkel, D. Lemke, J. Schubert, and M. Wells, "ISOPHOT-S: Capabilities and Calibration", Proc. First ISO Workshop on Analytical Spectroscopy, p. 113, ESA SP-419, December 1997

[14] D.A. Beintema, P.A.M. van Hoof, F. Lahuis, S.R. Pottasch, L.B.F.M. Waters, Th. de Graauw, D.R. Boxhorn, H. Feuchtgruber, and P.W. Morris, "The Central Stars of the Planetary Nebulae NGC 7027 and NGC 6543", A&A 315, L253, 1996

[15] I. Heinrichsen, H.J. Walker, and U. Klaas, "Infrared Mapping of the Dust Disc around Vega", MNRAS 293, L78, 1998

[16] J. Acosta & P. Ábrahám, "Correction of Signal Losses in Chopped Measurements", PIDT Calibration Report, in preparation

[17] H. Castañeda & J. Acosta, "Responsivity Variation vs. Orbit Position", PIDT Calibration Report, 19-February-1998

[18] U. Klaas, P. Ábrahám, M. Haas, U. Herbstmeier, and R.J. Laureijs, "General ISOPHOT Observing Strategies for Faint Sources", SAI/97-013/Wb, Version 1.3, 28-February-1997

[19] P. Ábrahám, U. Klaas, M. Haas, U. Herbstmeier, M. Linden, and D. Lemke, "Detection Limit and Observing Strategy for Very Faint Point Sources: Test Observations with P3, C100, and C200", Version 2.0, PHT/MPIA Calibration Report, 29-April-1997

[20] U. Klaas, "Determination of empirical PPSF correction factors for C200", PIDT Calibration Report, 08-May-1997

[21] B. Schulz & S. Huth, "Explanatory Supplement for FCS Monitoring Observations", Draft 2.0, 20-June-97 and related diagrams